

**GEOCHEMISTRY AND FRACTIONAL CRYSTALLIZATION  
HISTORY OF THE  
FALCON LAKE INTRUSIVE COMPLEX**

by

Patricia A. Tirschmann

presented to the University of Manitoba  
in fulfillment of the  
thesis requirement for the degree of  
Master of Science  
in  
Geology

Winnipeg, Manitoba, 1992

(c) Patricia A. Tirschmann, 1992



National Library  
of Canada

Acquisitions and  
Bibliographic Services Branch

395 Wellington Street  
Ottawa, Ontario  
K1A 0N4

Bibliothèque nationale  
du Canada

Direction des acquisitions et  
des services bibliographiques

395, rue Wellington  
Ottawa (Ontario)  
K1A 0N4

*Your file* *Votre référence*

*Our file* *Notre référence*

The author has granted an irrevocable non-exclusive licence allowing the National Library of Canada to reproduce, loan, distribute or sell copies of his/her thesis by any means and in any form or format, making this thesis available to interested persons.

L'auteur a accordé une licence irrévocable et non exclusive permettant à la Bibliothèque nationale du Canada de reproduire, prêter, distribuer ou vendre des copies de sa thèse de quelque manière et sous quelque forme que ce soit pour mettre des exemplaires de cette thèse à la disposition des personnes intéressées.

The author retains ownership of the copyright in his/her thesis. Neither the thesis nor substantial extracts from it may be printed or otherwise reproduced without his/her permission.

L'auteur conserve la propriété du droit d'auteur qui protège sa thèse. Ni la thèse ni des extraits substantiels de celle-ci ne doivent être imprimés ou autrement reproduits sans son autorisation.

ISBN 0-315-77867-9

Canada

**GEOCHEMISTRY AND FRACTIONAL CRYSTALLIZATION  
HISTORY OF THE FALCON LAKE INTRUSIVE COMPLEX**

**BY**

**PATRICIA A. TIRSCHMANN**

**A Thesis submitted to the Faculty of Graduate Studies of the University of Manitoba in  
partial fulfillment of the requirements for the degree of**

**MASTER OF SCIENCE**

**© 1992**

**Permission has been granted to the LIBRARY OF THE UNIVERSITY OF MANITOBA to  
lend or sell copies of this thesis, to the NATIONAL LIBRARY OF CANADA to microfilm  
this thesis and to lend or sell copies of the film, and UNIVERSITY MICROFILMS to  
publish an abstract of this thesis.**

**The author reserves other publication rights, and neither the thesis nor extensive extracts  
from it may be printed or otherwise reproduced without the author's permission.**

I hereby declare that I am the sole author of this thesis. I authorize the University of Manitoba to lend this thesis to other institutions or individuals for the purpose of scholarly research.

Patricia A. Tirschmann

I further authorize the University of Manitoba to reproduce this thesis by photocopying or by other means, in total or in part, at the request of other institutions or individuals for the purpose of scholarly research.

Patricia A. Tirschmann

The University of Manitoba requires the signatures of all persons using or photocopying this thesis. Please sign below, and give address and date.

## ABSTRACT

The Falcon Lake Intrusive Complex (FLIC) is a small (9 km<sup>2</sup>) compositionally zoned, composite intrusion located in the southwestern part of the Superior Structural Province. The complex was emplaced in Archean metavolcanic and metasedimentary rocks of the Lake of the Woods greenstone belt and represents a post-tectonic intrusion in its original intrusive orientation. The complex is comprised of six lithologic units: four outer gabbroic units (Gabbro #1-Gabbro #4), a central diorite-granodiorite unit and a quartz monzonite core. A K-AR (Wanless, 1968) date on biotite from the core rocks yielded a minimum age of 2.3 Ga.

Geochemical data and field relationships indicate that the rock types comprising the FLIC represent a genetically-related magma suite derived from a LREE-enriched parental source with "alkaline-like" characteristics. The lithologies present, however do not represent a single continuous liquid line of descent. Gabbro #1 and Gabbro #2 are geochemically the most primitive rock types of the complex. Gabbro #3, Gabbro #4, as well as some of the more mafic dioritic rocks, are distinctly more evolved, but are geochemically indistinct from each other. The dioritic-granodioritic and quartz monzonitic rocks collectively display major and trace element trends consistent with a single liquid line of descent.

The overall compositional zonation from oldest gabbroic rocks inward to youngest quartz monzonitic rocks can be explained by a combination of multiple intrusion and fractional crystallization processes. Formation of the mafic portions of the FLIC involved multiple intrusions of a) more primitive basic magma(s) and b) more evolved basic magmas. Evolution of the earlier, more primitive mafic

units (Gabbro #1 and Gabbro #2) involved the fractionation of clinopyroxene and plagioclase while the later, more evolved, mafic units (Gabbro #3, Gabbro #4 and some of the diorites) were dominated by plagioclase crystallization and accumulation. Subsequent evolution of the intermediate to felsic portions of the complex appears to have taken place via inward fractional crystallization, the later stages of which involved upward movement and convective homogenization of mobile felsic differentiates followed by rapid cooling and crystallization forming the quartz monzonite core.

## ACKNOWLEDGEMENTS

The author wishes to acknowledge Dr. N.M. Halden at the University of Manitoba who initiated the thesis project and provided supervision and guidance throughout. Norman also provided constructive criticism of earlier drafts of the thesis as well as timely "encouragement".

Ward Edwards and Stan Beaubien provided excellent field support (especially in the accurate and successful wielding of 10lb sampling sledges!). Technical support at the University of Manitoba was provided by a host of able-bodied and helpful persons including Wayne Blonski (XRF analyses), Tad Foniuk (volumetric FeO determinations), Ron Chapman (microprobe analyses), Irene Berta (thin section and stained rock slab preparation) and Ron Prihtko (photography and drafting).

Funding for the project was provided by the Geological Survey of Canada (G.S.C.) as part of the Canada-Manitoba Mineral Development Agreement (1984-1989). Jon Scoates of the G.S.C. was instrumental in the formulation of the research topic and also contributed to the work with advice and constructive criticism.

Special thanks are due to Falconbridge Limited, my employer throughout most of the thesis sojourn. Falconbridge generously made available drafting and computer facilities as well as covered the costs of slides for a 1990 GAC-MAC talk.

## TABLE OF CONTENTS

	<u>Page</u>
<b>ABSTRACT</b> .....	<b>iv</b>
<b>ACKNOWLEDGMENTS</b> .....	<b>vi</b>
<b>CHAPTER 1 - INTRODUCTION</b> .....	<b>1</b>
1.1 General Statement and Objectives .....	1
1.2 Location, Access .....	2
1.3 Topography, Vegetation .....	4
1.4 Previous Work .....	4
<b>CHAPTER 2 - REGIONAL GEOLOGY</b> .....	<b>8</b>
2.1 General Geology .....	8
2.2 Keewatin Series Rocks .....	8
2.2.1 Metavolcanic Rocks .....	11
2.2.2 Metasedimentary Rocks .....	12
2.3 Archean to Proterozoic Granitic Intrusive Rocks .....	13
2.3.1 Gneissic Granodiorite and Quartz Diorite .....	14
2.3.2 Rennie Batholith .....	14
2.3.3 Caddy Lake Granite .....	14
2.3.4 Porphyritic Granodiorite .....	15
2.4 Structural Geology .....	15
2.5 Regional Metamorphism .....	16
<b>CHAPTER 3 - METHODS OF RESEARCH</b> .....	<b>17</b>
3.1 Field .....	17
3.2 Laboratory .....	19
3.2.1 Major and Trace Elements .....	19
3.2.2 Rare Earth Elements .....	19
3.2.3 Microprobe Analyses .....	20
3.2.4 Petrography .....	20
<b>CHAPTER 4 - GEOLOGY OF THE FALCON LAKE INTRUSIVE COMPLEX</b> .....	<b>22</b>
4.1 General Features .....	22
4.1.1 External Contacts .....	24
4.1.2 Internal Contacts .....	25
4.1.3 Inclusions .....	26
4.1.4 Dykes .....	27
4.1.5 Breccia Pipes .....	27
4.1.6 Faults/Shear Zones .....	28
4.2 Contact Metamorphism .....	30
4.3 Gabbro #1 .....	30
4.3.1 Field Observations .....	30
4.3.2 Texture .....	31

	<u>Page</u>
4.3.3 Petrography . . . . .	31
4.4 Gabbro #2 . . . . .	33
4.4.1 Field Observations . . . . .	33
4.4.2 Texture . . . . .	34
4.4.3 Petrography . . . . .	34
4.5 Gabbro #3 . . . . .	36
4.5.1 Field Observations . . . . .	36
4.5.2 Texture . . . . .	37
4.5.3 Petrography . . . . .	37
4.6 Gabbro #4 . . . . .	43
4.6.1 Field Observations . . . . .	43
4.6.2 Texture . . . . .	45
4.6.3 Petrography . . . . .	45
4.7 Deformation in Gabbroic Units . . . . .	48
4.8 Diorite-Granodiorite . . . . .	48
4.8.1 Field Observations . . . . .	48
4.8.2 General Statement . . . . .	49
4.8.3 Diorites - Texture and Petrography . . . . .	49
4.8.4 Granodiorites - Texture and Petrography . . . . .	51
4.8.5 Large-scale Variations . . . . .	53
4.9 Quartz Monzonite . . . . .	55
4.9.1 Field Observations . . . . .	55
4.9.2 Texture . . . . .	55
4.9.3 Petrography . . . . .	55
4.10 Rock Nomenclature . . . . .	59
<b>CHAPTER 5 - WHOLE ROCK GEOCHEMISTRY . . . . .</b>	<b>66</b>
5.1 Major Element Geochemistry . . . . .	66
5.1.1 General Characterization . . . . .	66
5.1.2 Harker Variation Diagrams . . . . .	74
5.1.3 Normative Mineralogy . . . . .	76
5.2 Trace Element Geochemistry . . . . .	77
5.3 Rare Earth Element Geochemistry . . . . .	80
<b>CHAPTER 6 - MINERAL CHEMISTRY . . . . .</b>	<b>84</b>
6.1 Plagioclase . . . . .	84
6.2 Alkali Feldspar . . . . .	88
6.3 Oxide Minerals . . . . .	90
6.4 Pyroxenes . . . . .	93
6.5 Amphiboles . . . . .	97
6.6 Biotites . . . . .	100

	<u>Page</u>
<b>CHAPTER 7 - ESTIMATE OF INTENSIVE PARAMETERS</b> .....	<b>102</b>
7.1 Pressure and Temperature .....	102
7.2 $fO_2$ and Temperature .....	109
7.3 Summary .....	112
<b>CHAPTER 8 - DISCUSSION AND PETROGENESIS</b> .....	<b>114</b>
8.1 General Statement .....	114
8.2 Differentiation and Liquid Lines of Descent .....	115
8.3 Relationship Between Gabbroic Units .....	117
8.4 Relationships Between Diorite-Granodiorite and Quartz Monzonite .....	118
8.5 Trace Elements .....	122
8.5.1 Rb and Sr .....	122
8.5.2 Zr, Nb .....	129
8.6 Rare Earth Elements (REEs) .....	130
8.7 Eu Anomalies .....	131
8.8 Alkaline Characteristics .....	133
8.9 Petrogenetic Model .....	135
<b>CHAPTER 9 - CONCLUSIONS</b> .....	<b>139</b>
<b>REFERENCES</b> .....	<b>142</b>
<b>APPENDIX 1</b> .....	<b>151</b>
<b>APPENDIX 2</b> .....	<b>168</b>
<b>APPENDIX 3</b> .....	<b>170</b>

## LIST OF PLATES

PLATE		<u>Page</u>
1	Sunbeam-Kirkland Breccia Pipe . . . . .	29
2	Porphyritic Gabbro #1 . . . . .	32
3	Gabbro #2 . . . . .	35
4	Gabbro #3 . . . . .	38
5	Gabbro #3 . . . . .	40
6	Photomicrograph of Gabbro #3 . . . . .	42
7	Photomicrograph of Gabbro #3 . . . . .	44
8	Gabbro #4 . . . . .	46
9	Orthocumulate to mesocumulate Gabbro #4 . . . . .	47
10	Diorite and granodiorite . . . . .	50
11	Photomicrograph of granodiorite . . . . .	54
12	Quartz monzonite/granodiorite contact . . . . .	56
13	Quartz monzonite . . . . .	56
14	Porphyritic quartz monzonite . . . . .	57
15	Stained rock slabs . . . . .	64
16	Photomicrographs of oxide minerals . . . . .	92
17	Photomicrograph of relict pyroxene core . . . . .	94
18	Photomicrographs of allanite . . . . .	132

## LIST OF FIGURES

FIGURE		<u>Page</u>
1	Location map for the Falcon Lake Intrusive Complex . . . . .	3
2	Regional geology . . . . .	9
3	Geology of the West Hawk Lake-Falcon Lake area . . . . .	10
4	Sample location map . . . . .	18
5	General geology of the Falcon Lake Intrusive Complex . . . . .	23
6	Modal QAP plot . . . . .	62
7	K <sub>2</sub> O + Na <sub>2</sub> O vs SiO <sub>2</sub> plot . . . . .	70
8	Na <sub>2</sub> O vs K <sub>2</sub> O diagram . . . . .	71
9	AFM diagram . . . . .	72
10	CaO vs SiO <sub>2</sub> diagram . . . . .	73
11	Harker variation diagrams . . . . .	75
12	Trace element variation diagrams . . . . .	79
13	Chondrite-normalized REE plots . . . . .	82
14	OR-Ab-An feldspar triangle . . . . .	87
15	Alkali feldspar compositions in the Or-Ab-An triangle . . . . .	89
16	Classification of pyroxenes . . . . .	96
17	Classification of amphiboles . . . . .	99
18	Plot of Fe/Fe+Mg ratios in biotite . . . . .	101
19	FLIC quartz monzonites plotted in Qtz-Ab-Or-H <sub>2</sub> O system . . . . .	104
20	FLIC quartz monzonites plotted in granite system at 2 and 5 kbar pressure . . . . .	105
21	Experimental basalt-water systems . . . . .	107
22	Determinative curves for temperature based on a two-feldspar geothermometer . . . . .	110
23	FO <sub>2</sub> vs temperature diagram for selected buffer assemblages . . . . .	111
24	AFM diagrams . . . . .	116
25	Harker variation diagrams for the diorite-granodiorite and quartz monzonite samples . . . . .	119
26	Trace element variation diagrams for the diorite-granodiorite and quartz monzonite samples . . . . .	120
27	Log Rb vs log Sr diagrams . . . . .	124
28	Chondrite-normalized plot . . . . .	134
29	Petrogenetic model . . . . .	136

## LIST OF TABLES

TABLE		<u>Page</u>
1	Nomenclature for rocks of the Falcon Lake Intrusive Complex . . . . .	59
2	Point counting data . . . . .	61
3	Representative analyses of gabbros . . . . .	67
4	Representative analyses of diorite-granodiorite and quartz monzonite . . . . .	68
5	Degree of silica-saturation in rocks of the FLIC . . . . .	76
6	Ranges in trace element content . . . . .	78
7	Rare earth element data . . . . .	81
8	Representative plagioclase analyses . . . . .	85
9	Representative alkali feldspar analyses . . . . .	89
10	Representative oxide mineral analyses . . . . .	91
11	Representative pyroxene analyses . . . . .	95
12	Representative biotite analyses . . . . .	101
13	Calculated temperatures and $f_{O_2}$ 's for co-existing Fe-Ti oxides . . . . .	113
14	Rb and Sr mineral distribution coefficients . . . . .	126
15	Estimated modal mineralogy . . . . .	126

## CHAPTER 1

### INTRODUCTION

#### 1.1 General Statement and Objectives

The Falcon Lake Intrusive Complex (FLIC) is a small (9 km<sup>2</sup>), layered, concentrically zoned, composite intrusion emplaced in the eastern portion of the Lake of the Woods greenstone belt. It is comprised of four outer gabbroic units, a diorite-granodiorite unit and a quartz monzonite core, spanning a wide compositional range (42.4-68.8 wt% SiO<sub>2</sub>) and exhibiting no distinct compositional breaks between phases. Sharp internal intrusive contacts exist between phases and layering is present to some extent in all phases with the possible exception of Gabbro #2. The complex has sharp discordant contacts with host rocks and is thought to be in its original intrusive orientation.

Much research has been done in recent years by numerous geological workers on the processes involved in forming a normally zoned intrusion encompassing a relatively wide compositional range. Proposed mechanisms capable of producing a spatially-related differentiated suite of rocks include the following: crystal fractionation (Tindle and Pearce, 1981; Perfit et al, 1980; Bateman and Chappell, 1979; Bateman and Nokleberg, 1978; Raglan and Butler, 1972), assimilation (McBirney, 1984) and restite-minimum melt models (Scambos et al, 1986) and multiple intrusion (McBirney, 1984). Liquid-state diffusion and convective fractionation are also thought to result in chemical zonation but are more applicable to high-silica systems exhibiting a restricted compositional range (Tuach and Strong, 1986; Sparks and Huppert, 1984; Hildreth, 1981).

Previous studies on the FLIC, notably Brownell (1941), Gibbins (1967) and Mandziuk (1988), were focused on the petrology and primary igneous structures. Geochemical data, existing prior to the present study, consisted of 19 whole rock major element analyses done by Gibbins (1967) on samples obtained from Brownell's (1941) collection.

The primary objective of this study was to expand the geochemical data base for the FLIC thus providing a framework for interpreting the geochemical evolution of the complex. The evolution of the complex was investigated through synthesis of field observations (both the author's and those of previous workers), petrography, major and trace element geochemistry and preliminary REE and mineral chemistry. Mapping done by Mandziuk (1989), at a scale of 1:5000, provided the geological base upon which the geochemical sampling was performed.

## 1.2 Location, Access

The Falcon Lake Igneous Complex is located 110 km east of Winnipeg, Manitoba between Star Lake and Falcon Lake immediately north of the Trans-Canada Highway. The Manitoba-Ontario border lies 6 km to the east of the complex.

The Star Lake area is easily accessible via Highway #1 (Trans-Canada) and secondary provincial highways #44 and #301. Highway #1 and #301 cut across the southern and eastern parts of the complex respectively (Figure 1). A 1.2 km long private dirt and gravel road transects the east central part of the complex starting in the north from a Star Lake cottage block access road and running south to Highway #1. A dirt logging road borders a large part of the northern margin of the FLIC. Most parts of the complex are easily accessible on foot off of the

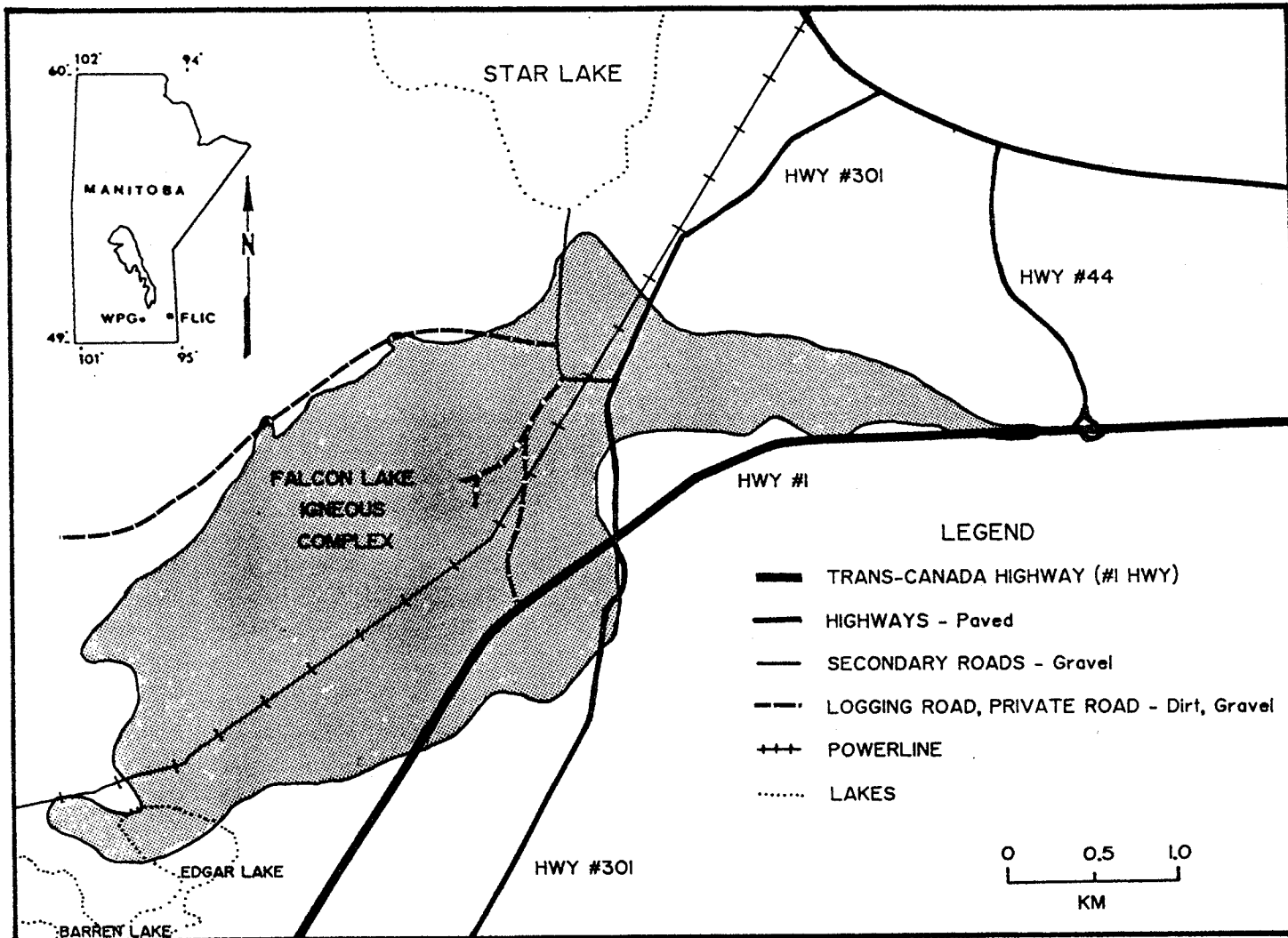


FIGURE 1: Location Map for the Falcon Lake Intrusive Complex. Modified after Mandziuk (1986).

above roads. Additional access is via a hydro-line cutting across the long axis of the FLIC.

### 1.3 Topography, Vegetation

Topography in the area is characterized by low gentle hills and ridges with intervening low-lying to swampy areas. Total relief is about 33 meters with the greatest relief occurring in the southwest part of the complex where 10 meter cliffs occur.

Vegetation on higher ground is predominantly mixed forest comprised of white spruce, poplar, birch and pine. Black spruce, tamarack and cedar are common in low-lying or swampy areas. Where thicker overburden comprised of glacial sand and gravel exists, jack pine and red pine are abundant and underbrush is fairly sparse.

### 1.4 Previous Work

In 1882, Bell subdivided rocks of the region into Laurentian gneisses and Huronian metavolcanic and metasedimentary rocks. A.C. Lawson (1885) carried out geological mapping in the Lake of the Woods area as far west as Falcon Lake. He showed the "Laurentian gneisses" to be younger than the volcanic and sedimentary rocks and was the first to use the term "Keewatin" with reference to these supracrustal rocks. As indicated by Davies (1954), the term "Laurentian" is no longer applied to the intrusive granitic rocks in eastern Manitoba and northwestern Ontario.

During the period between 1916 and 1921, various studies of the mineral deposits in the Falcon-West Hawk Lake area were done by DeLury, Bruce and

Marshall between the years 1916 and 1921. DeLury (1942) also did geological mapping in 1937. In the 1950's, more detailed mapping was done by Springer (1952) and Davies (1954) at scales of 1 inch:1 mile and 1 inch:1000 feet respectively. A petrologic study on the Archean sedimentary rocks in the West Hawk Lake area was completed by Binda in 1953.

Mapping to this point had outlined the presence of the zoned intrusive body then called the Falcon Lake stock, now referred to as the Falcon Lake Intrusive Complex. Studies concerned specifically with the FLIC are outlined below.

Brownell completed a detailed petrologic study of the complex in 1941. He defined three compositional zones: an outer zone comprising gabbro, diorite and quartz diorite, an intermediate zone of syenodiorite and granodiorite and a quartz monzonite core. The sequence of events hypothesized to have produced these zones involved differentiation via crystallization of the outer zone followed by intrusion of a felsic differentiate into the incompletely solidified core area with the intermediate zone formed by subsequent outward diffusion of potash and silica.

A study of the geology and radioactivity of the FLIC was done by House (1955). His model for the formation of the various rock types present involved intrusion of a felsic quartz monzonitic magma which reacted with basic igneous host rocks (either intrusive or extrusive). He suggested that reaction between the felsic magma and the basic rocks resulted in metasomatism and recrystallization forming the granodioritic through to gabbroic rocks. He further concluded that radioactivity was associated with apatite, magnetite, allanite, carbonate mineral(s) and to a lesser extent epidote and titanite in all phases of the FLIC, but with the most radioactive rocks being those of the intermediate zone.

Gibbins completed a petrogenetic study of the FLIC in 1967, expanding his data base to include geochemistry and specific gravity. Brownell's three compositional zones were retained but rock nomenclature was somewhat modified with the outer mafic zone defined as gabbro and diorite and the intermediate zone as monzodiorite and granodiorite. "Quartz monzonite" was retained for the core zone. Nineteen whole rock analyses comprising the three zones were obtained as part of the study and defined a calc-alkaline trend when plotted on an AFM diagram. A distinct compositional hiatus, correlatable with the contact between the intermediated zone rocks and rocks of the core, seemed to exist between 58 and 64 wt % SiO<sub>2</sub>. It was not clear whether or not this compositional hiatus represented a break in the physical evolution of the complex.

The following hypothesis was put forward by Gibbins (1967): initial intrusion of a crystal-liquid mush, in-situ differentiation by crystallization, segregation of a more felsic magma to the core of the intrusion, renewed movement of this felsic magma at some time after the outer structural zone was solidified and subsequent rapid cooling and crystallization of the quartz monzonite core. In a later paper, Gibbins (1971) suggested that the last stages of activity in the complex included resurgent boiling when  $P_{H_2O}$  exceeded  $P_{confining}$ . He used this phenomena to help explain the existence of breccia pipes, a locally brecciated inner contact, the finer grain size and porphyritic texture of the quartz monzonite as well as the homogeneity of the core rocks.

Haugh (1962) did a petrofabric study in which he measured and plotted the poles to (010) plagioclase composition planes and to crystallographic c axes of quartz crystals. He concluded that the quartz and plagioclase crystals from the

various parts of the complex exhibited preferred orientations related to primary magmatic flow layers.

The most recently completed study is that of Mandziuk (1989) whose work was concentrated on the primary igneous structures found within the complex and included remapping of the complex at a scale of 1:5000. Mandziuk (1989) defined six individual igneous rock units (four outer gabbroic units, a diorite-granodiorite unit and a quartz monzonite core) each characterized by unique primary fabric structures such as igneous laminations, mineral segregations, layering and unconformable structures. His study indicated that these primary structures were formed by magmatic flow processes related to intrusive emplacement mechanisms occurring within a magma conduit. Concentric, compositional zonation was attributed to periodic tapping of a lower level, progressively differentiating magma chamber.

Other studies relating to the FLIC or its host rocks are the following:

Fingler (1991) - precious metal mineralization related to the complex.

Beaubien (1988) and Quinn (1985) - studies of contact metamorphism in the rocks adjacent to the FLIC.

Chaytor (1985) - a report on the geochemistry of the complex

Johanasson (1985) - a gravity study of the complex

Barc (1985) and Halwas (1984) - studies of the Sunbeam-Kirkland and Moonbeam breccia pipes, respectively.

## CHAPTER 2

### REGIONAL GEOLOGY

#### 2.1 GENERAL GEOLOGY

The Falcon Lake Intrusive Complex is located in the Wabigoon Subprovince which is situated in the southwestern part of the Superior Structural Province (Figure 2). The complex occurs within a northwestern extension of what has been variously termed the Lake of the Woods greenstone belt (Blackburn et al, 1985) or the Kenora-Keewatin greenstone belt (Gibbins, 1971). Rocks comprising this west to southwest striking arm of the greenstone belt include Keewatin Series metavolcanic and metasedimentary rocks. The greenstones are bounded to the north and south by granitic intrusive rocks (Figure 3) which are interpreted to be Archean in age based on dating done by Farquharson and Clark (1970).

#### 2.2 KEEWATIN SERIES ROCKS

The band of metavolcanic and metasedimentary rocks hosting the FLIC extends from the main mass of the Lake of the Woods greenstone belt 35 km southeast of the Manitoba/Ontario border where it disappears beneath thick overburden. This sequence has a maximum thickness of 9.5 km near the inter-provincial border and narrows westward to a minimum thickness of 3 km.

Mapping done by Springer (1952) and Davies (1954) in the West Hawk-Falcon Lake area outlined a volcanic rock sequence comprised of mafic to intermediate flows, agglomerate and mafic tuff conformably overlain by a metasedimentary rock sequence. Recent mapping by Fingler (1991), Mandziuk (1989) and Beaubien (1988) immediately to the west and northwest of the FLIC

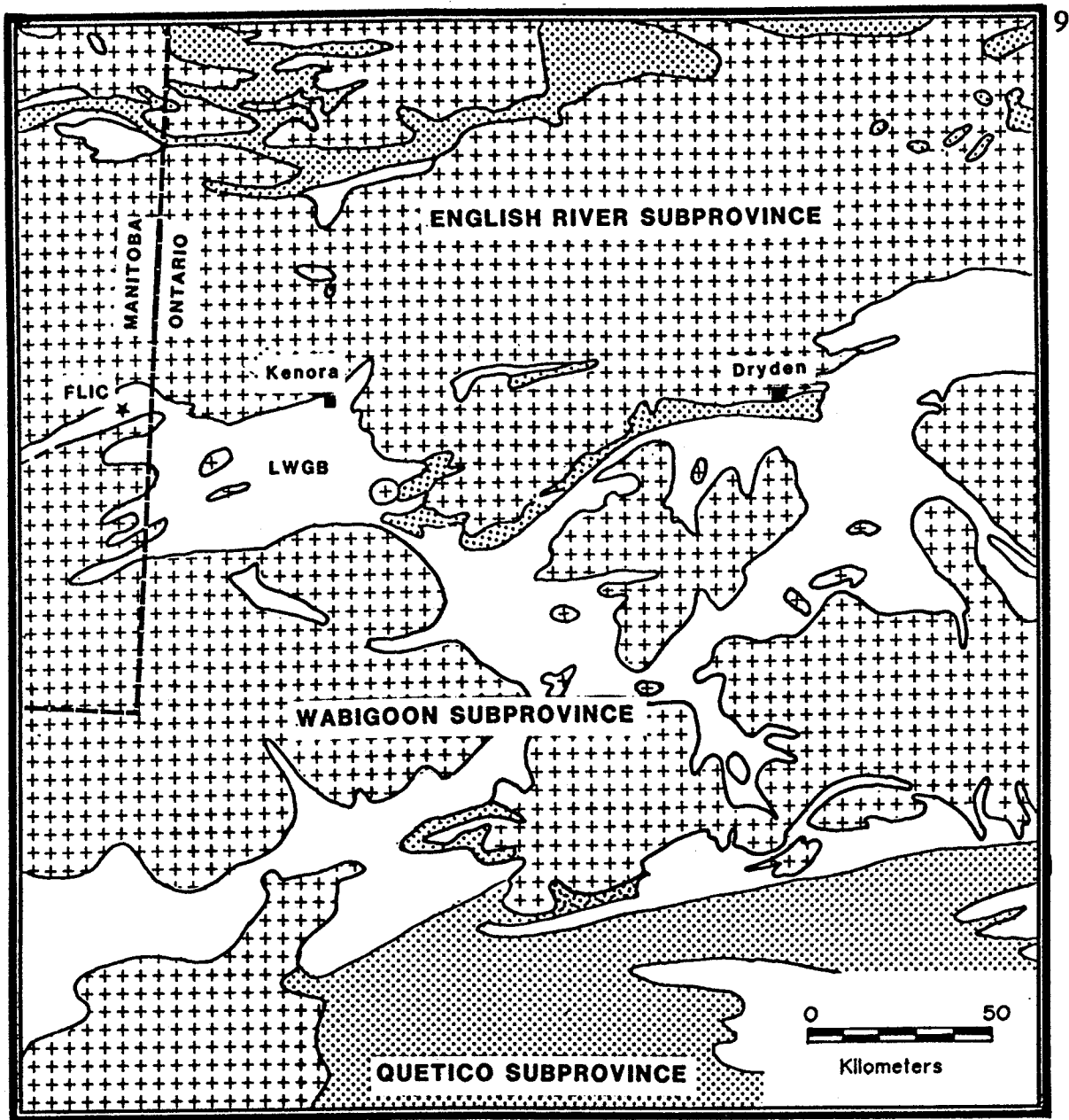


FIGURE 2: Regional Geology. Areas in white represent greenstone belts, crosses are granitoid terranes and the stippled patterns are metasedimentary units unrelated to those within greenstone belts.  
 LWGB = Lake of the Woods Greenstone Belt  
 FLIC = Falcon Lake Intrusive Complex  
 Note the location of the FLIC, shown by the star, within a west-striking extension of the LWGB. Map is modified after Pettijohn (1972) and Blackburn et al (1985).

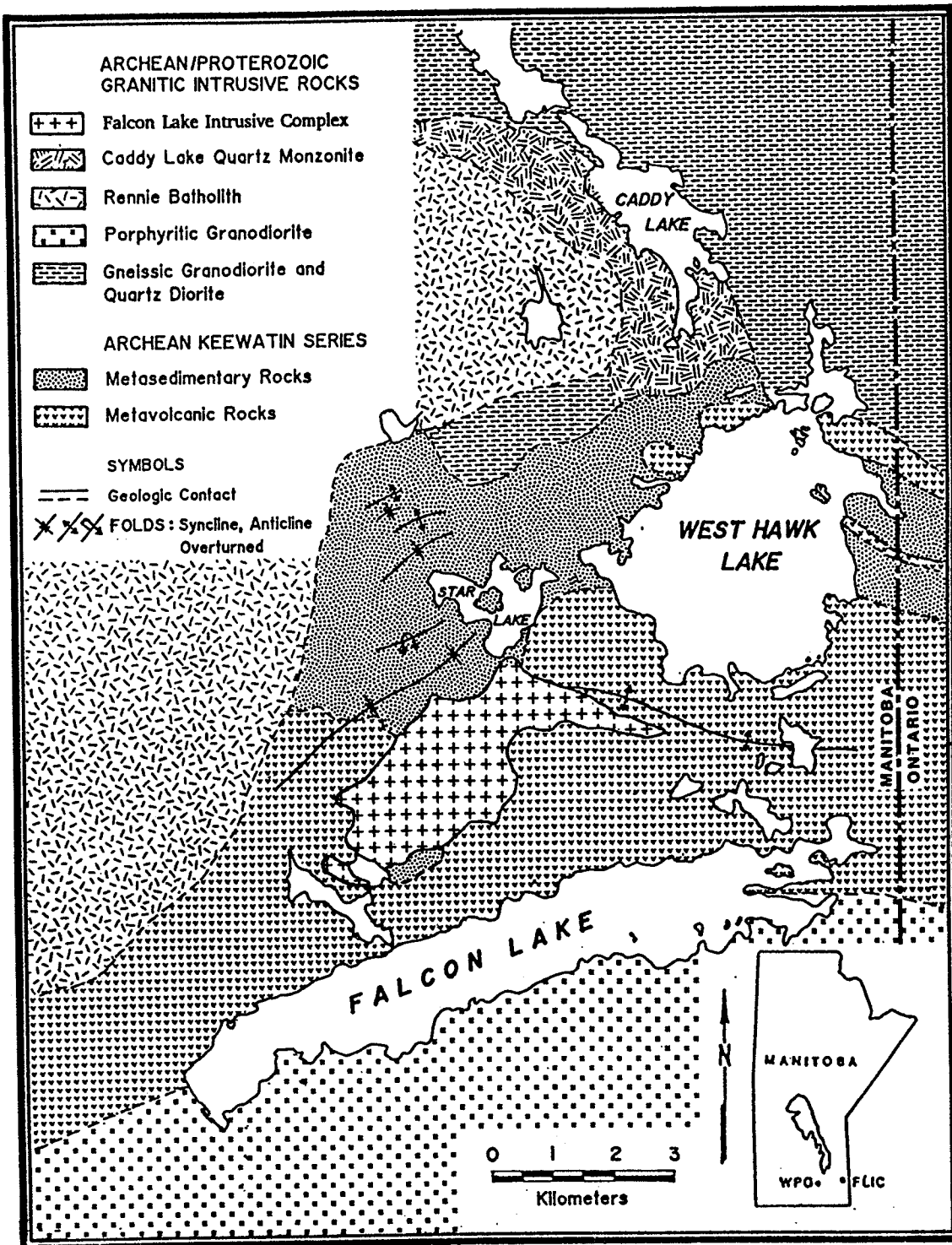


FIGURE 3: Geology of the West Hawk Lake-Falcon Lake area, southeastern Manitoba. Modified after Mandziuk (1988), Lamb (1975) and Davies (1954).

defined a lower sequence of intermediate to mafic flows unconformably overlain by a metasedimentary sequence comprised, in this area, of interbedded conglomerates, arkoses and arenites.

A major discrepancy between older and more recent mapping seems to lie in the fact that large parts of the agglomerate\tuff units of Springer and Davies are grouped as metasedimentary units by more recent workers. The subdivisions of Mandziuk (1989) are retained in Figure 3 and are in accordance with the limited field observations made by the author in the immediate vicinity of the FLIC. Proceeding descriptions of individual rock units are summarized from Springer (1952), Davies (1954) and Beaubien (1988).

### 2.2.1 Metavolcanic Rocks

The metavolcanic rocks form a broad band outcropping between Falcon Lake to the south and West Hawk and Star lakes to the north. The predominant units in this area are andesitic to basaltic pillowed to massive flows. Andesite is typically comprised of subequal amounts of andesine and green hornblende or actinolite with quartz, magnetite, calcite, biotite, sphene and sulphide minerals occurring as accessory phases. Epidote and chlorite are common constituents where the rocks exhibit a schistosity. Fabric in the rocks is defined, typically, by deformed pillows and locally by a mafic mineral schistosity. Units of tuff and "agglomerate" (Springer, 1952; Davies, 1954) are interstratified with the flows at some localities. The agglomerate and basic tuff units have been recently grouped with the metasedimentary rocks of the area.

The agglomerate unit defined by Davies (1954) outcrops southwest of Star Lake and is comprised of closely-packed oval-shaped andesitic fragments in a

darker gray andesitic matrix both consisting of andesine, hornblende and variable quantities of biotite, clinozoisite, epidote, calcite, quartz, magnetite and sulphide minerals. Andesite flows are intercalated with agglomerate at the base of this unit and agglomerate is intercalated with overlying tuff.

The basic tuff defined by Davies (1954) outcrops northwest of Star Lake and north of West Hawk Lake. This unit consists of finely (< 2.5 cm thick) bedded dark green tuff locally containing subangular to rounded andesitic fragments. Bedding is defined by variations in both grain size and composition. Andesine and hornblende or tremolite-actinolite are the main minerals present. Accessory minerals include quartz, biotite, magnetite and calcite.

At some localities, the tuff is recrystallized and is comprised of unoriented equidimensional hornblende with clear quartz and plagioclase. Hornblende can also occur as aligned needles or blades. Garnet is present in the rocks at some exposures.

### **2.2.2 Metasedimentary Rocks**

The reader is referred to Beaubien (1988) for specific descriptions of some of the metasedimentary arkoses, conglomerates and semi-pelites bordering the northwest margin of the FLIC.

The following general statement is summarized from Springer (1952) and Davies (1954) and refers to the metasedimentary rocks outcropping to the north of Star Lake and west to West Hawk Lake. The sequence is comprised mainly of fine grained to medium grained, bedded to massive quartz-feldspar-biotite-rich rocks which locally exhibit features indicative of silicification. Some fine grained brown to grey units comprised of quartz, plagioclase, microcline and biotite could

be compositionally classified as arkoses and greywackes. Localized occurrences of argillite and garnetiferous schist are found north of Star Lake.

### 2.3 ARCHEAN TO PROTEROZOIC GRANITIC INTRUSIVE ROCKS

Granitic intrusive rocks terminate against the northern and southern margins of the belt of Keewatin Series rocks. Situated to the north are the Rennie Lake Batholith, the Caddy Lake Granite as well as a large body of gneissic granodiorite and quartz diorite. To the south is a large body of pink to grey porphyritic granodiorite. Age relationships between the various intrusive rocks, including the FLIC, are not known precisely. However, Farquharson and Clark (1971) did a Rb-Sr whole-rock study of some granitic rocks from southeastern Manitoba and determined the following pertinent ages:

Pink porphyritic granodiorite	2664 ± 50 Ma
Porphyritic margin - Rennie Lake Batholith	2603 ± 320 Ma
Caddy Lake Granite	2558 ± 12 Ma

Wanless (1968) obtained a K-Ar minimum age of 2.3 Ga for biotite from the FLIC, whereas Gibbins (1971) reports that a Rb-Sr mineral-whole rock isochron falls within the time span of the Kenoran orogeny. Thus the FLIC is likely younger than any of the large intrusive bodies to the north and south, with the possible exception of the Caddy Lake Granite. Farquharson and Clark (1971) suggest that a major intrusive episode took place between 2620 and 2665 Ma with the Caddy Lake Quartz Granite being part of later igneous activity (as would be the FLIC based on existing age dates).

Proceeding descriptions of individual intrusive bodies are summarized from Springer (1952), Davies (1954) and Farquharson and Clark (1971).

### **2.3.1 Gneissic Granodiorite and Quartz Diorite**

This body (see Figure 3) is thought to be one of the oldest intrusive units in the area and is distinctive in that it displays a gneissosity defined by alignment of mafic minerals. Mineralogically, the rocks are comprised of 45% oligoclase, 30% quartz, 10% microcline, 10% biotite and 5% accessory minerals including calcite, muscovite, sausserite and garnet.

### **2.3.2 Rennie Batholith**

The batholith lies to the northwest of Falcon and West Hawk Lakes between Rennie and East Braintree and is the largest intrusive body in the area. It is composed of pink to brown and grey phases of granodiorite to quartz diorite with a distinctive porphyritic margin identified around the eastern side of the batholith. The porphyritic foliated margin contains microcline phenocrysts in an oligoclase, microcline, quartz and biotite groundmass.

### **2.3.3 Caddy Lake Granite**

This body, formerly referred to as the Caddy Lake Quartz Monzonite, outcrops in an arcuate band immediately adjacent to Caddy Lake, approximately 5 km N-NE of the FLIC. A recent petrogenetic study was done by Duncan (1989) who identified two lithologic phases comprising the granite; a predominant phase of two-mica leucogranite and subordinate areas of biotite granite. The granites are typically medium grained and comprised of microcline, plagioclase, quartz, biotite and muscovite as well as the accessory minerals apatite, allanite, zircon, epidote and altered Fe-Ti oxides. Rocks in the southern part of the pluton are locally garnetiferous.

### 2.3.4 Porphyritic Granodiorite

The 7 km wide granodiorite body is situated immediately south of Falcon Lake and is bounded along its southern edge by another westward arm of the Lake of the Woods greenstone belt. It consists of microcline phenocrysts in a groundmass of oligoclase, quartz, biotite and minor sphene, similar to the margin of the Rennie Lake Batholith.

## 2.4 STRUCTURAL GEOLOGY

The band of metavolcanic and metasedimentary rocks in the West Hawk-Falcon Lake area represent the west-trending north limb of a large anticline, the south limb of which is located in the greenstone rocks north of Shoal Lake. In the vicinity of the FLIC, the north limb of the anticline swings to the southwest and at this point is obscured by the complex. A synclinal axis to the south of this major anticline trends through the southern part of Shoal Lake into Ontario (Springer, 1952). To the west and northwest of the FLIC, a series of NE-SW trending, north-dipping minor folds occur in the Keewatin Series rocks. Fold axes are observed to plunge at approximately  $35^\circ$  to the northeast.

Metavolcanic rocks in this region are steeply dipping (up to  $80^\circ$  N or S) except near the Rennie Lake Batholith where dips as shallow as  $35^\circ$  occur (Davies, 1952). Foliation in the Rennie Lake Batholith, in the grey gneissic granite and in the porphyritic granodiorite south of Falcon Lake, is parallel to bedding in the greenstone rocks. Foliation measured in metasedimentary rocks adjacent to the FLIC (Beaubien, 1988) is typically Az  $030^\circ$  which is consistent with the trend of the minor fold series in that area.

In summary, major regional structural trends are east-west but swing to the southwest, as outlined above, west and southwest of Star Lake. This shift in structural trends, the presence of the closely-spaced minor folds northwest of the FLIC and the westward attenuation of the greenstone belt are all postulated to have accompanied or post-dated the intrusion of the large granitic masses which bound the greenstone belt rocks (Springer, 1954; Davies, 1952). Initial regional deformation resulted in the development of large-scale folds while the intrusion of the aerielly extensive Archean granitic bodies and/or subsequent events appears to have superimposed secondary deformational features on the area.

## 2.5 REGIONAL METAMORPHISM

Regional metamorphic grade in the Star Lake area ranges from medium greenschist facies to lower amphibolite facies. Metavolcanic rocks contain abundant actinolite, plagioclase ( $An_{40-50}$ ) and epidote defining a greenschist grade of metamorphism with temperatures of less than 500° C (Beaubien, 1988; Davies, 1962). Recent studies (Beaubien, 1988) of the metasedimentary rocks north of Star Lake identified a mineral assemblage including garnet and biotite indicating a middle amphibolite grade of metamorphism with temperatures greater than or equal to 600° C but below granite minimum melt temperatures. Beaubien also suggested that a second, possibly low pressure, high temperature metamorphic event may have occurred, the evidence for which includes cummingtonite asterisms, decussate muscovite and inclusion-free rims on garnet in the same metasedimentary rock samples.

## CHAPTER 3

### METHODS OF RESEARCH

#### 3.1 FIELD

Approximately seven weeks were spent during the 1986 and 1987 field seasons collecting samples of the six intrusive units comprising the FLIC for geochemical and petrological study. A total of 169 samples were obtained (Figure 4) with the following distribution between rock types: 10 samples of Gabbro #1, 4 samples of Gabbro #2, 26 samples of Gabbro #3, 12 samples of Gabbro #4, 59 diorite-granodiorite samples, 40 quartz monzonite samples and 18 other samples including dyke rocks, host rocks, contacts as well as mafic clots (see Plate 9b) and a mafic magnetite-rich layer occurring within Gabbro #4.

Sampling was based on previous mapping done by W. Mandziuk (1984-1986) and was carried out with a view to achieving a good aerial distribution across all phases while selecting only the most pristine samples with respect to alteration and deformation. Locally, areas of outcrop were eliminated as prospective sampling sites due to degree of weathering, alteration and deformation (the latter occurring in the form of small shear zones). In addition, areas containing various localized features such as layering, mafic clots and inclusions were generally avoided. This selective sampling process resulted, to some extent, in a limited number of samples over a restricted outcrop area, particularly in the case of the gabbroic units.

Detailed sampling and study of the layering within the complex was beyond the scope of this project. The layering is acknowledged as an important and

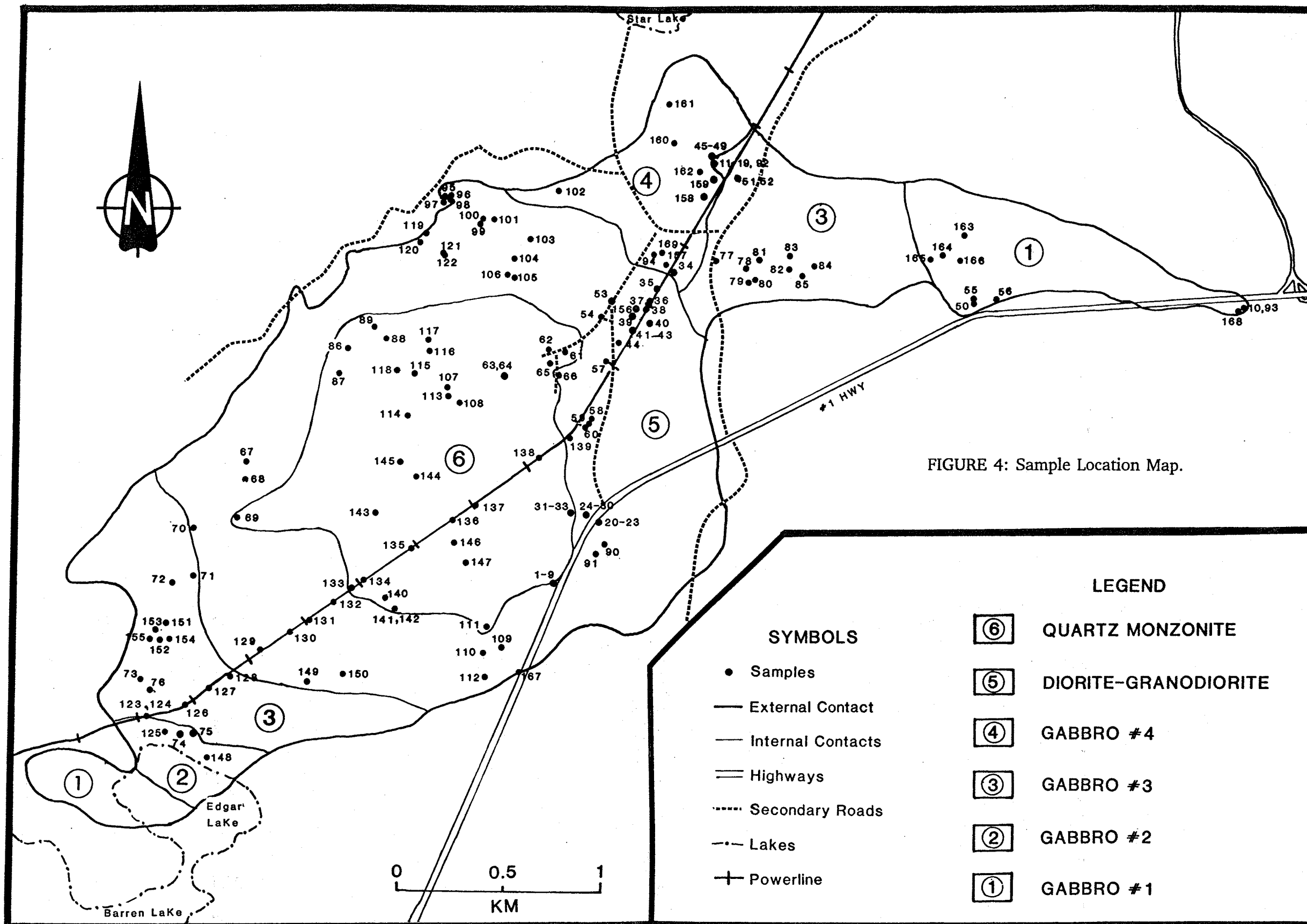


FIGURE 4: Sample Location Map.

integral part of the complex and future geochemical analyses of this and other internal structures, such as the mafic clots, would greatly contribute to an overall understanding of the evolution of the complex.

## **3.2 LABORATORY**

### **3.2.1 Major and Trace Elements**

Whole rock major and trace element analyses were obtained for 126 samples of FLIC rocks with the following distribution per intrusive phase: 9 Gabbro #1 analyses, 4 Gabbro #2 analyses, 23 Gabbro #3 analyses, 11 Gabbro #4 analyses, 51 diorite-granodiorite analyses, 25 quartz monzonite analyses, 2 analyses of mafic clots and 1 analysis of a mafic magnetite-rich layer (Appendix 1).

Major element analyses, including  $\text{SiO}_2$ ,  $\text{TiO}_2$ ,  $\text{Al}_2\text{O}_3$ ,  $\text{Fe}_2\text{O}_3$ ,  $\text{FeO}$ ,  $\text{MnO}$ ,  $\text{CaO}$ ,  $\text{Na}_2\text{O}$ ,  $\text{K}_2\text{O}$  and  $\text{P}_2\text{O}_5$ , were done primarily by X-ray fluorescence on fused glass discs. Glass discs were run on an ARL 8420 XRF spectrometer at the Department of Geological Sciences, University of Manitoba. The reader is referred to Appendix 1 for an account of sample preparation. Some of the gabbro analyses, indicated with an \* in Appendix 1, were done by directly coupled plasma emission spectroscopy (DCP) at Bondar-Clegg.  $\text{FeO}$  was determined volumetrically by the method practised by at the University of Manitoba which is modified after Donaldson (1982).

Trace element analyses, including Y, Zr, Nb, Rb and Sr were all done by X-ray fluorescence on pressed powder pellets. Pellets were run at the University of Manitoba (ARL 8420 XRF spectrometer as above). Appendix 1 lists detection limits.

### **3.2.2 Rare Earth Elements**

Thirteen samples of gabbroic to quartz monzonitic FLIC rocks were selected for REE analyses including La, Ce, Nd, Sm, Eu, Tb, Ho, Tm, Yb and Lu as well as the trace elements Th and Sc (Appendix 2). Analyses were done by Instrumental Neutron Activation Analysis (INAA) at Becquerel Laboratories Inc.. Appendix 2 lists detection limits.

### 3.2.3 Microprobe Analyses

Mineral chemistry data was obtained by electron microprobe analysis of 20 polished thin sections comprising the six principle intrusive units of the FLIC. The data set includes 235 microprobe analyses of seven different mineral phases as follows: 128 plagioclase analyses, 27 K-feldspar analyses, 30 oxide analyses (magnetite and ilmenite), 13 pyroxene analyses, 20 amphibole analyses and 17 biotite analyses (Appendix 3). All probe work was done at the Department of Geological Sciences, University of Manitoba on a MAC-5 electron microprobe. Microprobe methodology is given in Appendix 3 and a detailed discussion of the analytical accuracy and precision of this machine are given in Trembath (1986).

### 3.2.4 Petrography

Thin sections were made of most samples to allow for the coordination of geochemical data with observed mineralogy and petrographic features as well as to provide a check on possible alteration effects within any given sample.

A suite of representative rock slabs comprising all phases of the FLIC were stained with sodium cobaltinitrate to discriminate between plagioclase and K-feldspar. Modal analyses were done on each of the rock slabs under binocular microscope. Results are tabulated and discussed in Chapter 4.

The detailed petrographic descriptions of each phase found in Chapter 4 were obtained from a selected suite of thin sections and supplemented by stained rock slabs, microprobe analyses and field observations.

## CHAPTER 4

### GEOLOGY OF THE FALCON LAKE INTRUSIVE COMPLEX

#### 4.1 GENERAL FEATURES

The FLIC is a concentrically zoned, composite intrusion covering an area of approximately 9 km<sup>2</sup>. It is roughly elliptical in shape with slight sigmoidal distortions at the southwest and northeast ends of the body. The complex is 6.3 km along its NE-SW axis and 2 km across its NW-SE axis. The long axis is concordant with regional structural trends. However, the FLIC is locally discordant cutting across tectonic foliation in the host greenstone belt rocks as well as across the major anticlinal fold axis. Intrusion of the complex is interpreted to have occurred after deformation and regional metamorphism (Mandziuk et al, 1989; Gibbins, 1971).

Rock types comprising the FLIC range from gabbroic to quartz-monzonitic. Mandziuk (1989) defined six individual intrusive units; four outer gabbroic units, a dioritic to granodioritic unit and an inner quartz monzonitic core. These are subdivisions which will be used in proceeding sections of the thesis. Figure 5 shows the distribution of the various lithologies. Mandziuk (1989) defined the relative ages of the lithologies based on contact relationships, dykes of one unit cutting another unit and the presence of various cognate xenoliths. According to his interpretation, the units comprising the FLIC from oldest to youngest are as follows: Gabbro #1, Gabbro #2, Gabbro #3, Gabbro #4, diorite-granodiorite and quartz monzonite. The preceding terminology is that used by the author for this study and corresponds to intrusions A through F respectively in the terminology

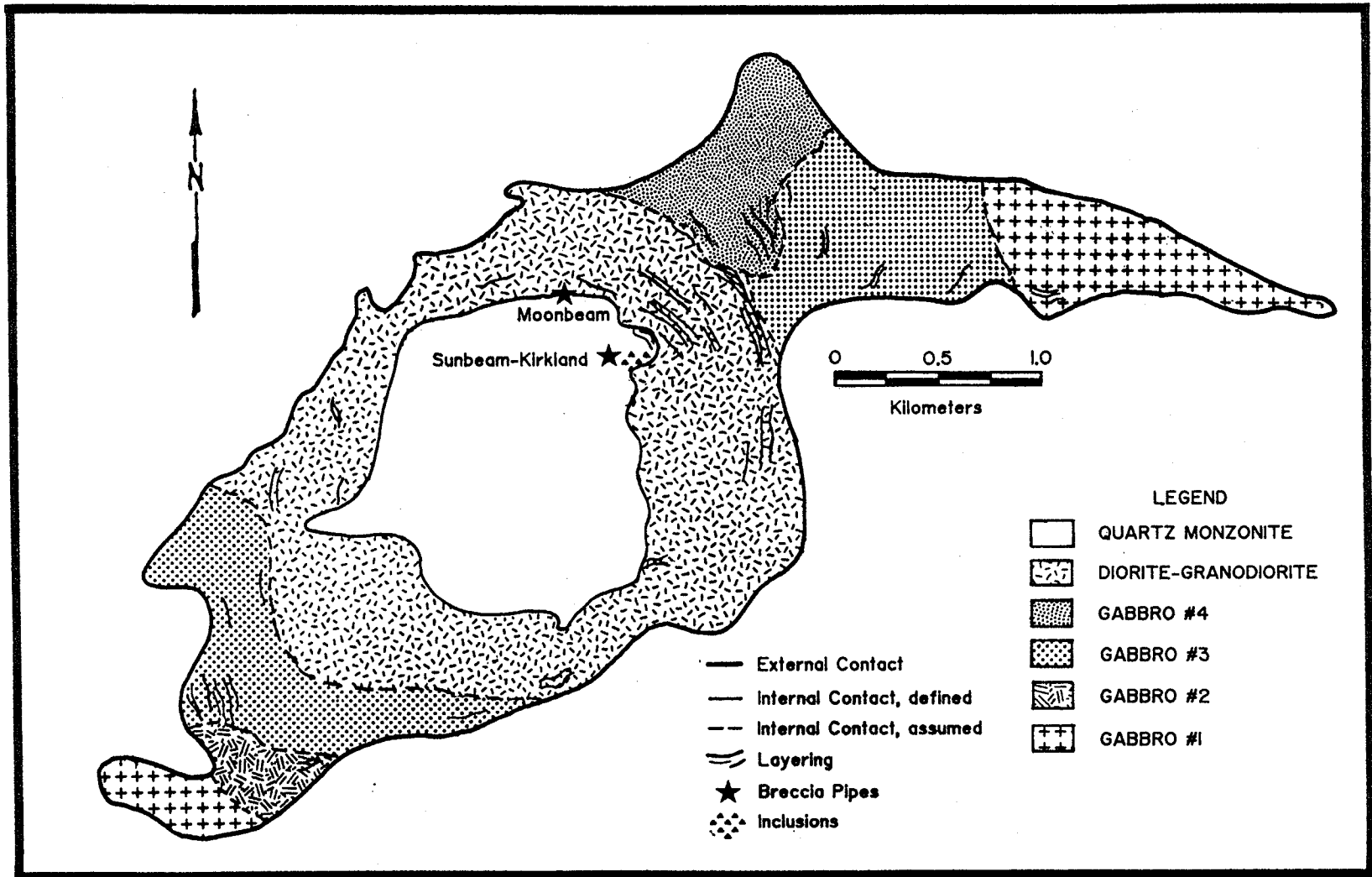


FIGURE 5: General Geology of the Falcon Lake Intrusive Complex. Modified after Mandziuk (1988).

used by Mandziuk (1989). The reader is referred to section 4.10 for a more detailed account of rock nomenclature.

#### 4.1.1 External Contacts

The FLIC is in sharp, disconformable intrusive contact with mafic metavolcanic rocks along its northeastern, southern and western margins. It is in contact with metasedimentary rocks along part of its northwestern and northern boundaries as well as an isolated part of its southern boundary.

The external contact is poorly exposed being covered by glacial drift and overburden or occurring in swampy areas. However, detailed mapping as well as observation of the contact (where exposed) indicates that it is highly irregular at outcrop scale. At some localities, dykes and apophyses of the FLIC intrude the adjacent country rocks cutting across bedding and foliation (Beaubien, 1988). Along the northeast extension of the body, contact relationships are quite complex with Gabbro #1 interfingered with mafic metavolcanic host rocks. Gabbro #2, north of Edgar Lake, is locally in sheared contact with mafic metavolcanic host rocks and displays a well-developed foliation (Az 282-290°) defined by alignment of amphibole.

The nature of the external contact is variable. In many cases, Gabbro #4 and dioritic rocks retain their coarse grain size right up to the contact with host rocks suggesting that the temperature gradient between the complex and surrounding rocks was not large. Gibbins (1967) documents a steep outward-dipping contact between diorite of the complex and mafic metavolcanic rocks which is "knife-edge sharp and shows no chill or baking effects on either side." In the same area, Beaubien (1988) noted numerous dykes intruded into the host

rocks, some of which contained angular mafic xenoliths, suggesting that the country rocks were cool enough to exhibit brittle behavior.

One chilled margin was observed in the northeast part of the complex where Gabbro #1 is in contact with mafic metavolcanic rocks. Gabbro #1 at this locality is only 80m wide and the country rocks here were probably substantially cooler than those bordering the central part of the complex due to the smaller volume of intruding magma and thus lower heat flow.

A unique contact relationship was documented by Beaubien (1988) between a diorite apophysis and host metavolcanic rocks along the northwest margin of the FLIC. A transition zone occurs between the two rock types and is comprised of metavolcanic fragments enclosed in a diorite matrix. The transition zone rocks may represent an intrusion breccia suggesting that the country rocks underwent brittle deformation (Beaubien, 1988).

#### **4.1.2 Internal Structures**

Numerous internal structures including mineral orientation structures, layering, unconformity and trough structures, as well as mineral segregations such as mafic clots are present. Mandziuk (1989) provides detailed descriptions and discussion of these features. Several general statements are made below as summarized from Mandziuk (1989), Mandziuk et al (1989) and the author's own observations, with specific examples of internal structures given in sections 4.3 - 4.9.

Mineral orientation structures include planar laminations, mineral lineations and lineate laminations. Laminations and lineations are defined primarily by the

orientations of feldspar crystals. The following comments are extracted from Mandziuk et al (1989):

"The orientation of planar laminations, mineral lineations, and lineate laminations is generally steep and parallels intrusive contacts and spatially associated layering. The alignments are taken as evidence of laminar flow in a crystal-liquid mixture where orientation of flow laminae is influenced by intrusive contacts."

Layering was observed in all phases , but is best developed in the gabbroic rocks, particularly in Gabbro #3 and Gabbro #4. Types of layering include rhythmic modal layering, graded layering and disrupted or semi-continuous layering. Grading is usually defined by compositional variations but rare examples of grain size grading were also observed. Trough and buttress structures are present locally. The general pattern of layering is illustrated in Figure 5 and is seen to be approximately parallel to internal and/or external contacts. Layering attitudes vary from sub-horizontal to sub-vertical or vertical with the latter being more prevalent. Severe constraints are put on the possible mechanisms producing layering in the FLIC given these predominantly vertical orientations and the fact that the complex is thought to be in its original intrusive position.

#### **4.1.3 Inclusions**

Inclusions are found in all phases of the FLIC and include xenoliths of metavolcanic and metasedimentary country rocks as well as cognate inclusions. Gabbro #3 and Gabbro #4 also contain mafic clots, lenses and irregular bodies which may represent disrupted layers or resistite. Mandziuk et al (1989) indicate that xenoliths and cognate inclusions appear to be concentrated near internal contacts and external contacts.

Inclusions range from rounded to angular in shape and may be submicroscopic to a meter or more in diameter. The largest inclusion observed was a 5x15 meter block of layered granodiorite in quartz monzonite. Contacts of inclusions may be sharp to diffuse with reaction rims being rare. The quartz monzonite phase appears to contain the greatest number and variety of inclusions and a particularly well-exposed concentration of xenoliths and cognate inclusions is observed along the northwest contact of this phase in what Mandziuk (1989) refers to as an embayment structure (Figure 5).

#### 4.1.4 Dykes

Previous workers referred to dykes as being uncommon in and around the FLIC. However, detailed mapping by Mandziuk (1989) and observations made by the author suggest that this is not the case. Mandziuk (1989) identified dykes of younger units cutting older units and used the various cross-cutting relationships to help define relative ages. Documented dyke types include gabbro, diorite, quartz monzonite, pegmatite and aplite. In addition, a porphyritic mafic "lamprophyre" dyke and hornblende-phyric intermediate composition dykes can be seen cutting across Gabbro #3 in the northern and southwestern parts of the complex respectively. Late mafic dykes are also present at the Moonbeam breccia pipe (Fingler, 1991).

#### 4.1.5 Breccia Pipes

The two main breccia pipes identified in the FLIC are the Sunbeam-Kirkland and Moonbeam pipes occurring in quartz monzonite and granodiorite respectively (Figure 5).

Sulphide mineralization and, locally, gold mineralization are associated with the breccia pipes particularly at the Sunbeam- Kirkland pipe. Here the breccia pipe is comprised of both massive and brecciated quartz monzonite. Brecciated rock (Plate 1a) consists of quartz monzonite fragments in quartz-sericite matrix (Halwas, 1984). A distinctive concentric fracture pattern is observed in the peripheral part of the pipe (Plate 1b). Sulphide minerals present include pyrite, pyrrhotite, arsenopyrite, sphalerite, galena, tennantite and chalcopyrite (Davies, 1954). Fractures and faults which displace the ore body are locally silicified and have gold concentrated along them. The reader is referred to Fingler (1991), Springer (1952) and Davies (1954) for more detailed information.

Halwas (1984) did a study on the Sunbeam-Kirkland pipe and mapped out in detail the fracture pattern associated with it. He suggested that pipe formed as the result of two events of fluid intrusion and implosion. Gibbins (1971) attributed the formation of the breccia pipes to a resurgent boiling event. The brecciation and fracture patterns indicate a violent process of origin which included rapid decompression of the surrounding quartz monzonite.

#### 4.1.6 Faults/Shear Zones

According to Gibbins (1967) there are no major regional scale faults in the immediate vicinity of the FLIC, but steeply dipping shear zones occur near the external and internal contacts of the complex. Locally, gold mineralization is associated with these shear zones (eg. Waverly showing). At the Sunbeam-Kirkland deposit the ore body is displaced by various faults, the largest of which dips  $38^{\circ}$  east and offsets the ore body by about 31 meters (Davies 1954). Both Davies



PLATE 1: Sunbeam Kirkland-Breccia Pipe

a) Quartz monzonite breccia within the Sunbeam Kirkland breccia pipe. Breccia is comprised of quartz monzonite fragments (f) in a fine grained, grey, quartz and sericite-rich groundmass (m). Lens cap for scale (52 mm in width).

b) Fracture pattern developed in quartz monzonite at the Sunbeam Kirkland breccia pipe. Note the close spacing and relatively uniform nature of the fractures. Sledge is approximately 40cm long.

(1954) and Gibbins (1967) suggest that the shear zones in around the FLIC are the result of late structural adjustments related to the intrusion of the complex.

## **4.2 CONTACT METAMORPHISM**

Observations by previous workers with respect to contact metamorphism are ambiguous. Davies et al (1962) indicated that samples of meta-andesite from 15 cm, 8 meters and 16 meters from the FLIC contact were petrographically the same as other "greenstones" in the area. Gibbins (1967) stated that "there is a tendency for the adjacent greenstones to have a more hornfelsic texture and traces of light blue quartz near the stock."

More recently, Beaubien (1988) did a study on the possible contact metamorphic effects using three specific study areas encompassing metavolcanic and metasedimentary rocks adjacent to diorite and Gabbro #4 rocks. He identified various subtle features in the country rocks indicative of static post-kinematic mineral growth such as asterisms and decussate textures. Decussate biotite and muscovite were observed by Beaubien (1988) to cross-cut the regional foliation. The mineral assemblages present suggest a hornblende hornfels facies grade of contact metamorphism with the temperature of the host rocks being between 425° and 600° C (Beaubien, 1988). Mandziuk et al (1989) also document contact metamorphism stating that the FLIC "... has upgraded the country-rock metamorphic level to amphibolite grade in a thermal contact aureole 0.5 to 1 km wide."

## **4.3 GABBRO #1**

### **4.3.1 Field Observations**

Gabbro #1 outcrops as part of the northeast and southwest extensions of the complex where it is in sharp, locally interfingered, contact with mafic metavolcanic host rocks. Internal contacts between this unit and Gabbro #3 and #2 were not observed in the field due to lack of outcrop.

Structures within Gabbro #1 include mafic clots, stringers and veins, plagioclase-rich clots, coarser grained gabbroic pods, a weak steeply dipping planar igneous lamination (Mandziuk et al, 1989) and flow textures. Layering was observed at only one exposure where modally graded layers and laminae comprise a 25 meter wide trough-like structure (Mandziuk et al, 1989).

Mafic mineral content varies from outcrop to outcrop with melanogabbroic to pyroxenitic zones present locally.

#### 4.3.2 Texture

Textures vary from equigranular to porphyritic (Plate 2). Where porphyritic, Gabbro #1 contains either plagioclase phenocrysts (up to 10.0 mm) or mafic megacrysts (up to 4.0 mm). Grain size varies from coarse to fine, but on average this phase is medium grained.

#### 4.3.3 Petrography

Gabbro #1 is comprised of 55-70% plagioclase (0.5-10.0 mm), 15-35% amphibole (<0.1-4.0 mm), 5% biotite (<0.1-1.0 mm), 5-7% K-feldspar, 0-5% quartz (<0.1-1.0 mm) and trace amounts of very fine grained sericite, epidote, clinozoisite, ilmenite, apatite and zircon.

Plagioclase occurs as subhedral to euhedral lath-shaped to blocky grains displaying albite twinning and ranging in composition from  $An_{31.2}$  to  $An_{47.7}$ .



PLATE 2: Porphyritic Gabbro #1 with 15% 3-7 mm blocky plagioclase phenocrysts. Phenocrysts are highlighted with arrows. Lens cap for scale (52 mm in width).

Commonly, plagioclase has undergone weak partial alteration to one or more of albite, sericite, carbonate or epidote.

Amphiboles present include fine grained fibrous uralite pseudomorphous after pyroxene and anhedral to subhedral grains of hornblende which may display either distinct amphibole cleavage or relict pyroxene cleavage. The hornblende commonly exhibits partial alteration to biotite ± fibrous uralite. Biotite occurs as anhedral grains intergrown with uralite after pyroxene, as tiny inclusions in the larger hornblende grains and, more rarely, as 1.0 mm large individual grains.

Quartz occurs as anhedral grains interstitial to both plagioclase and mafic minerals as well as in myrmekitic intergrowths with plagioclase. Myrmekite may be found as discrete interstitial patches and as lobate growths developed at plagioclase grain margins. Microcline also occupies interstitial positions to the main framework components.

Sericite, carbonate and epidote occur primarily as alteration products of plagioclase. Epidote and clinozoisite are also found as subhedral to euhedral grains associated with the mafic minerals. Apatite is an ubiquitous accessory phase found in close proximity to biotite and amphibole, but also locally occurs as inclusions in plagioclase.

#### **4.4 GABBRO #2**

##### **4.4.1 Field Observations**

Gabbro #2 has a restricted area of exposure, outcropping only in the southwest end of the complex along the north shore of Edgar Lake. Contacts between the adjacent Gabbro #1 and Gabbro #3 phases are not exposed.

Structures found within Gabbro #2 include a steeply dipping planar igneous lamination (Mandziuk, 1988), concentrations of mafic minerals in the form of clots, lenses and stringers and pyroxenitic fragments 2 x 4 cm to 8 x 8 cm in size.

Gabbro #2 is compositionally inhomogeneous on an outcrop scale ranging from melanogabbroic to pyroxenitic (Plate 3).

#### 4.4.2 Texture

Both equigranular and inequigranular porphyritic textures are observed in melanogabbroic portions of this unit. Equigranular rocks and the groundmass to porphyritic rocks typically have a fine to medium grain size. Pyroxenitic rocks exhibit cumulus textures comprised of coarse grained cumulus pyroxene crystals and/or pyroxene pseudomorphs with minor cumulus plagioclase and intercumulus pyroxene, plagioclase, oxide minerals, apatite and spinel (Mandziuk, 1989). A fine to medium grain size is typical of the equigranular rocks and of the groundmass in porphyritic rocks.

#### 4.4.3 Petrography

Gabbro #2 is comprised predominantly of variable amounts of mafic minerals (0.2-6.0 mm) and plagioclase (0.2-10.0 mm) with minor amounts (<1% each) of fine grained quartz, microcline, apatite, sericite, epidote, magnetite and locally disseminated sulphides. Mafic mineral content varies from 50-80% and plagioclase from 20-50%.

Mafic minerals present include amphibole ± biotite largely as pseudomorphs after pyroxene. Amphibole may be found as single grains of actinolite displaying polysynthetic twinning and as pyroxene pseudomorphs comprised of fine grained hornblende and actinolite fringed by a bright bluish-green amphibole or by biotite.

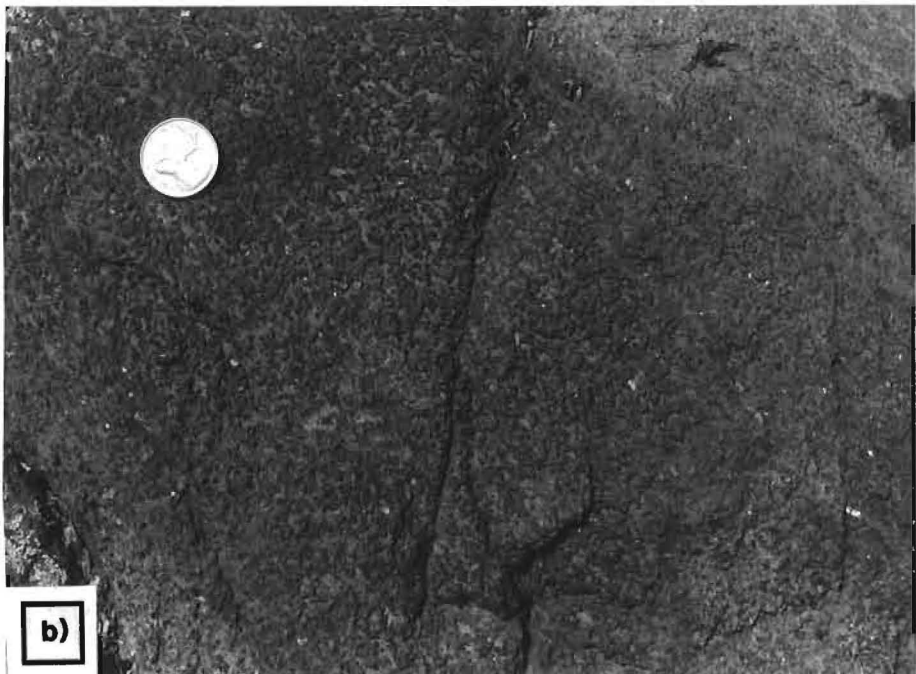
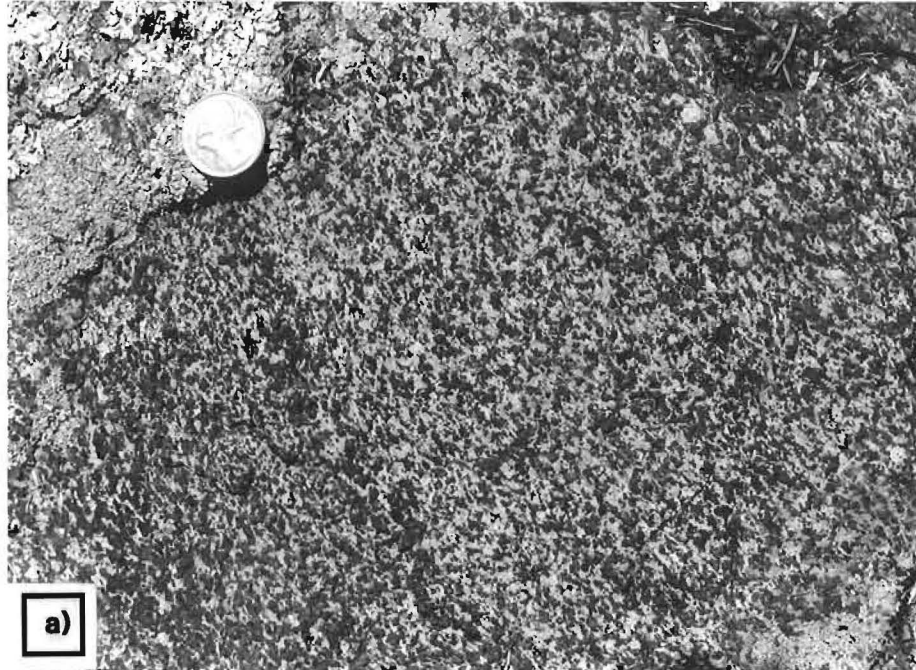


PLATE 3: Gabbro #2

a) Equigranular Gabbro #2 comprised of approximately subequal amounts of mafic minerals (black, high relief) and plagioclase (white, low relief). Quarter for scale.

b) Pyroxene-rich Gabbro #2. Quarter for scale.

Microprobe analyses of two anhedral to subhedral amphibole grains (samples 74-5 and 74-6, Appendix 3e) yielded Ca-rich actinolitic compositions. Sample 74-5 has the textural characteristics of primary amphibole, whereas sample 74-6 may represent amphibole pseudomorphous after pyroxene. Mafic minerals locally contain inclusions of apatite, quartz and opaque minerals.

Plagioclase occurs as subhedral to euhedral, lath-like to blocky grains displaying albite, carlsbad or pericline twinning and ranges in composition from  $An_{59.5}$  to  $An_{66.6}$ . Plagioclase is commonly albitized and some grains have myrmekitic margins where they are in contact with alkali feldspar.

Interstitial minerals include quartz and microcline with quartz also occurring as blebs in plagioclase or within myrmekitic intergrowths. Apatite is an accessory phase found in association with the mafic minerals whereas epidote and sericite are mainly alteration products of plagioclase.

## **4.5 GABBRO #3**

### **4.5.1 Field Observations**

Gabbro #3 outcrops in both the southwest and northeast parts of the complex and has the largest aerial exposure of the four gabbroic units. Contacts between this unit and adjacent host rocks as well as adjacent internal units are poorly exposed. One outcrop in the southwest part of the complex displays a sharp contact between Gabbro #3 and diorite-granodiorite.

Structures observed include, mafic clots, leuco-gabbro blocks, rhythmic modal layering and graded layering as well as angular unconformity and buttress structures. In addition, unlayered rocks display a weak planar lamination whereas layered rocks display well-developed planar and lineate laminations (Mandziuk,

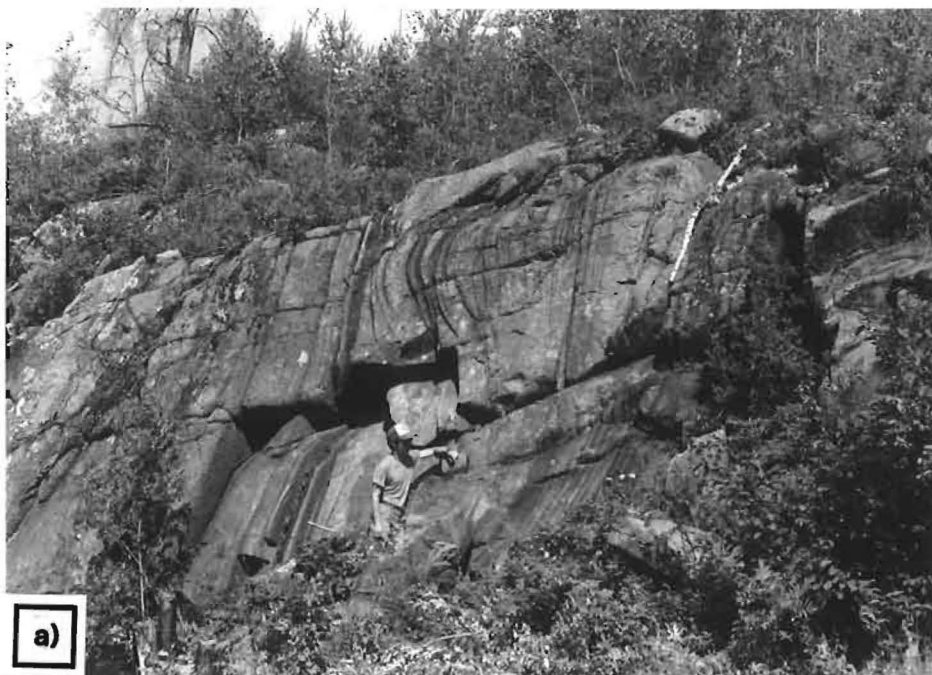
1989). Most of these features (Plate 4) are well-exposed on a ridge bordering the western side of a large beaver pond to the north of Edgar Lake which corresponds to the "southwest detailed study-area" of Mandziuk (1989). Vertical rhythmic layering consisting of alternating ultramafic and anorthositic layers is exposed on a vertical cliff face in this area . On one outcrop, a series of rhythmic layers comprised of alternating 3 mm - 7 cm wide mafic to ultramafic layers and 8-35 cm wide plagioclase-rich layers can be seen. Some of the plagioclase-rich layers display both compositional and grain size grading. In this same general area, several angular unconformities are present with earlier layered rocks cross-cut by younger layered rocks. Blocks of leucogabbro occur locally within rhythmically layered Gabbro #3 and in places disrupt the layers.

The majority of this unit is gabbroic, but localized zones of anorthositic to pyroxenitic gabbro are also present (Mandziuk, 1989).

#### 4.5.2 Texture

Massive Gabbro #3 is inequigranular consisting of a framework of coarse grained plagioclase with interstitial irregularly shaped clots or aggregates of medium to coarse grained mafic minerals. Rocks of this unit could be termed orthocumulates and mesocumulates with plagioclase representing the cumulus phase and the mafic minerals comprising intercumulus material (Plate 5). The coarser grain size and cumulus nature of this unit help to distinguish it from Gabbro #1 and Gabbro #2.

#### 4.5.3 Petrography



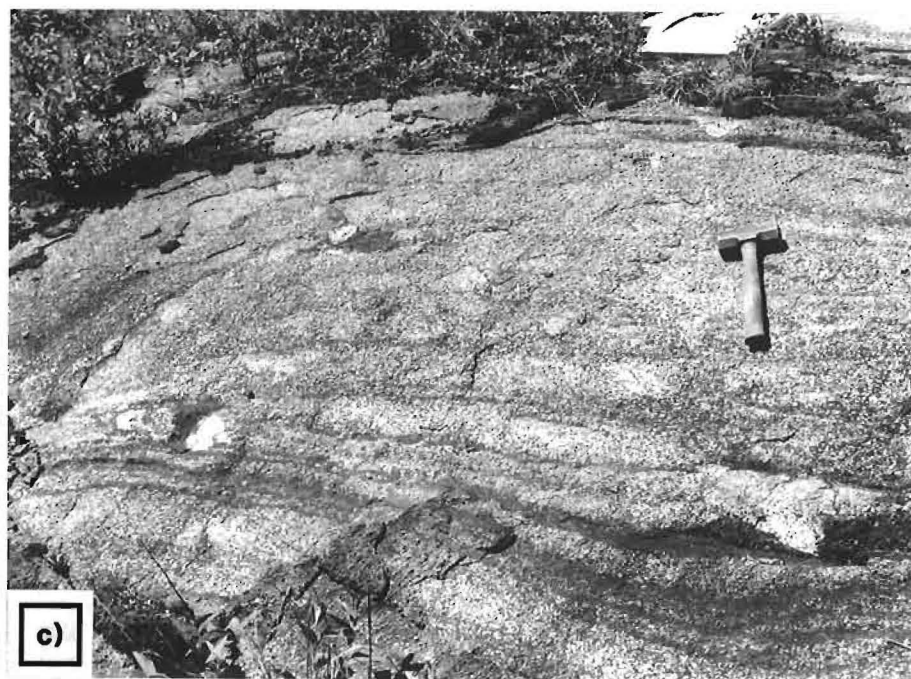


PLATE 4: Gabbro #3

a) Rhythmic modal layering in predominantly vertical orientations. Note the presence of a large trough structure visible in the center of the photo.

b) Pronounced angular unconformity with layered series in the upper right hand of the photo cutting across the older layered series in the remainder of the photo.

c) Inhomogeneous outcrop of rhythmically and modally graded Gabbro #3. Note the irregularly distributed blocks of leuco-gabbro locally disrupting layering.



PLATE 5: Gabbro #3 displaying orthocumulus texture defined by a framework of coarse grained plagioclase crystals with irregular interstitial clots of mafic minerals.

Gabbro #3 is comprised of 55-75% plagioclase (1.0-15.0 mm), 20-35% mafic minerals (0.2-7.0 mm), 1-5% quartz (0.4-5.0 mm), 1-3% apatite (0.1-1.0 mm), 1-3% microcline (1.0-10.0 mm) ± trace amounts of opaque minerals ( $\leq 2.0$ mm), allanite ( $\leq 2.0$  mm), epidote ( $<0.6$  mm) and carbonate ( $<0.6$  mm).

Plagioclase occurs as euhedral to subhedral blocky to rectangular grains displaying albite twinning and, more rarely, zoning or carlsbad twinning. Compositions range from  $An_{32.3}$  to  $An_{49.1}$ . Rare grains of plagioclase display evidence of adcumulus growth. Much of the plagioclase is albitized and minor alteration to sericite ± carbonate minerals ± epidote is ubiquitous. Strained or deformed plagioclase is also common with some deformed crystals containing irregular blebs of quartz. Myrmekitic rims partially to completely surrounding plagioclase grains are quite common, particularly where adjacent to grains of perthite or alkali feldspar.

Mafic minerals include amphibole, biotite and pyroxene, generally with amphibole having the highest abundance. The mafic minerals may occur as single discrete grains but more often form clumps or aggregates of grains (Plate 6). The pyroxene is identified by relict cores, twinning and cleavage planes. Three microprobe analyses of relict cores (samples 18-10, 73-3A and 85-5, Appendix 3d) gave augite compositions. The pyroxene is partially to totally pseudomorphed by either fine grained actinolite, locally with bright green hornblende rims, or by hornblende ± biotite. Amphibole partially pseudomorphed by biotite, but displaying amphibole cleavage and twinning appears to be of primary origin. Biotite may also occur as relatively fresh-looking discrete grains.

Quartz occurs predominantly as an interstitial mineral to plagioclase and the mafic minerals. Microcline occurs as relatively large interstitial grains locally

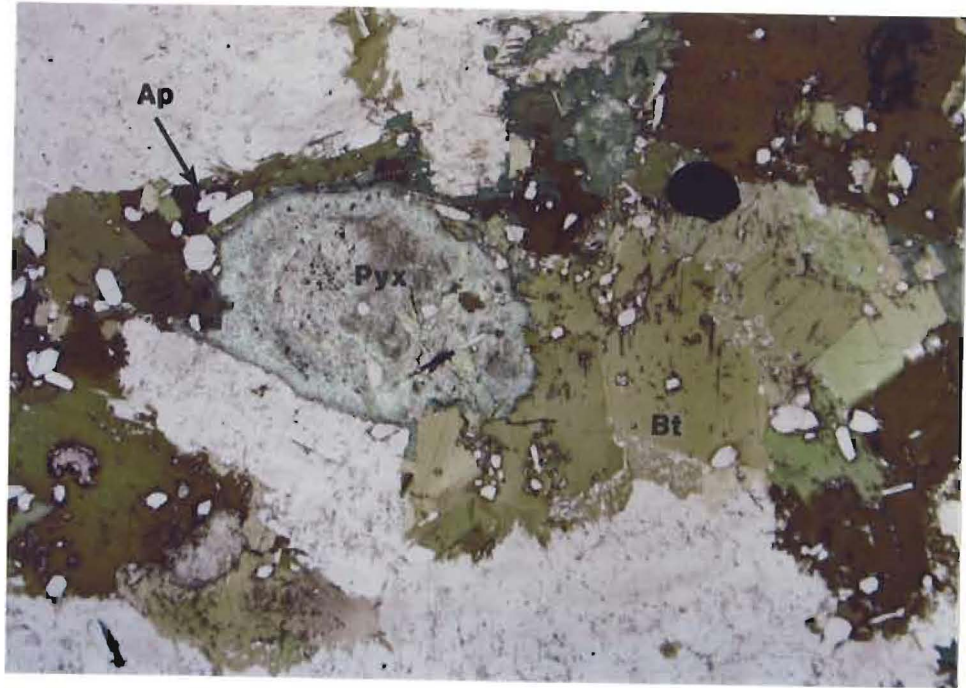


PLATE 6: Photomicrograph of Gabbro #3 showing the typical occurrence of mafic minerals in clots or aggregates of grains. Mafic minerals present include amphibole (A), biotite (Bt) and pyroxene (Pyx). Note the abundance of coarse grained brown to greenish brown biotite as well as the subhedral green-colored grain in the center of the picture which appears to be amphibole surrounding a relict pyroxene core. Numerous euhedral inclusions of apatite (Ap) are largely confined to the clots of mafic minerals. (Black dot in upper right hand side of photo is an ink spot). Plane Transmitted Light.

enclosing corroded grains of plagioclase which have reaction rims or myrmekitic margins (Plate 7). Apatite, allanite and the opaque minerals are generally found as accessory phases associated with the mafic minerals. Both apatite and allanite commonly form euhedral to subhedral crystals. Opaque minerals present include magnetite and ilmenite with ilmenite occurring as exsolutions in magnetite. Epidote and carbonate occur as alteration products of plagioclase with subhedral to euhedral epidote also observed within the mafic mineral clumps.

Both myrmekitic and perthitic intergrowths are found within Gabbro #3. The myrmekite, which may comprise as much as 1-2% of the rock, forms rims on plagioclase and occurs as patches interstitial to large feldspar grains. Perthite is observed as anhedral grains interstitial to feldspar and rarely contains tiny inclusions of plagioclase similar to those enclosed in microcline.

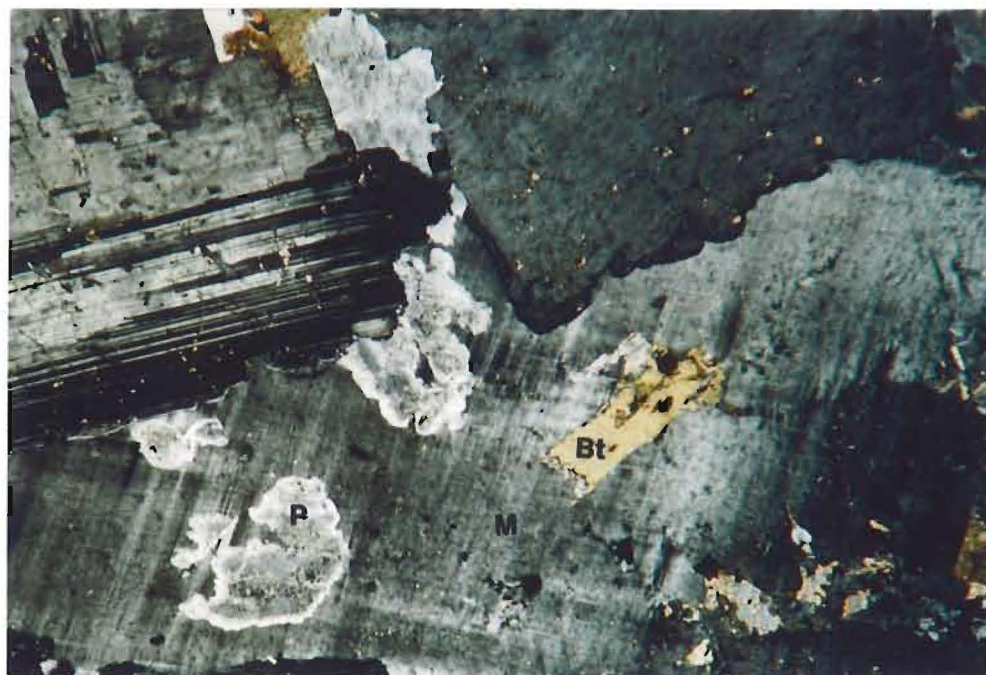
Higher percentages of plagioclase and apatite further distinguish Gabbro #3 from Gabbro #1 and #2.

## **4.6 GABBRO #4**

### **4.6.1 Field Observations**

Gabbro #4 outcrops in the northern portion of the complex immediately south of Star Lake where it is in contact with metasedimentary host rocks. Where exposed, the external contact is sharp, irregular and, locally, sheared. One outcrop displays a sharp, unchilled contact between Gabbro #4 and the diorite-granodiorite unit.

In the field, the inhomogeneous nature of Gabbro #4 helps to distinguish it from the other gabbro units. Mafic clots, stringers and irregular bodies as well as cognate gabbroic inclusions are found throughout Gabbro #4, particularly in or



0            0.5            1.0  
|-----|-----|  
millimeters

PLATE 7: Photomicrograph of Gabbro #3. Lower half of photo contains a large grain of microcline (M) enclosing corroded grains of plagioclase (P) and containing an inclusion of biotite (Bt). Note the reaction rims around the plagioclase grains. Crossed Polars.

near layered areas (see Plate 8). Layering is quite complex comprising rhythmic modal and graded layers and with layer compositions ranging from anorthositic to pyroxenitic. A steeply dipping planar igneous lamination exists in both layered and unlayered rocks (Mandziuk, 1989).

#### 4.6.2 Texture

Massive Gabbro #4 has a medium to very coarse grained cumulus texture comprised predominantly of subhedral to euhedral lath-shaped to blocky cumulus plagioclase and irregular intercumulus aggregates of mafic minerals (Plate 9).

#### 4.6.3 Petrography

Gabbro #4 consists of 60% plagioclase (0.5-10.0 mm), 15-17% amphibole (2.0-8.0 mm), 15-17% biotite (0.5-6.0 mm), 3-5% apatite (0.1-1.0 mm), 2% opaque minerals ( $\leq 1.0$  mm) and trace amounts of titanite (0.1-0.2 mm) and allanite.

Plagioclase ranges in composition from  $An_{37.3}$  to  $An_{68.4}$  and commonly contains inclusions of biotite and amphibole. The amphibole present is a greenish hornblende occurring as elongate to anhedral grains with bright green to blue rims and containing numerous apatite inclusions and minor opaque minerals. Anhedral grains of biotite commonly contain inclusions of apatite, opaque minerals and titanite. The predominant opaque mineral is magnetite, typically rimmed by titanite and, in places, containing irregular ilmenite exsolutions. Allanite occurs as anhedral to euhedral grains associated with the mafic minerals.

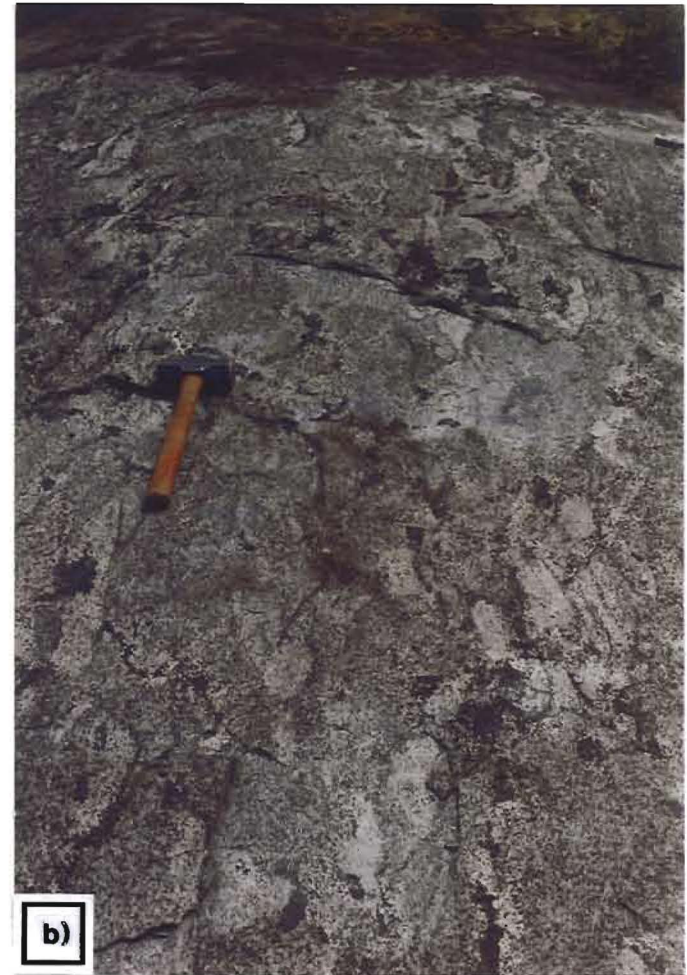
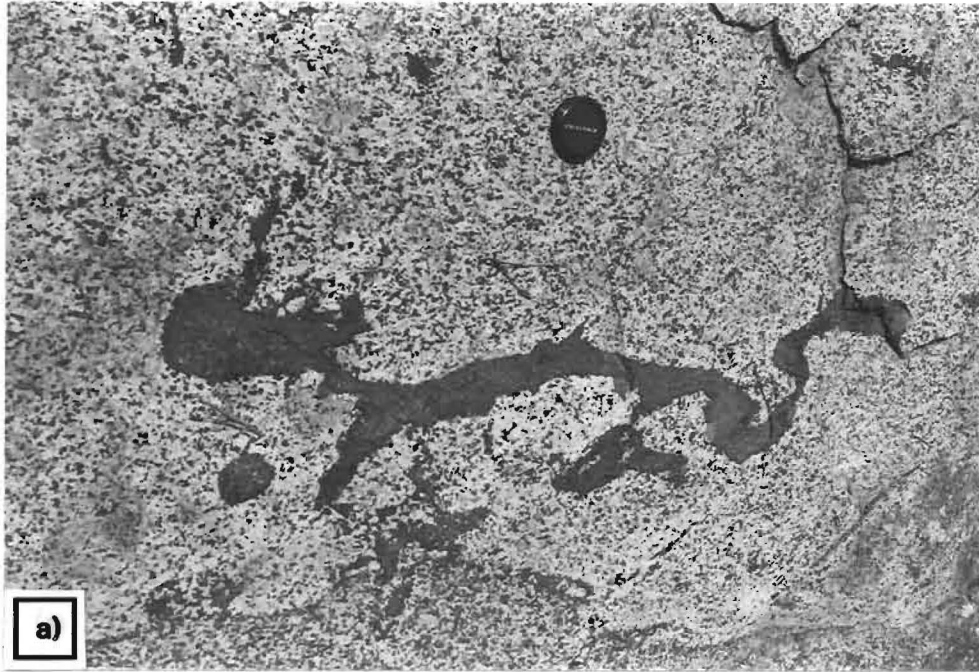


PLATE 8: Gabbro #4

a) Mafic mineral clots and an irregularly shaped 75 cm x 2-7 cm mafic body, possibly representing a disrupted layer.

b) Extremely inhomogeneous outcrop of Gabbro #4 containing numerous cognate gabbroic inclusions.



PLATE 9: Orthocumulate to mesocumulate Gabbro #4 comprised of coarse grained subhedral to euhedral lath-shaped plagioclase grains (white) and irregular intercumulus aggregates of mafic minerals (black).

#### 4.7 DEFORMATION IN GABBROIC UNITS

Microscopic evidence of deformation is present in all of the gabbroic units, particularly Gabbro #4. The following is a list of some of the features observed:

1. Fractured plagioclase including rotated individual fragments of a larger grain.
2. Bent grains.
3. Presence of mechanical twinning in plagioclase.
4. Presence of polygonal plagioclase.
5. Presence of granulated finer grained components including mafic minerals and quartz.

#### 4.8 DIORITE-GRANODIORITE

##### 4.8.1 Field Observations

Diorite-granodiorite is the most abundant of all the FLIC units and forms a roughly circular ring around the inner quartz monzonite core. It is bounded to the west and east by both metavolcanic and metasedimentary host rocks. At one locality, a steep, outwardly dipping contact between diorite and host mafic metavolcanic rocks exists with no evidence of chilling (Gibbins, 1967). Locally, however, the dioritic rocks appear to be finer grained immediately adjacent to the contact. Internal contacts with quartz monzonite are also sharp, irregular and lack evidence of chilling.

Layering is present within this unit but is not as extensively developed as in the gabbroic units. Layering is steeply dipping and includes both modally graded layers and unimodal mafic laminae (Mandziuk, 1989).

#### 4.8.2 General Statement

Various compositional and textural variations are observed across this unit with the outer portions comprised of dioritic to quartz dioritic rocks which grade into granodioritic rocks toward the core of the complex. Plate 10 shows some of the macroscopic textures seen in the field. Plagioclase compositions range from  $An_{25.7}$  to  $An_{49.4}$  in the unit. Although compositions are quite variable, even within a single sample, the diorites on average are observed to have higher An contents.

Due to the variability of this unit, a single petrographic description would not be meaningful. Instead, generalized descriptions of the diorites and granodiorites are given below.

#### 4.8.3 Diorites - Texture and Petrography

Diorites and quartz diorites are typically coarse grained and display an overall coreward transition from cumulus to inequigranular seriate to porphyritic textures.

The dioritic rocks are comprised of 50-70% plagioclase (1.0-15.0 mm), 25-35% mafic minerals (1.0-7.0 mm), 3-10% K-feldspar (up to 5.0 mm), trace to 10% quartz ( $\leq 2.0$  mm), 1-2% apatite ( $\leq 1.0$  mm), 1-2% opaque minerals ( $\leq 2.0$  mm) and trace allanite and titanite.

Plagioclase may occur as either a major framework component or as phenocrysts. Grains are euhedral to subhedral, lath-like to equant in shape, display albite twinning and locally have partial myrmekitic rims where adjacent to K-feldspar. Locally, plagioclase grains contain inclusions of biotite and amphibole.

The mafic minerals, which tend to occur in clumps or aggregates of grains, include amphibole, biotite and pyroxene. Amphiboles present include anhedral



PLATE 10: a) Diorite displaying inequigranular seriate texture. Note the occurrence of mafic minerals in irregular aggregates or clots.  
b) Granodiorite displaying porphyritic texture. Feldspar phenocrysts are highlighted by the black arrows.

hornblende grains, hornblende to actinolite rims around relict pyroxene cores (see samples 41-3 and 41-10, Appendix 3e) and, more rarely, patches of fine grained actinolite rimmed by hornblende  $\pm$  biotite (possibly pseudomorphous after pyroxene). Microprobe analyses of two pyroxene cores (samples 41-2 and 41-9, Appendix 3d) give augite compositions. Locally, these relict pyroxene grains appear to be partially resorbed displaying cusped outer margins. Biotite occurs as 1.0-7.0 mm equant to elongate grains (in some cases secondary after hornblende) containing inclusions of apatite and opaque minerals. Partial alteration to titanite is common.

K-feldspar is typically microcline or perthitic microcline which occurs as subhedral to anhedral grains interstitial to plagioclase. Locally, microcline contains oriented inclusions of plagioclase with myrmekitic rims. Quartz occurs as an anhedral interstitial mineral. Apatite is a ubiquitous accessory phase found near or within mafic mineral grains. The main opaque mineral present is magnetite which is commonly rimmed by titanite and locally contains intergrowths of ilmenite.

Effects of deformation can be recognized by the following features: multiple twinning of a mechanical type in plagioclase, serrated grain boundaries, preliminary development of polygonal plagioclase and slight granulation (particularly of quartz and mafic minerals). In general, the deformation observed in the diorites is not as great as that seen in the gabbros.

#### **4.8.4 Granodiorites - Texture and Petrography**

Most granodioritic rocks have a distinctly porphyritic texture containing 5-15% plagioclase + K-feldspar phenocrysts > 5.0 mm in size. Inequigranular seriate textures subtly transitional to porphyritic textures are observed locally. The

groundmass component in these rocks is commonly medium grained.

Granodiorites are comprised of 45-65% plagioclase (1.0-15.0 mm), 10-25% mafic minerals (1.0-6.0 mm), 15-25% K-feldspar (0.5-5.0 mm), 2-10% quartz (0.5-3.0 mm), 1-2% opaque minerals ( $\leq 2.0$  mm), trace to 1% apatite ( $< 1.0$  mm) and trace amounts of allanite, titanite, ( $\leq 2.0$  mm), epidote, carbonate and sericite (all  $\leq 0.5$  mm).

Plagioclase occurs as 5.0-15.0 mm blocky to rectangular, partially albitized phenocrysts and as 1.0-4.0 mm subhedral to euhedral equant albitized groundmass grains. Partial alteration to variable amounts of epidote and carbonate is common. Myrmekite is found as partial rims on plagioclase, as lobate patches extending outward from plagioclase margins into microcline and as discrete patches adjacent to quartz and microcline.

Hornblende, biotite and minor relict pyroxene comprise the mafic minerals which occur as both aggregates of grains and as single grains. Hornblende occurs as anhedral to subhedral grains commonly altered to biotite. Biotite is found as 1.0-4.0 mm equant to elongate grains and as fine grained flakes fringing larger mafic mineral grains. Both hornblende and biotite commonly contain inclusions of apatite and opaque minerals. Pyroxene grains typically have actinolite or hornblende rims (see samples 24-8 to 58-10B, Appendix 3e). Five out of seven pyroxene cores analyzed by microprobe have augite compositions whereas the other two contain slightly more Ca.

K-feldspar is present as microcline, perthitic microcline or perthite locally enclosing corroded, oriented inclusions of plagioclase or forming distinct rims around plagioclase. In some cases the plagioclase inclusions are non-oriented and display diffuse margins (Plate 11). These inclusions may represent relict primary

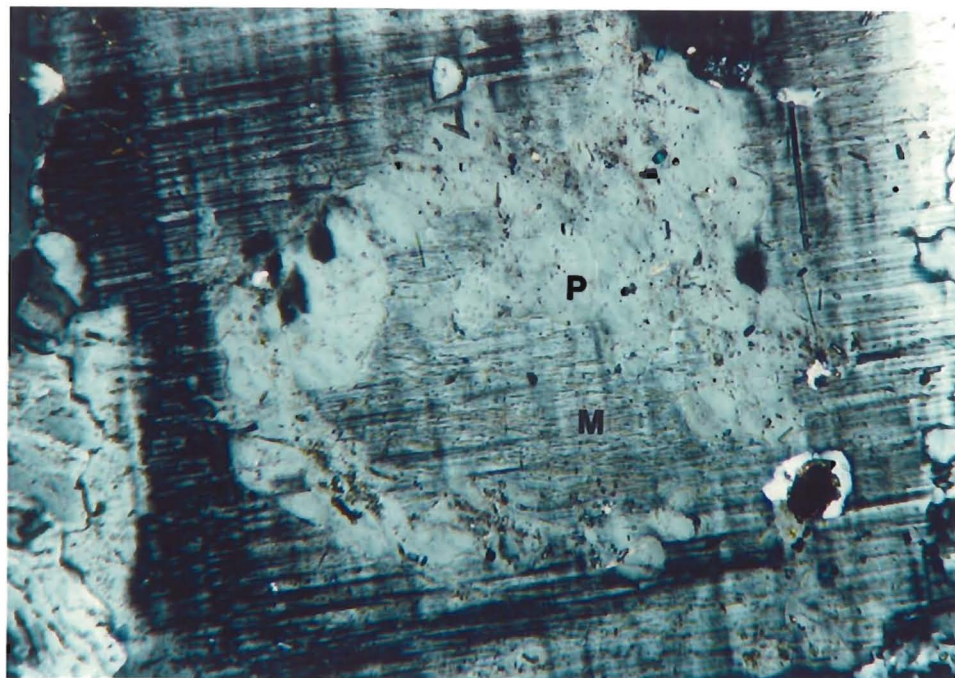
plagioclase now largely replaced by K-feldspar. K-feldspar also forms distinct rims around both groundmass and phenocryst plagioclase. Quartz is commonly anhedral and interstitial to the feldspar and mafic minerals.

The occurrence of apatite and the opaque minerals is similar to that described for the dioritic rocks with apatite also occurring as inclusions in feldspar. Opaque minerals include magnetite and minor ilmenite (see samples 21-10A to 68-7, Appendix 3c). Euhedral to subhedral allanite grains, locally exhibiting clearly defined zoning, are found in close proximity to mafic minerals. Rare euhedral grains of titanite, zircon and possible monazite were identified in isolated samples.

Deformation appears to be minimal in the samples examined. Some granulation of the finer grained components is observed with quartz regularly occurring as mosaic grains.

#### 4.8.5 Large-scale Variations

One of the most notable petrographic variations across this unit is the transition from cumulus to inequigranular seriate (and locally porphyritic) textures in the diorites to a more distinct porphyritic texture in the granodiorites. Accompanying this transition is a change in the occurrence of mafic minerals in the rocks. In the diorites, mafic minerals tend to congregate in aggregates of grains whereas in the granodiorites they tend to occur as single grains. Major changes coreward in mineralogy across this unit include decreases in the abundance of mafic minerals and apatite and increases in the abundance of K-feldspar as well as REE-bearing phases such as allanite and titanite.



0 0.25  
millimeters

PLATE 11: Photomicrograph of Granodiorite. Photomicrograph shows part of a microcline grain (M) containing a highly corroded inclusion?/core? of plagioclase (P). Note the diffuse margins and irregular shape of the plagioclase. Crossed polars.

## **4.9 QUARTZ MONZONITE**

### **4.9.1 Field Observations**

Quartz monzonite forms the core of the complex. The contact between quartz monzonite and diorite-granodiorite is the best exposed and most well-defined of all the internal contacts. The contact is sharp and rarely displays the effects of chilling. The quartz monzonite is locally layered and finer grained against the contact (Plate 12).

Structures found within this unit include a steeply plunging mineral lineation (Mandziuk, 1989) and discontinuous layering. The mineral lineation is defined by an alignment of feldspar phenocrysts whereas layering is defined by thin discontinuous, bifurcating unimodal mafic laminae (Plate 13).

Xenoliths and cognate inclusions are common in this unit and types include metavolcanic and metasedimentary host rocks as well internally derived dioritic and granodioritic rocks.

### **4.9.2 Texture**

Rocks of this unit are fine to medium grained with porphyritic to seriate textures (Plate 14). Porphyritic rocks contain both plagioclase and K-feldspar phenocrysts in a seriate groundmass. The finer grain size and a marked decrease in the abundance of mafic minerals readily distinguish quartz monzonite from granodiorite in the field.

### **4.9.3 Petrography**

Quartz monzonite is comprised of 40-60% plagioclase (0.5-15.0 mm), 20-25% K-feldspar (0.5-15.0 mm), 5-15% mafic minerals (up to 5.0 mm), 15-25%

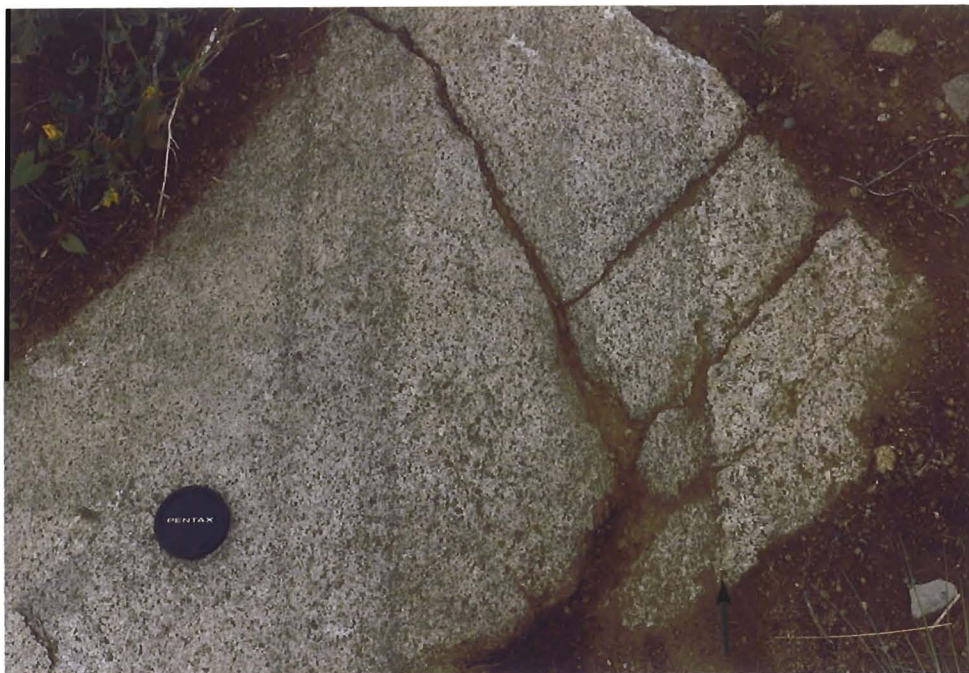


PLATE 12: Sharp intrusive contact between granodiorite (right) and finer grained quartz monzonite (left). Chilling is absent along the contact. Note that layering is developed in the quartz monzonite adjacent to the contact.

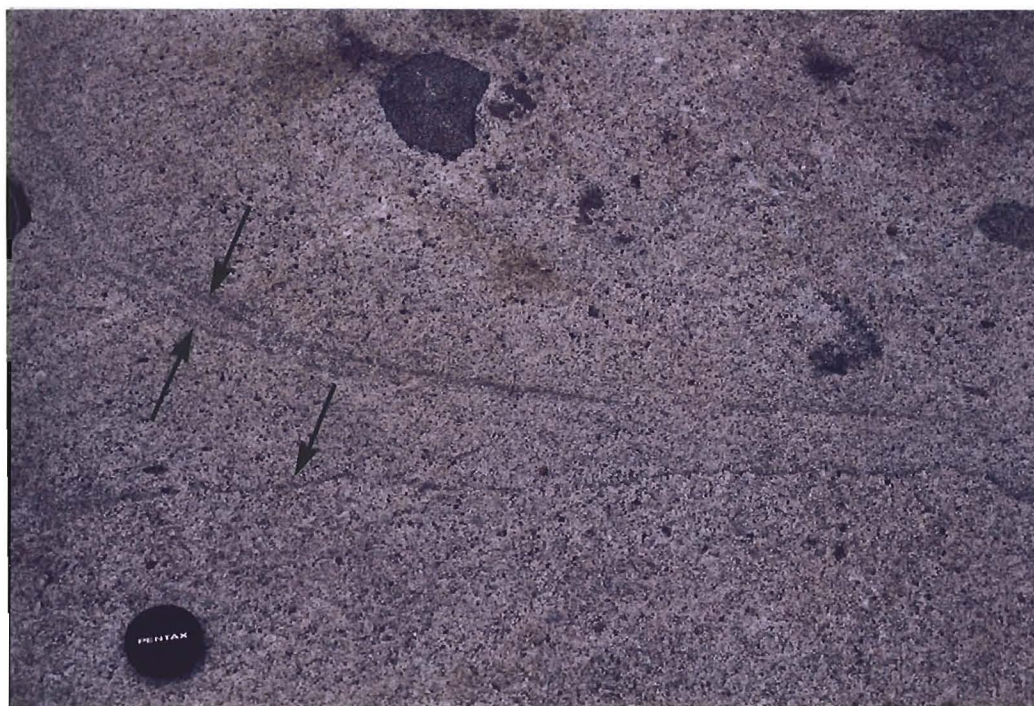


PLATE 13: Quartz monzonite containing discontinuous, wispy, bifurcating mafic laminae as indicated by the arrows.



PLATE 14: Fine grained porphyritic quartz monzonite.

quartz (up to 3.0 mm) and minor ( $\leq 2\%$ ) to trace amounts of epidote, magnetite, allanite, apatite, titanite, carbonate and sericite.

Plagioclase occurs as euhedral equant to rectangular grains displaying zoning, carlsbad twinning, albite twinning and, rarely, myrmekitic margins. Zoning is more prevalent in this unit than any of the other units. Anorthite contents range from  $An_{24.9}$  to  $An_{30.3}$ . Partial alteration to variable amounts of sericite, epidote and carbonate is common.

Both microcline and perthite are abundant occurring as coarse grained subhedral to euhedral framework components/phenocrysts or as smaller anhedral interstitial grains. The larger grains often display carlsbad twinning.

Mafic minerals include variable amounts of biotite and hornblende. Biotite is present either as equant to elongate grains or as fine grained flakes evenly distributed throughout the rock. Locally, hornblende appears to be partially altered to biotite.

Quartz is anhedral, locally mosaic and mainly found interstitial to feldspar. Epidote, allanite, titanite and apatite occur as euhedral to subhedral grains in close proximity to, or as inclusions within, the mafic minerals. Euhedral allanite locally exhibits well-developed zoning. Magnetite grains are commonly rimmed by titanite.

Also present within this unit are small (1.0-5.0 mm) inclusions with sharp to diffuse boundaries. They are comprised of very fine grained quartz, biotite and carbonate  $\pm$  epidote and may represent micro-xenoliths of meta-sedimentary host rock.

Quartz monzonite petrographically displays the least deformation of all the FLIC units. Deformation effects seem to be limited to a slight granulation of quartz and biotite and bent large feldspar grains.

#### 4.10 ROCK NOMENCLATURE

In the past, various names have been applied to the felsic to mafic rocks of the FLIC (Table 1). There is a general concensus by most workers in designating rocks comprising the outer, mafic parts of the complex as "gabbros" and "diorites" as well as defining the core rocks as "quartz monzonites". However, intermediate composition rock types of the complex have been variously classified as diorites, monzodiorites, syenodiorites and granodiorites.

For the present study, a selected suite of rock slabs were stained for K-feldspar with sodium cobaltinitrate. Of these, 22 slabs were point counted under binocular microscope to obtain modal mineral proportions to be used in application of Streckheisen's (1976) modal classification system.

**TABLE 1**  
**Nomenclature for rocks of the Falcon Lake Intrusive Complex**

	Brownell (1941)	House (1955)	Gibbins (1967)	Mandziuk et al (1988)
FELSIC ROCKS	Quartz Monzonite	Quartz Monzonite	Quartz Monzonite	Quartz Monzonite
INTERMEDIATE ROCKS	Granodiorite & Syenodiorite	Granodiorite- Syenodiorite	Monzodiorite & Granodiorite	Diorite- Granodiorite
MAFIC ROCKS	Quartz Diorite, Diorite & Gabbro	Diorite, Gabbro	Gabbro & Diorite	Gabbro, Melagabbro & Pyroxenite

Most rock slabs were point counted at a 1 mm spacing with a 2 mm spacing between successive traverses and a total 1500 points counted per slab. For some of the coarser gabbro samples, a spacing of 2 mm was used with 1000 points obtained per slab. Sample PT-56 (Gabbro #1) was quite fine grained and required a .5 mm spacing (1000 points). Components counted included plagioclase, K-feldspar, quartz and mafic minerals  $\pm$  inclusions. Table 2a lists the modal proportions obtained as well as the number of points counted per slab. Table 2b lists the proportions of plagioclase, K-feldspar and quartz normalized to 100% for plotting purposes.

The data are plotted on Streckheisen's (1976) modal QAP classification diagram in Figure 6 with the following results:

1. All quartz monzonitic samples plot in the quartz-poor, plagioclase-rich corner of the granite field.
2. Granodiorite samples plot in the quartz monzodiorite/quartz monzogabbro and quartz monzonite fields.
3. Diorite samples plot in the quartz monzodiorite/quartz monzogabbro and monzodiorite/monzogabbro fields.
4. Gabbro #2, Gabbro #4 and two out of three Gabbro #3 samples plot in the gabbro field.
5. The single Gabbro #1 sample and one of the Gabbro #3 samples plot in the monzodiorite/monzogabbro field.

Terminology obtained for the basic rocks is in fairly good agreement with that of previous workers. However, the present point counting reveals substantial amounts of K-feldspar in the intermediate rocks as well as quartz in the felsic rocks (see Plate 15). As a result, the dioritic to granodioritic rocks plot in a trend



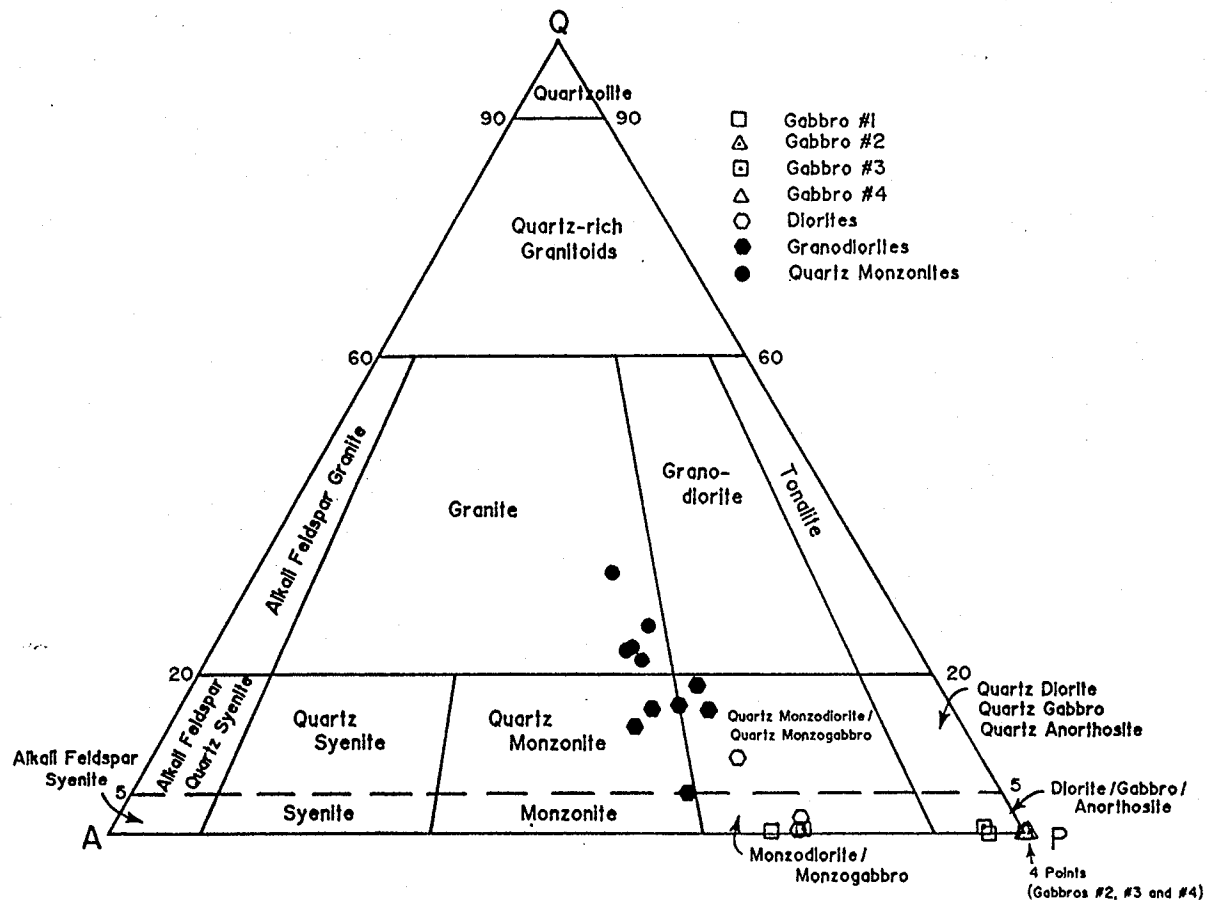
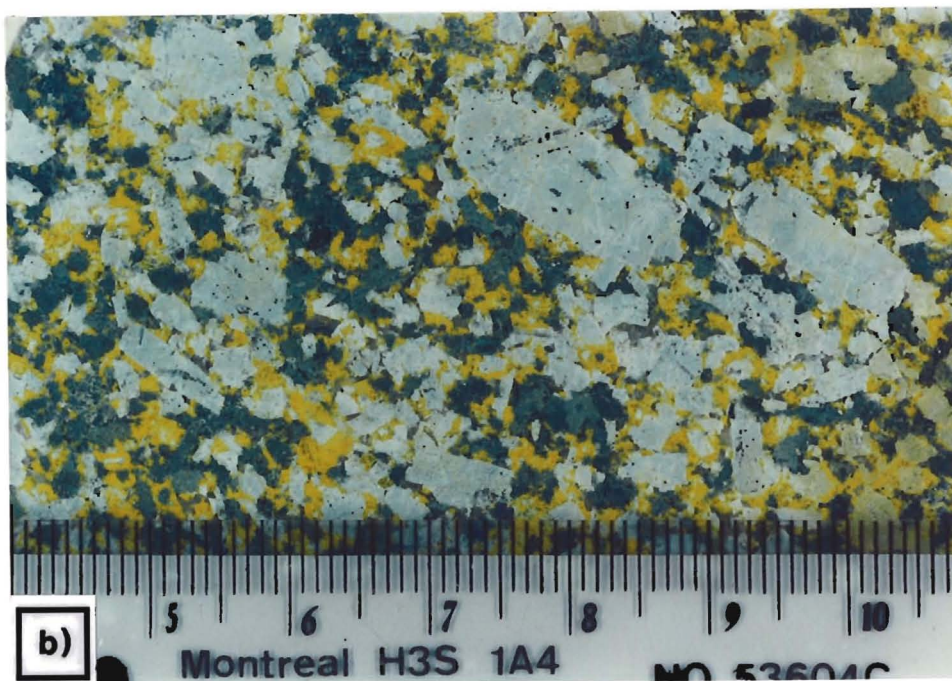
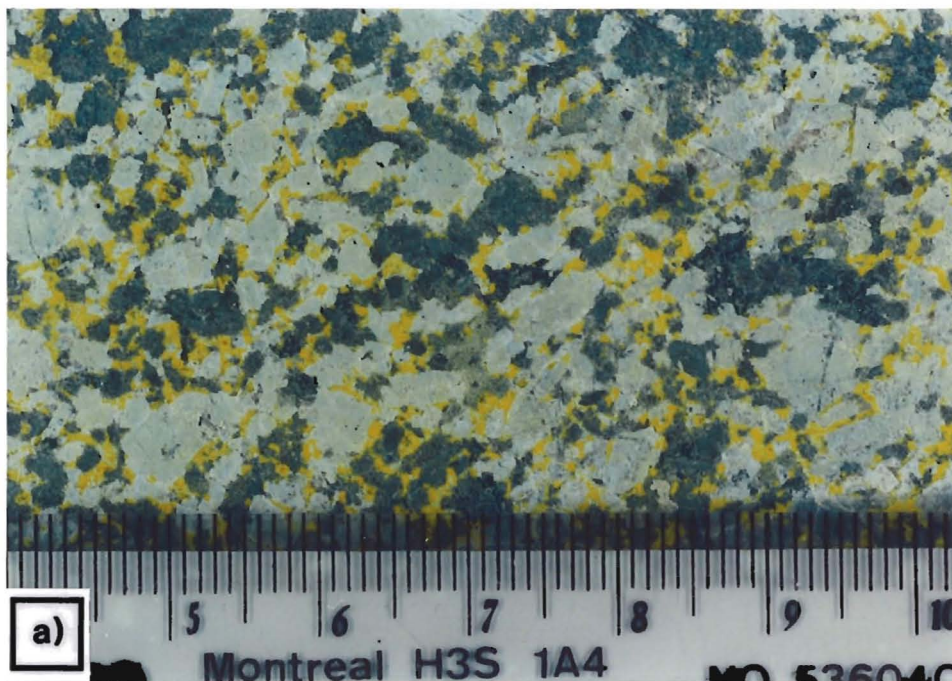


FIGURE 6: Modal QAP plot of point-counted FLIC rock samples listed in Table 2.  
(Plot after Streckheisen, 1976).

from monzodiorites to quartz monzodiorites and quartz monzonites whereas the quartz monzonitic rocks would be more properly classified as "granites".



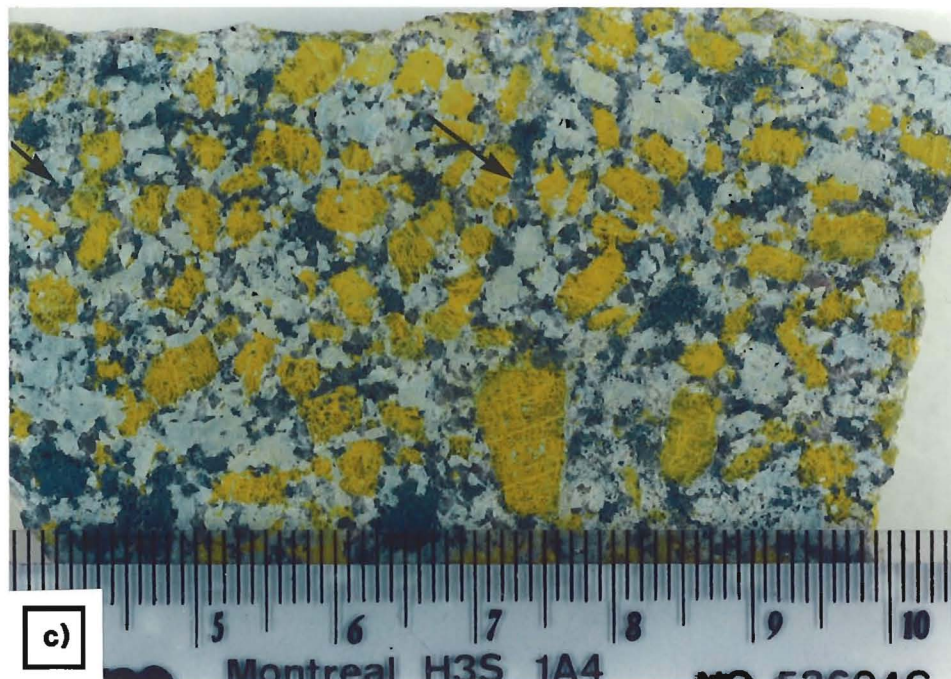


PLATE 15: Stained Rock Slabs

a) Diorite b) Granodiorite c) Quartz Monzonite

Abundant fine grained canary yellow K-feldspar occurs in an interstitial position to plagioclase and mafic minerals in the diorite (a) and granodiorite (b) samples. Fine grained clear groundmass quartz in the quartz monzonite sample (c) is highlighted by arrows. Note the transition from seriate to porphyritic textures in going from the diorite to granodiorites samples as well as the transition from plagioclase phenocrysts in diorite (b) to predominantly K-feldspar phenocrysts in the quartz monzonite (c). Scale shown is in centimeters.

## CHAPTER 5

### WHOLE ROCK GEOCHEMISTRY

Whole-rock major and trace element analyses were obtained on 126 samples from the Falcon Lake Intrusive Complex. These are listed in appendices 1a through 1e. Calculated for each analysis were the following: F/F+M, Rb/Sr and K/Rb ratios; crystal-free liquid densities calculated after the method of Bottinga and Weill (1970) and CIPW normative mineralogy. Table 3 lists representative analyses for the gabbroic rocks and similar representative data is given for the diorite-granodiorite and quartz monzonite rocks in Table 4.

#### 5.1 MAJOR ELEMENT GEOCHEMISTRY

##### 5.1.1 General Characterization

Geochemical classification of plutonic igneous rocks on the basis of whole rock geochemistry is complicated by the fact that these rocks rarely represent primary liquid compositions, particularly in the case of porphyritic and cumulate rocks. The plotting of FLIC rock types on the succeeding diagrams developed for the classification of volcanic rocks is done solely to obtain a broad picture of their chemical affinity.

General geochemical characterization of the FLIC rocks is illustrated by Figures 7, 8 and 9. On these and succeeding diagrams, only 91 of the 126 analyses are plotted (unless otherwise stated). A listing of the samples used for plotting is included in Appendix 1. This reduced data set was chosen to facilitate plotting of only the least altered samples as well as to improve clarity of variation diagrams. The following mineralogically and compositionally "anomalous" samples are included in Appendix 1:

**TABLE 3**  
Representative analyses of gabbros from the Falcon Lake Intrusive Complex.

KEY	PT-56 1	PT-163 1	PT-166 1	PT-168 1	PT-74 2	PT-125 2	PT-17 3
SiO <sub>2</sub>	56.50	51.71	53.39	49.81	48.60	46.27	51.00
TiO <sub>2</sub>	1.15	0.95	1.12	0.77	0.26	0.33	1.20
Al <sub>2</sub> O <sub>3</sub>	16.80	17.87	16.59	17.32	17.30	16.27	19.20
Fe <sub>2</sub> O <sub>3</sub>	3.19	2.75	3.40	2.74	3.18	3.24	3.20
FeO	5.92	7.90	7.01	7.90	6.39	7.44	6.19
MnO	0.13	0.15	0.14	0.15	0.16	0.17	0.13
MgO	3.35	4.94	4.59	6.78	8.87	11.17	3.62
CaO	5.75	9.20	7.23	9.51	13.20	12.66	8.15
Na <sub>2</sub> O	3.52	3.27	3.46	2.88	2.27	1.41	3.82
K <sub>2</sub> O	3.60	0.53	1.99	1.12	0.27	0.21	2.71
LOI	0.35	0.54	0.78	0.70	1.05	1.15	0.65
Total	101.20	100.10	100.21	99.69	101.96	100.33	100.94
Y	29	19	28	12	13	13	22
Zr	317	60	231	62	49	35	247
Nb	19	0	9	0	0	1	11
Rb	140	21	68	32	4	12	99
Sr	521	794	635	714	836	675	1216

KEY	PT-83 3	PT-84 3	PT-45 4	PT-46 4	PT-159 4	PT-162 4
SiO <sub>2</sub>	56.10	55.70	51.50	54.70	54.89	50.23
TiO <sub>2</sub>	0.77	1.02	1.26	1.03	0.85	1.17
Al <sub>2</sub> O <sub>3</sub>	21.20	19.20	17.90	17.10	19.46	20.11
Fe <sub>2</sub> O <sub>3</sub>	1.91	3.79	4.17	4.16	2.17	2.77
FeO	3.63	4.15	5.72	4.25	4.71	5.56
MnO	0.08	0.11	0.14	0.12	0.09	0.09
MgO	1.40	2.32	4.10	2.97	2.45	3.09
CaO	6.78	6.80	8.71	6.68	6.43	8.25
Na <sub>2</sub> O	4.64	3.78	3.50	3.30	3.38	3.72
K <sub>2</sub> O	2.98	3.27	2.48	3.49	3.27	2.54
P <sub>2</sub> O <sub>5</sub>	0.22	0.58	1.24	0.92	0.52	0.86
LOI	0.80	0.30	0.35	0.45	0.60	0.72
Total	100.51	101.02	101.07	99.17	98.82	99.11
Y	15	24	26	24	14	16
Zr	158	284	468	280	211	124
Nb	7	16	16	1	10	11
Rb	82	108	99	104	103	99
Sr	1223	1117	1111	1015	1120	1389

Key: 1=Gabbro #1    2=Gabbro #2    3=Gabbro #3    4=Gabbro #4

TABLE 4

Representative analyses of diorite-granodiorite and quartz monzonite from the Falcon Lake Intrusive Complex.

KEY	PT-38 5	PT-96 5	PT-121 5	PT-130 5	PT-24B 5	PT-43 5	PT-44 5	PT-60 5
SiO <sub>2</sub>	52.03	54.78	56.68	51.80	58.07	57.17	56.32	59.32
TiO <sub>2</sub>	1.23	0.94	0.82	1.01	0.76	0.77	0.76	0.68
Al <sub>2</sub> O <sub>3</sub>	19.28	17.15	16.71	15.99	16.73	17.26	16.39	16.59
Fe <sub>2</sub> O <sub>3</sub>	3.63	2.65	3.27	4.03	3.23	3.20	7.20	2.84
FeO	5.48	6.05	4.52	6.27	3.86	3.67	0.00	3.81
MnO	0.13	0.12	0.10	0.14	0.12	0.11	0.12	0.09
MgO	2.02	3.91	3.68	5.28	3.20	2.85	3.45	2.62
CaO	6.80	6.64	5.25	7.63	5.18	4.79	5.16	4.54
Na <sub>2</sub> O	3.98	3.62	3.89	3.06	3.50	3.70	4.30	3.87
K <sub>2</sub> O	3.39	2.63	4.36	2.76	3.96	4.95	4.34	4.21
P <sub>2</sub> O <sub>5</sub>	0.86	0.51	0.45	0.66	0.37	0.34	0.43	0.27
LOI	0.50	0.80	0.21	0.83	0.78	0.49	0.84	1.12
TOTAL	99.33	99.80	99.94	99.46	99.76	99.30	99.31	99.96
Y	21	19	16	22	20	24	26	21
Zr	217	343	299	243	385	318	428	373
Nb	9	16	23	15	18	20	21	21
Rb	76	109	181	108	155	183	154	176
Sr	1094	920	848	970	869	859	827	758

KEY	PT-66 5	PT-106 5	PT-132 5	PT-61 0	PT-107 0	PT-117 0	PT-137 0	PT-145 0
SiO <sub>2</sub>	62.82	59.23	60.24	65.79	66.51	67.42	67.95	68.46
TiO <sub>2</sub>	0.54	0.73	0.59	0.37	0.24	0.29	0.24	0.23
Al <sub>2</sub> O <sub>3</sub>	16.56	16.37	16.96	16.42	16.37	16.09	15.87	16.08
Fe <sub>2</sub> O <sub>3</sub>	2.61	2.99	2.69	2.15	1.54	1.35	1.75	1.82
FeO	2.84	3.98	3.19	1.88	1.29	1.60	1.29	1.24
MnO	0.07	0.10	0.09	0.09	0.05	0.03	0.05	0.05
MgO	1.93	2.77	2.42	1.35	0.91	0.84	0.96	0.84
CaO	3.93	4.72	4.46	3.01	2.74	2.70	2.62	2.79
Na <sub>2</sub> O	3.73	3.35	3.94	3.92	4.07	4.03	3.59	4.33
K <sub>2</sub> O	4.22	4.33	4.15	4.25	4.59	4.57	4.49	4.44
P <sub>2</sub> O <sub>5</sub>	0.21	0.37	0.28	0.05	0.01	0.02	0.02	0.03
LOI	0.89	0.39	0.41	0.72	0.49	0.68	0.35	0.35
TOTAL	100.35	99.33	99.42	100.00	98.81	99.62	99.18	100.66
Y	19	14	8	13	2	0	2	2
Zr	328	384	309	229	161	156	150	158
Nb	19	21	17	13	6	6	9	11
Rb	173	163	169	158	125	172	165	180
Sr	697	790	793	674	788	708	663	684

KEY: 5=Diorites-Granodiorites 0=Quartz Monzonites

PT-164 - pyroxenitic phase of Gabbro #1

PT-153 - pyroxenitic layer in Gabbro #3

PT-94 - magnetite-rich ultramafic layer in Gabbro #4

PT-157, PT-169A - mafic clots in Gabbro #4.

These five samples are labelled in the geochemical diagrams in which they are plotted but are omitted from discussions of general geochemical trends.

Figure 7 is a  $\text{Na}_2\text{O} + \text{K}_2\text{O}$  vs  $\text{SiO}_2$  diagram with a line shown dividing alkaline and subalkaline affinities. Gabbro #3, Gabbro #4 and diorite-granodiorite samples plot mainly in the alkaline field whereas Gabbro #1, Gabbro #2 and quartz monzonite samples plot mainly in the subalkaline field. Also shown for comparative purposes is a chemical classification system for volcanic rocks. The mafic to felsic FLIC rocks plot in the fields of basalts through hawaiites, mugearites and trachyandesites to rhyolites. The majority of the Gabbro #3, Gabbro #4 and diorite-granodiorite samples lie within the alkaline rock fields of hawaiites, mugearites and trachyandesites. The data set as a whole defines a continuous trend of increasing alkali content with increasing silica content progressing from the mafic to felsic rocks which is consistent with a differentiated series.

$\text{Na}_2\text{O}$  and  $\text{K}_2\text{O}$  contents each range between 1 and 5 wt% for nearly all Gabbro #3, Gabbro #4, diorite-granodiorite and quartz monzonite samples. (Exceptions include the previously mentioned "anomalous" samples). Many of the diorite-granodiorite and quartz monzonite samples are slightly potassic as shown by  $\text{K}_2\text{O}:\text{Na}_2\text{O}$  ratios being commonly greater than 1 (see Figure 8). The alkali contents, particularly  $\text{K}_2\text{O}$ , of Gabbro #3 and #4 are more like those found in alkaline mafic rocks than in their subalkaline equivalents. High  $\text{K}_2\text{O}$  contents in Gabbro #3 are reflected mineralogically by the presence of 1-3% interstitial

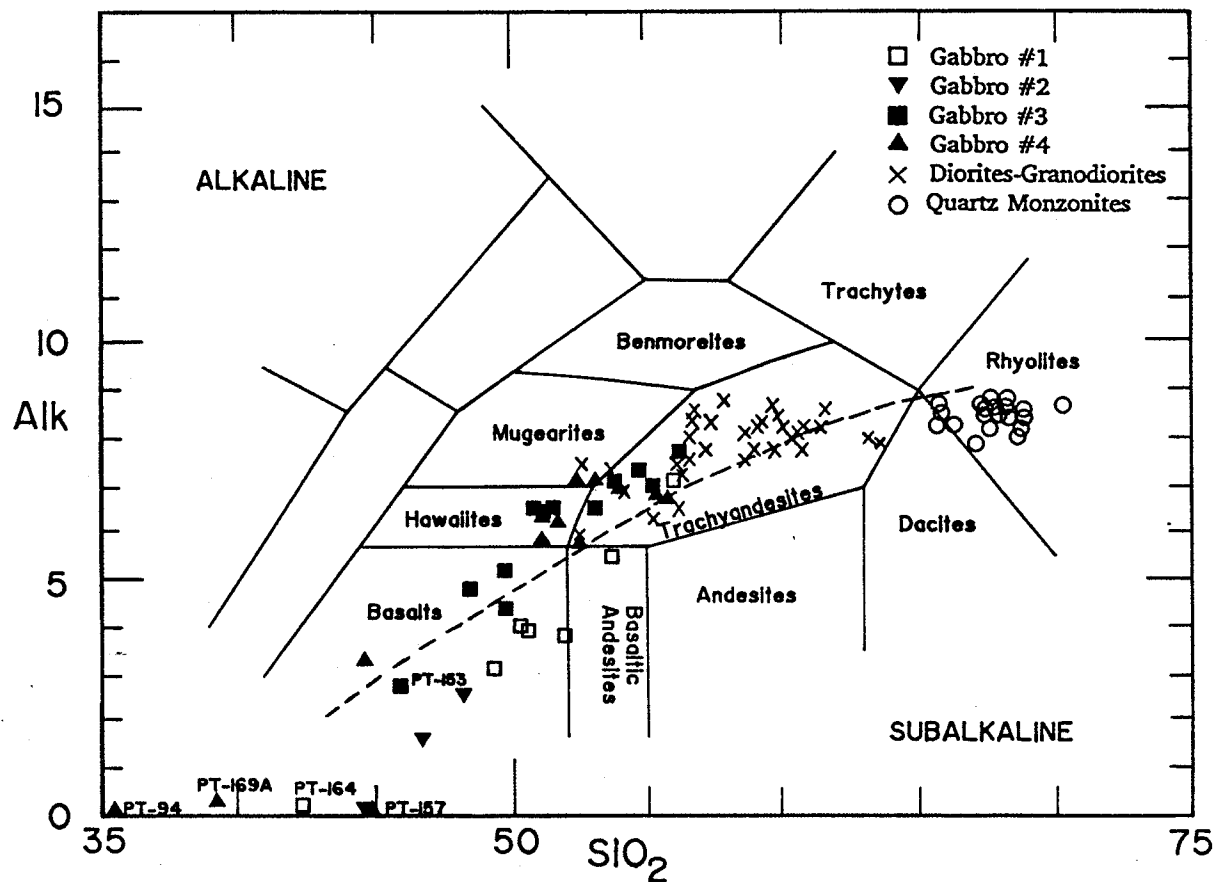


FIGURE 7:  $K_2O + Na_2O$  vs  $SiO_2$  plot for rocks of the Falcon Lake Intrusive Complex. All oxides are in wt %. The line dividing alkaline and subalkaline fields is from Irvine and Baragar (1971). Volcanic rock classification is from Fisher and Schmincke (1984) and Cox et al (1979).

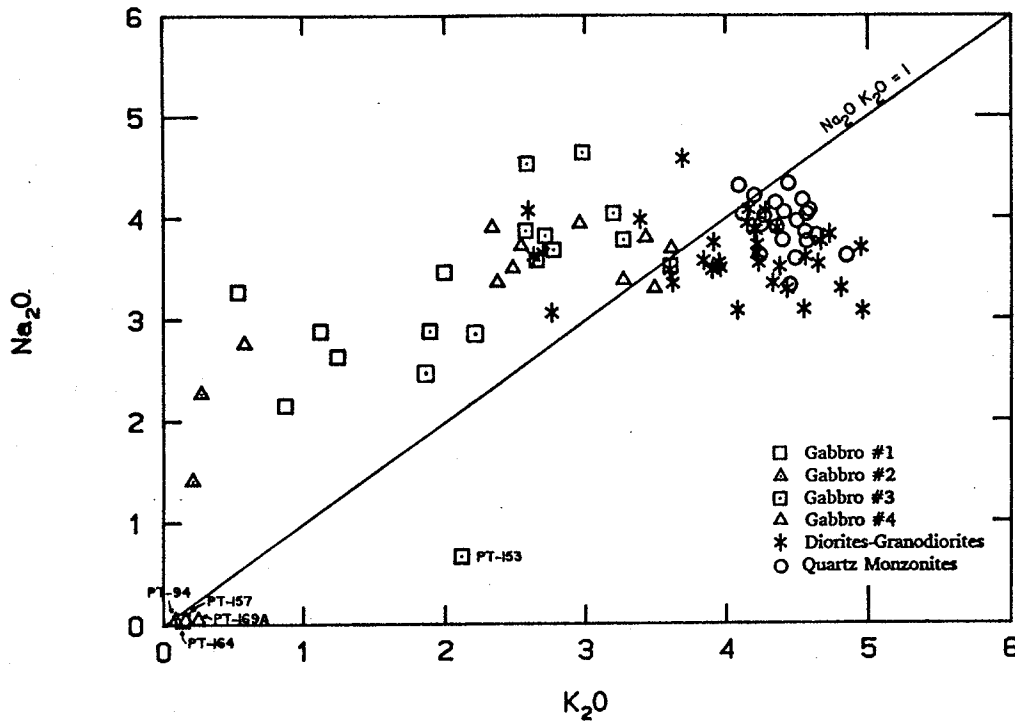


FIGURE 8: Na<sub>2</sub>O vs K<sub>2</sub>O diagram. Oxides in wt %.

microcline as well as primary biotite. Gabbro #4 rocks also contain abundant primary biotite.

The majority of FLIC rocks define a calc-alkaline trend on the AFM diagram (Figure 9). More mafic samples of Gabbro #1 and #4 as well as one sample each of Gabbro #3 and diorite plot in the tholeiitic field.

It is important to note that increases in silica content from mafic to felsic rock types are relatively continuous and, in some cases, overlapping. Plots of previous FLIC analyses (Gibbins, 1971) displayed a distinct silica gap between granodioritic and quartz monzonitic rocks. This gap appears to have been a function of sample distribution rather than a real geochemical feature. A number of the analyses from this study are observed to plot within this gap (Figure 10).

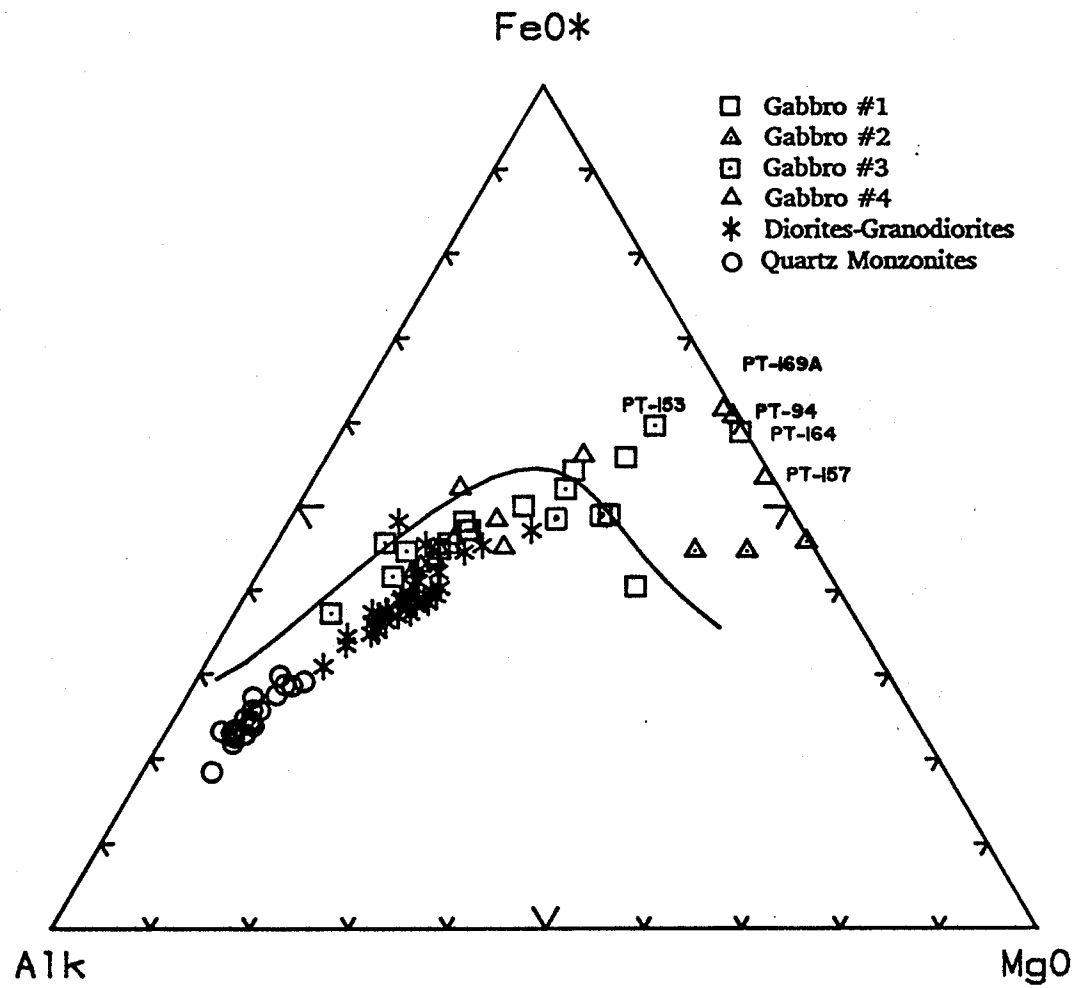


FIGURE 9: AFM diagram with data plotted for the Falcon Lake Intrusive Complex. The dividing line between calc-alkaline and tholeiitic fields is from Irvine and Baragar (1971).

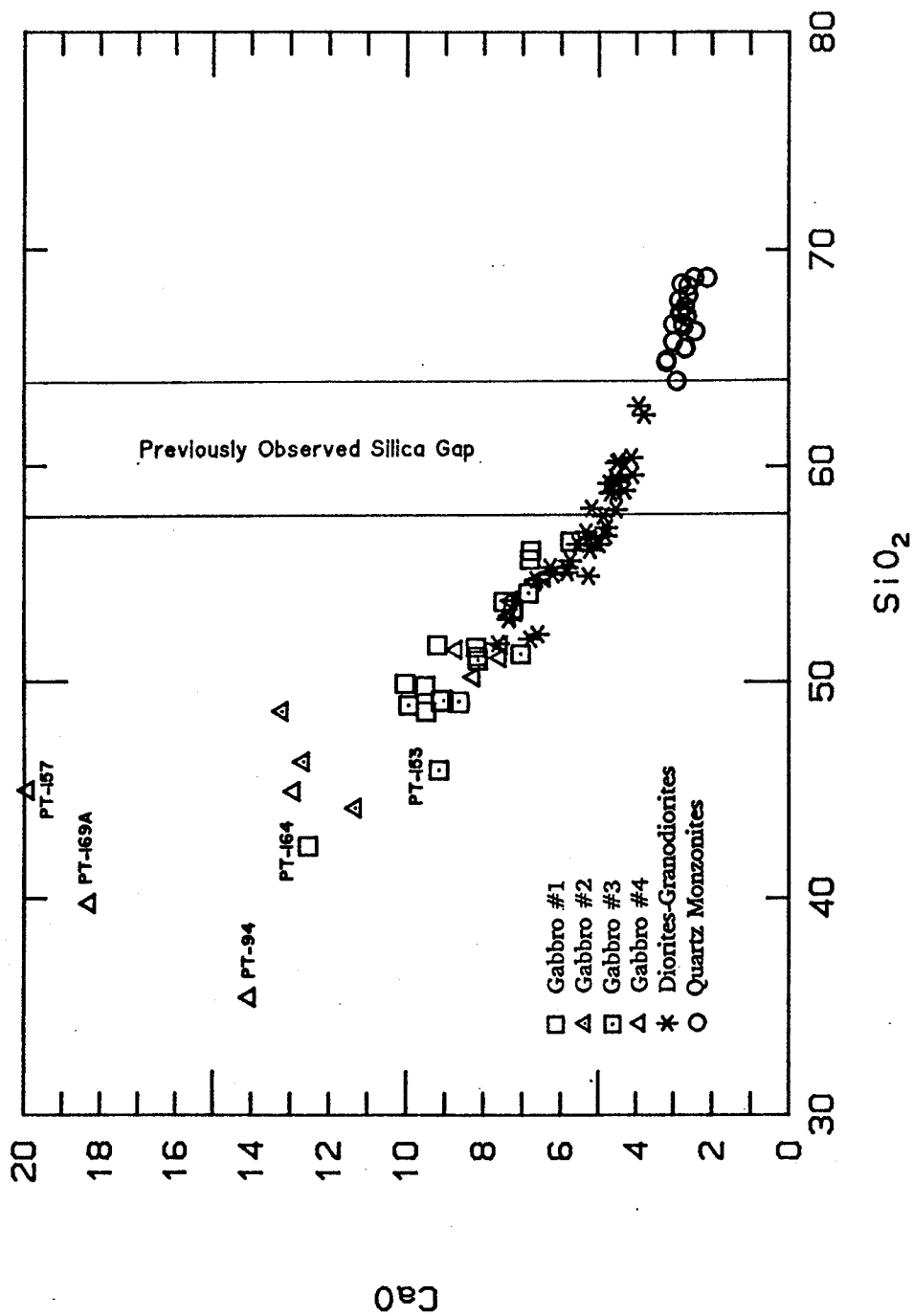


FIGURE 10: CaO vs SiO<sub>2</sub> diagram. Oxides in wt %. See text for discussion.

The analyses include granodiorite and quartz monzonite samples that were collected within 30 meters of the granodiorite-quartz monzonite contact.

### 5.1.2 Harker Variation Diagrams

Major element variations are illustrated by the Harker variation diagrams in Figure 11. Silica contents range from 42.41 to 70.04 wt% SiO<sub>2</sub> (all data excluding mafic clots and mt-rich layer). The trends broadly define a differentiated sequence progressing inward from the outer gabbroic units to the quartz monzonite core. FeO, MnO, MgO and CaO all display strong negative correlations with SiO<sub>2</sub>. TiO<sub>2</sub>, P<sub>2</sub>O<sub>5</sub> and Fe<sub>2</sub>O<sub>3</sub> are also negatively correlated with SiO<sub>2</sub>, but some scatter is observed in the gabbroic rocks reflecting variable modal proportions of accessory phases such as apatite, magnetite and ilmenite. K<sub>2</sub>O displays a positive correlation with SiO<sub>2</sub> as does Na<sub>2</sub>O to a more limited extent.

Deflections of trends are observed in most of the plots in Figure 11, most significantly in the plots involving MgO, CaO and K<sub>2</sub>O. In systems evolving via fractional crystallization, such deflections result from a change in crystallizing mineral phases or from a change in the modal proportion of crystallizing phases. Possible relationships between changing mineralogy and its affect on the chemical evolution of the FLIC rocks are evaluated in Chapter 8.

An important feature to note in all the oxide plots is the large amount of overlap between the diorite analyses and the Gabbro #3, #4 analyses, which is incompatible with a single liquid line of descent. Overlap in major element oxide contents also exists amongst the gabbroic units, particularly between Gabbro #3 and Gabbro #4.



### 5.1.3 Normative Mineralogy

Normative mineralogy for all units of the complex are dominated by variable proportions of anorthite, albite, orthoclase, hypersthene and accessory apatite, magnetite and ilmenite (see Appendix 1). Diopside is a normative mineral in all units, absent only in some of the quartz monzonite samples. Olivine is a typical mineral in the norm of Gabbro #2 samples and also occurs in 30-50% of samples from each of the other gabbroic units. Normative quartz is ubiquitous in granodiorite and quartz monzonite samples as well as in most diorite samples. It also occurs in the norm of some gabbro #1, #3 and #4 samples. The degree of silica-saturation, based on normative compositions, for each unit is summarized in Table 5.

**TABLE 5**

Degree of silica-saturation in rocks of the Falcon Lake Intrusive Complex as indicated by normative mineralogy. Percentages listed under normative minerals refer to the percentage of samples containing that particular mineral.

Q=Quartz HYP=Hypersthene OL=Olivine

ROCK TYPE	NORMATIVE Q	MINERAL HYP	PRESENT OL	DEGREE OF SILICA- SATURATION
Gabbro #1	60%	100%	25%	Silica-saturated
Gabbro #2	-	100%	100%	Silica-saturated to undersaturated
Gabbro #3	55%	100%	45%	Silica-saturated
Gabbro #4	45%	100%	45%	Silica-saturated
Diorite- Granodiorite	90%	100%	10%	Silica-saturated to oversaturated
Quartz Monzonite	100%	100%	-	Silica over- saturated

Variations in normative mineralogy from mafic to felsic rocks reflect major oxide trends and are consistent with trends expected in a differentiated series. Well-defined variations include: decreasing An, Di, Ol, Ap, Mt and Il contents with increasing SiO<sub>2</sub>; increasing Q, Or and Ab contents with increasing SiO<sub>2</sub>.

Greater abundances of madal magnetite and apatite in Gabbro #4 distinguish it from Gabbro #3 (based on criteria used by Mandziuk, 1989 and in this thesis). It is, therefore significant to note that the range of normative apatite, magnetite and ilmenite contents for these units are virtually identical suggesting that the above mineralogical criteria may not be valid.

## 5.2 TRACE ELEMENT GEOCHEMISTRY

Ranges in trace element (Y, Zr, Nb, Rb and Sr) contents for each unit of the complex are given in Table 6. Plots of Zr, Rb and Sr vs SiO<sub>2</sub> (Figure 12) contain trends which are compatible with a differentiated series progressing from gabbro to quartz monzonite. The trends are also compatible with crystal-liquid fractionation processes.

Zr abundance (Figure 12a) increases with increasing SiO<sub>2</sub> to a maximum in the diorite-granodiorite. Zr abundance decreases in the quartz monzonite with increasing SiO<sub>2</sub>. The lowest Zr abundances are observed in Gabbro #1 and Gabbro #2 with low values also occurring in the more mafic Gabbro #3 and #4 samples. Some overlap is seen amongst Gabbro #3, Gabbro #4 and dioritic rocks. A plot of Nb vs SiO<sub>2</sub> (not shown) displays a very similar trend to that of Zr.

A trend of continuously decreasing Sr with increasing SiO<sub>2</sub> is observed progressing from Gabbro #3 and #4 through diorite-granodiorite to quartz monzonite (Figure 12b). This reflects the decreasing plagioclase abundance in

these successively more felsic rock types. Gabbro #1 and #2, along with the quartz monzonite, have the lowest Sr contents. Here again there is overlap between Gabbro #3, Gabbro #4 and dioritic rocks. Strontium contents of the quartz monzonite fall within a fairly restricted range, exhibit no distinct trend and have similar Sr abundances to the more silica-rich granodiorite samples.

Rb contents increase with increasing SiO<sub>2</sub> through the gabbros and diorite and reach a maximum in granodiorite and quartz monzonite (Figure 12c). The lowest Rb contents are found in some of the Gabbro #1 and #2 samples. As in the previous two plots, extensive overlap amongst the Gabbro #3, Gabbro #4 and diorite data is evident. Quartz monzonite samples form a cluster of points.

TABLE 6

Ranges in trace element content for the six major intrusive units of the Falcon Lake Intrusive Complex. All values in parts per million (ppm).

	Y	Zr	Nb	Rb	Sr
Gabbro #1	12-29	40-321	0-19	18-138	492-794
Gabbro #2	13-25	32-69	0-3	2-12	47-836
Gabbro #3	13-31	113-325	0-24	49-139	747-1419
Gabbro #4	14-26	108-468	0-26	16-187	913-1759
Diorites- Granodiorites	8-26	178-558	6-30	75-203	667-1422
Quartz Monzonites	0-15	138-299	16-14	125-187	589-788

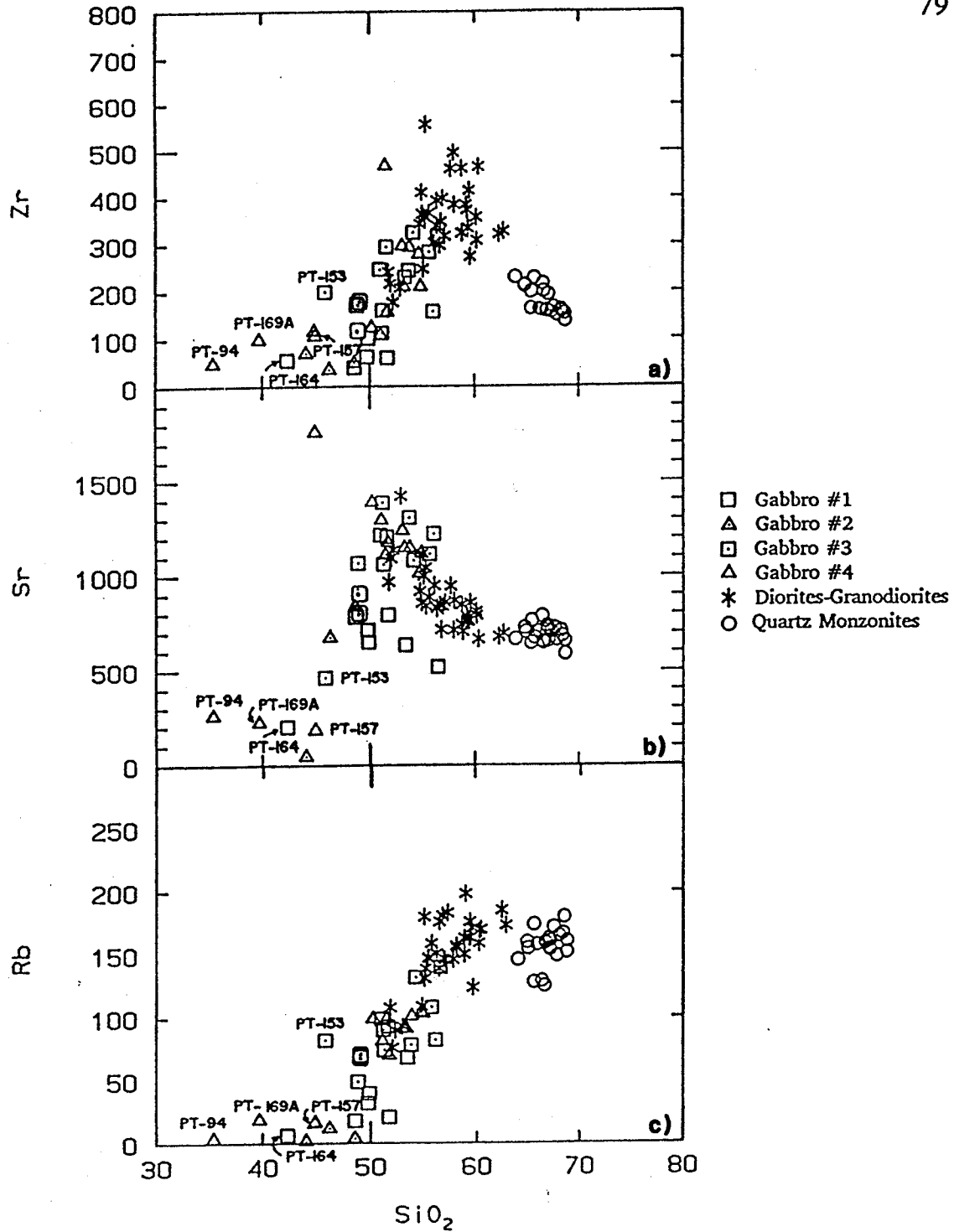


FIGURE 12: Trace element variation diagrams.  $\text{SiO}_2$  is in wt %, trace elements are in ppm. a) Zr vs  $\text{SiO}_2$  b) Sr vs  $\text{SiO}_2$  c) Rb vs  $\text{SiO}_2$

### 5.3 RARE EARTH ELEMENT GEOCHEMISTRY

Rare earth element (REE) data for thirteen selected gabbroic to quartz monzonitic rocks are listed in Table 7a. Also given are the total REE abundances, chondrite normalized La/Lu ratios ( $La/Lu_{CN}$ ) and Eu/Sm ratios. Listed for comparative purposes in Table 7b are total REE contents and  $La/Lu_{CN}$  ratios for various rock types with alkaline affinities. Although the data set is limited, several pertinent observations may be made which add to the geochemical characterization of the FLIC rocks.

The unique feature of these rocks is their pronounced light rare earth element (LREE) enrichments as evidenced by  $La/Lu_{CN}$  ratios ranging from 8.77 to 70.92 (typically  $> 25$ ). In addition, total REE contents range from 40 to 537 ppm (excluding Pr, Pm, Gd, Dy and Er which were not included in the analyses) with the majority of samples containing between 400 and 500 ppm total REEs. The  $La/Lu_{CN}$  ratios and total REE abundances of the FLIC rocks are comparable to those of mafic to felsic alkaline rocks, in particular those belonging to the K-rich basalt and alkali basalt groups (Cullers and Graf, 1984), and are much higher than typical calc-alkaline equivalent rock types.

Variations in REE geochemistry from rock type to rock type within the FLIC are illustrated in the chondrite normalized plots in Figure 13. Gabbro #2 samples have the lowest LREEs, lowest total REEs and lowest  $La/Lu_{CN}$  ratios of all the FLIC units displaying chondrite normalized patterns with the shallowest slopes (Figure 13a). Two Gabbro #1 samples are also plotted in Figure 13a and display patterns of similar slope to those of Gabbro #2 but reflect higher overall REE contents.

Gabbro #3, Gabbro #4 and the diorite-granodiorite samples have the highest LREE and total REE abundances. Chondrite normalized patterns for these three

TABLE 7  
REE DATA

a) Rare earth element data for selected gabbroic to quartz monzonitic rocks of the Falcon Lake Intrusive Complex. All data are expressed in parts per million (ppm).  $La/Lu_{CN}$  ratios calculated using the chondritic values from Thompson (1982).

	<u>PT-10</u>	<u>PT-55</u>	<u>PT-74</u>	<u>PT-125</u>	<u>PT-18</u>	<u>PT-126</u>	<u>PT-34</u>	<u>PT-46</u>
La	27.60	104.00	7.66	14.70	123.00	123.00	82.60	144.00
Ce	50.00	207.00	15.40	29.50	247.00	243.00	176.00	271.00
Nd	23.60	83.30	12.20	20.20	95.80	92.40	85.50	102.00
Sm	3.23	12.30	2.32	3.37	13.60	12.90	11.90	14.40
Eu	1.07	1.91	1.01	1.04	3.03	2.49	2.85	2.99
Tb	0.52	1.34	0.60	0.58	1.09	0.84	0.63	0.87
Yb	0.96	2.57	0.86	0.52	1.35	1.79	1.42	1.81
Lu	0.11	0.37	0.09	0.08	0.19	0.25	0.12	0.27
Total	107.09	412.79	40.14	69.99	485.06	476.67	361.02	537.34
$La/Lu_{CN}$	25.85	28.96	8.77	18.93	66.70	50.69	70.92	54.95
Eu/Sm	0.33	0.16	0.44	0.31	0.22	0.19	0.24	0.21

	<u>PT-44</u>	<u>PT-36</u>	<u>PT-24</u>	<u>PT-87</u>	<u>PT-136</u>	<u>Key:</u>	
La	121.00	112.00	120.00	55.90	60.40	PT-10	Gabbro #1
Ce	245.00	221.00	237.00	100.00	107.00	PT-55	Gabbro #1
Nd	96.50	95.40	82.30	32.80	32.90	PT-74	Gabbro #2
Sm	14.30	13.50	12.00	4.70	4.86	PT-125	Gabbro #2
Eu	2.59	3.27	2.29	1.07	1.08	PT-18	Gabbro #3
Tb	1.04	0.78	0.62	0.32	0.42	PT-126	Gabbro #3
Yb	2.08	1.92	1.84	0.92	1.14	PT-34	Gabbro #4
Lu	0.38	0.18	0.22	0.16	0.17	PT-46	Gabbro #4
Total	482.89	448.05	456.27	195.87	207.97	PT-44	Diorite
$La/Lu_{CN}$	32.81	64.11	56.20	36.00	36.61	PT-35	Diorite
Eu/Sm	0.18	0.24	0.19	0.23	0.22	PT-24	Granodiorite
						PT-87	Quartz Monzonite
						PT-136	Quartz Monzonite

b) Ranges in total REE content and  $(La/Lu)_{CN}$  ratios for various rocks with alkaline affinities. Values are from Cullers and Graf (1984).

	Total REE ppm	$(La/Lu)_{CN}$
<u>Alkali basalt group</u>		
Alkali basalts	130-250	5.35-28.40
Intermediate rocks associated with alkali basalts	235-988	4.80-41.80
<u>Shoshonite group</u>		
Shoshonites	69-240	2.70-18.30
Intermediate and felsic rocks associated with shoshonites	124-387	3.20-23.10
<u>K-rich basalt group</u>		
K-rich mafic rocks	255-1453	19.50-262.00
Intermediate rocks associated with K-rich mafic rocks	92-688	3.80-114.00

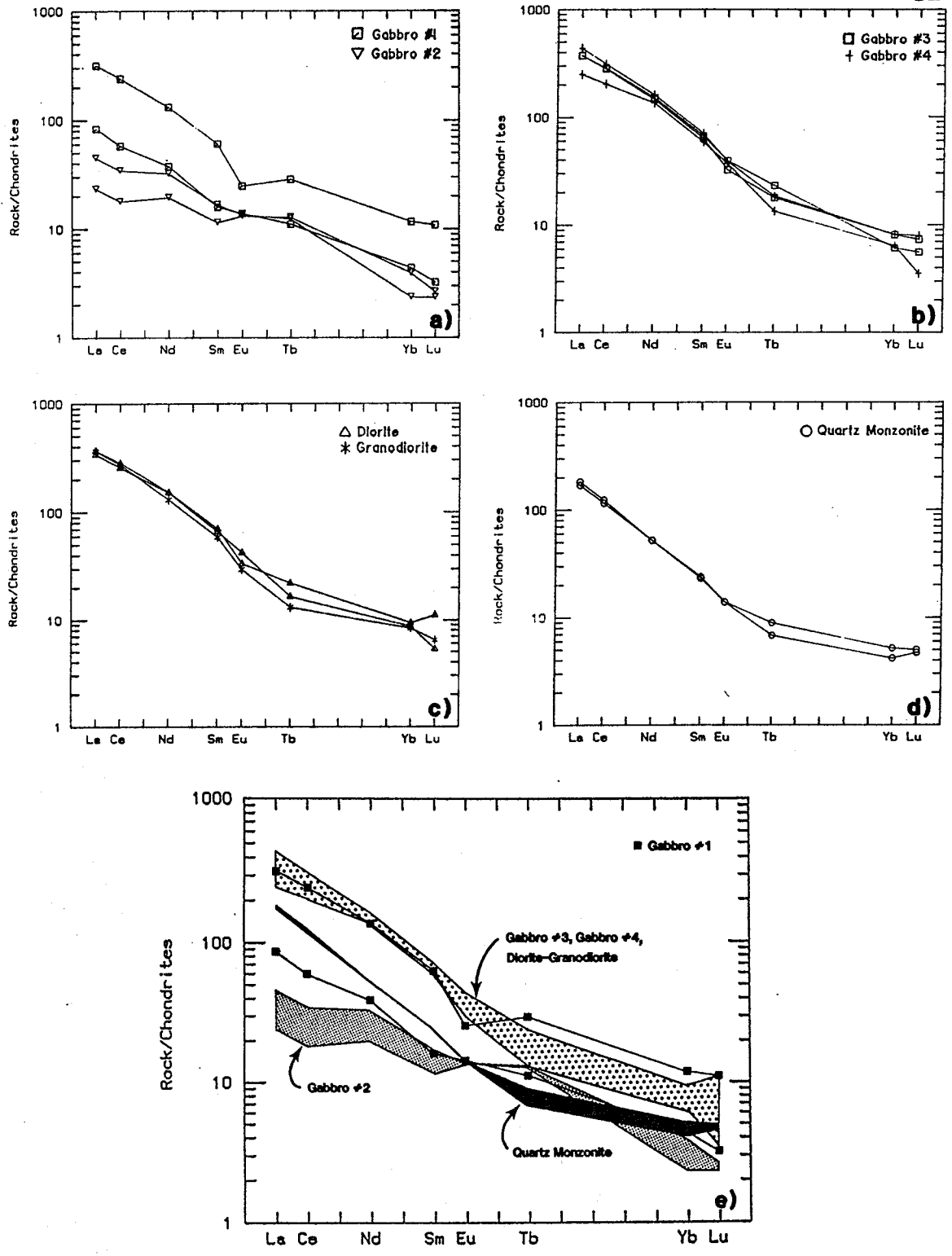


FIGURE 13: Chondrite-normalized REE plots of selected mafic to felsic whole rock samples from the Falcon Lake Intrusive Complex. Normalization values are from Thompson (1982).

rock types (Figure 13b and c) are virtually identical except for slight scatter in the heavy rare earth elements (HREE). In comparison, quartz monzonite samples (Figure 13d) have patterns of similar slope to these rock types, but contain lower LREE and total REE abundances.

REE data is summarized in Figure 13e where the less pronounced LREE enrichment of the Gabbro #1 and Gabbro #2 phases relative to the other phases is clearly evident.

Eu anomalies are absent in all plots except for those of one Gabbro #1 and one Gabbro #2 samples which have negative and positive anomalies respectively. The paucity of Eu anomalies is unusual given the abundance of plagioclase (into which Eu is commonly partitioned) in all units of the complex. Factors governing the development of Eu anomalies and possible reasons for their absence in the FLIC rocks are discussed in Chapter 8.

## CHAPTER 6

### MINERAL CHEMISTRY

Seven different mineral phases from a total of 20 mafic to felsic rock samples were analyzed by electron microprobe as outlined in Chapter 3. The data are listed in Appendix 3. Over half of the data are plagioclase analyses obtained from each rock type of the complex in order to determine plagioclase compositions and document cryptic compositional variations. The remainder of the data set includes limited alkali feldspar, oxide mineral, pyroxene, amphibole and biotite analyses collected from selected rock types of the complex primarily for the purpose of documenting compositions.

#### 6.1 PLAGIOCLASE

Plagioclase is an ubiquitous and abundant mineral phase in all rock types of the FLIC, variably occurring as cumulus crystals, intercumulus grains, phenocrysts and/or groundmass components. All analyses are reported in Appendix 3a and depicted (by rock type) in the series of triangular plots in Figure 14. Representative analyses are listed in Table 8. (Note: The first two to three digits in all electron microprobe sample numbers correspond to the sample numbers of the whole rock samples listed in Appendix 3).

Plagioclase compositions in Gabbro #1, #3, #4 and in the dioritic rocks are all largely overlapping but an overall progression to more albitic compositions is observed progressing from dioritic to quartz monzonitic rocks. Extensive overlap in plagioclase compositions is observed between most rock types of the complex.

TABLE 8  
Representative Plagioclase Analyses

SAMPLE	55-1	55-9B	74-1	18-2	18-3	73-6	47-5	34-11A	38-4
SiO <sub>2</sub>	60.92	59.77	53.26	60.77	58.31	56.34	56.53	52.87	58.76
Al <sub>2</sub> O <sub>3</sub>	24.62	25.21	29.95	24.79	26.27	27.69	27.09	30.21	26.26
CaO	6.44	7.36	12.62	6.47	8.26	9.97	9.47	12.83	8.21
Na <sub>2</sub> O	7.74	6.66	4.00	7.44	6.52	5.85	5.65	3.83	6.45
K <sub>2</sub> O	0.15	0.12	0.00	0.09	0.08	0.17	0.12	0.00	0.12
Total	99.87	99.12	99.83	99.56	99.44	100.02	98.86	99.74	99.80
Cations per 24 Oxygens									
Si	8.129	8.035	7.228	8.122	7.850	7.593	7.681	7.185	7.875
Al	3.872	3.994	4.789	3.906	4.168	4.398	4.337	4.839	4.148
Ca	0.920	1.061	1.835	0.926	1.191	1.439	1.379	1.868	1.179
Na	2.002	1.737	1.052	1.927	1.702	1.529	1.489	1.008	1.677
K	0.026	0.020	0.000	0.015	0.014	0.029	0.020	0.000	0.020
Total	14.949	14.847	14.905	14.896	14.925	14.988	14.906	14.900	14.899
SAMPLE	39-4	39-5	70-8B	42-11	42-15	58-1	58-14	86-7	86-12
SiO <sub>2</sub>	57.43	58.43	60.71	60.32	59.09	59.88	57.10	61.45	61.86
Al <sub>2</sub> O <sub>3</sub>	26.66	25.72	24.70	25.54	25.97	25.57	27.38	23.91	23.97
CaO	8.79	7.86	6.86	7.26	7.95	7.45	9.72	5.66	5.57
Na <sub>2</sub> O	6.16	6.78	7.53	7.16	6.91	7.25	5.77	8.16	8.35
K <sub>2</sub> O	0.23	0.13	0.10	0.14	0.13	0.09	0.15	0.10	0.07
Total	99.27	98.92	99.90	100.42	100.05	100.24	100.12	99.28	99.82
Cations per 24 Oxygens									
Si	7.764	7.904	8.104	8.015	7.906	7.982	7.668	8.230	8.239
Al	4.248	4.101	3.886	4.001	4.094	4.018	4.334	3.774	3.762
Ca	1.273	1.140	0.981	1.034	1.140	1.064	1.398	0.812	0.794
Na	1.614	1.778	1.949	1.845	1.793	1.875	1.502	2.118	2.157
K	0.039	0.023	0.017	0.024	0.022	0.015	0.026	0.017	0.011
Total	14.938	14.946	14.937	14.919	14.955	14.954	14.928	14.951	14.963
55-1	:	Phenocryst, Gabbro #1							
55-9B	:	Medium grained groundmass plagioclase, Gabbro #1							
74-1	:	Medium grained plagioclase, Gabbro #2							
18-2	:	Medium grained cumulus plagioclase, Gabbro #3							
18-3	:	Very fine grained intercumulus plagioclase, Gabbro #3							
73-6	:	Coarse grained cumulus plagioclase, Gabbro #3							
47-5	:	Coarse grained cumulus plagioclase, Gabbro #4							
34-11A	:	Coarse grained cumulus plagioclase, Gabbro #4							
38-4	:	Coarse grained cumulus plagioclase, diorite							
39-4	:	Phenocryst, quartz diorite							
39-5	:	Fine grained groundmass plagioclase, quartz diorite							
70-8B	:	Medium grained groundmass plagioclase, diorite							
42-11	:	Medium grained groundmass plagioclase, granodiorite							
42-15	:	Phenocryst, granodiorite							
58-1	:	Medium grained groundmass plagioclase, granodiorite							
58-14	:	Phenocryst, granodiorite							
86-7	:	Phenocryst, quartz monzonite							
86-12	:	Medium grained groundmass plagioclase, quartz monzonite							

Comparison of plagioclase composition between the four gabbroic phases is hampered by the paucity of data with analyses from only one Gabbro #1, one Gabbro #2, three Gabbro #3 and two Gabbro #4 samples. The highest An contents are found in the single Gabbro #2 sample (An<sub>59.5-66.6</sub>) and in one of the Gabbro #4 samples (An<sub>62.5-68.4</sub>). Ranges in An content for the remainder of the data from gabbroic rocks are as follows:

Gabbro #1 - An<sub>31.2-47.7</sub>

Gabbro #3 - An<sub>32.3-49.1</sub>

Gabbro #4 - An<sub>37.3-47.7</sub>

Compositions of cumulus vs intercumulus plagioclase as well as phenocryst vs groundmass plagioclase are largely overlapping and lack any coherent variation (Figure 14a,b and c).

Plagioclase analyses for the dioritic rocks are subdivided into cumulus grains, phenocrysts and groundmass grains and those for the granodioritic rocks into phenocryst and groundmass grains (Figure 14d and e). Ranges in An content are summarized as follows:

Diorite - cumulus plagioclase An<sub>37.5-49.4</sub>

- phenocrysts An<sub>28.5-44.5</sub>

- groundmass plagioclase An<sub>28.7-38.7</sub>

Granodiorite - phenocrysts plagioclase An<sub>26.2-38.6</sub>

- groundmass plagioclase An<sub>25.7-44.3</sub>

A large amount of overlap is observed between phenocryst and groundmass plagioclase in each of these rock types.

Plagioclase compositions in the quartz monzonites are tightly grouped (Figure 14f) ranging from An<sub>24.9-30.3</sub> and overlapping with some of the diorite-

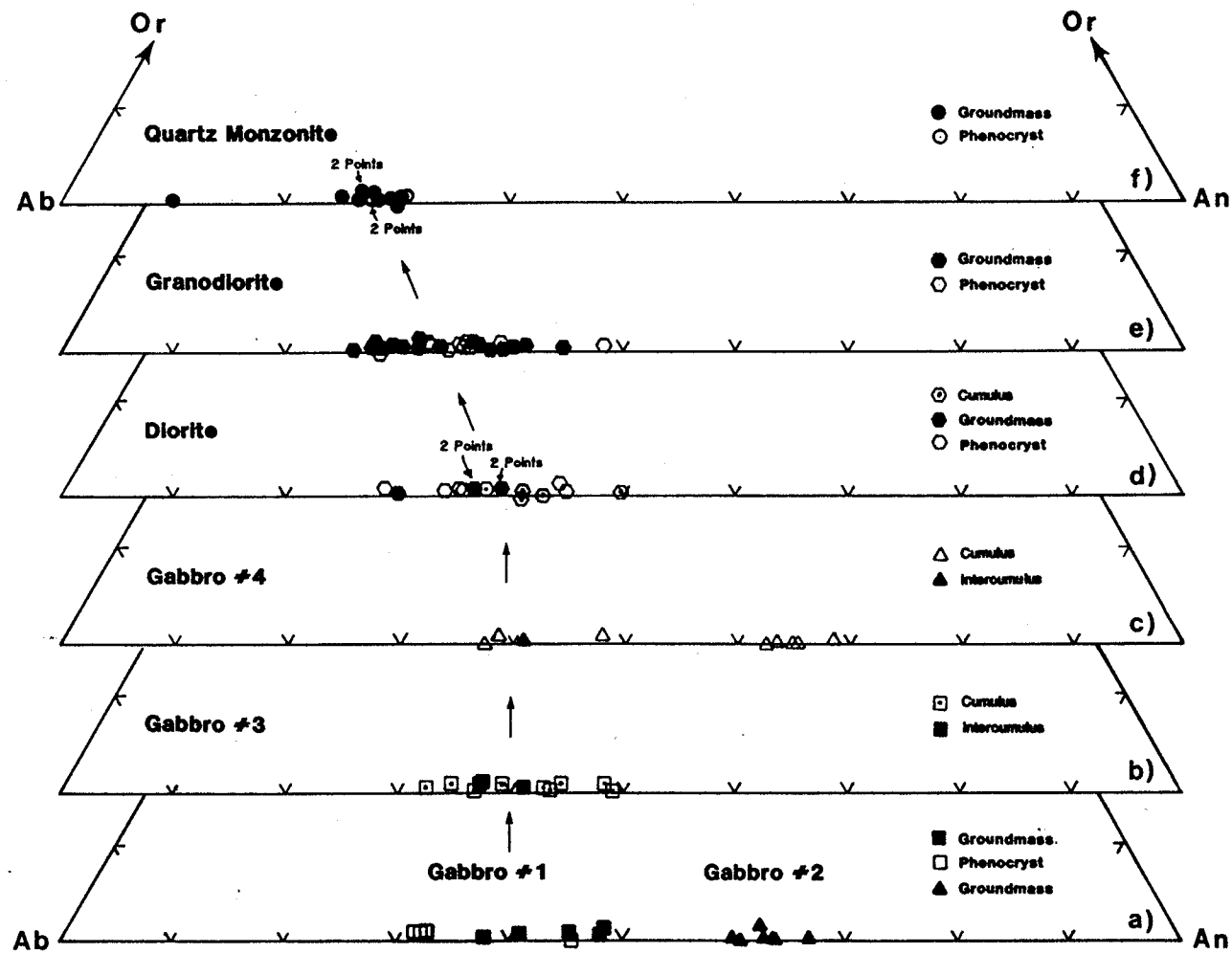


FIGURE 14: Plagioclase analyses from rocks of the Falcon Lake Intrusive Complex plotted by rock and grain type in the Or-Ab-An feldspar triangle. Note the general transition toward more albitic compositions from the dioritic through granodioritic to quartz monzonitic rocks.

granodiorite data. As in the other rock types, phenocryst and groundmass components are compositionally indistinct.

## 6.2 ALKALI FELDSPAR

Alkali feldspar occurs as an interstitial to intercumulus mineral in some of the gabbroic rocks (see Chapter 4) and is an ubiquitous groundmass  $\pm$  phenocryst phase in the dioritic to quartz monzonitic rocks. The 27 analyses obtained from samples of gabbro #3, Gabbro #4, diorite, granodiorite and quartz monzonite are listed in Appendix 3b. The majority of the data was obtained from analysis of fine to medium grained anhedral to subhedral grains of microcline, perthitic microcline and perthite.

Compositions are plotted in Figure 15 and representative analyses are given in Table 9. All grains analyzed, with the exception of sample 68-2, are K-rich exhibiting the following end member compositions:  $Ab_{0.0-14.5} An_{0.0-0.1} Or_{85.5-100.0}$ . Microcline grains contain between 87.6 and 100% of the Or end member. In grains comprised of feldspar intergrowths (ie. perthitic feldspars), Or contents of the alkali feldspar component range from  $Or_{85.5-100.0}$ .

The uniformly K-rich nature of alkali feldspars observed in intrusions elsewhere has been, in some cases, attributed to non-magmatic processes. In the Wooley Creek Batholith (California) K-rich alkali feldspar compositions are thought to be a result of subsolidus equilibration (Barnes, 1983) whereas in the Center Pond Pluton (Maine), alkali feldspars are interpreted to have undergone post crystallization alkali element exchange with deuteric fluids (Scambos et al, 1986).

TABLE 9  
Representative Alkali Feldspar Analyses

SAMPLE	39-2	70-10	68-2	86-5	86-10
SiO <sub>2</sub>	64.09	64.58	63.89	64.39	64.21
Al <sub>2</sub> O <sub>3</sub>	18.15	17.73	19.70	17.83	18.31
CaO	0.02	0.00	1.55	0.00	0.00
Na <sub>2</sub> O	0.00	0.00	3.06	0.00	0.00
K <sub>2</sub> O	16.53	16.77	11.21	16.72	16.61
BaO	0.68	0.38	0.44	0.45	0.65
Total	99.47	99.46	99.85	99.39	99.78
Cations per 24 Oxygens					
Si	8.990	9.045	8.784	9.030	8.978
Al	3.001	2.927	3.192	2.946	3.018
Ca	0.002	0.000	0.229	0.000	0.000
Na	0.000	0.000	0.815	0.000	0.000
K	2.958	2.997	1.967	2.992	2.963
Ba	0.037	0.021	0.024	0.025	0.035
Total	14.988	14.990	15.011	14.993	14.994
End Member Compositions					
Ab:An:Or	Ab <sub>0</sub> :An <sub>0.1</sub> :Or <sub>99.9</sub>	Ab <sub>0</sub> :An <sub>0</sub> :Or <sub>100</sub>	Ab <sub>27.1</sub> :An <sub>7.6</sub> :Or <sub>65.3</sub>	Ab <sub>0</sub> :An <sub>0</sub> :Or <sub>100</sub>	Ab <sub>0</sub> :An <sub>0</sub> :Or <sub>100</sub>

39-2 : Fine grained groundmass perthite, quartz diorite  
 70-10: Fine grained groundmass microcline, diorite  
 68-2 : Fine grained groundmass perthitic microcline, granodiorite  
 86-5 : Medium grained microcline, quartz monzonite  
 86-10: Coarse grained microcline phenocryst, quartz monzonite

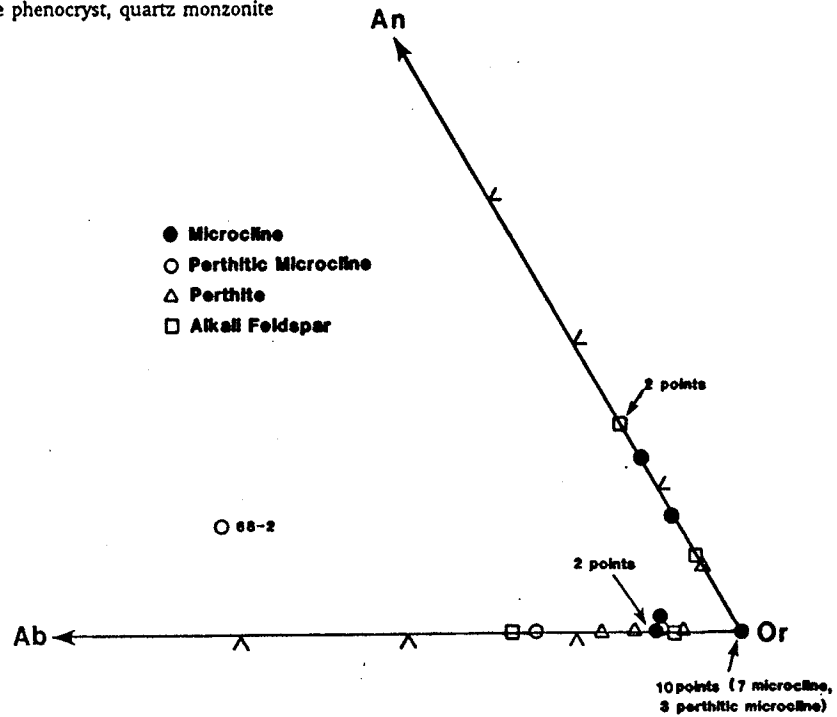


FIGURE 15: Alkali feldspar compositions from samples of quartz diorite, granodiorite and quartz monzonite plotted in the Or-Ab-An feldspar triangle.

### 6.3 OXIDE MINERALS

Oxide minerals are ubiquitous accessory phases in all rock types of the FLIC occurring as intercumulus or groundmass components as well as inclusions within mafic minerals.

Two or more oxide analyses were obtained from each rock type of the FLIC except Gabbro #2 and are tabulated in Appendix 3c. Brief sample descriptions are also given. Oxides identified included magnetite and ilmenite with magnetite grains commonly containing trellis and/or composite granular intergrowths of ilmenite (cf. Haggerty, 1976). Where intergrowths were encountered during probing, both phases were analyzed. Pairs of analyses may be identified by their sample numbers (eg. 73-8A and 73-8B). Representative analyses are given in Table 10. A summary of oxide types identified in each rock type is as follows:

- |           |  |
|-----------|--|
| Gabbro #1 | - subhedral to euhedral ilmenite with titanite rims  |
| Gabbro #3 | - subhedral to anhedral magnetite  |
|           | - euhedral ilmenite with titanite rims   |
|           | - euhedral magnetite with ilmenite lamellae (trellis type intergrowths) and/or composite ilmenite intergrowths (Plate 16a)   |
| Gabbro #4 | - anhedral magnetite (as an accessory phase and as inclusions in amphibole) with composite ilmenite intergrowths (Plate 16b) |
| Diorites  | - anhedral to euhedral magnetite with composite ilmenite intergrowths  |

**TABLE 10**  
Representative Oxide Mineral Analyses

SAMPLE	MAGNETITES				ILMENITES			
	85-4A	38-5B	21-10A	65-10	85-4B	38-5A	21-10B	42-17
SiO <sub>2</sub>	0.00	0.00	0.00	0.39	0.00	0.00	0.00	0.00
TiO <sub>2</sub>	0.00	0.00	0.00	0.00	51.30	50.39	50.49	51.26
Fe <sub>2</sub> O <sub>3</sub>	66.66	67.50	67.65	67.95	2.62	4.46	3.62	2.41
FeO	32.59	32.22	32.08	31.80	43.11	42.26	40.34	38.77
MnO	0.00	0.00	0.00	0.00	2.98	3.01	5.00	7.23
Cr <sub>2</sub> O <sub>3</sub>	0.00	0.00	0.43	0.63	0.00	0.00	0.00	0.00
V <sub>2</sub> O <sub>5</sub>	0.94	0.67	0.52	0.00	0.00	0.00	0.00	0.00
Total	100.19	100.39	100.68	100.77	100.01	100.13	99.44	99.67
	Calculated on basis of 32 anions & 24 cations				Calculated on basis of 6 anions & 4 cations			
Si	0.000	0.000	0.000	0.119	0.000	0.000	0.000	0.000
Ti	0.000	0.000	0.000	0.000	1.950	1.915	1.931	1.954
Fe <sup>3+</sup>	15.427	15.592	15.581	15.610	0.100	0.170	0.138	0.092
Fe <sup>2+</sup>	8.382	8.272	8.210	8.119	1.823	1.786	1.715	1.644
Mn	0.000	0.000	0.000	0.000	0.128	0.129	0.215	0.310
Cr	0.000	0.000	0.104	0.152	0.000	0.000	0.000	0.000
V	0.191	0.136	0.105	0.000	0.000	0.000	0.000	0.000
Total	24	24	24	24	4	4	4	4

Note: Fe<sub>2</sub>O<sub>3</sub> and Fe<sup>3+</sup> determined by stoichiometry.

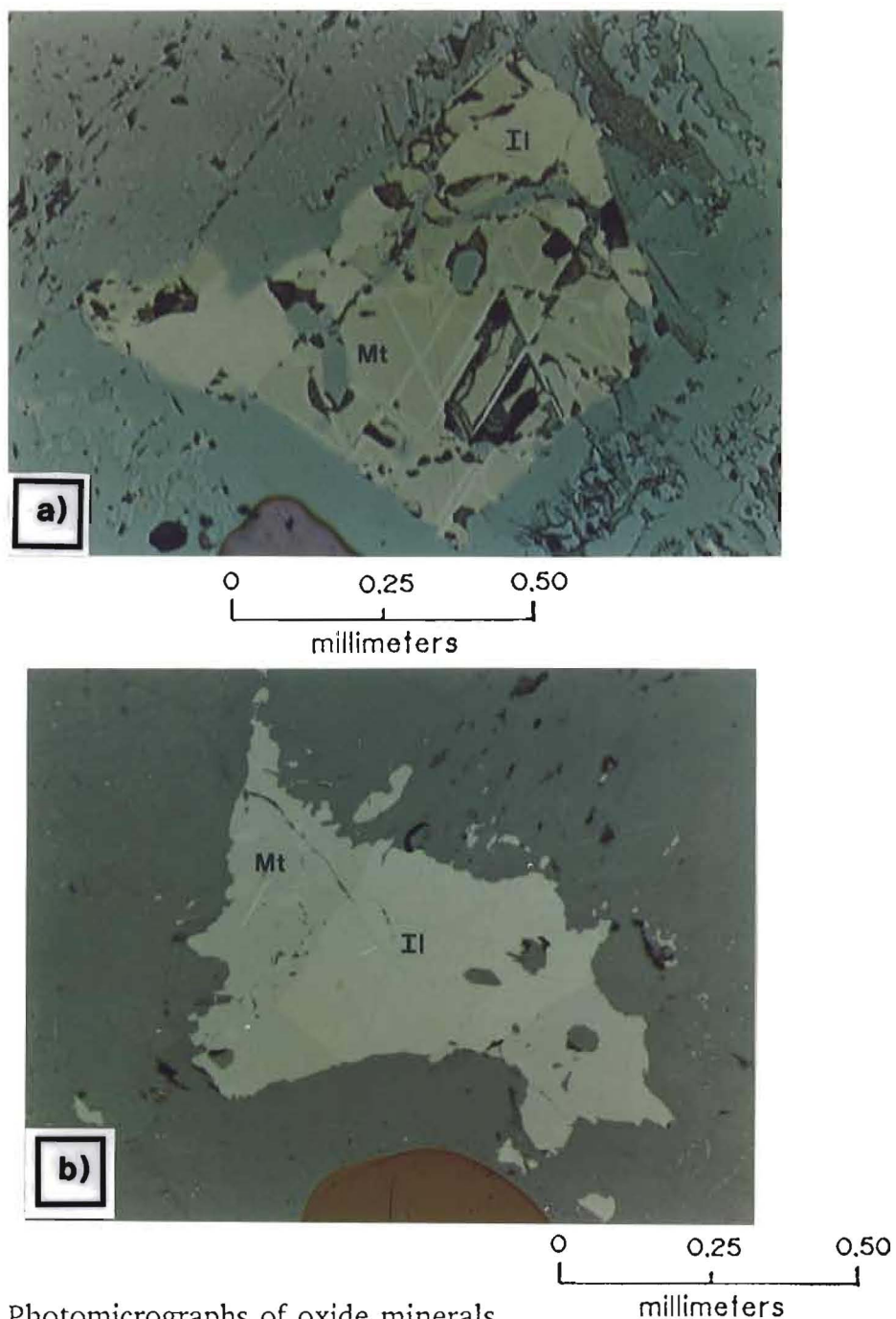


PLATE 16: Photomicrographs of oxide minerals.

a) Photomicrograph of Gabbro #3. Center of photomicrograph contains a subhedral magnetite grain (Mt) containing trellis and composite ilmenite intergrowths (Il). Reflected light.

b) Photomicrograph of Gabbro #4. An anhedral oxide mineral comprised of magnetite (Mt) with composite ilmenite intergrowths (Il) is shown in the center of the picture. Reflected light.

Granodiorites - anhedral to subhedral magnetite with pronounced titanite rims + composite intergrowths of ilmenite

Quartz Monzonites - euhedral magnetite

All magnetites are close to pure end member compositions and range from  $Mt_{93.89-100} : Usp_{0-6.11}$ . (End member compositions were calculated using the computer program "GPP"; Geist et al, 1983).

Oxide minerals within all rock types of the FLIC appear to be strongly oxidized as indicated by the presence of partial to complete titanite rims around many of the oxide mineral grains. In addition, ilmenite lamellae within magnetite grains, such as that observed in Gabbro #3 are commonly accepted to be oxidation products of  $Mt-Usp_{ss}$  (Haggerty, 1976). Composite ilmenite intergrowths may be either the result of oxidation or of primary magmatic precipitation (Haggerty, 1976). The composite intergrowths found in the FLIC rocks are most likely the result of oxidation given the common presence of titanite rims and occurrence of trellis type ilmenite intergrowths (lamellae). Oxide thermometers applied to these rocks yield subsolidus temperatures as discussed in Chapter 7.

#### 6.4 PYROXENES

Primary pyroxene has been identified in, or is inferred to be present in, all rock types of the complex except the quartz monzonites and is most abundant in the gabbroic rocks. Within Gabbro #3 and the dioritic to granodioritic rocks, pyroxene typically occurs as relict cores displaying pyroxene cleavage or diallage structures (Plate 17). Cores are surrounded by various types of amphibole (see section 6.5 below). In the Gabbro #1 and Gabbro #2 rocks, primary pyroxene



0            0.25            0.50  
 millimeters

Plate 17: Photomicrograph of a relict pyroxene core (center;P) displaying diagenetic structure and surrounded by amphibole (A). Plane transmitted light.

(inferred from crystal outlines) appears to have been completely pseudomorphed by one or more of uralitic amphibole, hornblende and actinolite.

Thirteen analyses of relict pyroxene cores from Gabbro #3 rocks, diorites and granodiorites are reported in Appendix 3d with representative analyses given in Table 11. End member compositions (Wo:En:F<sub>s</sub>) were calculated using the computer program "GPP" (Geist et al, 1983) and are plotted in Figure 16. Ca-rich clinopyroxenes predominate with all but three analyses plotting in the augite field. The three data points plotting outside the field contain slightly higher amounts



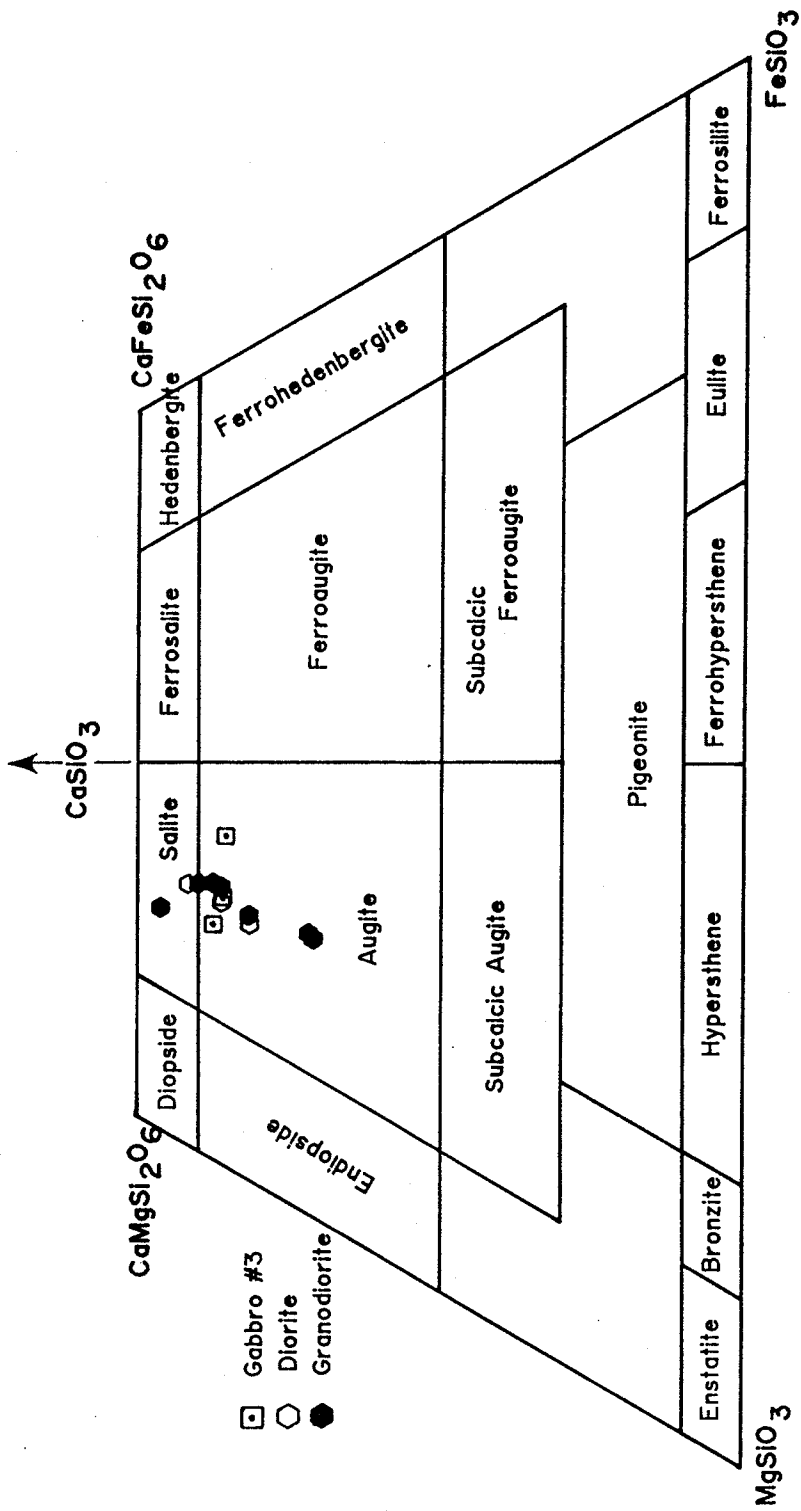


FIGURE 16: Classification of pyroxenes from Gabbro #3, diorite and granodiorite samples in the end member system CaSiO<sub>3</sub>-MgSiO<sub>3</sub>-FeSiO<sub>3</sub>. After McBirney (1984).

of Ca and lie in the salite field. In terms of end member components, pyroxenes from each rock type span similar compositional ranges with no distinct trends apparent.

Pyroxenes in alkali basaltic rocks typically have higher  $\text{Al}_2\text{O}_3$ ,  $\text{TiO}_2$  and  $\text{Na}_2\text{O}$  contents than pyroxenes in subalkaline counterparts (Wilkinson, 1974). Listed for comparison in Table 11 are two Ca-rich augite analyses from mafic alkaline rocks and one augite analysis from a calcalkaline diorite. Based on this comparison, pyroxenes analyzed from the FLIC are compositionally more similar to those found in subalkaline rock types. With the exception of sample 42-3, they have relatively low contents of  $\text{TiO}_2$  and  $\text{Al}_2\text{O}_3$  (0.13-0.65 and 0.75-1.95 respectively) and contain no  $\text{Na}_2\text{O}$ . However, all but one sample (85-5) contain trace to small amounts of  $\text{K}_2\text{O}$  ranging from 0.04-0.39 wt%.

## 6.5 AMPHIBOLES

Amphibole occurs as either a primary or secondary mineral phase in all rock types of the complex (see Chapter 4). In Gabbro #1 and #2, amphibole is mainly a secondary mineral after pyroxene. In Gabbro #3 and the dioritic to granodioritic rocks, amphiboles commonly surround relict pyroxene cores and, more rarely, occur in fine grained patches which appear to be pseudomorphous after pyroxene. Primary amphibole occurs as an intercumulus to framework component in Gabbro #1, #3 and #4. In diorite, granodiorite and quartz monzonite it is a groundmass mineral having its greatest abundance in the diorite-granodiorite unit.

All amphibole analyses are reported in Appendix 3e along with brief descriptions of each sample. Approximately half of the analyses are of amphibole rims surrounding the pyroxene cores previously reported in section 6.4. The

remainder of the amphibole data includes analyses of both primary and secondary grains.

Classification of the amphiboles was attempted using the classification scheme of Hawthorne (1981). (Cation proportions used for plotting purposes were calculated after the method of Deer, Howie and Zussman (1985) using a "LOTUS 123" computer spreadsheet program.  $\text{Fe}_2\text{O}_3$  and FeO were determined by stoichiometry.) All of the data is plotted in Figure 17a with the majority of the amphiboles being either magnesio-hornblendes or actinolites. The total range in Mg/Mg +  $\text{Fe}^{2+}$  ratios, barring Gabbro #2 samples 74-5 and 74-6, is small (0.47-0.65).

Analyzed amphibole rims to pyroxene grains are plotted in Figure 17b whereas other primary and secondary amphiboles are plotted in Figure 17c. Both magnesio-hornblende and actinolite rims around pyroxene are present in Gabbro #3, diorite and granodiorite (Figure 17b). One rim analysis (18-11) yielded a ferro-hornblende composition. The two Gabbro #2 amphibole grains (74-5 and 74-6), which appear to be pseudomorphous after pyroxene, have the highest Mg/Mg +  $\text{Fe}^{2+}$  contents and are also quite Ca-rich, plotting in the actinolite and actinolitic hornblende fields (Figure 17c). The primary amphiboles from the diorite-granodiorite unit are all either magnesio- or ferro-hornblendes. Several Gabbro #3 amphiboles (18-8, 85-2 and 85-12), which appear to represent recrystallized primary grains, yield actinolite and ferro-hornblende compositions. Analysis 34-8, obtained from a Gabbro #4 sample, contains the lowest Si content and plots in the alumino-tschemakite field.

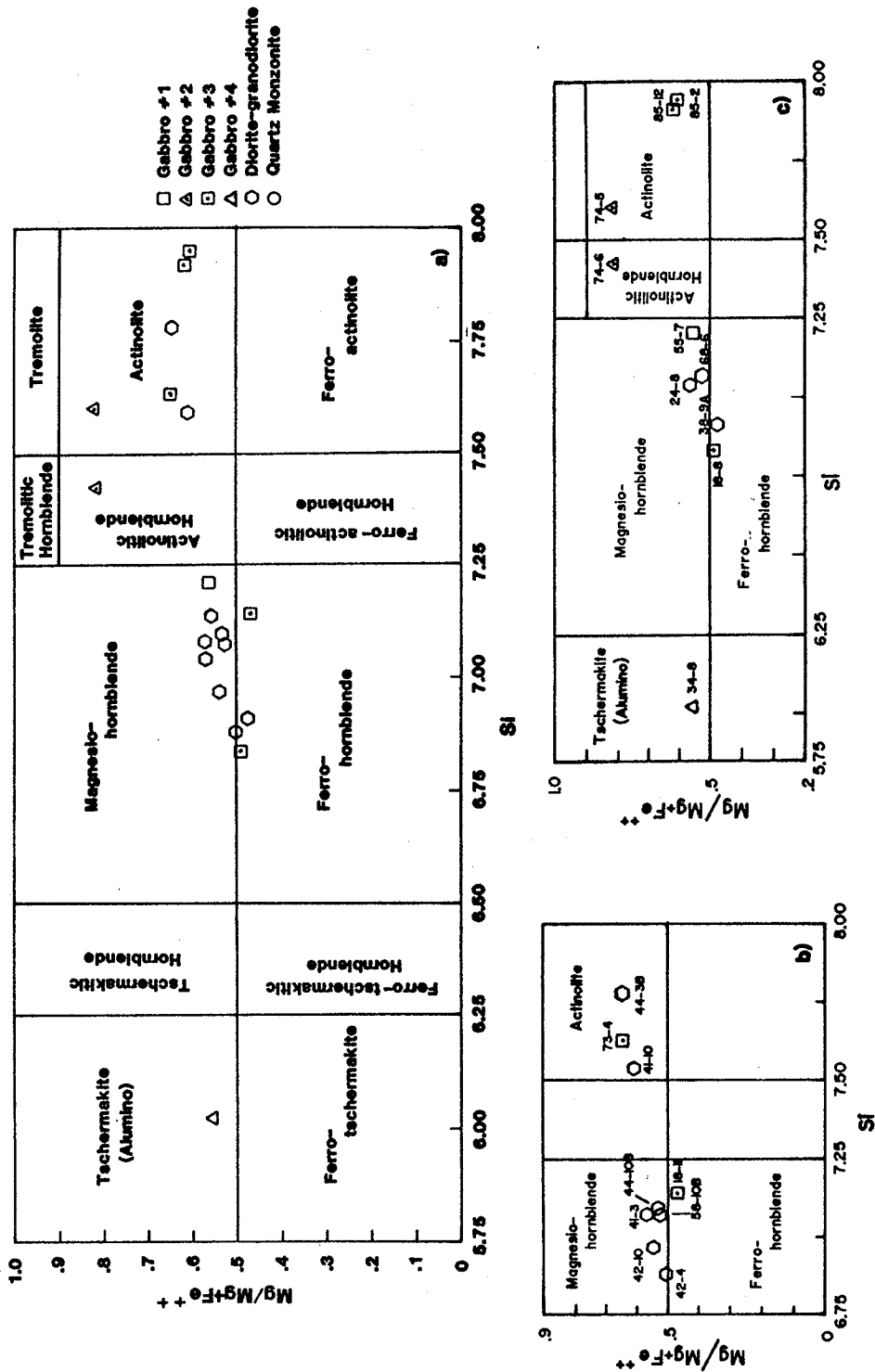


FIGURE 17: Classification of amphiboles from rocks of the Falcon Lake Intrusive Complex using the Mg/Mg+Fe<sup>++</sup> vs Si scheme of Hawthorne (1981).  
 a) All amphibole analyses b) Amphibole rims to pyroxene grains  
 c) Primary and secondary amphibole grains (see descriptions in Appendix 3e Sample numbers are plotted for reference in b) and c).

## 6.6 BIOTITES

Biotite is found in all FLIC units and occurs as a primary mineral phase in Gabbro #3, Gabbro #4, diorite-granodiorite and quartz monzonite. Primary biotite in the gabbroic to granodioritic rocks commonly contains inclusions of apatite, oxide minerals and titanite. Secondary biotite occurs a) with amphibole as pseudomorphs of pyroxene in Gabbro #2, Gabbro #3 and diorite and b) as an alteration product of hornblende in Gabbro #1, Gabbro #3, diorite-granodiorite and quartz monzonite.

Appendix 3f contains 24 biotite analyses from mafic to felsic FLIC rocks with representative analyses listed in Table 12. Most grains are K-rich containing between 9.19 and 10.15 wt% K<sub>2</sub>O.

In Figure 18, the Fe/Fe+Mg ratios of primary biotite grains are plotted against whole rock SiO<sub>2</sub> contents. A general trend of Fe depletion is broadly observed progressing from gabbro to granodiorite. The total range of Fe/Fe+Mg ratios is small (0.419-0.640).

**TABLE 12**  
Representative Biotite Analyses

SAMPLE	85-10	38-6	41-8	24-6
Key	3	5	5	6
SiO <sub>2</sub>	35.84	35.42	36.41	36.49
TiO <sub>2</sub>	2.99	2.20	1.58	2.22
Al <sub>2</sub> O <sub>3</sub>	13.93	15.26	14.70	14.39
FeO	24.13	24.73	21.43	21.01
MnO	0.29	0.00	0.19	0.33
MgO	8.39	8.31	10.45	10.72
K <sub>2</sub> O	9.95	9.92	9.61	10.72
Total	95.52	95.84	94.37	95.19
Cations per 24 Oxygens				
Si	6.140	6.051	6.198	6.168
Ti	0.386	0.282	0.203	0.283
Al	2.813	3.071	2.949	2.867
Fe	3.457	3.632	3.051	2.969
Mn	0.042	0.000	0.027	0.047
Mg	2.143	2.116	2.653	2.700
K	2.174	2.161	2.088	2.163
Total	17.155	17.213	17.169	17.197

Key: 3 = Gabbro #3    5 = Diorite    6 = Granodiorite

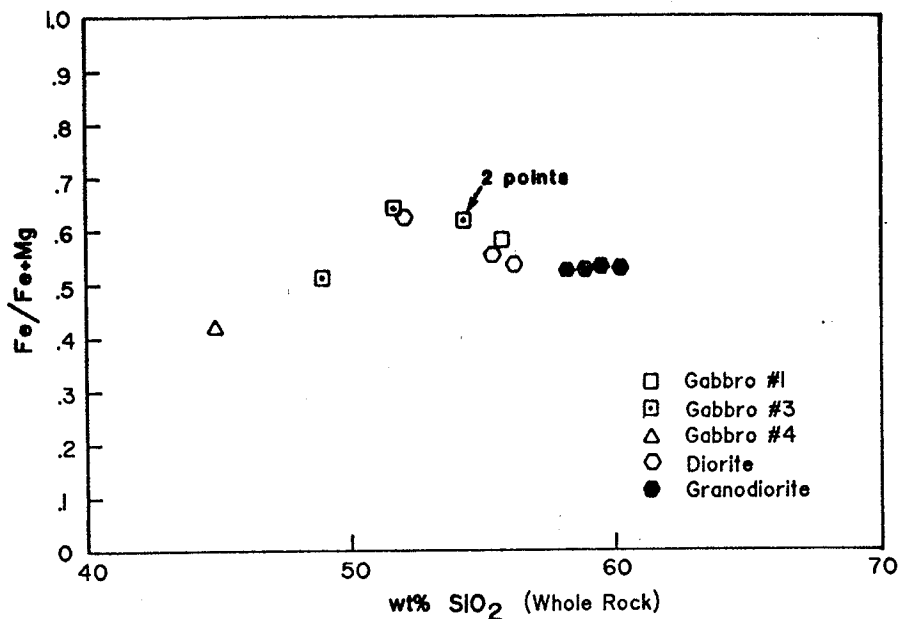


**FIGURE 18:** Plot of Fe/Fe+Mg ratios in biotite vs whole rock SiO<sub>2</sub> contents for primary biotites from rocks of the Falcon Lake Intrusive Complex.

## CHAPTER 7 ESTIMATE OF INTENSIVE PARAMETERS

Semi-quantitative estimates of the intensive parameters (namely pressure (P), temperature (T) and oxygen fugacity ( $fO_2$ )) which were likely to have prevailed during the evolution of FLIC were attempted, primarily through comparison of the existing mineral assemblages in the FLIC rocks with work done on various experimental and natural systems. It was originally anticipated that estimates of T and  $fO_2$  could be made from analysis of co-existing oxide pairs in combination with a two-feldspar geothermometer, however, these results were largely negative as discussed below.

### 7.1 Pressure and Temperature

A first approximation of the temperature-pressure conditions of emplacement for an intrusion can, in some cases be obtained, from the contact metamorphosed host rocks. As stated in section 4.2, observations relating to contact metamorphism around the FLIC are ambiguous. According to Beaubien (1988), mineral assemblages present in the host rocks suggest a hornblende hornfels facies grade of contact metamorphism with host rock temperatures of between 425°C and 600°C. According to Mandziuk et al (1989), the FLIC has a 0.5-1.0km wide aureole in which country rocks have been upgraded to amphibolite facies which would indicate temperatures of between ~475°C and 700°C and pressures up to ~8kb.

### Quartz Monzonites

Many workers use the data of Tuttle and Bowen (1958) in the granite system Qtz-Ab-Or-H<sub>2</sub>O to obtain estimates of pressure and temperature for rocks thought to represent felsic residual H<sub>2</sub>O-saturated melts. Increasing H<sub>2</sub>O content from mafic to felsic FLIC rocks is clearly evident in the increasing proportion of hydrous mafic mineral phases to the point where the quartz monzonites contain mainly biotite with subordinate amphibole. The presence of late-stage breccia pipes in the complex also indicates substantial build-up of volatiles. However, features indicative of H<sub>2</sub>O-saturation such as aplite dykes, pegmatite dykes and mariolitic cavities are rare to absent.

It is not known if any of the more felsic FLIC rocks crystallized under water-saturated conditions but the most likely candidates, for which geochemical data is available, are the quartz monzonites. Figure 19 shows normative data for the quartz monzonites plotted in the Qtz-Ab-Or-H<sub>2</sub>O system with experimentally derived minima shown for pressures ranging from 0.5 to 10 kb. The quartz monzonites lie on the feldspathic side of the minima. The positioning of the data points on the diagram could be interpreted as representing crystallization under water-undersaturated conditions at > 2 kb pressure. The data also plot in an apparent trend from lower to higher water pressures, possibly suggesting variations in P<sub>H<sub>2</sub>O</sub> during crystallization. Several of the most quartz-rich samples lie very close to the point representing a 1 kb minimum under water-undersaturated conditions and with 4.5 wt% B<sub>2</sub>O<sub>3</sub> added to the system. This serves to emphasize the possible effects that volatiles other than H<sub>2</sub>O may have on pressure. The influence of boron in the granite system might be particularly interesting with respect to the FLIC considering tourmaline was identified petrographically and by probe analysis in isolated samples of granodiorite and quartz monzonite.

Figure 20a & b show the quartz monzonites plotted in the granite system at 2 and 5 kb pressure respectively. The data points lie within the 725-760° C temperature range at 2 kb and between 690° and 700° C at 5 kb.

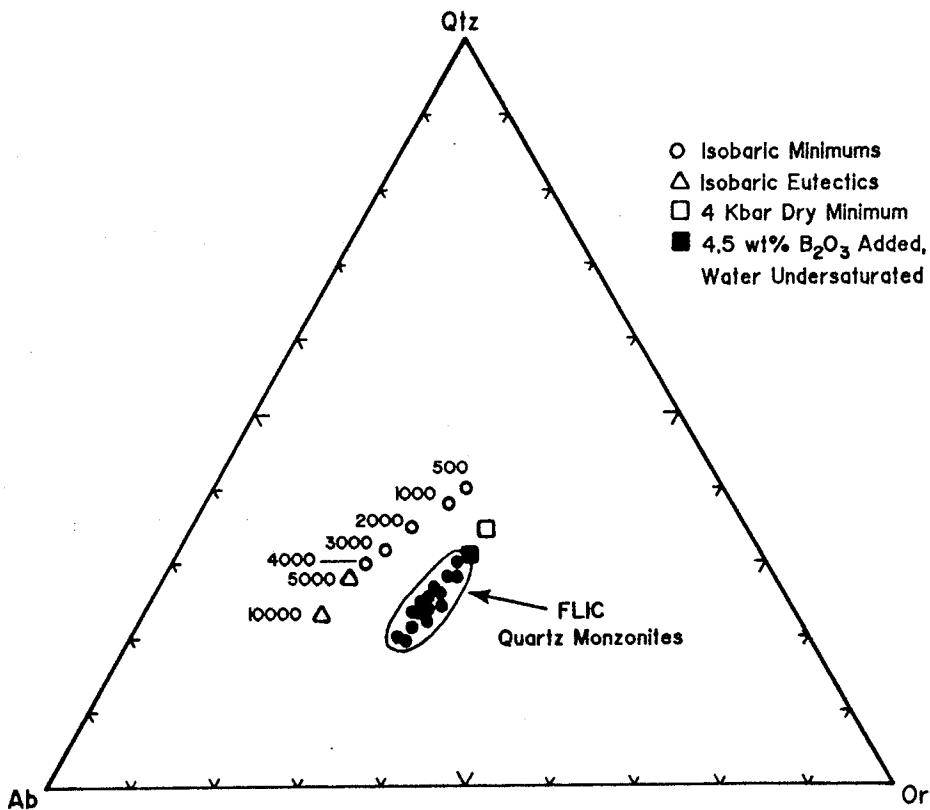


FIGURE 19: FLIC quartz monzonites plotted in the Qtz-Ab-Or-H<sub>2</sub>O system. Shown are experimentally derived minima and eutectics at P<sub>H<sub>2</sub>O</sub>s ranging from 0.5 - 10 kbar, a 4 kbar dry minimum and a 1 kbar water-saturated minimum in a system containing 4.5 wt% B<sub>2</sub>O<sub>3</sub> (Tuttle and Bowen, 1958; Luth, 1976; Manning and Pichavant, 1985). H<sub>2</sub>O pressures are given in bars. Diagram after Manning and Pichavant (1985).

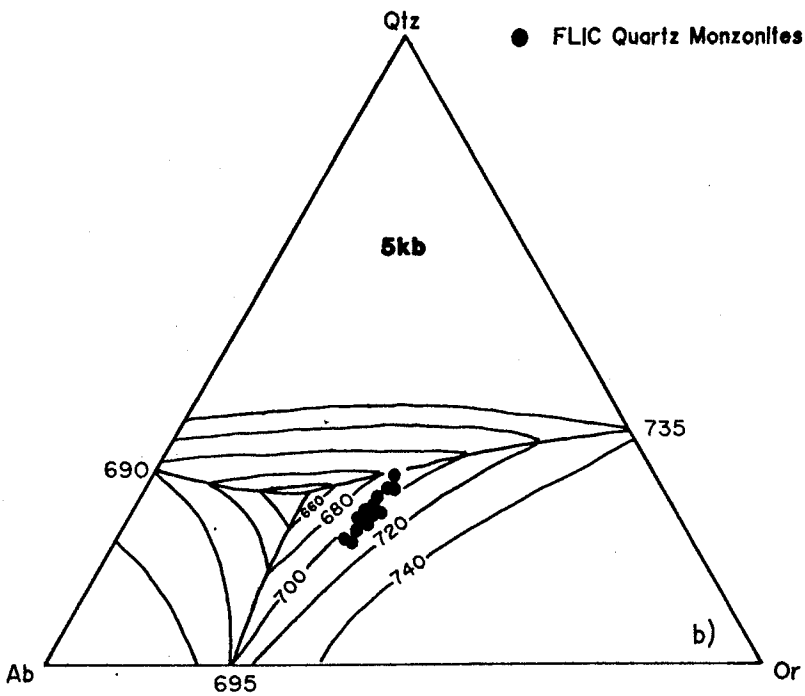
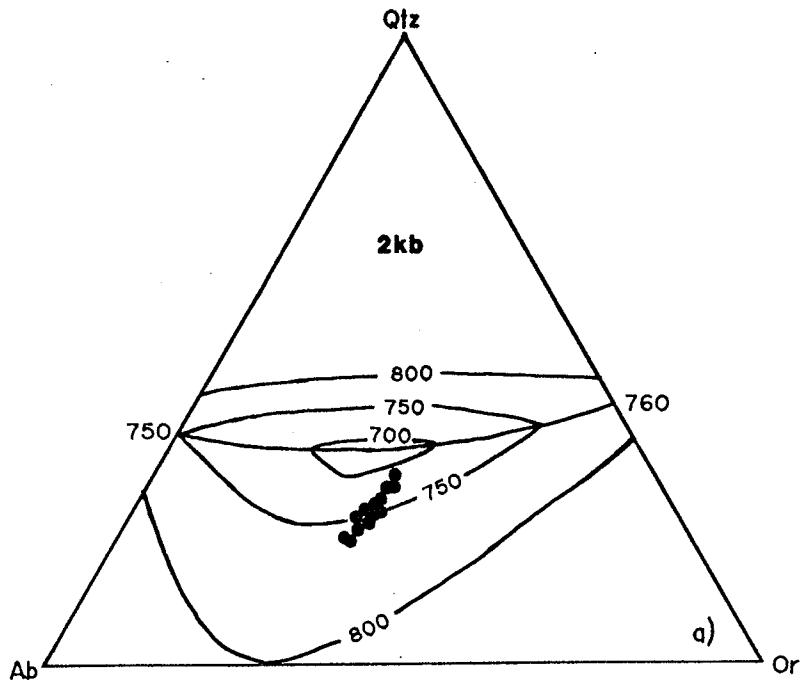


FIGURE 20: FLIC quartz monzonites plotted in the granite system at 2 kbar and 5 kbar water pressure (a and b respectively). After Tuttle and Bowen (1958), Luth et al (1964) and McBirney (1984).

### Gabbros

Comparison of a lithology with any experimental system requires assumptions to be made about the liquidus mineral phases in that rock type. Gabbroic rocks of the FLIC are dominated by cumulus textures and as such do not represent primary liquid compositions. It would therefore be erroneous to attempt pressure-temperature estimates through direct comparison of FLIC gabbros with experimental basalt systems which represent liquid equivalents. Nevertheless, experimental systems can be used to comment on specific features observed in the gabbros such as amphibole rimming and replacing pyroxene and the presence of primary hydrous mafic mineral phases (ie. amphibole and biotite).

As the FLIC is interpreted by previous workers (Mandziuk, 1989; Gibbins, 1971) to be post-metamorphic, most mafic mineral reaction textures and pseudomorphs observed in the gabbros are likely to be products of magmatic processes. The preponderance of hydrous mafic minerals and the alkali-rich nature of some of the gabbros make them amenable to comparison with the basalt water systems of Yoder and Tilley (1962).

Gabbro #1, #3 and #4 were compared to the natural alkali basalt-water and the hawaiite-water systems shown in Figure 21. Liquidus and solidus curves for an anhydrous alkali olivine basalt are also plotted in Figure 21a. Mineral stability curves in the alkali basalt-water system indicate that the assemblage plagioclase-pyroxene-amphibole (which is observed in gabbros #1 and #3) could co-exist within the hachured field shown in Figure 21a. The field is defined by water pressures ranging from 0.8-2.8kb and temperatures of 920-980°C. The same assemblage in the hawaiite-water system would be stable at about 835-950° C and 2-2.8 kb water pressure (hachured field in Figure 21b).

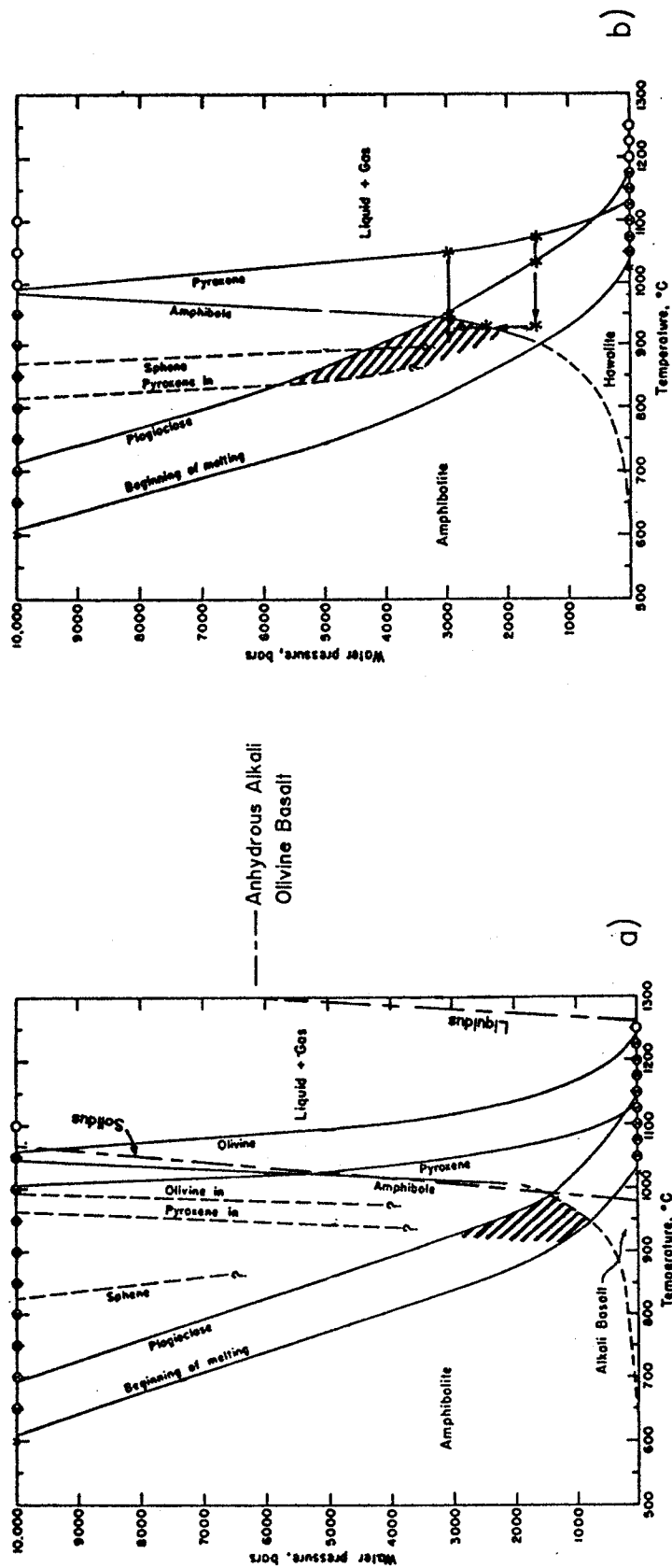


FIGURE 21: Experimental basalt-water systems. See text for discussion.

a) Natural alkali basalt-water system from Yoder and Tilley (1962). Also shown are the liquidus and solidus curves for an anhydrous alkali olivine basalt (Thompson, 1974. In Basaltic Volcanism Project, 1981).

b) Natural oxidized hawaiiite-water system from Yoder and Tilley (1962). (See text for explanation of paths marked by \* and arrows).

Formation of amphiboles in the basaltic systems noted in the previous paragraph could occur via two different types of crystallization paths under variable sets of pressure-temperature conditions. For example, a magma in the hawaiite system at  $P_{H_2O} = 3\text{kb}$  (denoted by an \* in Figure 21b) would start crystallizing pyroxene at  $\sim 1050^\circ\text{C}$ . After cooling to  $950^\circ\text{C}$ , plagioclase would start to crystallize and amphibole would start to form, probably at the expense of pyroxene. Final solidification would have to occur at temperatures  $> 890^\circ\text{C}$  if all pyroxene is not to be consumed. Alternatively, a magma in the same system at  $P_{H_2O} = 1.5\text{kb}$  (denoted by \* in Figure 21b) would start crystallizing pyroxene at  $1070^\circ\text{C}$ . A drop of only  $40^\circ$  in temperature would allow plagioclase to start crystallizing at  $1030^\circ\text{C}$ . Continued cooling at this pressure would not allow for the formation of amphibole in the rocks. However, if the system cools to  $925^\circ\text{C}$  and  $P_{H_2O}$  is increased to  $2.4\text{kb}$  at this point, amphibole will begin to crystallize. Complete solidification at this new water pressure would occur at temperatures  $> 900^\circ\text{C}$ . A practical application of variable gas pressure to crystallization is seen in the appinites of Scotland where Bowes and McArthur (1976) use increasing gas pressure to explain the presence of rhythmic amphibole overgrowths on reacted hornblende crystals with pyroxene cores.

Relict pyroxene cores were not identified in Gabbro #4, possibly suggesting lower solidification temperatures than those for the Gabbro #1 and Gabbro #3 rocks based on the position of the pyroxene out (cooling) curves in Figure 21.

#### Two-feldspar Geothermometer

Estimates of temperature were also attempted using a two-feldspar geothermometer based on the partitioning of the albite component between alkali

feldspar and plagioclase. Stormer (1975) developed a series of determinative curves from which a quick graphical estimate of temperature can be obtained (Figure 22). Most alkali feldspar grains analyzed from FLIC rocks were deemed inappropriate for use in this geothermometer since they were either perthites or perthitic microclines. Feldspar data from two granodiorite samples and one quartz monzonite sample are plotted in Figure 22. Feldspar from the granodiorites yields temperatures of 400° C or less at both 2 and 5 kb pressure. The quartz monzonite feldspar data yields temperatures of a) 450-500° C at 2 kb and 475-525° C at 5 kb and b) < 400° C at both 2 and 5 kb.

The temperatures are clearly too low to be magmatic. Stormer (1975) indicates that results may be poor for very Ca-rich or K-rich alkali feldspars. All alkali feldspars plotted here are in fact K-rich containing Or > 0.862 with two out of the four grains used being microclines. Alternatively, submagmatic temperatures could result from alteration of alkali feldspar after crystallization as suggested by Scambos (1986) who obtained low temperatures when applying the same geothermometer to rocks of the Center Pond pluton.

## 7.2 $fO_2$ and Temperature

Observed primary mineralogy may be compared with known buffer assemblages in Figure 23 to estimate the general  $fO_2$  and temperature conditions under which the rocks may have crystallized. Microprobe analysis identified ilmenite grains surrounded by or intergrown with fine grained biotite in one sample of Gabbro #1.  $fO_2$  conditions above the HM-MT (hematite-magnetite) buffer (ie.  $\log fO_2 < -10$  at temperatures above 800° C) are indicated if ilmenite is the dominant oxide phase in Gabbro #1. No comment may be made on Gabbro

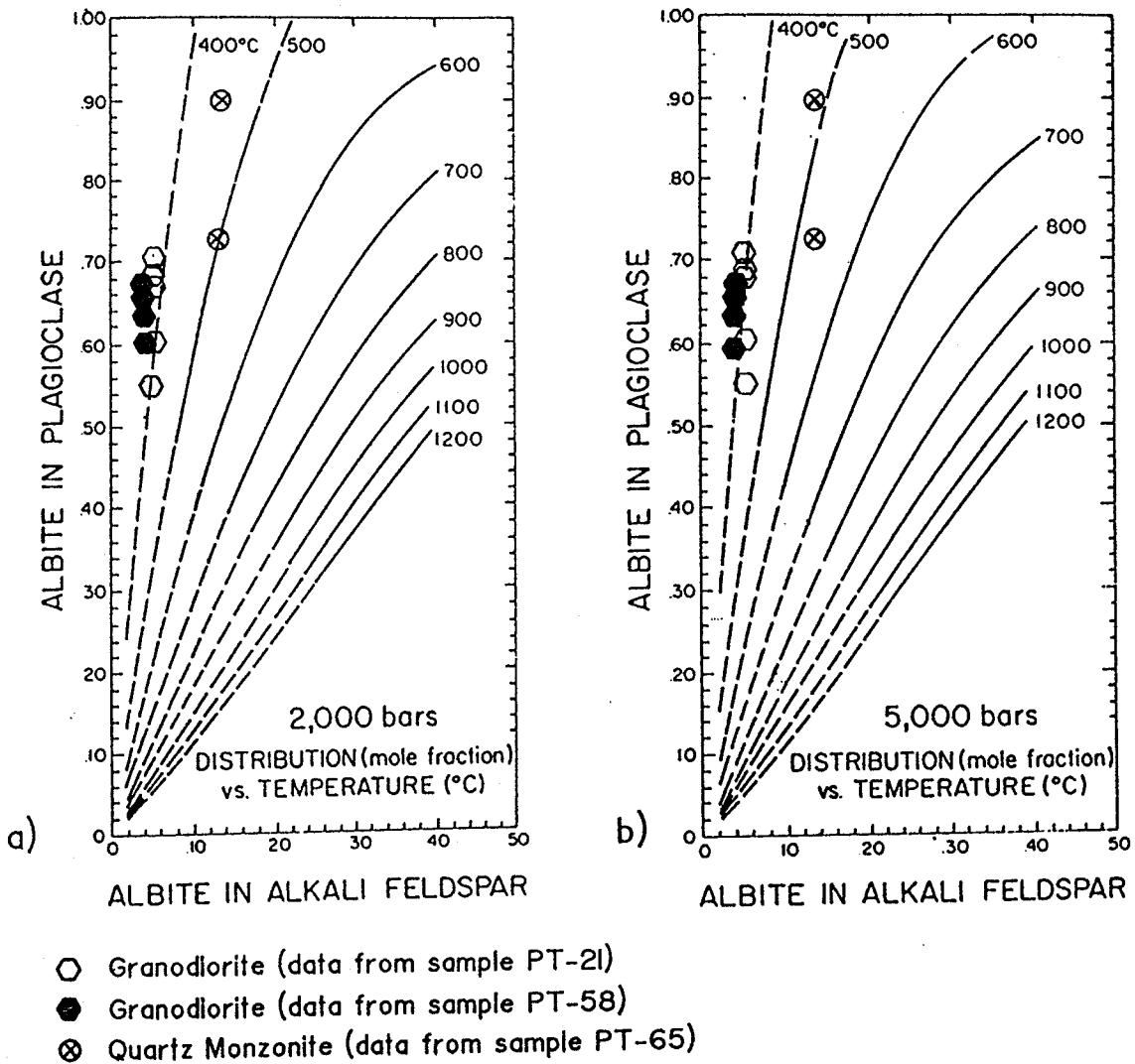


FIGURE 22: Determinative curves for temperature based on a two-feldspar geothermometer utilizing albite distribution between coexisting plagioclase and alkali feldspar (Storner, 1975). Plotted are data from two FLIC granodiorite samples and one FLIC quartz monzonite sample.

#2 since probe analyses of oxide minerals from this unit are lacking. In all other rock types of the FLIC, magnetite appears to be the dominant oxide mineral phase indicating  $f_{O_2}$ -T conditions between HM-MT and FA-MT-QTZ (fayalite-magnetite-

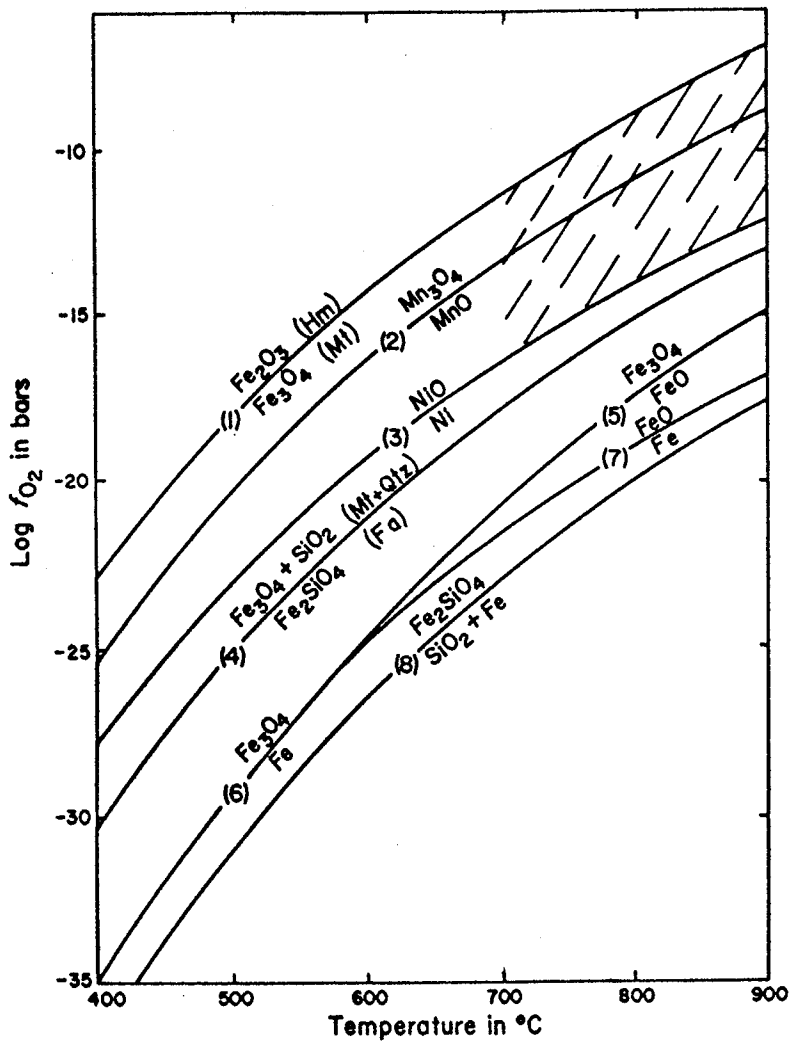


FIGURE 23:  $f_{O_2}$  vs temperature diagram for selected buffer assemblages from Ernst (1976). Shaded area represents possible range of  $f_{O_2}$ -T conditions prevailing during crystallization of rocks from the Falcon Lake Intrusive Complex (excluding Gabbro #1 and Gabbro #2).

quartz) assemblages. At temperatures between 700° and 900° C, this area corresponds to  $\text{Log } f\text{O}_2 = -17$  to  $> -10$  as shown by the shaded area in Figure 23. In addition to magnetite, possible primary ilmenite was identified in one sample of Gabbro #3 and one sample of granodiorite indicating slightly higher  $f\text{O}_2$  than those given above.

Application of a geothermometer based on co-existing Fe-Ti oxides (Anderson, 1985) to grains of magnetite containing intergrowths of ilmenite in gabbros #3 and #4 yielded unrealistically low temperatures and  $f\text{O}_2$  (see Table 13). This supports the contention made in Chapter 6 that the ilmenite intergrowths in magnetite are the result of oxidation. Re-equilibration of oxide minerals is further indicated by the presence of titanite rims around many of the oxide grains.

### 7.3 Summary

Pressures under which rocks of the FLIC crystallized could not be precisely determined but a consideration of the metamorphic grade exhibited by the host rocks in combination with estimates made from quartz monzonites in the granite system indicate pressures between 2 and 8 kb. Comparison of observed mineral assemblages with basalt-water systems suggest a minimum temperature range of 835°-920°C. Temperatures were probably between 690 and 760° C when the quartz monzonites crystallized based on comparisons with the Qtz-Ab-Or-H<sub>2</sub>O system. Oxygen fugacity appears to have been high ( $\text{Log } f\text{O}_2 > -17$  bars) throughout the crystallization history of the pluton as indicated by the occurrence of magnetite and/or ilmenite in all phases of the complex.

Table 13

Calculated temperatures and  $fO_2$ 's for co-existing Fe-Ti oxides in gabbros from the Falcon Lake Intrusive Complex. Calculations after the method of Anderson (1985) using the computer program "GPP" (McBirney, 1984).

<u>Mt-II Pair</u>	<u>Temperature</u> <u>°C</u>	<u>Mol Fraction Ulspl</u> <u>Mol Fraction Il</u>	<u>Log(10) <math>fO_2</math></u>	Key: Mt = Magnetite Il = Ilmenite Ulspl = Ulvöspinel
73-8B (Mt) 73-8A (Il)	573	0.036 0.956	-20.107	
73-10A (Mt) 73-10B (Il)	476	0.013 0.977	-25.037	
34-3B (Mt) 34-3A (Il)	544	0.038 0.968	-22.165	
34-10A (Mt) 34-10B (Il)	588	0.056 0.958	-20.055	

Sample Descriptions

73-8B & A: Fine grained euhedral magnetite in Gabbro #3 with ilmenite lamellae and inter-granular ilmenite (Gabbro #3) exsolutions. No titanite rim.

73-10A & B: Fine grained euhedral magnetite in Gabbro #3 with ilmenite lamellae and internal sandwich-type (Gabbro #3) exsolutions. No titanite rim.

34-3A & B: Fine grained euhedral magnetite in Gabbro #4 with ilmenite core. No titanite rim. (Gabbro #4)

34-10A & B: Fine grained euhedral magnetite occurring as an inclusion in an amphibole grain. Contains what (Gabbro #4) appear to be ilmenite exsolutions.

## CHAPTER 8

## DISCUSSION AND PETROGENESIS

## 8.1 General Statement

The Falcon Lake Intrusive Complex is comprised of a genetically related suite of rocks exhibiting normal compositional zoning from outer, older mafic rock types inward to younger felsic rock types. A number of different mechanisms, particularly pertinent to zoned plutons, have been proposed for the generation of a suite of rocks comprising a large compositional range: fractional crystallization (Barnes, 1983; Tindle and Pearce, 1981; Perfit et al, 1980; Bateman and Chappell, 1979; Brown et al, 1979; Bateman and Nokelberg, 1978; Erikson, 1977; Raglan and Butler, 1972), partial melting and unmixing of a single parental source (Scambos et al, 1986), assimilation of different wallrocks (McBirney, 1984) and multiple intrusion of separate magmatic pulses (Mandziuk, 1989; McBirney, 1984). Magma mixing may play a subordinate evolutionary role as advocated by Barnes (1987) in the case of the Wooley Creek Batholith and Frost and Mahood (1987) for the Lamarck Granodiorite. In any given pluton, field, petrographic, geochemical and/or isotopic data may suggest the operation of a combination of the above processes. Specific features of the rocks may also indicate a host of other internal processes such as crystal accumulation, flow differentiation, convection, density currents and liquid state diffusion.

Various origins have been proposed for the FLIC including fractional crystallization (Brownell, 1941; Gibbins, 1967), assimilation (House, 1955) and multiple intrusion (Mandziuk, 1988). The following discussion attempts to identify and evaluate processes which may have been important in the evolution of the

complex based largely on geochemical data of unlayered rocks. Geochemistry is inseparable from field and petrographic data as well as the observations and hypotheses of previous workers, and as such, attempts have been made to integrate all layers of data into the discussion where applicable.

## 8.2 Differentiation and Liquid Lines of Descent

The suite of rocks comprising the FLIC appears to represent a differentiated series as indicated by relatively continuous increases in silica content coreward, the broad compositional spectrum of rock types present and well-defined trends on AFM and Harker variation diagrams. The continuous trends of a) decreasing FeO, Fe<sub>2</sub>O<sub>3</sub>, MgO, MnO, CaO, TiO<sub>2</sub> and P<sub>2</sub>O<sub>5</sub> as well as increasing K<sub>2</sub>O and Na<sub>2</sub>O with increasing SiO<sub>2</sub> (Figure 11) and b) decreasing normative An, Di, Ol, Ap, Mt, Il as well as increasing Q, Or and Ab with increasing SiO<sub>2</sub> (Section 5.2) are particularly diagnostic of a differentiated series. Closer inspection, however, of geochemical plots in Figures 7 through 12 as well as Figure 24 reveals a large amount of overlap amongst the gabbroic units as well as amongst Gabbro #3, Gabbro #4 and the dioritic rocks. A single liquid line of descent encompassing all lithologic phases cannot account for the observed overlap, making a simple scenario of in-situ fractional crystallization of one magmatic pulse improbable.

Mandziuk (1989) documented the existence of sharp intrusive contacts between different phases of the FLIC and suggested a sequential emplacement history from outer, oldest mafic intrusion A (Gabbro #1) through to inner, youngest felsic intrusion F (quartz monzonite). Consequently, his model for the formation of the complex involved periodic tapping of a deeper differentiating magma chamber with early dyke-like and later diapir-like ascent of magma in a

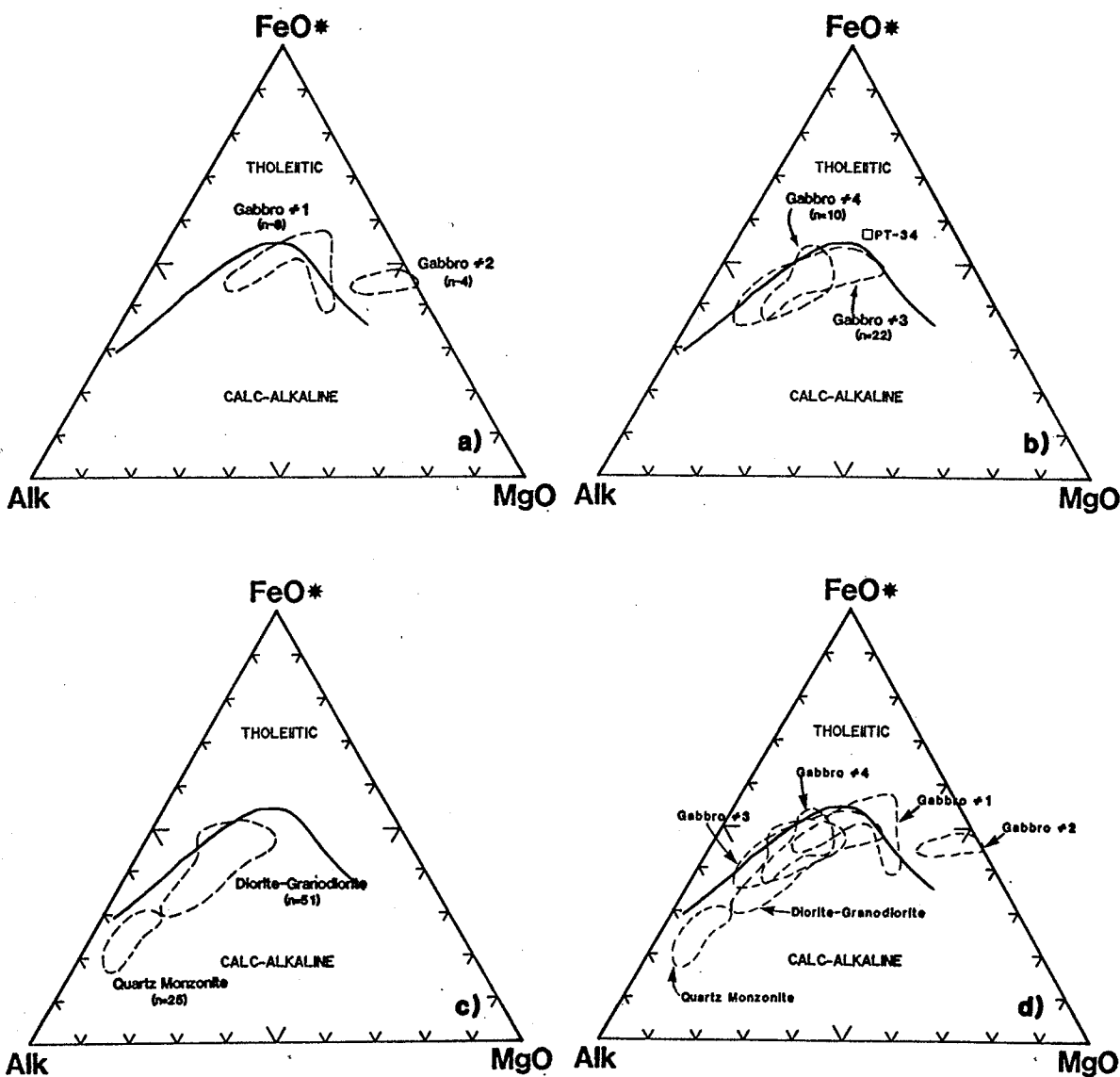


FIGURE 24: AFM Diagrams for Rock Types of The Falcon Lake Intrusive Complex.

- a) Gabbros #1 and #2
- b) Gabbros #3 and #4
- c) Diorite-Granodiorite and Quartz Monzonite
- d) All Rock Types

Fields shown for each rock type are based on the same data set used in previous geochemical plots except for the five mineralogically and compositionally anomalous samples (PT-164, PT-153, PT-94, PT-157 & PT-169A) which are not plotted.

common conduit. Geochemical data supports the existence of separate batches of magma giving rise to the gabbroic portion of the complex, but indicates a more complex history than simply successive intrusions of progressively more differentiated magma.

### 8.3 Relationship Between Gabbroic Units

Broad petrological and geochemical similarities exist between Gabbro #1 and Gabbro #2 as well as between Gabbro #3 and Gabbro #4:

1. Gabbro #1 and #2 are the most primitive of the gabbros as indicated by their lower average Rb, Zr, total REE and LREE abundances.
2. Gabbro #1 and #2 plot largely in the subalkaline field on a alkali vs silica diagram (Figure 7) whereas Gabbro #3 and #4 lie in the alkaline field.
3. Unlayered rocks of Gabbro #3 and Gabbro #4 are texturally distinct, both displaying cumulus textures consisting of a framework of coarse grained plagioclase with irregularly-shaped interstitial mafic mineral aggregates which include primary biotite.
4. Gabbro #3 and #4 have comparable trace element and REE contents and display the highest LREE enrichments of all the gabbros. Distinct Eu anomalies are also lacking for Gabbro #3 and #4.

A more detailed analysis of the data also reveals differences between Gabbro #1 and #2 as well as between Gabbro #3 and #4. Gabbro #2 stands out as the most primitive of all the gabbros comprising rocks of tholeiitic affinity which border on ultramafic compositions (eg. samples PT-75 and PT-148). All samples

studied contain normative olivine, are silica-saturated to under-saturated and have the lowest total REE and LREE contents (Figure 13a). In addition, plagioclase from Gabbro #2 has the highest An contents<sub>(An<sub>59.5-66.6</sub>)</sub> and amphiboles, which appear to be secondary after pyroxene, have the highest Mg/Mg+Fe<sup>2+</sup> ratios (Figure 17). Mineralogically, Gabbro #2 differs from Gabbro #1 in its greater abundance of mafic minerals (including abundant cumulus pyroxene) and general absence of interstitial K-feldspar.

Differences between Gabbro #3 and #4 are more subtle and confined mainly to mineralogical and geophysical data with Gabbro #4 rocks being strongly magnetic and lacking interstitial K-feldspar. Specific gravity and magnetometer surveys over parts of the complex also indicate that Gabbro #4 forms a distinct specific gravity low and magnetic high in comparison to the other FLIC rock types (cf. Gibbins, 1967 and Johanasson, 1985 respectively).

The above observations collectively outline at least three geochemically distinct and four petrologically distinct gabbroic units. The overlap of major and trace element data observed in variation diagrams (Figures 11 and 12), however, precludes the four gabbroic units from being successive intrusions of more differentiated magma. Gabbro #1 and Gabbro #2 are clearly the more primitive of all the gabbros with Gabbro #2 being the most primitive rock type based on geochemistry.

#### 8.4 Relationships Between Diorite-Granodiorite and Quartz Monzonite

Smooth transitions in major and trace element geochemistry (Figure 24, Figure 25 and Figure 26) are observed in progressing from the diorite-granodiorite to quartz monzonite with neither compositional overlap nor a compositional hiatus

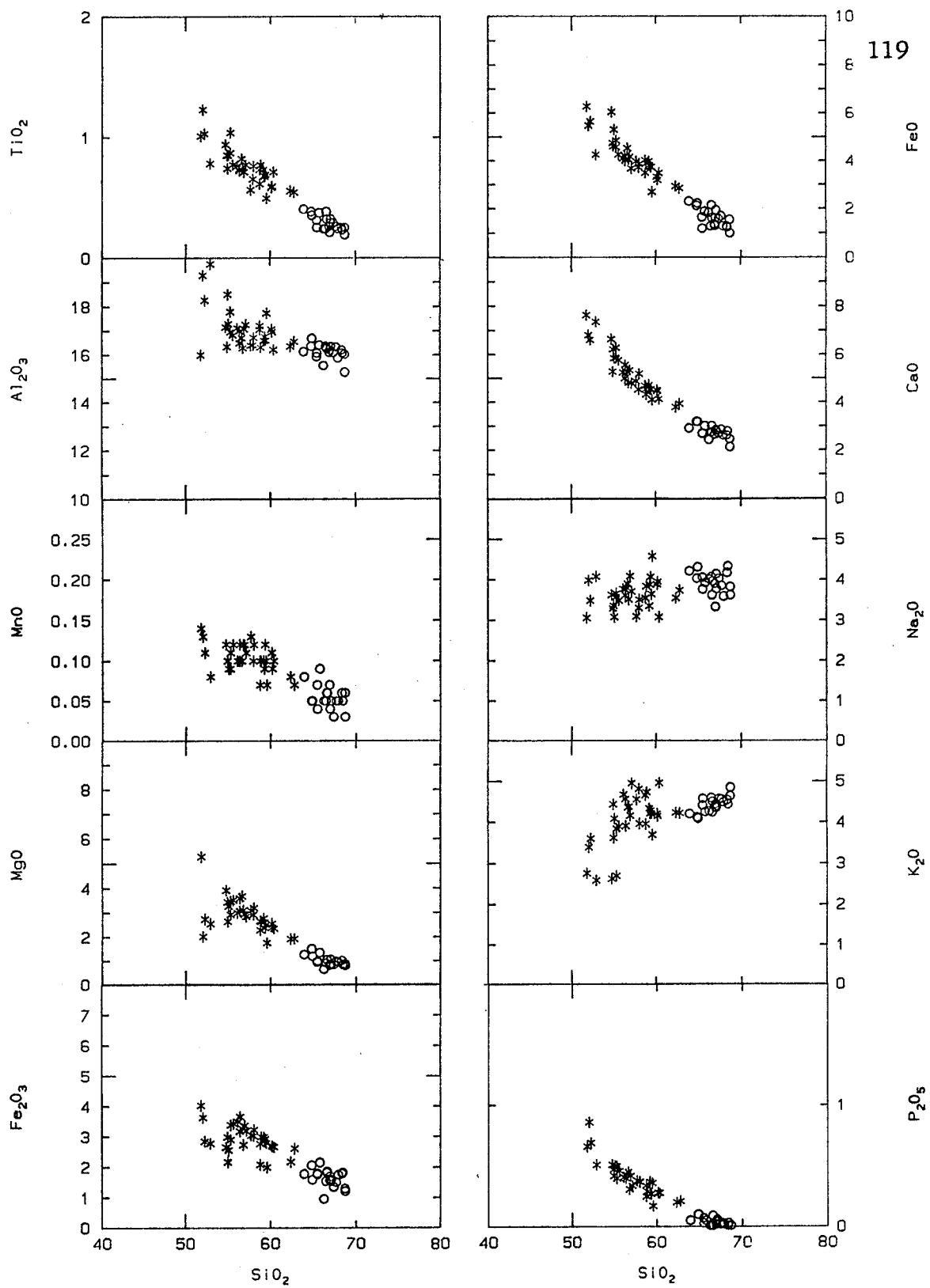


FIGURE 25: Harker variation diagrams for the diorite-granodiorite and quartz monzonite samples. All data are expressed in wt%.  
 \* = Diorite-Granodiorites o = Quartz Monzonites

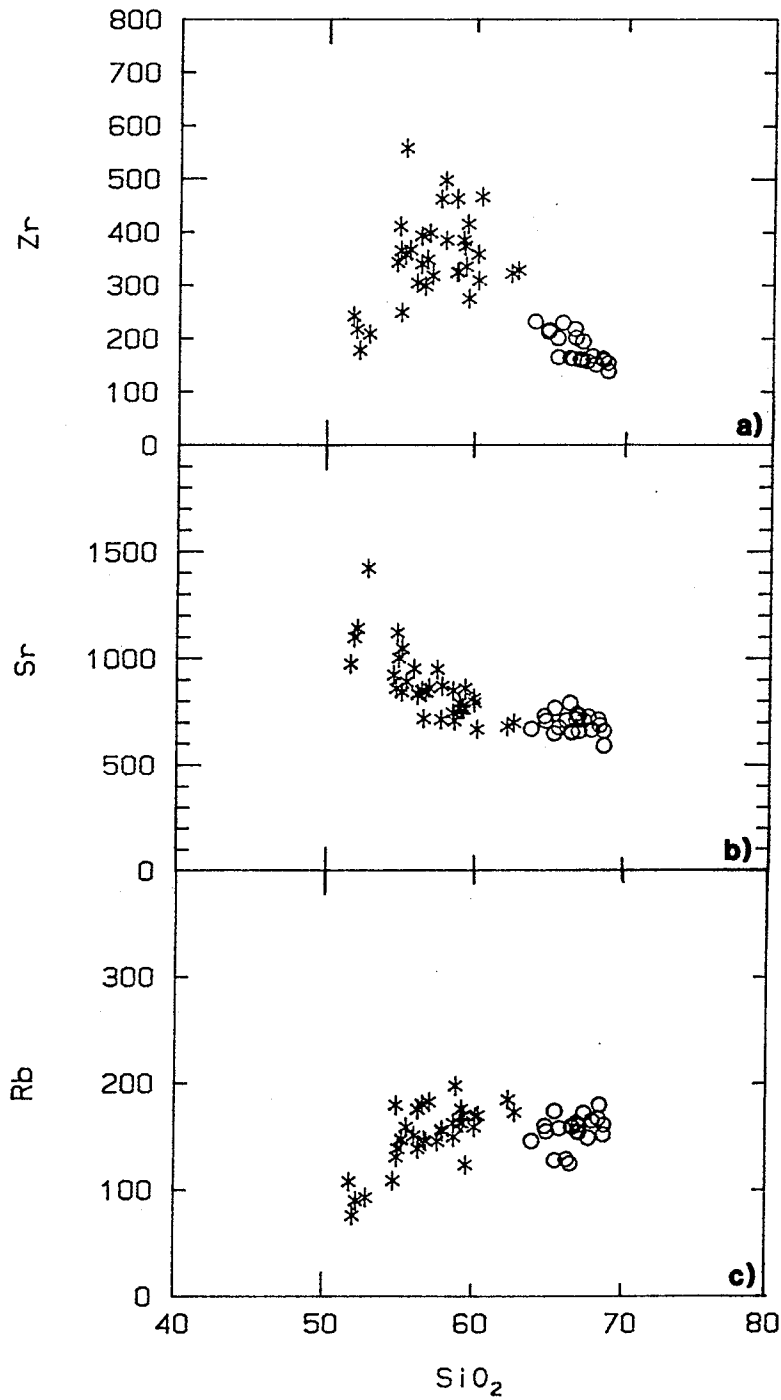


FIGURE 26: Trace element variation diagrams for the diorite-granodiorite and quartz monzonite samples.  $\text{SiO}_2$  is in wt%, trace elements are in ppm.

a) Zr vs  $\text{SiO}_2$    b) Sr vs  $\text{SiO}_2$    c) Rb vs  $\text{SiO}_2$

\* = Diorite-Granodiorites

o = Quartz Monzonites

being observed. The linear to curvilinear trends of  $\text{TiO}_2$ ,  $\text{FeO}$ ,  $\text{CaO}$ ,  $\text{MnO}$ ,  $\text{MgO}$ ,  $\text{Fe}_2\text{O}_3$  and  $\text{P}_2\text{O}_5$  with increasing  $\text{SiO}_2$  and increasing  $\text{K}_2\text{O}$  and  $\text{Na}_2\text{O}$  with increasing  $\text{SiO}_2$  (Figure 26) are compatible with a single liquid line of descent as well as with a system dominated by fractional crystallization. The close coherence between the Harker diagram trends of Ca and Sr as well as Rb and  $\text{K}_2\text{O}$  stress the importance of feldspar crystallization in the evolution of these FLIC rock types. Sharp deflections in major and trace element (vs silica) trends typically signal the appearance of a new crystallizing mineral phase or, conversely the disappearance of a particular mineral phase. The deflection in the  $\text{K}_2\text{O}$  vs  $\text{SiO}_2$  plot is best explained by the transition from plagioclase phenocrysts in the granodiorites to mainly K-feldspar phenocrysts in the quartz monzonites.

The observed geochemical, textural and mineralogical continuum from dioritic to granodioritic to quartz monzonitic rocks argues strongly for their origin from one fractionally crystallizing magma. However, a strictly in-situ process is complicated by the existence of a sharp intrusive contact between granodiorite and quartz monzonite (Plate 12). The contact indicates a physical separation such that the felsic residual magma (ie. quartz monzonite) intruded granodiorite. The lack of chilling along the contact suggests that intrusion of quartz monzonite occurred before complete cooling and crystallization of the granodioritic rocks.

The presence of internal contacts in a sequence of rocks exhibiting concentric compositional zoning can result from one of two processes: multiple injection of magmas which differentiate in a separate magma chamber or movements or intrusion of mobile "core" magma into consolidated or partially consolidated marginal rock, in some cases breaking through solidified carapaces (Bateman and Chappell, 1979, Pitcher, 1978). With respect to the granodiorite-quartz monzonite

contact in the FLIC, geochemical continuity and time constraints argue against the first scenario and in favour of the second. In addition, compositional variations, the textural transitional from cumulate to inequigranular porphyritic textures and the coreward decrease in the abundance of well-defined layering suggest that the evolution of the diorite-granodiorite unit took place in a more closed, static system compared to the gabbroic units.

In a closed, static system, concentric compositional zonation can be accompanied by crystallization at the walls, floor and roof of the chamber causing displacement of the residual melt and volatiles to the core area (Bateman and Chappell, 1979, Pitcher, 1978). Subsequent decreases in the density and increases in volatile content could lead to upward movement and perhaps convective homogenization of the mobile residual magma. Such a model seems plausible for the core rocks of the FLIC. Liquid densities calculated after the method of Bottinga and Weill (1970) are slightly lower for the quartz monzonites than for the granodiorites (Appendix 1) and mafic minerals found in the quartz monzonites are primarily hydrous phases (biotite and amphibole) signifying a high water content. Late stage build up of volatiles can also account for the presence of breccia pipes in the core rocks as suggested by Gibbins (1971). Upward intrusion of quartz monzonite, possibly involving stoping, would aid in explaining the localized concentration of both cognate and country rock inclusions along the granodiorite-quartz monzonite contact and the presence of widely dispersed micro-xenoliths, of apparently sedimentary origin, throughout the core rocks.

## 8.5 Trace Elements

### 8.5.1 Rb and Sr

Sr and Rb contents decrease and increase respectively with increasing SiO<sub>2</sub> (Figure 12) progressing from Gabbro #3 and #4 through to granodiorite and level off in quartz monzonite. The variation diagram trends for Rb display a strong coherence with that of K<sub>2</sub>O. In a like manner, Sr and CaO closely correlate except for the Gabbro #1 and Gabbro #2 data. Collectively the above features suggest that feldspar crystallization was of primary importance in the evolution of most of the FLIC rock types. The high CaO contents coupled with low Sr contents in Gabbro #1 and #2 appear to reflect the crystallization of a Ca-rich mafic mineral(s) (such as clinopyroxene) as opposed to plagioclase crystallization in the other gabbros.

The relationship between trace element geochemistry and crystal fractionation are illustrated in Figure 27 which contains a series of log Rb vs log Sr plots onto which mineral vectors and data from the various FLIC rock types are plotted. Mineral vectors were calculated using a Rayleigh fractional crystallization model according to the following equation:

$$Cl/Co = F^{(Kd-1)}$$

- where
- Co = concentration of a given trace element in the original melt
  - Cl = concentration of a given trace element in the residual melt
  - F = weight fraction of melt remaining
  - D = bulk distribution coefficient for a given trace element
  - Kd<sup>i</sup> = mineral/melt weight distribution coefficient of a given trace element in phase i

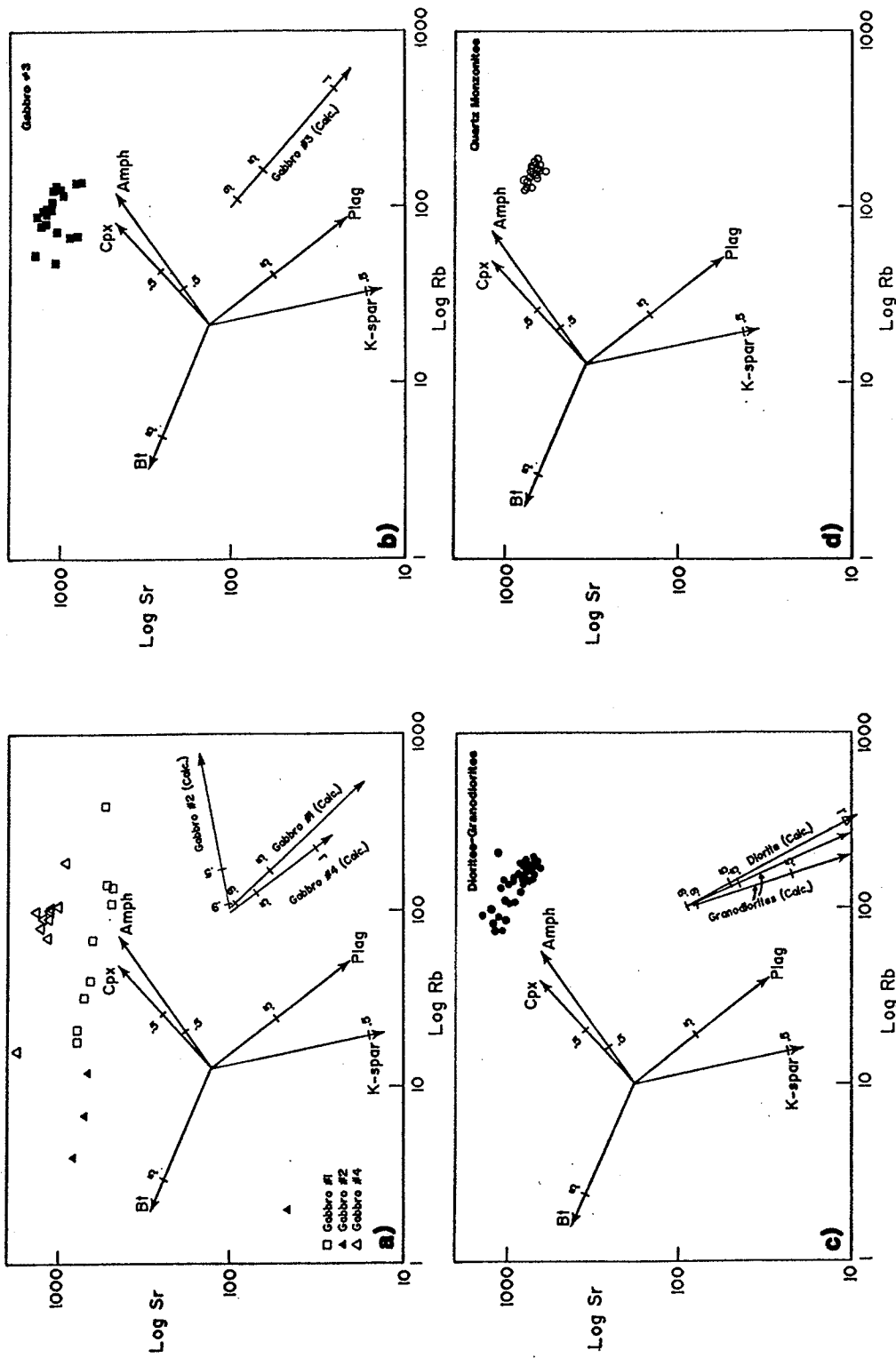


FIGURE 27: Log Rb vs Log Sr Diagrams. All data plotted for each rock type except samples PT-164, PT-153, PT-94, PT-157 and PT-169A. Mineral fractionation vectors calculated assuming Rayleigh fractionation and using  $K_p$  values in Table 14. a) Gabbro #1, #2 and #4 b) Gabbro #3 c) Diorite-Granodiorite d) Quartz Monzonite

(After Cox et al, 1979; Tindle and Pearce, 1981; Hanson, 1978).

Rayleigh fractionation as defined by McBirney (1984) is "crystallization in which crystals are segregated from the liquid and do not re-equilibrate as crystallization advances". As such, this model is more applicable to the FLIC rocks than an equilibrium fractional crystallization model, particularly in the case of the gabbroic and dioritic cumulate-textured rocks.

The D values used in the calculation of various mineral vectors are given in Table 14. It should be noted that the accuracy of calculated CI values is strongly dependent on the choice of distribution coefficients, which for some minerals, can be heavily influenced by the melt composition and temperature and thus are subject to change during fractional crystallization (Cox et al, 1979; Tindle and Pearce, 1981). The arbitrary Co values used were 100 ppm for each Rb and Sr.

Rb-Sr data for Gabbro #1, #2 and #4 are shown in Figure 27a. Data for Gabbro #2 is scattered whereas that of Gabbro #4 is largely overlapping with that of Gabbro #3 (Figure 27b). Gabbro #1, however, appears to display a trend, which on comparison with mineral vectors, could be dominated by clinopyroxene  $\pm$  amphibole crystallization with some plagioclase crystallization. In Figures 27b and c respectively, the Gabbro #3 and diorite-granodiorite data define two short similar trends which appear to be controlled mainly by plagioclase crystallization and minor mafic mineral crystallization.

The quartz monzonites (Figure 27d) are unique in that a tight clustering of data points is observed suggesting little fractionation of Rb and Sr occurred during the formation of this unit, even though the rocks span a SiO<sub>2</sub> range of approximately 5%. Restricted amounts of trace element fractionation would be expected if the entire quartz monzonite unit crystallized over a short time

**TABLE 14**  
**Rb and Sr Mineral Distribution Coefficients**

Rb and Sr distribution coefficients for clinopyroxene, plagioclase, amphibole, Fe-mica and K-feldspar. Values are those given in Cox et al (1979).

A = intermediate or acidic liquid compositions

B = basaltic liquid composition

MINERAL		Rb	Sr
Clinopyroxene	A	0.03	0.50
	B	0.001	0.07
Amphibole	A	0.01	0.02
	B	0.30	0.50
Fe-mica	A	2.0	-
	B	3.1	0.08
Plagioclase	A	0.04	4.4
	B	0.07	2.2
K-feldspar		0.4	4.0

**TABLE 15**  
**Estimated Modal Mineralogy**

Modal mineralogy used in calculation of bulk rock vectors shown in Figure 28. Percentages of minerals were derived from point counting data on stained rocks slabs (Table 2) in combination with visual estimates of rock slabs and/or thin sections. (Quartz and accessory minerals omitted).

PLAG = Plagioclase CPX = Clinopyroxene AMPH = Amphibole BT = Biotite

K-SPAR = K-feldspar

ROCK TYPE	PLAG	CPX	AMPH	BT	K-SPAR
Gabbro #1	65%	-	25%	5%	5%
Gabbro #2	25%	25%	46%	3%	1%
Gabbro #3	63%	12%	15%	7%	3%
Gabbro #4	62%	-	20%	18%	-
Diorite	54%	5%	12%	12%	17%
Granodiorite	46%	3%	15%	11%	25%
Granodiorite	47%	3%	13%	10%	27%

span and/or if this unit underwent convective homogenization. In his petrogenetic model of the complex, Gibbins (1967) also suggested rapid cooling and crystallization of the quartz monzonite core. Gibbins (1971) further speculated that during the latest stages of activity,  $P_{H_2O}$  exceeded  $P_{confining}$  causing resurgent boiling and giving rise to the following series of features associated with the core rocks: breccia pipes, textural homogeneity of the core rocks, finer grain size and porphyritic textures and locally brecciated inner contact. Also of interest to note is that a log Rb vs log Sr plot of all the FLIC rock types (mafic to felsic) does not display a single continuous linear trend, precluding a single liquid line of descent. In fact, a large amount of overlap occurs between Gabbro #3 and diorite-granodiorite samples and complete overlap occurs between quartz monzonite and more felsic granodiorite samples.

As stated by Hanson (1978), "A common misconception is that the trace element composition of a rock is controlled by the mineral present...". In order to evaluate the extent to which the observed trends for Gabbro #1, Gabbro #3 and the diorite-granodiorites in Figure 27 could be explained by fractionation of the actual minerals present in the rock, bulk rock vectors for each rock type were calculated and have been added to Figures 27a-c. Vectors were calculated using the same Rayleigh fractionation model as described earlier but substituting D for Kd where  $D = \sum X^i Kd^i$  and  $X^i$  = weight fraction of phase i in the solid. The modal mineralogy used was taken from point counting data on stained rock slabs (Table 2) in combination with visual petrographic estimates and is listed in Table 15.

The calculated bulk rock vector for Gabbro #1 (Figure 27a) is subparallel to the plagioclase vector but is dissimilar from the actual Gabbro #1 trend suggesting that evolution of this phase involved earlier crystallization and

separation of one or more Ca-rich mafic mineral phases in which Sr is incompatible. Gabbro #2 represents the only phase of the complex containing rocks transitional to ultramafic compositions and containing cumulus mafic minerals. A bulk rock vector calculated for a pyroxenitic Gabbro #2 sample (PT-74) is also plotted in Figure 27a and is consistent with dominantly clinopyroxene ( $\pm$  amphibole) and minor plagioclase fractionation.

The bulk rock vector for Gabbro #3 (Figure 27b) is very similar to the observed trend supporting the role of plagioclase fractionation (and accumulation?) in the formation of this unit.

Three bulk rock vectors representing a spectrum of progressively more differentiated compositions were calculated for the diorite-granodiorite (Figure 27c). These vectors are consistent with a scenario whereby the fractionation of K-feldspar  $\pm$  biotite are of increasing importance as the rocks evolve from diorite to granodiorite compositions. The trend of data points for this unit is more similar in slope to that of the plagioclase vector than to the calculated bulk rock vectors but, in general, is compatible with fractionation of plagioclase and variable proportions of K-feldspar and mafic minerals which agrees well with observed mineralogy.

In the preceding discussion, Rayleigh fractionation was used as a first approximation in commenting on the relationship between trace element geochemistry and fractionation of specific mineral phases. The effect of changing bulk distribution coefficients with differentiation and the precise nature of the crystal-liquid fractionation which may have occurred cannot be evaluated. Alternative models might include accumulated Rayleigh fractionation and equilibrium fractionation which are applicable to closed systems.

### 8.5.2 Zr, Nb

Ionic radius and charge are the two main factors governing incorporation of trace elements into the lattice of major mineral phases (Cox et al, 1979). The +4 charge on Zr makes this element incompatible in virtually all major mineral phases. Thus Zr contents in the FLIC rocks are more likely controlled by the distribution of the accessory mineral zircon. Zircon was observed petrographically only Gabbro #1, but may have remained undetected in other rock types due to its fine grain size.

A non-linear trend for Zr variation with increasing silica, similar to that observed in the FLIC rocks, is documented by Sawka (1987) in the zoned McMurray Meadows Pluton where Zr contents increase in outer granodioritic rocks and then decrease in the inner granitic rocks. Sawka (1987) attributed this trend to progressive zircon accumulation in sidewall granodiorites, resulting in a decrease in Zr in the melt fraction. In the FLIC, zircon crystallization in the gabbroic and dioritic-granodioritic rocks (maximum 58% SiO<sub>2</sub> content) may have caused the residual melt to be depleted in this element, accounting for the trend seen in Figure 12a.

A similar, though more scattered, non-linear variation is observed for Nb suggesting that Nb contents are closely tied to those of zircon. The ionic radius and charge of Nb make it amenable to substitution for Zr in the zircon lattice. However, titanite can also accommodate small amounts of Nb (in substitution with Ti). Incorporation of some Nb into this mineral, which is found in the Gabbro #4, diorite-granodiorites and quartz monzonites, could account for observed scatter on the Nb vs SiO<sub>2</sub> plot.

## 8.6 Rare Earth Elements (REEs)

Excluding Gabbro #1 and #2, all FLIC rock types contain significant total REE contents (approximately 196-537 ppm), have high La/Lu<sub>CN</sub> ratios (32-71) and display strong LREE-enriched chondrite normalized patterns (Figure 13). Gabbro #2 stands out as the most primitive gabbro phase having the lowest total REE contents and displaying the flattest, though still distinctly LREE-enriched, chondrite-normalized patterns. REE characteristics of Gabbro #1 are transitional between those of Gabbro #2 and Gabbro #3. In general, the LREE-enrichment displayed, in varying degrees, by all rocks of the complex is further evidence of their genetic relationships. REE trends in Figure 13e are inconsistent with the evolution of the FLIC rocks via a single liquid line of descent, however progressive increases in the total REE and LREE contents are observed in progressing from Gabbro #2 to Gabbro #1 to Gabbro #3. The nearly identical chondrite-normalized patterns of the Gabbro #3, Gabbro #4 and diorite-granodiorite samples are compatible with derivation from a common LREE-enriched parental magma. The similar REE contents of these rock types correlates well with the large amount of overlap between these phases on major and trace element variation diagrams.

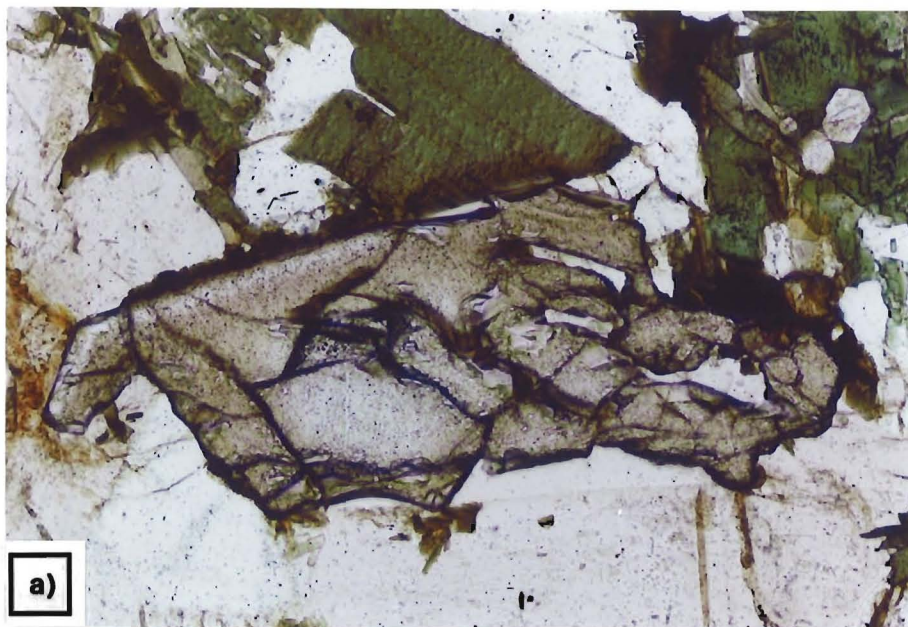
Recent studies (Sawka, 1987; Sawka et al, 1984; Gromet and Silver, 1983) have emphasized the importance of accessory mineral phases such as allanite, titanite, apatite and monazite on REE contents, particularly in felsic systems. For example, the study by Gromet and Silver (1983) on REE distribution in a Peninsular Range granodiorite revealed that titanite and allanite together contained 80-95% of each REE whereas plagioclase, alkali feldspar, biotite, epidote and apatite each accounted for  $\leq 1\%$  of each REE. The patterns of extreme LREE-enrichment in the Gabbro #3, Gabbro #4, diorite-granodiorite and quartz

monzonite samples are most likely attributable to fractionation of allanite and/or apatite for which  $K_d$ 's can be exceedingly high (eg.  $K_{d_{La}}$  for allanite = 820; Henderson, 1984). Both of these minerals are accessory phases in each of these rock types, typically occurring as subhedral to euhedral grains in close proximity to, and locally included within, mafic minerals. Euhedral grains appear to represent early primary mineral phases (Plate 18a) but rounded, corroded, metamict allanite grains (Plate 18b) were observed in one Gabbro #3 sample and suggest that Gabbro #3 chemistry was not in equilibrium with allanite.

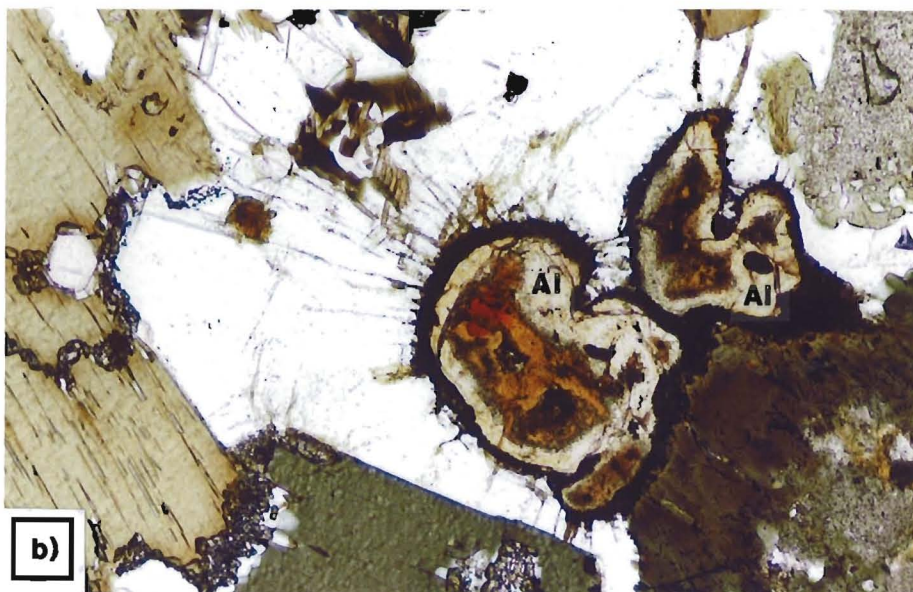
The abrupt decrease in total REE and LREE contents from diorites-granodiorites to quartz monzonites could be explained by allanite and/or apatite fractionation in the diorite-granodiorites resulting in a depletion of REEs in the remaining melt from which the quartz monzonites crystallized. Mittlefehldt and Miller (1983) observed a similar depletion in LREE with progressive crystallization in the felsic Sweetwater Wash Pluton and attributed it to early monazite fractionation.

### 8.7 Eu Anomalies

All but two chondrite-normalized patterns in Figure 13 lack Eu anomalies. Eu is most commonly partitioned into plagioclase, in the +2 oxidation state, where its ionic radius makes it amenable to substitution for  $Ca^{+2}$ . Thus the lack of Eu anomalies in most of the FLIC rocks is unusual given the abundance of plagioclase in all rock types. The bulk distribution coefficients ( $K_d$ 's) for Eu are strongly dependent on oxygen fugacities (Cox et al, 1979) with  $K_d$ 's for  $Eu^{+3}$  in plagioclase being substantially lower than for  $Eu^{+2}$ . Consequently, at high oxygen fugacities, exclusion of trivalent Eu from the plagioclase structure could result in an absence



0 0.25 0.50  
millimeters



0 0.25 0.50  
millimeters

PLATE 18: Photomicrographs of allanite.

a) Subhedral, zoned allanite in granodiorite. Plane light.

b) Rounded, corroded, partially metamict allanite grains (Al) in Gabbro #3. Note cracks, resulting from metamictization, radiating out from the larger allanite grain into the adjacent quartz grain. Plane light.

of whole rock anomalies. This is a likely scenario for the FLIC given petrographic evidence supporting high  $fO_2$ 's throughout much of the crystallization history of the complex (see section 7.4). Post-magmatic changes in the oxidation state of Eu are also a possibility given mineralogical evidence of oxidation and re-equilibration (see section 6.3).

### 8.8 Alkaline Characteristics

The Gabbro #3, Gabbro #4 and diorite-granodiorite rocks of the FLIC have geochemical and mineralogical features suggestive of an alkaline affinity. Samples of these lithologies plot largely in the alkaline field (Figure 7) and their  $Na_2O$  and  $K_2O$  contents (1-5 wt%) are much higher than typical calc-alkaline rocks of similar  $SiO_2$  content. High alkali contents are manifest mineralogically in the presence of abundant primary biotite in all three rock types and interstitial K-feldspar (generally microcline or perthitic microcline) in the Gabbro #3 and diorite-granodiorite rocks.  $K_2O$  contents of analyzed biotites (Appendix 3f) are typically 9-10 wt%. The high total REE abundances (361-537 ppm) extreme LREE-enrichments and lack of Eu anomalies are similar to those of the alkali basalt and K-rich basalt groups (cf. Cullers and Graf, 1984). The similarity between chondrite-normalized patterns of FLIC samples and those of K-rich basalts is illustrated in Figure 28.

Brownell (1941) postulated that the intermediate composition rocks of the complex formed by an outward diffusion of potash and silica from a felsic differentiate which had intruded the core area. The REE data and the presence of  $K_2O$ -rich biotite in the rocks suggests that the "alkaline-like" features are linked

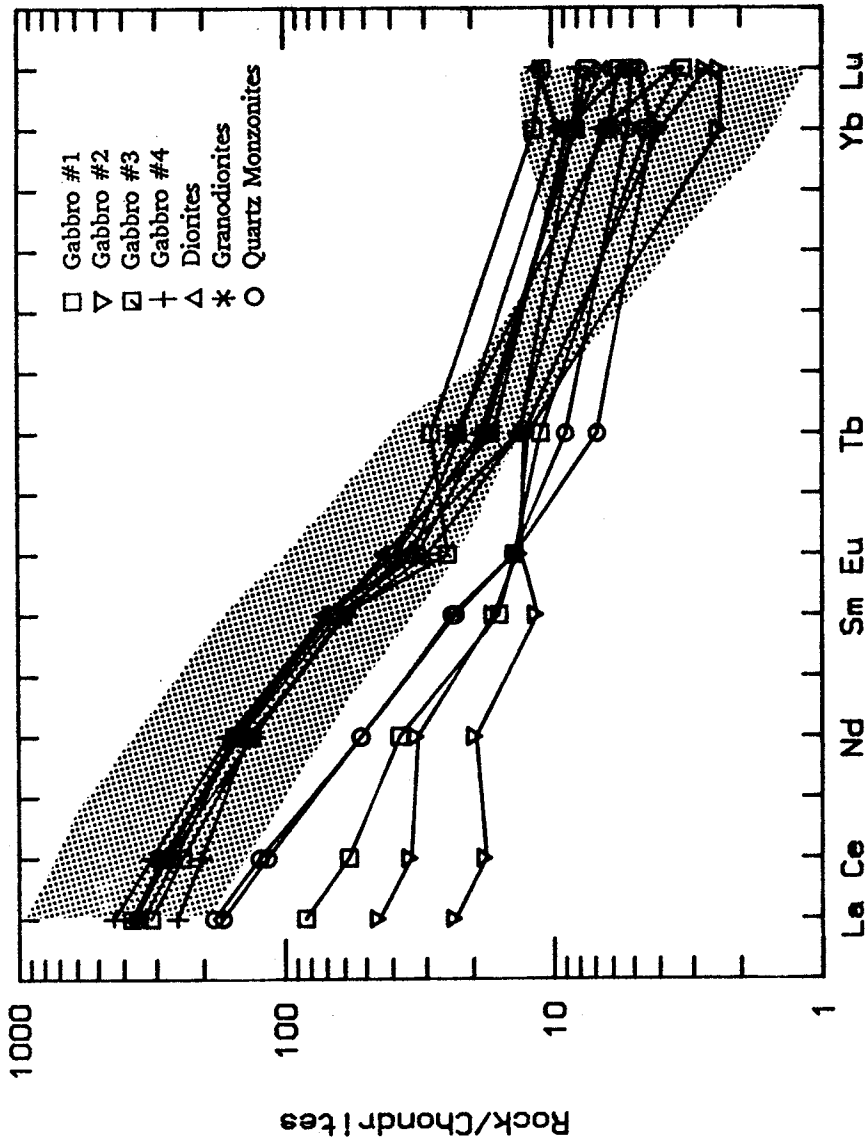


FIGURE 28: Chondrite-normalized plot of mafic to felsic whole rock samples from the Falcon Lake Intrusive Complex. Normalization values are from Thompson (9182). The stippled field shows the range of chondrite normalized REE contents for K-rich basalts (from Cullers and Graf, 1984).

to the parental magma from which the Gabbro #3, Gabbro #4 and diorite-granodiorite rocks were derived rather than a result of secondary processes. Important constraints are thus put on both the derivation and composition of possible parent magmas.

Various origins involving anatexis, metasomatism, assimilation of crustal components, magmatic differentiation, volatile fluxing and liquid immiscibility have been proposed for alkaline rocks (Sorenson, 1974; McBirney, 1984). Models involving a mantle derivation for the formation of alkaline basaltic magma include: very small degrees of partial melting of a garnet peridotite (Cullers and Graf, 1984), anatexis of mantle metasomatized source rocks (Upton and Emeleus, 1987; Cullers and Graf, 1984) and disequilibrium melting of mantle containing a LREE-enriched accessory phase (Gorton and Campbell, 1980).

Observed geochemistry indicates that a parental magma or magmas from which the FLIC rocks evolved was LREE-enriched and, to some extent, exhibited alkaline characteristics. The composition and origin of such a parental magma remains speculative. Further consideration of the "parental magma problem" would be aided by the following: isotopic studies, identification of LREE-enriched rocks in the vicinity of the complex and a more regional geochemical characterization of plutonic rocks similar in age to the FLIC.

### 8.8 Petrogenetic Model

The diagram in Figure 29 attempts to outline a possible sequence of events which might have occurred during the evolution of the FLIC based on the integration of presented data and discussions as well as incorporation of Mandziuk's (1989) hypothesis of multiple intrusions in a magma conduit. The

**FIGURE 29**  
**Petrogenetic Model for the Falcon Lake Intrusive Complex**

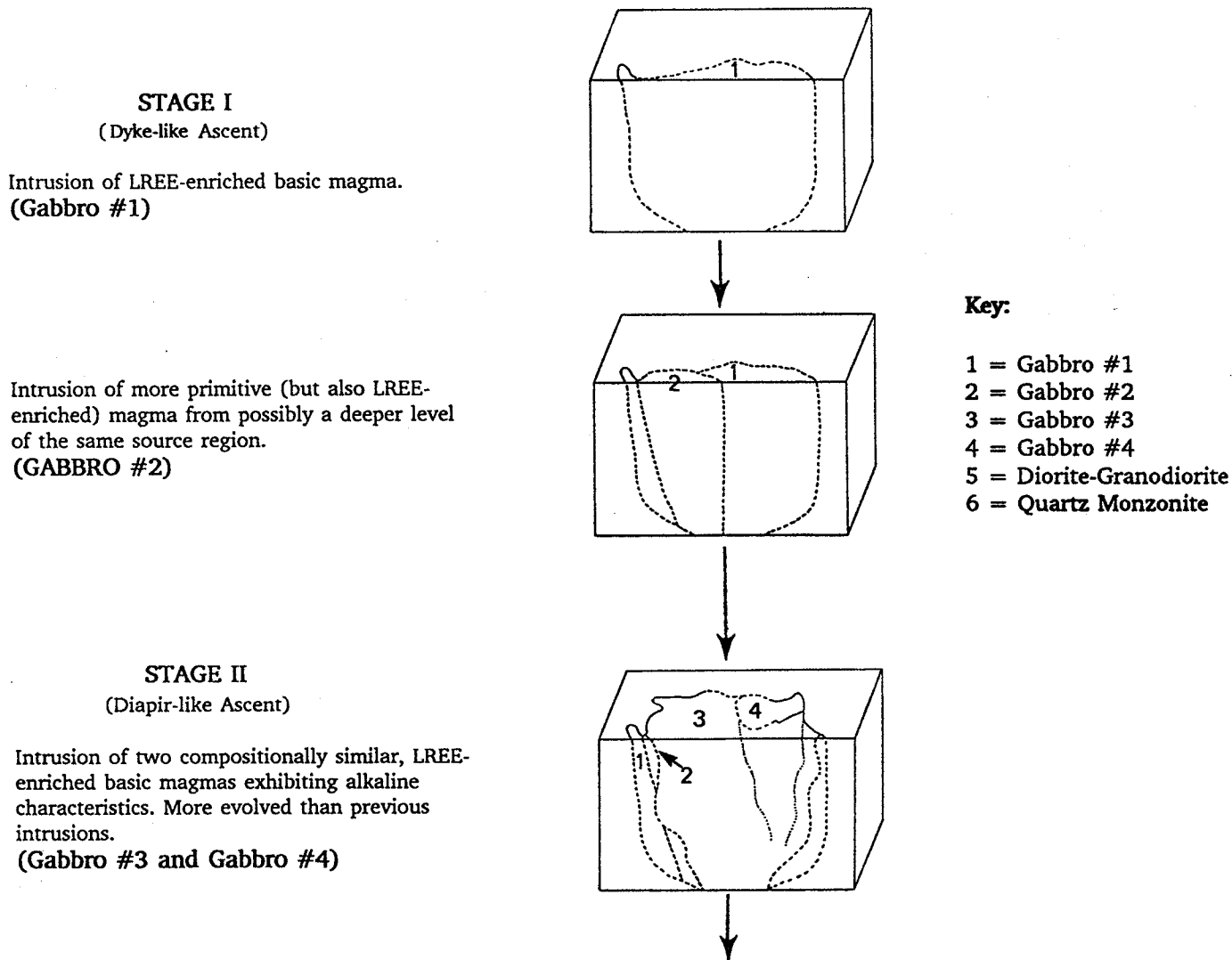
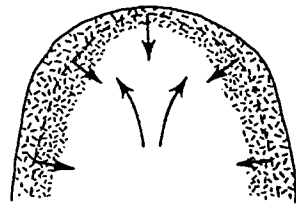
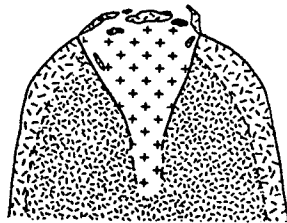


FIGURE 29 (continued)



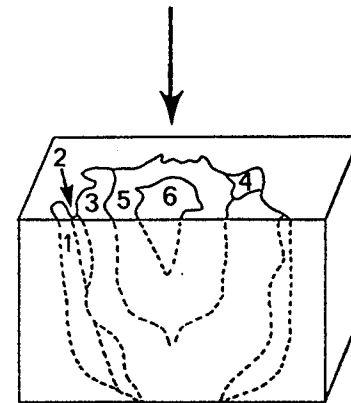
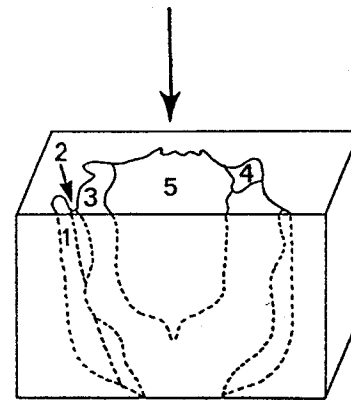
Inward Fractional Crystallization



- \* Brecciation Of Cap Rock And Incorporation Of Xenoliths
- \* Late-stage Formation Of Breccia Pipes

STAGE II (Continued)

Intrusion of basic magma similar in composition to gabbros #3 and #4 and derived from same source region. (Diorite-Granodiorite)



Upward movement of mobile, slightly REE-depleted residual liquid. (Quartz Monzonite)

model is separated into two stages. Formation of Gabbro #1 and #2 occurs in Stage I with intrusion occurring via a dyke-like ascent mechanism (Mandziuk, 1989) under open system conditions. Stage II comprises evolution of the remaining rock types of the FLIC with intrusion of magma occurring via a diapir-like ascent of magma (Mandziuk, 1989). A transition to closed system conditions is interpreted to have occurred during evolution of the diorite-granodiorite unit.

## CHAPTER 9

### CONCLUSIONS

Major, trace and REE geochemistry combined with field relationships indicate that the rock types of the Falcon Lake Intrusive Complex form a genetically related suite exhibiting a calc-alkaline trend and derived from a LREE-enriched parent magma. Large amounts of compositional overlap between various phases preclude relationship of all FLIC lithologies via a single liquid line of descent. Alkaline characteristics exhibited by most rock types are more likely to be primary features inherited from the parental source rather than the product of secondary processes. Consistently high  $\text{Na}_2\text{O}$  and  $\text{K}_2\text{O}$  contents in all units (except Gabbro #2) and the presence of primary biotite and/or interstitial K-feldspar in the gabbroic rocks coupled with LREE-enriched chondrite-normalized patterns suggest that alkaline features were characteristic of the source region. Additional data collection, particularly of isotopic data, along with petrogenetic modelling is required for further evaluation of possible parental magma compositions.

The FLIC represents a dynamic intrusive magma system encompassing a variety of lithologies spanning a large silica range and separated by intrusive contacts, further complicated by the presence of unique internal structural features such as layering, mineral orientation structures and mineral segregations. In addition to providing documentation of whole rock geochemistry and preliminary mineral chemistry, the present study of unlayered FLIC rocks allows the following main conclusions to be made:

1. Gabbros #1 and #2 exhibit the most primitive trace and REE geochemistry of all rock types present, in keeping with their designation as the earliest

intrusive units. Petrographic data, Rb-Sr data and CaO contents suggest development of these units was controlled by fractionation of a Ca-rich mineral(s), likely pyroxene.

2. Gabbros #3 and #4 are geochemically similar and their formation was dominated by plagioclase fractionation.

3. Geochemistry of diorite through granodiorite to quartz monzonite is collectively consistent with a single liquid line of descent and evolution involving inward fractional crystallization. More mafic dioritic rocks are chemically similar to Gabbro #3 and Gabbro #4 suggesting withdrawal from a common source undergoing little differentiation.

4. Geochemical continuity across the granodiorite/quartz monzonite contact is consistent with the crystallization of the quartz monzonite core from the residual liquid remaining after formation of the diorite-granodiorite unit.

5. The LREE-enrichment exhibited by the Gabbro #3, Gabbro #4 and diorite-granodiorites can most reasonably be attributed to allanite  $\pm$  apatite fractionation with early crystallization of these accessory phases in the diorite-granodiorites causing the observed total REE depletion in the quartz monzonites. LREE-enrichment in general, however, appears to have been an intrinsic feature of the source region.

The spatial distribution of rock types and the compositional zonation in the FLIC from outer gabbros inward to a quartz monzonite core can be explained by multiple intrusions of magma in combination with fractional crystallization processes. Early development of the mafic portions of the complex appears to have involved intrusion of LREE-enriched magmas from which Gabbro #1 and #2 evolved. Age relationships between these two units cannot be conclusively

determined from field data. Geochemically, Gabbro #2 has the more primitive composition. Subsequent evolution of the complex involved successive intrusions of compositionally similar, but more evolved, basic magma which gave rise to the Gabbro #3, Gabbro #4 and cumulate-textured diorites. The magmas were dominated by plagioclase crystallization and accumulation. A transition to closed system conditions may have occurred during crystallization of the diorites. Given, this scenario progressive crystallization and inward concentration of residual liquids could have produced the compositional zonation from diorite to granodiorite to quartz monzonite. Upward, erosive movement of felsic differentiate accompanied by rapid cooling and crystallization and/or by convective homogenization can explain the granodiorite-quartz monzonite contact as well as specific structural and textural features of the core rocks.

REFERENCES

- Barc, P.S., 1985. Moonbeam claim, S.E. Manitoba; Reconnaissance geology and petrography. B.Sc. Thesis, University of Manitoba.
- Barnes, C.G., 1987. Mineralogy of the Wooley Creek batholith, Slinkard pluton, and related dikes, Klamath Mountains, northern California. Am. Min., 72:879-9012.
- Basaltic Volcanism Study Project, 1981. Basaltic Volcanism on the Terrestrial Planets. Pergamon Press, Inc., New York, 1286p.
- Bateman, P.C. and Chappell, B.W., 1979. Crystallization, fractionation and solidification of the Tuolumne Intrusive Series, Yosemite National Park, California. Geol. Soc. Am. Bull., 90:465-482.
- Bateman, P.C. and Nokleberg, W.J., 1978. Solidification of the Mount Givens, Granodiorite, Sierra Nevada, California. Jour. of Geol., 86:563-579.
- Bell, R., 1880-1882. On the geology of the Lake of the Woods and adjacent Country. Geol. Surv. of Can., Report of Progress 1880-1882.
- Blackburn, C.E, Bond, W.D., Breaks, F.W., Davis, D.W., Edwards, G.R., Poulsen, K.H., Trowell, N.F. and Wood, J., 1985. Evolution of the Archean Volcanic-Sedimentary Sequences of the Western Wabigoon Subprovince and its Margins: a Review. In: Evolution of Archean Supracrustal Sequences, L.D. Ayres, P.C. Thurston, K.D. Card and W. Weber (eds). GAC Spec. Paper 28, p. 89-117.
- Bottinga, Y. and Weill, D.F., 1970. Densities of liquid silicate systems calculated from partial molar volumes of oxide components. Am. Jour. Sci. 269, p. 169-182.

- Bowes, D.R. and McArthur, A.C., 1976. Nature and Genesis of the Appinite Suite.  
Krystalinikum 12, p. 31-46.
- Brownell, G.M., 1941. Geology of the Falcon Lake Stock, southeastern Manitoba.  
Trans. Can. Inst. Mining Met., 44:230-250.
- Bruce, E.L., 1918. Gold Quartz Veins and Scheelite Deposits in Southeastern  
Manitoba. Geol. Surv., Canada, Sum. Rept. 1918, pt. D, pp. 11-15.
- Bruce, E.L., 1917. Molybdenite near Falcon Lake, Manitoba, Geol. Surv., Canada,  
Sum. Rept. 1917, pt. D, pp. 22-25.
- Carr, M.J., 1987. IGPET II. Copywrite 1987, Terra Soft Inc., 25 Moran Ave.,  
Princeton, N. J. 08542.
- Chaytor, M., 1985. A report on the geochemistry of the Falcon Lake stock. BSc.  
Thesis, University of Manitoba, 138p.
- Colby, J.W., 1980. MAGIC V Program, Kevex. Foster City, California.
- Cox, K.G., Bell, J.D. and Pankhurst, R.J., 1979. The Interpretation of Igneous  
Rocks,. George Allen and Unwin, London, 450p.
- Cullers, R.L. and Graf, J.L., 1984. Rare Earth Elements in Igneous Rocks of the  
Continental Crust: Predominantly Basic and Ultrabasic Rocks. In: Henderson  
P. (ed.) Rare Earth Element Geochemistry, Developments in Geology 2,  
Elsevier, pp. 237-274.
- Davies, J.F., 1954. Geology of the West Hawk - Falcon Lake area. Man. Dept.  
Mines Nat. Res., Publication 53-4, 28p.
- DeLury, J.S., 1942. West Hawk and Falcon Lakes Area, Southeastern Manitoba.  
Man. Mines Branch, Map 37-3.
- DeLury, J.S., 1921b. The Mineral Resources of Southeastern Manitoba. Ind. Dev.  
Bd., Manitoba.

- DeLury, J.S., 1919. Some economic aspects of the Falcon Lake District, Manitoba. Trans. Can. Inst. Min. and Met., 22:320-328.
- DeLury, J.S., 1918. Tungsten ore deposits near Falcon Lake, Manitoba. Can. Min. Jour., 39:186-188.
- DeLury, J.S., 1917. Molybdenite at Falcon Lake, Manitoba, Can. Min. Jour. 38:460-462.
- Donaldson, E.M., 1982. Determination of ferrous iron in acid-soluble iron oxides and iron oxide ores and mill products by titration with potassium dichromate after acid-decomposition in an air-free atmosphere. In: methods for analysis of ores, rocks and related materials. Can. Center for Mineral and Energy Technology, Energy, Mines and Resources Canada, p. 465-468.
- Duncan, C., 1989. Constraints on petrogenetic models of the Caddy Lake granite in Southeastern Manitoba. Unpublished B.Sc. Thesis, University of Manitoba, 186p.
- Ehlers, E.G. and Blatt, H., 1982. Petrology Igneous, Metamorphic and Sedimentary. W.H. Freeman and Company, San Francisco, 19:606-607.
- Ercit, T.S., 1987. FORMULA - A general purpose program for formula calculation. Royal Ontario Museum.
- Ernst, W.G., 1976. Petrologic Phase Equilibria. W.H. Freeman and Company, San Francisco, 2:33.
- Farquharson, R.B. and Clark, G.S., 1971. Rb-Sr geochronology of some granitic rocks in Southeastern Manitoba. In Turnock A.C. (ed) Geoscience Studies in Manitoba. Geol. Assoc. Can. Spec. Paper 9, p. 111-117.
- Fingler, J., 1991. Precious metal mineralization related to the Falcon Lake Intrusive Complex, southeastern Manitoba. Unpublished M.Sc. Thesis, University of

Manitoba, 145p.

- Fisher, R.V. and Schmincke, H. -U., 1984. Pyroclastic Rocks. Springer Verlag, Berlin, Heidelberg, 472p.
- Geist, D.J., Baker, B.H., McBirney, A.R., 1985. GPP, A program package for creating and using geochemical data files (Version for IBM-PC and compatible microcomputers).
- Gibbins, W.A., 1971. Geology of the Falcon lake stock, southeastern Manitoba. In Geoscience Studies in Manitoba, A.C. Turnock (ed). Geol. Assoc. of Can. Spec. Paper 9, p. 129-135.
- Gibbins, W.A., 1967. Geology of the Falcon Lake stock, Manitoba. MSc. Thesis, Northwestern University, 99p.
- Gromet, L.P. and Silver, L.T., 1983. Rare earth element distribution among minerals in a granodiorite and their petrogenetic implications. *Geochemica et Cosmochimica Acta*, 47:925-939.
- Haggerty, S.E., 1976. Oxidation of Opaque Mineral Oxides in Basalts. In Rumble D. III (ed) Oxide Minerals. Volume 3, *Reviews in Mineralogy*, . HG-1 to HG-100.
- Halwas, D., 1984. The Sunbeam-Kirkland breccia pipe, Southeastern Manitoba. B.Sc. Thesis, University of Manitoba, 56p.
- Hanson, G.N., 1978. The application of trace elements to the petrogenesis of igneous rocks of granitic composition. *Earth and Planet. Sci. Letters*, 38:26-43.
- Harvey, P.K., Taylor, D.M., Hendry, R., Bancroft, F., 1972. An accurate fusion method for the analysis of rocks and chemically related materials by X-ray fluorescence spectrometry. *X-ray Spectrometry*, 2:33-44.

- Haskin, L.A., 1984. Petrogenetic modelling - use of rare earth elements. In: Rare Earth Element Geochemistry, Developments in Geology 2, Elsevier, P. Henderson (ed). 4:115-152.
- Hawthorne, F., 1981. Crystal chemistry of the amphiboles. Min. Soc. Am. Reviews in Mineralogy, 9A, p. 1-102.
- Henderson, P., 1984. General geochemical properties and abundances of the rare earth elements. In: Rare Earth Elements, Developments in Geology 2, Elsevier, P. Henderson (ed., 1:1-32.
- Hildreth, W., 1981. Gradients in silicic magma chambers: implications for lithospheric magmatism. Jour. Geophys. Res., 86:10153-10192.
- House, R.D., 1955. Radioactivity and geology of the Falcon Lake stock, southern Manitoba. M.Sc. Thesis, Northwestern University.
- Irvine, T.N. and Barager, W.R.A., 1971. A guide to the chemical classification of the common volcanic rocks. Can. Jour. of Earth Sciences, 8:523-548.
- Johanasson, P.R., 1985. A gravity study of the Falcon Lake Intrusive Complex. B.Sc. Thesis, University of Manitoba, 28p.
- Lamb, C.F., 1975. Southeastern Manitoba - Preliminary Compilation. Man. Min. Res. Div. Prelim. Map 1975 F-8.
- Lawson, A.C., 1886. Report on the geology of the Lake of the Woods region with special reference to the Keewatin (Huronian?) Belt of Archean Rocks. Geol. Surv. of Can., Annual Report 1885, pt. CC.
- Leake, B.E., Henry, G.L., Kemp, A., Plant, A.G., Harvey, P.K., Wilson, J.R., Coats, J.S., Aucott, J.W., Lund, T., Howarth, R.J., 1969. The chemical analysis of rock powders by automatic X-ray fluorescence. Chem. Geol. 5, p. 7-86.
- Luth, W.C., 1976. Granitic rocks. In: The evolution of crystalline rocks, Bailey,

- D.K., and Macdonald R., (eds.). Academic Press, London, p. 335-417.
- Luth, W.C., Jahns, R.H. and Tuttle, O.F., 1964. The granite system at pressures of 4-10 kilbars. Jour. of Geophys. Research, v. 69, No. 4, p. 759-773.
- McBirney, A.R., 1984. Igneous Petrology. Freeman, Cooper and Co., San Francisco, California, 504p.
- Mandziuk, W.S., 1989. Primary structures of the Falcon Lake Intrusive Complex, Southeastern Manitoba. M.Sc. Thesis, University of Manitoba, 103p.
- Mandziuk, W.S, Brisbin, W.C. and Scoates, R.F.J., 1989. Igneous structures in the Falcon Lake Intrusive Complex, southeastern Manitoba. Can. Min., 27:81-92.
- Manning, D.A.C. and Pichavant, M., 1985. Volatiles and their bearing on the behavior of metals in granite systems. In: Taylor, R.P. and Strong, D.F. (eds.) Recent Advances in the Geology of Granite-related Mineral Deposits. Spec. Vol. 39, Can. Instit. of Mining and Metall., p. 13-23, Figure 6.
- Marshall, J.R., 1917. Star Lake Area, Manitoba. Geol. Surv., Canada, Sum. Rept. 1917, pt. D, p. 21-22.
- Mittlefehldt, D.W. and Miller, C.F., 1983. Geochemistry of the Sweetwater Wash Pluton, California: Implications for "anomalous" trace element behavior during differentiation of felsic magmas. Geochimica et Cosmochimica Acta, 47: 109-124.
- Quinn, W., 1985. A petrologic study of the host rocks along the northwestern contact of the Falcon Lake stock. B.Sc. Thesis, University of Manitoba, 42p.
- Perfit, M.R., Bruechner, H., Lawrence, J.R., Kay, R.W., 1980. Trace element and isotopic variations in a zoned pluton and associated volcanic rocks, Unalaska Island, Alaska: A model for fractionation in the Aleutian calc-alkaline suite. Contrib. Mineral. Petrol., 73:69-87.

- Pettijohn, F.J., 1972. The Archean of the Canadian shield: A Resume. In Studies in Mineralogy and Precambrian Geology. Geol. Soc. of Am., Memoir 135, p. 131-149.
- Raglan, P.C. and Butler, J.R., 1972. Crystallization of the West Farrington Pluton, North Carolina, U.S.A. Jour. of Petrol., v. 13, Part 3, p. 381-404.
- Sawka, W.N., 1987. REE and trace element variation in accessory minerals and hornblende from the strongly zoned McMurray Meadows Pluton, California. In: Transactions of the Royal society of Edinburgh: Earth Sciences, 79:156-168.
- Sawka, W.N., Chappell, B.W. and Norrish, K., 1984. Light-rare-earth-element zoning in sphene and allanite during granitoid fractionation. Geology, 12:131-134.
- Scambos, T.A., Loisselle, M.C., Wones, D.R., 1986. The Center Pond Pluton: The Restite of the Story (Phase Separation and Melt Evolution Granitoid Genesis). Am. Jour. of Sci., 286:241-280.
- Scoates, R.F.J., Williamson, B.L., Duke, J.M., Mandziuk, W., Brisbin, W.C., Sutcliffe, R.H., 1986. Layered intrusions of southeastern Manitoba and Northwestern Ontario. GAC-MAC Field Trip 13: Guide Book, Geol. Assoc. of Can., Ottawa '86 Committee.
- Snoke, A.W., Quick, J.E. and Bowman, H.R., 1981. Bear Mountain Igneous Complex, Klamath Mountains, California: an ultrabasic to silicic calc-alkaline suite. Jour of Petrol., v. 22, Part 4, p. 501-552.
- Sorensen, H., 1974. Origin of the alkaline rocks - a summary and retrospect: In Sorensen, H (ed.) The Alkaline Rocks. John Wiley and Sons, p. 535-537.
- Sparks, R.S.J. and Huppert, H.E., 1984. Density changes during the fractional

- crystallization of basaltic magmas: fluid dynamic implications. Contrib. Mineral. Petrol., 85:300-309.
- Springer, G.D., 1959. Geology of the Rennie-West Hawk Lake area, Lac du Bonnet Mining Division Manitoba. Dept. of Mines and Natural Resources, Province of Manitoba, Publication 50-6, 24p.
- Stormer, Jr., J.C., 1975. A practical two-feldspar geothermometer. Am. Mineral. 60:667-674.
- Streckheisen, A.C., 1976. To each plutonic rock its proper name. Earth Science reviews, 12:1-33.
- Tauch, J. and Strong, D.F., 1986. Geochemical trends in the Ackley Granite, southeast Newfoundland: their relevance to magmatic-metallogenic processes in high-silica granitoid systems. Can. Jour. Earth Sci., 23:747-765.
- Taylor, R.P. and Strong, D.F., 1985. Recent Advances in the Geology of Granite-Related Mineral Deposits. Spec. Vol. 39, Can. Instit. of Mining and Metallurgy.
- Thompson, R.N., 1982. Magmatism of the British Tertiary Volcanic Province. Scottish Jour. Geol., 18:49-107.
- Tindle, A.G. and Pearce, J.A., 1981. Petrogenetic modelling of in-situ fractional crystallization in the zoned Loch Doon pluton. Contrib. Mineral. Petrol., 78:196-207.
- Trembath, G.D., 1986. The compositional variation of staurolite in the area of Anderson Lake Mine, Snow Lake, Manitoba, Canada. Unpublished M.Sc. Thesis, University of Manitoba, 187p.
- Tuttle, O.F. and Bowen, N.L., 1958. Origin of granite in the light of experimental studies in the system NaAlSi<sub>3</sub>O<sub>8</sub>-KAlSi<sub>3</sub>O<sub>8</sub>-SiO<sub>2</sub>-H<sub>2</sub>O. Geol. Soc. Am. Memoir

74, 153p.

Wanless, R.K., Stevens, R.D., Lachance, G.R. and Edmonds, C.M., 1968. Age determinations and geological studies. K-Ar isotopic ages. Report 8, Geol. Surv. Can., Paper 67-2, Part A, pp 90-91.

Yoder, H.S. and Tilley, C.E., 1962. Origin of basaltic magmas: An experimental study of natural and synthetic rock systems. Jour. of Petrol., v. 3, Part 3, p. 342-532.

## APPENDIX 1 WHOLE ROCK ANALYSES

- 1a) Gabbro #1
- 1b) Gabbro #2
- 1c) Gabbro #3
- 1d) Gabbro #4
- 1e) Diorites-Granodiorites
- 1f) Quartz Monzonites

Preliminary sample preparation consisted of trimming off all weathered surfaces from each sample, grinding down to -250 mesh size via jaw crusher, agate swing mill and agate ball mill and then drying rock powders.

Most major element analyses were done at the Department of Geological Sciences, University of Manitoba by X-ray fluorescence on an ARL 8420 sequential spectrometer. Analyses were performed on glass beads prepared by the method of Harvey et al (1972) using a flux comprised of 80% lithium tetraborate and 20% lanthanum oxide. Samples were fused in platinum crucibles. Some of the major element gabbro analyses were done by directly coupled plasma emission spectroscopy (DCP) at Bondar Clegg Laboratories and are indicated in this Appendix with an asterisk (\*).

Trace element analyses were done at the University of Manitoba by X-ray fluorescence on the same spectrometer as above. Analyses were performed on pressed powder pellets prepared in a manner similar to that described in Leake et al (1969). Lower limits of detection for Rb, Sr, Y, Nb and Zr were 2, 2, 2, 5 and 5 ppm respectively. Analytical machine precision (analytical runs, n=10) for Rb, Sr, Y, Nb and Zr is  $\pm 4$ ,  $\pm 4$ ,  $\pm 3$ ,  $\pm 5$  and  $\pm 2$  ppm respectively.

Major element oxides are expressed in wt % oxide; trace elements in parts per million (ppm). Trace elements below detection limits are listed as 0 ppm. Normative values are CIPW weight norms. Densities were calculated after the method of Bottinga and Weill. (CIPW norms and densities were calculated using the computer program "IGPET" (Carr, 1987)).

Abbreviations:      N.D. = No Data  
                              Den = Density

LISTING OF SAMPLES USED IN GEOCHEMICAL PLOTS

GABBRO #1:PT-10	GABBRO #3:PT-17	GABBRO #4:PT-34
PT-56	PT-18	PT-45
PT-163	PT-19	PT-46
PT-165	PT-52	PT-47
PT-166	PT-73	PT-48
PT-168	PT-77	PT-49
	PT-83	PT-159
GABBRO #2:PT-74	PT-84	PT-161
PT-125	PT-85	PT-162
PT-148	PT-123	
	PT-124	
DIORITE-GRANODIORITE:		
(Diorites) PT-29	PT-122	PT-54
PT-36	PT-130	PT-58
PT-38	(Granodiorites)	PT-59
PT-39B	PT-7B	PT-60
PT-41	PT-24B	PT-62
PT-67	PT-27	PT-66
PT-96	PT-30	PT-68
PT-109	PT-42	PT-70
PT-110	PT-43	PT-100
PT-121	PT-53	PT-101
QUARTZ MONZONITES:		
PT-32	PT-111	PT-138
PT-61	PT-113	PT-140
PT-64	PT-116	PT-141
PT-69	PT-117	PT-143
PT-88	PT-133	PT-144
PT-89	PT-134	PT-145
PT-107	PT-136	PT-146
PT-108	PT-137	
OTHER:	PT-164 (Pyroxenitic phase of Gabbro #1)	PT-157, PT-169A (Mafic clots
	PT-153 (Pyroxenitic layer in Gabbro #3)	in Gabbro #4)
	PT-94 (Magnetite-rich layer in Gabbro #4)	

a) Gabbro #1

Sample	PT-10	*PT-50	*PT-55	*PT-56	PT-163	PT-164	PT-165	PT-166	PT-168
SiO <sub>2</sub>	49.88	54.80	55.70	56.50	51.71	42.41	48.60	53.39	49.81
TiO <sub>2</sub>	0.21	1.11	1.09	1.15	0.95	1.75	1.34	1.12	0.77
Al <sub>2</sub> O <sub>3</sub>	19.18	15.80	16.10	16.80	17.87	8.06	16.36	16.59	17.32
Fe <sub>2</sub> O <sub>3</sub>	2.29	2.89	3.01	3.19	2.75	7.09	2.71	3.40	2.74
FeO	5.59	5.55	5.51	5.92	7.90	13.46	9.77	7.01	7.90
MnO	0.13	0.12	0.12	0.13	0.15	0.26	0.19	0.14	0.15
MgO	7.36	3.18	3.15	3.35	4.94	13.67	6.63	4.59	6.78
CaO	10.03	5.58	5.31	5.75	9.20	12.54	9.49	7.23	9.51
Na <sub>2</sub> O	2.63	3.24	3.43	3.52	3.27	0.05	2.15	3.46	2.88
K <sub>2</sub> O	1.24	3.45	3.08	3.60	0.53	0.14	0.87	1.99	1.12
P <sub>2</sub> O <sub>5</sub>	0.01	0.78	0.59	0.94	0.29	0.76	0.44	0.51	0.01
LOI	1.18	2.10	0.85	0.35	0.54	1.72	0.64	0.78	0.70
Total	99.73	98.60	97.94	101.20	100.10	101.91	99.19	100.21	99.69
Y	12	28	29	29	19	34	24	28	12
Zr	102	288	321	317	60	55	40	231	62
Nb	0	8	9	19	0	5	2	9	0
Rb	40	138	112	140	21	7	18	68	32
Sr	651	492	499	521	794	202	783	635	714
AN	62.4	40.1	40.1	39.5	54.0	98.1	64.1	44.9	56.0
Q	0.0	6.3	7.5	5.2	1.8	0.0	0.0	2.8	0.0
Or	7.3	20.4	18.2	21.3	3.1	0.8	5.1	11.8	6.6
Ab	22.3	27.4	29.0	29.8	27.7	0.4	18.2	29.3	24.4
An	36.9	18.4	19.4	19.4	32.5	21.4	32.4	23.9	31.0
Di	10.4	3.5	2.5	2.4	9.3	29.0	9.7	7.1	13.1
Hy	8.6	12.4	12.7	13.7	18.7	24.6	25.6	16.4	9.4
Ol	9.4	0.0	0.0	0.0	0.0	8.6	0.0	0.0	9.0
Mt	3.3	4.2	4.4	4.6	4.0	10.3	3.9	4.9	4.0
Il	0.4	2.1	2.1	2.2	1.8	3.3	2.5	2.1	1.5
Ap	0.0	1.8	1.4	2.2	0.7	1.8	1.0	1.2	0.0
FeO*	7.65	8.15	8.22	8.79	10.38	19.84	12.21	10.07	10.37
F/F+M	0.514	0.722	0.726	0.727	0.681	0.595	0.652	0.690	0.608
Rb/Sr	0.061	0.280	0.224	0.269	0.026	0.035	0.023	0.107	0.045
K/Rb	257	208	228	213	209	166	401	243	291
Den	2.61	2.52	2.51	2.52	2.62	2.88	2.68	2.58	2.64

\* Note: PT-164 is from a pyroxenitic phase of Gabbro #1.

## b) Gabbro #2

Sample	*PT-74	PT-75	PT-125	PT-148
SiO <sub>2</sub>	48.60	45.58	46.27	44.15
TiO <sub>2</sub>	0.26	0.29	0.33	0.75
Al <sub>2</sub> O <sub>3</sub>	17.30	16.11	16.27	3.96
Fe <sub>2</sub> O <sub>3</sub>	3.18	3.49	2.84	9.18
FeO	6.39	7.73	7.80	8.96
MnO	0.16	0.16	0.17	0.22
MgO	8.87	11.36	11.17	20.18
CaO	13.20	12.98	12.66	11.31
Na <sub>2</sub> O	2.27	0.60	1.41	0.05
K <sub>2</sub> O	0.27	0.09	0.21	0.09
P <sub>2</sub> O <sub>5</sub>	0.41	0.01	0.01	0.08
LOI	1.05	1.21	1.15	3.50
Total	101.96	99.61	100.29	102.43
Y	13	17	13	26
Zr	49	32	35	69
Nb	0	3	0	0
Rb	4	7	12	2
Sr	836	712	675	47
AN	65.4	89.0	75.8	96.1
Or	1.6	0.5	1.2	0.5
Ab	19.2	5.1	11.9	0.4
An	36.2	41.0	37.5	10.3
Di	21.4	18.8	20.4	35.8
Hy	5.2	19.6	6.8	26.0
Ol	11.2	7.8	16.5	11.0
Mt	4.6	5.1	4.1	13.3
Il	0.5	0.6	0.6	1.4
Ap	1.0	0.0	0.0	0.2
FeO*	9.25	10.87	10.36	17.22
F/F+M	0.515	0.493	0.485	0.463
Rb/Sr	0.005	0.010	0.018	0.043
K/Rb	560	107	145	374
Den	2.67	2.73	2.72	2.84

## c) Gabbro #3

Sample	*PT-17	*PT-18	PT-19	*PT-51	*PT-52	*PT-71	*PT-72	*PT-73	*PT-76	*PT-77	*PT-78
SiO <sub>2</sub>	51.00	51.60	53.74	53.30	51.20	52.40	52.00	48.90	51.90	51.30	53.30
TiO <sub>2</sub>	1.20	1.16	0.90	1.11	1.09	0.79	1.06	1.26	1.16	0.82	0.96
Al <sub>2</sub> O <sub>3</sub>	19.20	19.20	20.92	15.60	20.80	18.20	18.00	16.40	17.30	18.20	18.50
Fe <sub>2</sub> O <sub>3</sub>	3.20	3.33	2.49	3.20	2.48	3.20	3.71	4.85	4.35	2.82	3.41
FeO	6.19	6.14	4.40	6.52	5.36	4.53	4.90	7.04	5.07	6.06	5.01
MnO	0.13	0.13	0.08	0.13	0.09	0.11	0.13	0.15	0.13	0.13	0.12
MgO	3.62	3.36	2.20	4.45	2.85	3.29	3.51	5.71	3.35	3.39	2.89
CaO	8.15	8.20	7.48	6.57	8.16	7.72	8.94	9.94	8.25	7.05	6.63
Na <sub>2</sub> O	3.82	3.68	4.53	3.15	3.87	3.67	3.50	2.88	3.41	3.58	3.63
K <sub>2</sub> O	2.71	2.77	2.58	2.74	2.57	2.74	1.83	1.89	2.66	2.65	3.30
P <sub>2</sub> O <sub>5</sub>	1.07	1.09	0.55	0.57	0.68	1.00	0.95	1.66	1.19	0.63	0.54
LOI	0.65	0.55	0.89	1.00	0.60	1.60	0.95	0.65	0.65	0.65	1.05
Total	100.94	101.21	100.76	98.34	99.75	99.25	99.48	101.33	99.42	97.28	99.34
Y	22	19	19	31	23	19	17	26	24	23	26
Zr	247	295	245	318	113	247	199	171	282	161	254
Nb	11	9	0	24	3	10	2	0	6	4	17
Rb	99	93	78	137	90	93	53	49	95	74	118
Sr	1216	1206	1308	819	1388	1255	1419	1069	1255	1063	982
AN	45.7	47.1	43.2	43.3	49.3	44.7	48.6	51.9	45.5	46.0	44.3
Q	0.0	0.0	0.0	3.7	0.0	1.3	3.1	0.0	2.7	0.0	1.3
Or	16.0	16.4	15.3	16.2	15.2	16.2	10.8	11.2	15.7	15.7	19.5
Ab	32.3	31.1	38.3	26.7	32.8	31.1	29.6	24.4	28.9	30.3	30.7
An	27.2	27.7	29.1	20.3	31.8	25.1	28.0	26.2	24.0	25.8	24.4
Ne	0.0	0.0	0.0	0.0	0.0	0.0	0.0	0.0	0.0	0.0	0.0
Di	5.1	4.8	3.6	7.0	3.5	5.4	8.2	9.9	7.4	4.2	4.0
Hy	1.3	6.2	3.0	15.4	0.8	10.1	9.2	13.6	8.8	12.4	10.3
Ol	8.9	4.8	3.9	0.0	7.9	0.0	0.0	2.1	0.0	1.3	0.0
Mt	4.6	4.8	3.6	4.6	3.6	4.6	5.4	7.0	6.3	4.1	4.9
Il	2.3	2.2	1.7	2.1	2.1	1.5	2.0	2.4	2.2	1.6	1.8
Ap	2.5	2.5	1.3	1.3	1.6	2.3	2.2	3.9	2.8	1.5	1.3
FeO*	9.07	9.14	6.64	9.40	7.59	7.41	8.24	11.41	8.99	8.60	8.08
F/F+M	0.718	0.734	0.753	0.682	0.729	0.696	0.705	0.669	0.731	0.720	0.739
Rb/Sr	0.081	0.077	0.060	0.167	0.065	0.074	0.037	0.046	0.076	0.070	0.120
K/Rb	227	247	275	166	237	245	287	320	232	297	232
Den	2.57	2.57	2.51	2.56	2.55	2.53	2.56	2.63	2.55	2.55	2.52

Sample	*PT-79	*PT-80	*PT-82	*PT-83	*PT-84	PT-85	PT-123	PT-124	PT-126	PT-127	PT-128
SiO <sub>2</sub>	48.40	48.80	55.00	56.10	55.70	54.15	49.12	49.06	53.70	52.60	53.28
TiO <sub>2</sub>	1.45	1.24	0.74	0.77	1.02	0.95	1.04	1.08	0.85	0.89	0.82
Al <sub>2</sub> O <sub>3</sub>	14.50	19.80	20.50	21.20	19.20	19.00	16.14	17.47	19.31	18.32	17.99
Fe <sub>2</sub> O <sub>3</sub>	5.05	3.33	2.46	1.91	3.79	3.49	3.68	3.70	2.59	2.78	2.68
FeO	8.06	6.04	3.96	3.63	4.15	4.49	7.26	6.59	4.36	5.04	4.89
MnO	0.18	0.14	0.08	0.08	0.11	0.11	0.14	0.12	0.08	0.09	0.09
MgO	6.31	3.76	2.07	1.40	2.32	1.84	6.83	5.58	2.89	3.62	3.47
CaO	8.53	8.08	6.23	6.78	6.80	6.84	9.04	8.65	6.93	6.93	6.80
N <sub>2</sub> O	1.96	3.49	4.38	4.64	3.78	4.04	2.47	2.86	3.40	3.18	3.25
K <sub>2</sub> O	3.70	3.55	3.52	2.98	3.27	3.20	1.86	2.21	3.27	3.45	3.50
P <sub>2</sub> O <sub>5</sub>	0.98	0.71	0.35	0.22	0.58	0.65	1.09	1.19	0.64	0.55	0.53
LOI	2.20	2.05	1.25	0.80	0.30	0.74	0.89	0.95	1.38	1.05	1.03
Total	<u>101.32</u>	<u>100.99</u>	<u>100.54</u>	<u>100.51</u>	<u>101.02</u>	<u>99.50</u>	<u>99.56</u>	<u>99.46</u>	<u>99.40</u>	<u>98.50</u>	<u>98.33</u>
Y	31	29	18	15	24	26	25	24	18	15	13
Zr	285	373	228	158	284	325	175	116	246	208	268
Nb	12	12	3	7	16	19	8	8	16	9	20
Rb	139	105	97	82	108	132	70	67	125	108	127
Sr	747	1105	1180	1223	1117	1084	800	903	1098	1119	1021
AN	54.5	57.0	41.1	41.8	44.6	41.5	56.8	53.9	49.1	48.7	46.8
Q	0.0	0.0	0.0	0.8	4.3	2.2	0.0	0.0	2.5	0.8	1.5
Or	21.9	21.0	20.8	17.6	19.3	18.9	11.0	13.1	19.3	20.4	20.7
Ab	16.6	21.1	37.1	39.3	32.0	34.2	20.9	24.2	28.8	26.9	27.5
An	19.8	27.9	25.9	28.2	25.8	24.3	27.5	28.3	27.8	25.5	24.2
Ne	0.0	4.6	0.0	0.0	0.0	0.0	0.0	0.0	0.0	0.0	0.0
Di	13.1	6.2	2.3	3.3	3.4	4.5	8.3	5.5	2.0	4.3	5.0
Hy	8.8	0.0	5.6	5.8	7.1	6.4	19.5	13.4	10.8	12.6	11.8
Ol	6.7	9.4	1.9	0.0	0.0	0.0	1.7	3.9	0.0	0.0	0.0
Mt	7.3	4.8	3.6	2.8	5.5	5.1	5.3	5.4	3.8	4.0	3.9
Il	2.8	2.4	1.4	1.5	1.9	1.8	2.0	2.1	1.6	1.7	1.6
Ap	2.3	1.6	0.8	0.5	1.3	1.5	2.5	2.8	1.5	1.3	1.2
FeO*	12.61	9.04	6.17	5.35	7.56	7.63	10.57	9.92	6.69	7.54	7.30
F/F+M	0.670	0.709	0.751	0.795	0.768	0.808	0.611	0.643	0.701	0.678	0.681
Rb/Sr	0.186	0.095	0.082	0.067	0.097	0.122	0.088	0.074	0.114	0.097	0.124
K/Rb	221	281	301	302	251	201	221	274	217	265	229
Den	2.64	2.58	2.49	2.48	2.50	2.51	2.63	2.61	2.51	2.53	2.52

Sample	PT-153
SiO <sub>2</sub>	45.90
TiO <sub>2</sub>	1.64
Al <sub>2</sub> O <sub>3</sub>	9.91
Fe <sub>2</sub> O <sub>3</sub>	6.83
FeO	12.51
MnO	0.31
MgO	9.85
CaO	9.16
Na <sub>2</sub> O	0.66
K <sub>2</sub> O	2.12
P <sub>2</sub> O <sub>5</sub>	0.95
LOI	0.56
Total	<u>100.40</u>
Y	36
Zr	199
Nb	7
Rb	82
Sr	462
AN	76.1
Q	0.0
Or	12.5
Ab	5.6
An	17.8
Ne	0.0
Di	17.5
Hy	31.2
Ol	0.0
Mt	9.9
Il	3.1
Ap	2.2
FeO*	18.66
F/F+M	0.658
Rb/Sr	0.177
K/Rb	215
Den	2.77

\* Note: PT-153 is from a pyroxenitic layer in Gabbro #3.

d) Gabbro #4

Sample	*PT-34	*PT-45	*PT-46	*PT-47	*PT-48	*PT-49	PT-94	PT-102	PT-158	PT-159	PT-161
SiO <sub>2</sub>	44.90	51.50	54.70	53.80	53.10	53.30	35.45	57.55	51.13	54.89	51.73
TiO <sub>2</sub>	1.08	1.26	1.03	1.00	1.04	0.93	1.73	0.78	0.97	0.85	1.29
Al <sub>2</sub> O <sub>3</sub>	21.50	17.90	17.10	19.30	19.80	19.40	5.19	17.89	18.33	19.46	18.90
Fe <sub>2</sub> O <sub>3</sub>	5.00	4.17	4.16	3.54	2.82	2.71	14.20	2.37	3.15	2.17	3.04
FeO	5.90	5.72	4.25	4.87	5.55	4.77	9.94	4.48	6.10	4.71	6.49
MnO	0.13	0.14	0.12	0.12	0.12	0.10	0.28	0.13	0.12	0.09	0.10
MgO	4.81	4.10	2.97	3.12	3.17	2.69	14.52	2.56	4.61	2.45	2.72
CaO	12.90	8.71	6.68	7.29	7.34	7.17	14.04	5.14	6.43	6.43	7.54
Nb <sub>2</sub> O	2.76	3.50	3.30	3.80	3.69	3.94	0.05	3.75	3.90	3.38	3.36
K <sub>2</sub> O	0.58	2.48	3.49	3.43	3.61	2.96	0.09	4.47	2.33	3.27	2.37
P <sub>2</sub> O <sub>5</sub>	1.16	1.24	0.92	0.96	0.93	0.83	4.39	0.38	0.72	0.52	0.88
LOI	0.45	0.35	0.45	0.45	0.30	0.60	2.27	0.21	1.07	0.60	0.97
Total	<u>101.17</u>	<u>101.07</u>	<u>99.17</u>	<u>101.68</u>	<u>101.47</u>	<u>99.40</u>	<u>102.15</u>	<u>99.71</u>	<u>100.01</u>	<u>98.82</u>	<u>99.39</u>
Y	20	26	24	21	19	22	53	15	17	14	21
Zr	116	468	280	294	297	211	48	399	108	211	157
Nb	5	16	0	10	0	10	6	26	5	10	9
Rb	16	99	104	101	91	91	4	187	81	103	70
Sr	1759	1111	1015	1149	1240	1149	261	913	1295	1120	1178
AN	68.3	46.6	43.6	44.2	46.2	44.3	97.0	37.2	43.7	49.7	50.9
Q	0.0	0.0	5.9	0.0	0.0	0.5	0.0	3.4	0.0	4.2	2.5
Or	3.4	14.7	20.6	20.3	21.3	17.5	0.5	26.4	13.8	19.3	14.0
Ab	20.7	29.6	27.9	32.2	31.2	33.3	0.4	31.7	33.0	28.6	28.4
An	44.6	25.8	21.5	25.5	26.8	26.5	13.7	18.8	25.6	28.3	29.5
Ne	1.5	0.0	0.0	0.0	0.0	0.0	0.0	0.0	0.0	0.0	0.0
Di	9.6	7.5	4.5	3.6	2.9	3.0	21.5	3.5	5.9	0.2	1.8
Hy	0.0	11.8	8.1	10.1	4.8	10.4	28.4	9.9	3.8	11.6	13.3
Ol	9.1	0.0	0.0	0.4	5.9	0.0	1.3	0.0	8.8	0.0	0.0
Mt	7.3	6.1	6.0	5.1	4.1	3.9	20.6	3.4	4.6	3.2	4.4
Il	2.1	2.4	2.0	1.9	2.0	1.8	3.3	1.5	1.8	1.6	2.5
Ap	2.7	2.9	2.1	2.2	2.2	1.9	10.2	0.9	1.7	1.2	2.0
FeO*	10.4	9.47	7.99	8.06	8.09	7.21	22.72	6.61	8.94	6.66	9.23
F/F+M	0.686	0.701	0.732	0.724	0.721	0.731	0.613	0.725	0.663	0.734	0.774
Rb/Sr	0.009	0.089	0.102	0.088	0.073	0.079	0.015	0.205	0.063	0.092	0.059
K/Rb	301	208	279	282	329	270	187	198	239	264	281
Den	2.66	2.57	2.51	2.53	2.54	2.52	2.92	2.48	2.57	2.51	2.56

Sample	PT-162	PT-169A	PT-157
SiO <sub>2</sub>	50.23	39.78	44.97
TiO <sub>2</sub>	1.17	2.75	1.25
Al <sub>2</sub> O <sub>3</sub>	20.11	3.90	3.35
Fe <sub>2</sub> O <sub>3</sub>	2.77	10.21	4.86
FeO	5.56	10.83	10.04
MnO	0.09	0.25	0.25
MgO	3.09	12.19	12.37
CaO	8.25	18.28	19.90
Na <sub>2</sub> O	3.72	0.05	0.05
K <sub>2</sub> O	2.54	0.25	0.16
P <sub>2</sub> O <sub>5</sub>	0.86	2.80	3.14
LOI	0.72	0.27	1.44
Total	<u>99.11</u>	<u>101.56</u>	<u>101.78</u>
Y	16	54	66
Zr	124	98	106
Nb	11	4	0
Rb	99	19	17
Sr	1389	224	185
An	49.4	95.8	95.2
Q	0.0	0.0	1.1
Or	15.0	1.5	1.0
Ab	31.5	0.4	0.4
An	30.7	9.7	8.4
Ne	0.0	0.0	0.0
Di	3.8	49.9	56.2
Hy	1.5	11.5	16.5
Ol	7.6	1.8	0.0
Mt	4.0	14.8	7.1
Il	2.2	5.2	2.4
Ap	2.0	6.5	7.3
FeO*	8.05	20.02	14.41
F/F+M	0.725	0.624	0.542
Rb/Sr	0.071	0.085	0.092
K/Rb	213	109	78
Den	2.56	2.91	2.84

\* Note: PT-94 is from a magnetite-rich layer and PT-169A and PT-157 are mafic clots all found within Gabbro #4.

## e) Diorites-Granodiorites

Diorites Sample	PT-9	PT-20	PT-29	PT-36	PT-37A	PT-38	PT-39B	PT-40	PT-41	PT-67	PT-95
SiO <sub>2</sub>	59.25	56.35	56.81	52.25	50.98	52.03	55.33	51.58	56.15	58.90	57.26
TiO <sub>2</sub>	0.88	0.73	0.75	1.03	1.17	1.23	0.87	1.04	0.76	0.77	0.71
Al <sub>2</sub> O <sub>3</sub>	16.00	16.01	16.29	18.26	19.52	19.28	17.79	18.13	17.11	16.32	17.05
Fe <sub>2</sub> O <sub>3</sub>	3.10	3.15	2.74	2.84	2.78	3.63	2.91	3.66	3.49	3.00	2.47
FeO	3.98	3.87	4.06	5.65	5.71	5.48	4.58	5.94	4.09	3.87	4.28
MnO	0.12	0.13	0.12	0.11	0.10	0.13	0.09	0.14	0.10	0.10	0.11
MgO	3.13	3.07	3.11	2.74	2.31	2.02	2.92	3.10	2.99	2.63	2.72
CaO	4.90	4.78	4.81	6.61	6.94	6.80	5.85	7.66	5.23	4.31	5.30
Na <sub>2</sub> O	3.45	3.24	3.51	3.48	3.37	3.98	3.57	3.41	3.76	3.83	3.74
K <sub>2</sub> O	3.61	4.49	4.38	3.60	3.30	3.39	3.84	2.34	4.67	4.73	3.49
P <sub>2</sub> O <sub>5</sub>	0.28	0.34	0.31	0.69	0.84	0.86	0.40	0.83	0.41	0.29	0.35
LOI	0.78	0.66	0.82	0.66	0.93	0.50	0.60	0.66	0.82	0.70	0.58
Total	99.48	96.82	97.71	97.92	97.95	99.33	98.75	98.49	99.58	99.45	98.06
Y	23	20	19	19	21	21	25	25	26	24	15
Zr	365	446	348	178	262	217	357	219	304	325	276
Nb	27	15	16	10	6	9	20	13	18	22	18
Rb	160	150	147	90	75	76	147	87	151	198	125
Sr	705	744	719	1138	1228	1094	1045	1055	951	707	864
An	37.5	36.7	34.7	44.5	49.9	42.3	41.2	48.6	33.5	29.2	38.0
Q	10.5	6.1	5.0	0.0	0.0	0.0	3.1	2.3	1.8	5.9	6.5
Or	21.3	26.5	25.9	21.3	19.5	20.0	22.7	13.8	27.6	28.0	20.6
Ab	29.2	27.4	29.7	29.5	28.5	33.7	30.2	28.9	31.8	32.4	31.7
An	17.5	15.9	15.8	23.6	28.4	24.7	21.2	27.3	16.0	13.4	19.4
Di	4.0	4.5	4.9	3.9	0.5	2.8	4.3	4.4	5.9	5.0	3.8
Hy	9.4	9.0	9.5	11.3	11.9	5.4	9.9	12.0	8.2	7.7	9.8
Ol	0.0	0.0	0.0	0.1	0.0	2.6	0.0	0.0	0.0	0.0	0.0
Mc	4.5	4.6	4.0	4.1	4.0	5.3	4.2	5.3	5.1	4.4	3.6
Il	1.7	1.4	1.4	2.0	2.2	2.3	1.7	2.0	1.4	1.5	1.4
Ap	0.7	0.8	0.7	1.6	2.0	2.0	0.9	1.9	1.0	0.7	0.8
FeO*	6.77	6.71	6.53	8.21	8.21	8.75	7.20	9.23	7.23	6.57	6.50
F/F+M	0.688	0.690	0.681	0.752	0.783	0.815	0.714	0.751	0.710	0.717	0.709
Rb/Sr	0.227	0.202	0.204	0.079	0.061	0.069	0.141	0.082	0.159	0.280	0.145
K/Rb	187	248	247	332	365	370	217	223	257	198	232
Den	2.47	2.47	2.47	2.53	2.54	2.53	2.50	2.56	2.48	2.46	2.48

Sample	PT-96	PT-109	PT-110	PT-112	PT-120	PT-121	PT-122	PT-129	PT-130	PT-149	PT-150	85874
SiO <sub>2</sub>	54.78	58.80	56.42	56.92	51.58	56.68	54.95	52.26	51.80	53.63	53.67	55.88
TiO <sub>2</sub>	0.94	0.61	0.72	0.85	0.98	0.82	0.85	0.81	1.01	0.71	0.73	0.94
Al <sub>2</sub> O <sub>3</sub>	17.15	17.21	16.50	16.83	18.57	16.71	16.34	19.08	15.99	19.27	17.85	16.77
Fe <sub>2</sub> O <sub>3</sub>	2.65	2.09	3.66	2.73	2.66	3.27	2.99	3.29	4.03	2.48	3.06	2.93
FeO	6.05	3.50	4.01	4.41	5.31	4.52	4.74	4.40	6.27	4.51	5.30	4.95
MnO	0.12	0.07	0.12	0.11	0.11	0.10	0.10	0.10	0.14	0.09	0.12	0.13
MgO	3.91	2.30	3.59	3.09	3.61	3.68	3.44	2.89	5.28	2.64	3.90	3.64
CaO	6.64	4.53	5.55	5.09	6.19	5.25	5.27	7.09	7.63	7.00	7.28	5.26
Na <sub>2</sub> O	3.62	3.55	3.75	3.59	3.85	3.89	3.29	3.97	3.06	4.09	3.46	3.13
K <sub>2</sub> O	2.63	3.95	3.91	4.35	3.61	4.36	4.43	3.09	3.06	3.17	3.05	4.15
P <sub>2</sub> O <sub>5</sub>	0.51	0.25	0.43	0.43	0.61	0.45	0.47	0.68	0.66	0.54	0.52	0.45
LOI	0.80	0.49	0.56	0.86	1.73	0.21	0.80	1.12	0.83	1.40	0.86	1.36
Total	99.80	97.35	99.22	99.26	98.81	99.94	97.67	98.78	99.46	99.53	99.80	99.59
Y	19	13	17	16	16	16	17	19	22	14	18	16
Zr	343	324	340	408	487	299	411	210	243	192	249	379
Nb	16	17	18	22	29	23	25	12	15	8	9	16
Rb	109	150	139	164	203	181	180	83	108	98	113	151
Sr	920	847	828	832	1138	848	857	1229	970	1245	1061	1076
AN	42.7	39.2	34.4	35.8	41.1	31.7	37.5	42.8	45.7	41.8	45.2	42.4
Q	3.1	9.2	3.8	4.2	0.0	1.6	2.9	0.0	0.5	0.0	0.9	4.7
Or	15.5	23.3	23.1	25.7	21.3	25.8	26.2	18.3	16.3	18.7	18.0	24.5
Ab	30.6	30.0	31.7	30.4	32.6	32.9	27.8	33.6	25.9	34.6	29.3	26.5
An	22.8	19.4	16.6	17.0	22.7	15.3	16.7	25.1	21.8	24.9	24.2	19.5
Di	5.6	1.2	6.5	4.5	3.3	6.4	5.2	4.6	9.6	5.2	7.0	3.0
Hy	14.6	9.0	9.2	10.2	0.6	10.5	11.1	5.7	15.3	6.6	12.5	13.0
Ol	0.0	0.0	0.0	0.0	9.4	0.0	0.0	2.5	0.0	2.0	0.0	0.0
Mt	3.8	3.0	5.3	4.0	3.9	4.7	4.3	4.8	5.8	3.6	4.4	4.3
Il	1.8	1.2	1.4	1.6	1.9	1.6	1.6	1.5	1.9	1.4	1.4	1.8
Ap	1.2	0.6	1.0	1.0	1.4	1.0	1.1	1.6	1.5	1.3	1.2	1.0
FeO	8.44	5.38	7.30	6.87	7.70	7.46	7.43	7.36	9.90	6.74	8.05	7.59
F/F+M	0.686	0.703	0.674	0.693	0.684	0.673	0.686	0.721	0.655	0.721	0.677	0.679
Rb/Sr	0.118	0.177	0.168	0.197	0.178	0.213	0.210	0.068	0.111	0.079	0.107	0.140
K/Rb	200	219	233	220	148	200	204	309	212	268	224	228
Den	2.54	2.45	2.49	2.48	2.53	2.49	2.50	2.52	2.58	2.51	2.54	2.50

NOTE: Sample 85874 is from a piece of drill core provided by the Manitoba Mines Branch.

Granodiorites  
Sample

	PT-1	PT-3B	PT-5	PT-7B	PT-24B	PT-27	PT-28	PT-30	PT-42	PT-43	PT-44
SiO <sub>2</sub>	58.56	59.07	59.90	60.41	58.07	57.73	57.52	58.01	55.65	57.17	56.32
TiO <sub>2</sub>	0.68	0.63	0.59	0.71	0.76	0.56	0.71	0.65	0.77	0.77	0.76
Al <sub>2</sub> O <sub>3</sub>	16.43	16.08	16.99	16.22	16.73	16.40	16.72	16.41	16.83	17.26	16.39
Fe <sub>2</sub> O <sub>3</sub>	2.32	2.37	2.59	2.67	3.23	3.05	2.67	3.03	3.43	3.20	7.20
FeO	3.85	3.38	3.17	3.49	3.86	3.98	4.05	3.73	4.26	3.67	N.D.
MnO	0.10	0.07	0.10	0.10	0.12	0.13	0.12	0.10	0.12	0.11	0.12
MgO	2.55	2.19	2.16	2.36	3.20	3.10	3.10	2.92	3.52	2.85	3.45
CaO	4.33	4.01	4.38	4.13	5.18	4.87	4.79	4.53	5.75	4.79	5.16
Na <sub>2</sub> O	3.39	3.36	4.02	3.08	3.50	3.09	3.41	3.30	3.48	3.70	4.30
K <sub>2</sub> O	4.73	4.38	3.85	4.96	3.96	4.55	4.69	4.81	3.90	4.95	4.34
P <sub>2</sub> O <sub>5</sub>	0.23	0.21	0.17	0.28	0.37	0.38	0.36	0.37	0.46	0.34	0.43
LOI	1.61	1.46	0.74	0.80	0.78	0.70	1.49	0.62	0.64	0.49	0.84
Total	98.78	97.21	98.66	99.21	99.76	98.54	99.63	98.48	98.81	99.30	99.31
Y	24	24	18	24	20	23	21	23	25	24	26
Zr	409	359	327	466	385	462	380	497	367	318	428
Nb	23	17	15	21	18	12	16	14	19	20	21
Rb	185	153	141	170	155	146	148	157	159	183	154
Sr	702	702	788	667	869	947	772	714	888	859	827
AN	35.3	35.8	33.3	37.7	38.1	40.0	36.3	36.1	39.0	33.6	25.7
Q	7.3	10.6	9.1	11.1	7.3	7.4	5.0	6.7	3.9	3.0	1.9
Or	28.0	25.9	22.8	29.3	23.4	26.9	27.7	28.4	23.1	29.3	25.7
Ab	28.7	28.4	34.0	26.1	29.6	26.2	28.9	27.9	29.5	31.3	36.4
An	15.7	15.9	17.0	15.8	18.3	17.4	16.5	15.8	18.8	15.9	12.6
Di	3.5	2.2	3.0	2.3	4.1	3.4	4.0	3.5	5.4	4.6	6.2
Hy	8.8	7.7	6.8	8.0	9.4	10.2	10.1	9.1	10.1	7.9	5.7
Mt	3.4	3.4	3.8	3.9	4.7	4.4	3.9	4.4	5.0	4.6	0.0
Il	1.3	1.2	1.1	1.4	1.4	1.1	1.4	1.2	1.5	1.5	0.3
Hem	0.0	0.0	0.0	0.0	0.0	0.0	0.0	0.0	0.0	0.0	7.2
Ti	0.0	0.0	0.0	0.0	0.0	0.0	0.0	0.0	0.0	0.0	1.5
Ap	0.5	0.5	0.4	0.7	0.9	0.9	0.8	0.9	1.1	0.8	1.0
FeO*	5.94	5.51	5.50	5.89	6.77	6.73	6.45	6.46	7.35	6.55	6.48
F/F+M	0.703	0.718	0.722	0.717	0.683	0.689	0.680	0.692	0.680	0.700	0.657
Rb/Sr	0.264	0.218	0.179	0.255	0.178	0.154	0.192	0.220	0.179	0.213	0.186
K/Rb	212	238	227	242	212	259	263	254	204	225	234
Den	2.46	2.44	2.44	2.44	2.48	2.47	2.47	2.46	2.50	2.47	2.44

Sample	PT-53	PT-54	PT-57	PT-58	PT-59	PT-60	PT-62	PT-66	PT-68	PT-70	PT-100
SiO <sub>2</sub>	56.41	56.97	55.29	59.40	59.51	59.32	59.61	62.82	58.79	60.18	55.02
TiO <sub>2</sub>	0.73	0.71	0.73	0.67	0.69	0.68	0.49	0.54	0.73	0.58	0.74
Al <sub>2</sub> O <sub>3</sub>	16.99	17.07	16.14	16.77	16.62	16.59	17.74	16.56	17.06	17.06	18.50
Fe <sub>2</sub> O <sub>3</sub>	3.18	3.37	6.88	2.93	2.79	2.84	2.00	2.61	2.77	2.70	2.17
FeO	4.19	4.16	N.D.	3.74	3.74	3.81	2.69	2.84	4.02	3.32	4.61
MnO	0.10	0.12	0.11	0.12	0.10	0.09	0.07	0.07	0.10	0.11	0.10
MgO	3.07	2.94	3.15	2.38	2.52	2.62	1.76	1.93	2.67	2.55	2.65
CaO	4.99	5.33	4.80	4.53	4.55	4.54	4.10	3.93	4.68	4.51	6.21
Na <sub>2</sub> O	3.61	4.08	3.52	4.06	3.64	3.87	4.58	3.73	3.54	3.88	3.35
K <sub>2</sub> O	4.56	4.16	4.55	4.28	4.22	4.21	3.69	4.22	4.65	4.20	3.62
P <sub>2</sub> O <sub>5</sub>	0.40	0.42	0.40	0.27	0.36	0.27	0.17	0.21	0.34	0.28	0.42
LOI	1.32	0.45	0.52	0.76	1.03	1.12	1.05	0.89	0.86	0.68	0.47
Total	<u>99.55</u>	<u>99.78</u>	<u>96.09</u>	<u>99.91</u>	<u>99.77</u>	<u>99.96</u>	<u>97.95</u>	<u>100.35</u>	<u>100.21</u>	<u>100.05</u>	<u>97.86</u>
Y	23	23	13	23	24	21	16	19	23	18	18
Zr	393	398	399	335	415	373	275	328	463	358	365
Nb	24	17	25	19	24	21	12	19	19	16	12
Rb	176	146	188	163	171	176	124	173	163	159	131
Sr	834	841	780	775	760	758	858	697	744	812	1118
AN	35.3	31.6	33.2	30.2	35.0	32.1	30.4	33.6	36.1	33.8	46.6
Q	3.2	2.6	4.9	6.5	8.8	7.3	7.2	13.7	6.4	8.3	3.8
Or	27.0	24.6	26.9	25.3	24.9	24.9	21.8	24.9	27.5	24.8	21.4
Ab	30.6	34.5	29.8	34.3	30.8	32.8	38.8	31.6	30.0	32.8	28.4
An	16.7	16.0	14.8	14.9	16.5	15.5	17.0	16.0	16.9	16.7	24.8
Di	4.4	6.3	3.3	4.7	3.0	4.3	1.9	1.7	3.3	3.1	2.7
Hy	9.6	8.2	6.3	7.2	8.4	8.1	6.1	6.3	9.1	8.0	10.9
Mt	4.6	4.9	0.0	4.3	4.1	4.1	2.9	3.8	4.0	3.9	3.2
Il	1.4	1.4	0.2	1.3	1.3	1.3	0.9	1.0	1.4	1.1	1.4
Hem	0.0	0.0	6.9	0.0	0.0	0.0	0.0	0.0	0.0	0.0	0.0
Ti	0.0	0.0	1.5	0.0	0.0	0.0	0.0	0.0	0.0	0.0	0.0
Ap	0.9	1.0	0.9	0.6	0.8	0.6	0.4	0.5	0.8	0.7	1.0
FeO*	7.05	7.19	6.19	6.38	6.25	6.37	4.49	5.19	6.51	5.75	6.56
F/F+M	0.700	0.713	0.667	0.732	0.716	0.711	0.722	0.732	0.712	0.697	0.715
Rb/Sr	0.211	0.174	0.241	0.210	0.225	0.232	0.145	0.248	0.219	0.196	0.117
K/Rb	215	236	201	218	205	199	247	202	237	219	229
Den	2.48	2.48	2.44	2.46	2.46	2.46	2.43	2.42	2.46	2.45	2.50

Sample	PT-101	PT-103	PT-106	PT-131	PT-132	PT-139
SiO <sub>2</sub>	55.11	52.95	59.23	55.35	60.24	62.39
TiO <sub>2</sub>	0.85	0.78	0.73	1.04	0.59	0.55
Al <sub>2</sub> O <sub>3</sub>	17.29	19.75	16.61	16.95	16.96	16.36
Fe <sub>2</sub> O <sub>3</sub>	2.56	2.78	2.99	3.39	2.69	2.18
FeO	5.31	4.26	3.98	4.85	3.19	2.92
MnO	0.09	0.08	0.10	0.11	0.09	0.08
MgO	3.27	2.55	2.77	3.47	2.42	1.92
CaO	5.84	7.35	4.72	6.28	4.46	3.79
Na <sub>2</sub> O	3.08	4.07	3.35	3.65	3.94	3.55
K <sub>2</sub> O	4.08	2.59	4.33	2.70	4.15	4.23
P <sub>2</sub> O <sub>5</sub>	0.50	0.51	0.37	0.50	0.28	0.20
LOI	0.68	0.99	0.39	0.70	0.41	0.62
Total	<u>98.66</u>	<u>98.66</u>	<u>99.57</u>	<u>98.99</u>	<u>99.42</u>	<u>98.79</u>
Y	16	18	14	23	8	10
Zr	249	209	384	558	309	322
Nb	15	12	21	30	17	22
Rb	139	93	163	148	169	185
Sr	1001	1422	790	842	793	680
AN	45.0	44.8	38.2	41.5	32.9	35.1
Q	3.6	0.4	9.0	5.8	8.6	14.1
Or	24.1	15.3	25.6	16.0	24.5	25.0
Ab	26.1	34.4	28.4	30.9	33.3	30.0
An	21.3	28.0	17.5	21.9	16.3	16.2
Di	3.6	4.2	2.8	4.9	3.2	1.0
Hy	12.8	8.7	9.3	10.9	7.3	7.1
Mt	3.7	4.0	4.3	4.9	3.9	3.2
Il	1.6	1.5	1.4	2.0	1.1	1.0
Ap	1.2	1.2	0.9	1.2	0.7	0.5
FeO*	7.61	6.76	6.67	7.90	5.61	4.88
F/F+M	0.702	0.728	0.710	0.698	0.702	0.721
Rb/Sr	0.139	0.065	0.206	0.176	0.213	0.272
K/Rb	244	231	220	151	204	190
Den	2.51	2.52	2.47	2.52	2.44	2.42

Q Quartz Monzonites

Sample	PT-32	PT-61	PT-64	PT-65	PT-69	PT-88	PT-89	PT-90	PT-107	PT-108	PT-111
SiO <sub>2</sub>	66.65	65.79	65.48	64.18	63.97	70.04	66.27	65.42	66.51	65.52	66.60
TiO <sub>2</sub>	0.32	0.37	0.31	0.36	0.40	0.26	0.24	0.36	0.24	0.25	0.38
Al <sub>2</sub> O <sub>3</sub>	16.26	16.42	15.93	16.36	16.14	16.73	15.55	16.95	16.37	16.08	16.32
Fe <sub>2</sub> O <sub>3</sub>	1.86	2.15	1.80	1.69	1.78	1.76	0.96	1.77	1.54	1.76	1.82
FeO	1.63	1.88	1.65	1.85	2.30	1.39	1.84	2.07	1.29	1.19	2.14
MnO	0.06	0.09	0.07	0.08	0.08	0.06	0.05	0.06	0.05	0.04	0.06
MgO	1.06	1.35	0.95	1.11	1.27	1.08	0.65	1.26	0.91	0.99	1.06
CaO	2.76	3.01	2.71	3.02	2.91	2.72	2.43	3.26	2.74	2.68	3.01
Na <sub>2</sub> O	3.96	3.92	4.05	4.12	4.21	4.15	4.01	5.75	4.07	3.76	3.62
K <sub>2</sub> O	4.50	4.25	4.41	4.31	4.20	4.69	4.27	3.92	4.59	4.57	4.24
P <sub>2</sub> O <sub>5</sub>	0.01	0.05	0.07	0.04	0.05	0.03	0.01	0.07	0.01	0.03	0.09
LOI	1.45	0.72	0.82	1.17	0.82	0.72	1.42	0.93	0.49	0.29	0.41
Total	100.52	100.00	98.25	98.24	98.13	103.63	97.70	101.82	98.81	97.16	99.75
Y	15	13	10	12	14	11	6	6	2	3	8
Zr	201	229	200	210	231	172	163	206	161	164	217
Nb	12	13	11	10	13	11	6	9	6	4	14
Rb	159	158	174	141	146	155	129	128	125	128	160
Sr	649	674	646	762	667	687	706	782	788	764	655
AN	28.4	30.6	26.4	27.8	26.3	27.3	25.8	15.4	27.2	29.2	31.9
Q	18.5	17.8	17.6	15.2	14.7	20.3	19.5	8.9	17.9	18.8	20.7
Or	26.6	25.1	26.1	25.5	24.8	27.7	25.2	23.2	27.1	27.0	25.1
Ab	33.5	33.2	34.3	34.9	35.6	35.1	33.9	48.7	34.4	31.8	30.6
An	13.3	14.6	12.3	13.4	12.7	13.2	11.8	8.9	12.8	13.1	14.4
C	0.0	0.0	0.0	0.0	0.0	0.0	0.0	0.0	0.0	0.2	0.5
Di	0.3	0.0	0.6	1.1	1.1	0.1	0.1	5.6	0.6	0.0	0.0
Hy	3.6	4.6	3.2	3.9	4.9	3.4	3.8	2.3	2.8	2.9	4.6
Mt	2.7	3.1	2.6	2.5	2.6	2.6	1.4	2.6	2.2	2.6	2.6
Il	0.6	0.7	0.6	0.6	0.8	0.5	0.5	0.7	0.5	0.5	0.7
Ap	0.0	0.1	0.2	0.1	0.1	0.1	0.0	0.2	0.0	0.1	0.2
FeO*	3.30	3.82	3.27	3.37	3.90	2.97	2.70	3.66	2.68	2.77	3.78
F/F+M	0.760	0.743	0.779	0.757	0.758	0.737	0.809	0.747	0.750	0.740	0.784
Rb/Sr	0.245	0.234	0.269	0.185	0.219	0.226	0.183	0.164	0.159	0.168	0.244
K/Rb	235	223	210	254	239	251	275	254	305	296	220
Den	2.38	2.39	2.38	2.39	2.39	2.37	2.37	2.39	2.37	2.37	2.39

\* Note: PT-90 is a sample of a quartz monzonite dyke.

Sample	PT-113	PT-116	PT-117	PT-133	PT-134	PT-136	PT-137	PT-138	PT-140	PT-141	PT-143
SiO <sub>2</sub>	68.75	66.94	67.42	64.94	64.85	68.36	67.95	67.08	67.12	65.80	67.71
TiO <sub>2</sub>	0.19	0.26	0.29	0.35	0.38	0.25	0.24	0.29	0.32	0.33	0.26
Al <sub>2</sub> O <sub>3</sub>	15.27	16.11	16.09	16.70	16.37	16.21	15.87	16.33	16.36	16.14	16.33
Fe <sub>2</sub> O <sub>3</sub>	1.22	1.57	1.35	1.59	2.06	1.79	1.75	1.54	1.60	2.08	1.51
FeO	1.00	1.37	1.60	2.22	2.12	1.29	1.29	1.62	1.94	1.57	1.70
MnO	0.03	0.07	0.03	0.05	0.05	0.06	0.05	0.05	0.05	0.08	0.05
MgO	0.80	0.82	0.84	1.20	1.51	1.02	0.96	1.07	0.85	0.95	0.99
CaO	2.13	2.66	2.70	3.18	3.19	2.62	2.62	2.81	2.84	2.75	2.86
Na <sub>2</sub> O	3.62	3.90	4.03	4.31	4.03	4.17	3.59	4.14	3.77	3.66	3.85
K <sub>2</sub> O	4.85	4.36	4.57	4.09	4.12	4.54	4.49	4.35	4.40	4.36	4.56
P <sub>2</sub> O <sub>5</sub>	0.01	0.04	0.02	0.10	0.10	0.01	0.02	0.05	0.06	0.06	0.03
LOI	0.39	0.35	0.68	0.74	0.53	0.33	0.35	0.50	0.17	0.47	0.74
Total	98.26	98.45	99.62	99.47	99.31	100.65	99.18	99.83	99.48	98.25	100.59
Y	6	0	0	5	4	3	2	6	6	4	4
Zr	138	161	156	215	212	162	150	159	194	185	166
Nb	12	9	6	11	12	11	9	8	10	11	8
Rb	161	163	172	155	160	167	165	154	161	167	149
Sr	589	710	708	705	727	710	663	725	657	654	725
AN	25.5	28.2	26.5	27.9	29.7	25.5	29.8	27.3	30.0	30.0	29.8
Q	23.1	20.3	19.1	15.1	16.2	19.5	22.6	18.4	20.3	20.3	19.7
Or	28.7	25.8	27.0	24.2	24.4	26.8	26.5	25.7	26.0	25.8	27.0
Ab	30.6	33.0	34.1	36.5	34.1	35.3	30.4	35.0	31.9	31.0	32.6
An	10.5	12.9	12.3	14.1	14.4	12.1	12.9	13.1	13.7	13.3	13.8
C	0.2	0.2	0.0	0.0	0.0	0.0	0.4	0.0	0.4	0.5	0.0
Di	0.0	0.0	0.8	0.8	0.6	0.7	0.0	0.4	0.0	0.0	0.2
Hy	2.6	3.0	3.1	4.9	5.1	2.8	3.0	3.8	3.9	3.1	3.9
Mt	1.8	2.3	2.0	2.3	3.0	2.6	2.5	2.2	2.3	3.0	2.2
Il	0.4	0.5	0.6	0.7	0.7	0.5	0.5	0.6	0.6	0.6	0.5
Ap	0.0	0.1	0.1	0.2	0.2	0.0	0.1	0.1	0.1	0.1	0.1
FeO*	2.10	2.78	2.82	3.65	3.97	2.90	2.87	3.01	3.38	3.44	3.06
F/F+M	0.727	0.777	0.772	0.755	0.727	0.744	0.752	0.741	0.801	0.788	0.758
Rb/Sr	0.273	0.230	0.243	0.220	0.220	0.235	0.249	0.212	0.245	0.255	0.206
K/Rb	250	222	221	219	214	226	226	234	227	217	254
Den	2.35	2.37	2.37	2.39	2.40	2.37	2.37	2.38	2.38	2.38	2.37

Sample	PT-144	PT-145	PT-146
SiO <sub>2</sub>	68.73	68.46	66.99
TiO <sub>2</sub>	0.25	0.23	0.21
Al <sub>2</sub> O <sub>3</sub>	16.03	16.08	16.21
Fe <sub>2</sub> O <sub>3</sub>	1.30	1.82	1.70
FeO	1.55	1.24	1.30
MnO	0.06	0.05	0.04
MgO	0.87	0.84	0.83
CaO	2.46	2.79	2.65
Na <sub>2</sub> O	3.82	4.33	3.33
K <sub>2</sub> O	4.64	4.44	4.45
P <sub>2</sub> O <sub>5</sub>	0.01	0.03	0.02
LOI	0.64	0.35	0.82
Total	<u>100.36</u>	<u>100.66</u>	<u>98.55</u>
Y	2	2	4
Zr	153	158	158
Nb	7	11	7
Rb	152	180	155
Sr	658	684	738
AN	27.3	23.6	31.6
Q	21.5	19.4	23.4
Or	27.4	26.2	26.3
Ab	32.3	36.6	28.2
An	12.1	11.3	13.0
C	0.3	0.0	1.2
Di	0.0	1.8	0.0
Hy	3.6	1.7	2.8
Mt	1.9	2.6	2.5
Il	0.5	0.4	0.4
Ap	0.0	0.1	0.1
FeO*	2.72	2.88	2.83
F/F+M	0.762	0.777	0.776
Rb/Sr	0.231	0.263	0.210
K/Rb	253	205	238
Den	2.37	2.37	2.37

## APPENDIX 2

### WHOLE ROCK RARE EARTH ELEMENT ANALYSES

Thirteen whole rock rare earth element analyses (La, Ce, Nd, Sm, Eu, Tb, Ho, Tm, Yb and Lu) were done on selected gabbroic to quartz monzonitic samples by Becquerel Laboratories Inc.. Analyses also included the trace elements Th and Sc. Lower limits of detection (in ppm) were as follows:

La	0.5
Ce	5
Nd	10
Sm	0.1
Eu	1
Tb	1
Ho	1
Tm	0.5
Yb	0.5
Lu	0.1
Th	0.5
Sc	0.05

In all samples, Ho and Tm were lower than detection limits and are not included in the analyses. All data are expressed in parts per million (ppm). La/Lu<sub>CN</sub> ratios were calculated using the chondritic values from Thompson (1982).

	<u>PT-10</u>	<u>PT-55</u>	<u>PT-74</u>	<u>PT-125</u>	<u>PT-18</u>	<u>PT-126</u>	<u>PT-34</u>	<u>PT-46</u>
La	27.60	104.00	7.66	14.70	123.00	123.00	82.60	144.00
Ce	50.00	207.00	15.40	29.50	247.00	243.00	176.00	271.00
Nd	23.60	83.30	12.20	20.20	95.80	92.40	85.50	102.00
Sm	3.23	12.30	2.32	3.37	13.60	12.90	11.90	14.40
Eu	1.07	1.91	1.01	1.04	3.03	2.49	2.85	2.99
Tb	0.52	1.34	0.60	0.58	1.09	0.84	0.63	0.87
Yb	0.96	2.57	0.86	0.52	1.35	1.79	1.42	1.81
Lu	0.11	0.37	0.09	0.08	0.19	0.25	0.12	0.27
Th	6.06	27.40	0	1.16	15.40	28.50	3.25	27.50
Sc	15.60	14.80	24.60	31.30	13.60	10.90	13.20	12.20
REE <sub>T</sub>	107.09	412.79	40.14	69.99	485.06	476.67	361.02	537.34
La/Lu <sub>CN</sub>	25.85	28.96	8.77	18.93	66.70	50.69	70.92	54.95
Eu/Sm	0.33	0.16	0.44	0.31	0.22	0.19	0.24	0.21
	<u>PT-44</u>	<u>PT-36</u>	<u>PT-24</u>	<u>PT-87</u>	<u>PT-136</u>	<u>Key:</u>	<u>PT-10</u>	<u>Gabbro #1</u>
La	121.00	112.00	120.00	55.90	60.40		<u>PT-55</u>	<u>Gabbro #1</u>
Ce	245.00	221.00	237.00	100.00	107.00		<u>PT-74</u>	<u>Gabbro #2</u>
Nd	96.50	95.40	82.30	32.80	32.90		<u>PT-125</u>	<u>Gabbro #2</u>
Sm	14.30	13.50	12.00	4.70	4.86		<u>PT-18</u>	<u>Gabbro #3</u>
Eu	2.59	3.27	2.29	1.07	1.08		<u>PT-126</u>	<u>Gabbro #3</u>
Tb	1.04	0.78	0.62	0.32	0.42		<u>PT-34</u>	<u>Gabbro #4</u>
Yb	2.08	1.92	1.84	0.92	1.14		<u>PT-46</u>	<u>Gabbro #4</u>
Lu	0.38	0.18	0.22	0.16	0.17		<u>PT-44</u>	<u>Diorite</u>
							<u>PT-35</u>	<u>Diorite</u>
							<u>PT-24</u>	<u>Granodiorite</u>
Th	40.30	7.91	35.80	20.40	20.50		<u>PT-87</u>	<u>Quartz Monzonite</u>
Sc	13.30	13.30	11.70	4.23	4.25		<u>PT-136</u>	<u>Quartz Monzonite</u>
REE <sub>T</sub>	482.89	448.05	456.27	195.87	207.97			
La/Lu <sub>CN</sub>	32.81	64.11	56.20	36.00	36.61			
Eu/Sm	0.18	0.24	0.19	0.23	0.22			

### APPENDIX 3 MICROPROBE ANALYSES

- 3a) Plagioclase
- 3b) Alkali Feldspar
- 3c) Oxide Minerals
- 3d) Pyroxene
- 3e) Amphibole
- 3f) Biotite

KEY: 1 = Gabbro #1      2 = Gabbro #2  
3 = Gabbro #3      4 = Gabbro #4  
5 = Diorites      6 = Granodiorites  
0 = Quartz Monzonites

A total of 229 analyses comprising seven different minerals were obtained at the Department of Geological Sciences, University of Manitoba with a MAC-5 electron microprobe using an energy dispersive system via a Kevex 7100 multichannel analyzer with a Li drifted Si detector. Analysis was at 15kv, 6-7uamps (on fayalite reference standard) and for 200 live counting seconds. Synthetic fayalite was used as a current and voltage standard. Corrections for peak overlap and  $k\alpha$ - $k\beta$  element interference were made using peak modelling and overlay techniques practised at the University of Manitoba. Processing was with the MAGIC V program of Colby (1980).

The data set includes 128 plagioclase analyses, 27 alkali feldspar analyses, 17 magnetite analyses, 7 ilmenite analyses, 13 pyroxene analyses, 20 amphibole analyses and 17 biotite analyses. The first two digits of each sample number correspond to the whole rock sample numbers listed in Appendix 1 and to the sample location given in Figure 4 (minus the prefix designator "PT").

## a) Plagioclase Analyses

Sample Key	55-1 1	55-2 1	55-3 1	55-4 1	55-5 1	55-8 1	55-9A 1	55-9B 1	55-10 1	74-1 2
SiO <sub>2</sub>	60.92	59.12	56.82	61.29	57.04	60.90	56.14	59.77	57.80	53.26
Al <sub>2</sub> O <sub>3</sub>	24.62	26.65	26.89	24.45	26.60	24.71	27.26	25.21	26.85	29.95
FeO	0.00	0.00	0.51	0.00	0.00	0.00	0.00	0.00	0.00	0.00
CaO	6.44	8.36	9.13	6.28	9.10	6.33	9.52	7.36	9.00	12.62
Na <sub>2</sub> O	7.74	6.70	5.39	7.19	6.10	7.51	5.73	6.66	6.01	4.00
K <sub>2</sub> O	0.15	0.14	0.23	0.17	0.12	0.13	0.12	0.12	0.00	0.00
Total	99.87	100.97	98.97	99.38	98.96	99.58	98.77	99.12	99.66	99.83
Cations per 24 Oxygens										
Si	8.129	7.844	7.715	8.189	7.741	10.849	7.642	8.035	7.770	7.228
Al	3.872	4.166	4.303	3.851	4.255	5.189	4.373	3.994	4.254	4.790
Fe	0.000	0.000	0.058	0.000	0.000	0.000	0.000	0.000	0.000	0.000
Ca	0.920	1.189	1.328	0.899	1.323	1.208	1.389	1.061	1.297	1.835
Na	2.002	1.724	1.419	1.863	1.604	2.594	1.513	1.737	1.566	1.052
K	0.026	0.024	0.041	0.028	0.021	0.031	0.021	0.020	0.000	0.000
Total	14.949	14.947	14.864	14.830	14.944	19.871	14.938	14.847	14.887	14.905
End Member Compositions										
Ab	67.9	58.7	50.9	66.7	54.4	67.7	51.8	61.6	54.7	36.5
An	31.2	40.5	47.7	32.2	44.9	31.5	47.5	37.6	45.3	63.5
Or	0.9	0.8	1.4	1.0	0.7	0.8	0.7	0.7	0.0	0.0

Sample Key	74-2 2	74-3 2	74-4 2	74-7 2	74-8 2	74-9 2	18-1 3	18-2 3	18-3 3	18-4 3
SiO <sub>2</sub>	53.49	52.99	53.71	53.03	53.63	51.44	57.97	60.77	58.31	59.20
Al <sub>2</sub> O <sub>3</sub>	29.38	29.85	29.40	29.29	29.59	30.31	26.36	24.79	26.27	25.48
CaO	12.28	12.39	11.98	12.11	11.82	13.20	8.58	6.47	8.26	7.42
Na <sub>2</sub> O	4.04	3.99	4.51	4.00	4.28	3.64	6.28	7.44	6.52	7.03
K <sub>2</sub> O	0.00	0.00	0.00	0.26	0.00	0.03	0.09	0.09	0.08	0.04
Total	99.19	99.22	99.60	98.69	99.32	98.62	99.28	99.56	99.44	99.17
Cations per 24 Oxygens										
Si	7.294	7.230	7.299	7.278	7.297	7.089	7.822	8.122	7.850	7.972
Al	4.722	4.801	4.709	4.739	4.745	4.923	4.191	3.906	4.168	4.044
Ca	1.795	1.811	1.744	1.781	1.723	1.948	1.241	0.926	1.191	1.070
Na	1.068	1.055	1.188	1.064	1.130	0.973	1.643	1.927	1.702	1.836
K	0.000	0.000	0.000	0.045	0.000	0.006	0.016	0.015	0.014	0.006
Total	14.879	14.897	14.940	14.907	14.895	14.939	14.913	14.896	14.925	14.928
End Member Compositions										
Ab	37.3	36.8	40.5	36.8	39.6	33.2	56.7	67.2	58.5	63.0
An	62.7	63.2	59.5	61.6	60.4	66.6	42.8	32.3	41.0	36.8
Or	0.0	0.0	0.0	1.6	0.0	0.2	0.5	0.5	0.5	0.2

Sample Key	18-5 3	18-12 3	73-2 3	73-5 3	73-6 3	73-7 3	73-9 3	85-1 3	85-3 3	85-7 3
SiO <sub>2</sub>	58.65	57.20	57.28	57.57	56.34	57.30	55.66	56.30	58.40	58.89
Al <sub>2</sub> O <sub>3</sub>	25.47	26.98	26.39	26.63	27.69	26.73	26.96	27.46	25.90	25.68
FeO	0.57	0.00	0.00	0.00	0.00	0.00	0.54	0.35	0.00	0.00
CaO	7.49	9.06	8.57	8.90	9.97	8.86	9.72	9.74	7.84	7.57
Na <sub>2</sub> O	6.93	6.25	6.19	6.34	5.85	6.27	5.57	5.72	6.78	7.02
K <sub>2</sub> O	0.20	0.14	0.05	0.07	0.17	0.12	0.00	0.14	0.12	0.15
Total	99.31	99.63	98.48	99.51	100.02	99.28	98.45	99.71	99.04	99.31

## Cations per 24 Oxygens

Si	7.923	7.715	7.792	7.765	7.593	7.748	7.622	7.612	7.891	7.932
Al	4.055	4.288	4.231	4.233	4.398	4.259	4.352	4.376	4.124	4.076
Fe	0.064	0.000	0.000	0.000	0.000	0.000	0.062	0.039	0.000	0.000
Ca	1.084	1.310	1.250	1.286	1.439	1.284	1.426	1.411	1.134	1.093
Na	1.814	1.633	1.632	1.658	1.529	1.644	1.479	1.500	1.775	1.832
K	0.034	0.024	0.008	0.011	0.029	0.020	0.000	0.025	0.021	0.027
Total	14.974	14.970	14.913	14.953	14.988	14.955	14.941	14.963	14.945	14.960

## End Member Compositions

Ab	61.9	55.1	56.5	56.1	51.0	55.8	50.9	51.1	60.6	62.1
An	37.0	44.1	43.2	43.5	48.0	43.5	49.1	48.1	38.7	37.0
Or	1.2	0.8	0.3	0.4	1.0	0.7	0.0	0.8	0.7	0.9

Sample Key	85-8 3	85-9 3	34-2 4	34-4 4	34-5 4	34-7 4	34-9 4	34-11 4	47-1 4	47-2 4
SiO <sub>2</sub>	59.12	59.24	52.76	52.05	53.71	52.90	52.15	52.87	58.44	58.27
Al <sub>2</sub> O <sub>3</sub>	25.89	25.19	30.39	30.34	29.74	29.77	29.96	30.21	25.93	25.58
CaO	7.86	7.10	13.10	13.45	12.42	12.48	12.89	12.83	8.04	7.66
Na <sub>2</sub> O	6.89	7.37	3.85	3.37	4.11	3.95	3.71	3.83	6.68	6.74
K <sub>2</sub> O	0.14	0.18	0.00	0.10	0.00	0.00	0.00	0.00	0.08	0.19
Total	99.90	99.08	100.10	99.31	99.98	99.10	98.71	99.74	99.17	98.44

## Cations per 24 Oxygens

Si	7.918	7.994	7.153	7.119	7.271	7.229	7.165	7.185	7.886	7.917
Al	4.087	4.005	4.857	4.891	4.745	4.795	4.852	4.839	4.123	4.097
Ca	1.128	1.026	1.903	1.970	1.802	1.827	1.897	1.868	1.163	1.116
Na	1.789	1.927	1.011	0.895	1.079	1.047	0.989	1.008	1.747	1.776
K	0.024	0.031	0.000	0.018	0.000	0.000	0.000	0.000	0.014	0.034
Total	14.946	14.983	14.924	14.893	14.897	14.898	14.903	14.900	14.933	14.940

## End Member Compositions

Ab	60.8	64.6	34.7	31.0	37.5	36.4	34.2	35.1	59.8	60.7
An	38.4	34.4	65.3	68.4	62.5	63.6	65.8	64.9	39.8	38.1
Or	0.8	1.0	0.0	0.6	0.0	0.0	0.0	0.0	0.5	1.1

Sample Key	47-3 4	47-4 4	47-5 4	38-1 5	38-2 5	38-3 5	38-4 5	38-10 5	38-11 5	39-1 5
SiO <sub>2</sub>	58.60	58.34	56.53	56.71	57.56	58.92	58.76	58.71	58.24	59.22
Al <sub>2</sub> O <sub>3</sub>	25.52	25.95	27.09	27.46	26.71	25.97	26.26	26.00	25.75	25.21
CaO	7.43	8.22	9.47	9.88	8.76	7.81	8.21	8.29	8.19	7.17
Na <sub>2</sub> O	6.89	6.53	5.65	5.53	6.49	7.08	6.45	6.48	6.49	7.30
K <sub>2</sub> O	0.00	0.09	0.12	0.11	0.00	0.15	0.12	0.14	0.00	0.13
Total	98.44	99.13	98.86	99.69	99.52	99.93	99.80	99.62	98.67	99.03
Cations per 24 Oxygens										
Si	7.947	7.877	7.681	7.647	7.760	7.897	7.875	7.888	7.894	7.992
Al	4.079	4.130	4.337	4.365	4.244	4.102	4.148	4.117	4.113	4.009
Ca	1.080	1.189	1.379	1.427	1.266	1.121	1.179	1.193	1.190	1.037
Na	1.813	1.709	1.489	1.445	1.696	1.839	1.677	1.689	1.705	1.910
K	0.000	0.016	0.020	0.019	0.000	0.026	0.020	0.025	0.000	0.023
Total	14.919	14.921	14.906	14.903	14.966	14.985	14.899	14.912	14.902	14.971
End Member Compositions										
Ab	62.7	58.7	51.5	50.0	57.3	61.6	58.3	58.1	58.9	64.3
An	37.3	40.8	47.7	49.4	42.7	37.5	41.0	41.1	41.1	34.9
Or	0.0	0.5	0.7	0.7	0.0	0.9	0.7	0.8	0.0	0.8

Sample Key	39-3 5	39-4 5	39-5 5	39-6 5	39-8 5	41-1 5	41-4 5	41-6 5	41-7 5	41-11 5
SiO <sub>2</sub>	58.86	57.43	58.43	58.64	59.73	61.08	59.26	60.46	56.96	59.19
Al <sub>2</sub> O <sub>3</sub>	25.18	26.66	25.72	25.85	25.15	24.14	25.18	24.17	27.06	25.71
FeO	0.23	0.00	0.00	0.00	0.00	0.00	0.00	0.00	0.00	0.00
CaO	7.21	8.79	7.86	7.59	6.88	5.86	7.29	6.07	9.22	7.54
Na <sub>2</sub> O	7.22	6.16	6.78	6.60	7.39	8.00	7.16	7.88	6.27	7.19
K <sub>2</sub> O	0.16	0.23	0.13	0.11	0.12	0.16	0.10	0.07	0.11	0.13
Total	98.86	99.27	98.92	98.79	99.27	99.24	98.99	98.65	99.62	99.76
Cations per 24 Oxygens										
Si	7.969	7.764	7.904	7.925	8.029	8.191	7.997	8.160	7.690	7.938
Al	4.019	4.248	4.101	4.118	3.985	3.815	4.005	3.844	4.305	4.063
Fe	0.026	0.000	0.000	0.000	0.000	0.000	0.000	0.000	1.333	0.000
Ca	1.046	1.273	1.140	1.099	0.991	0.843	1.054	0.878	0.000	1.084
Na	1.895	1.614	1.778	1.729	1.927	2.080	1.874	2.061	1.641	1.869
K	0.028	0.039	0.023	0.019	0.021	0.028	0.017	0.011	0.019	0.022
Total	14.983	14.938	14.946	14.890	14.953	14.957	14.947	14.954	14.988	14.976
End Member Compositions										
Ab	63.8	55.2	60.5	60.7	65.6	70.5	63.6	69.9	54.8	62.8
An	35.2	43.5	38.7	38.6	33.7	28.5	35.8	29.7	44.5	36.4
Or	0.9	1.4	0.8	0.7	0.7	0.9	0.6	0.4	0.6	0.7

Sample Key	41-12 5	70-1 6	70-4 6	70-6 6	70-8 6	70-9 6	70-11 6	70-12 6	21-1 6	21-2 6
SiO <sub>2</sub>	59.03	60.30	61.50	60.71	60.71	60.45	60.54	61.43	57.43	59.58
Al <sub>2</sub> O <sub>3</sub>	25.25	24.97	23.81	24.26	24.70	24.75	24.92	23.83	26.67	25.91
CaO	7.20	6.89	5.46	6.02	6.86	6.83	6.82	5.88	8.84	7.83
Na <sub>2</sub> O	6.88	7.30	8.25	8.08	7.53	7.47	7.44	7.96	6.09	6.80
K <sub>2</sub> O	0.09	0.11	0.16	0.12	0.10	0.14	0.15	0.15	0.09	0.16
Total	98.45	99.57	99.18	99.19	99.90	99.64	99.87	99.25	99.12	100.28
Cations per 24 Oxygens										
Si	7.998	8.072	8.244	8.155	8.104	8.091	8.083	8.231	7.768	7.942
Al	4.032	3.940	3.761	3.840	3.886	3.905	3.922	3.764	4.251	4.071
Ca	1.045	0.989	0.785	0.866	0.981	0.980	0.976	0.844	1.281	1.119
Na	1.807	1.895	2.145	2.104	1.949	1.938	1.926	2.069	1.598	1.757
K	0.015	0.019	0.027	0.021	0.017	0.025	0.026	0.026	0.015	0.027
Total	14.897	14.915	14.962	14.986	14.937	14.939	14.933	14.934	14.913	14.916
End Member Compositions										
Ab	63.0	65.3	72.5	70.3	66.1	65.9	65.8	70.4	55.2	60.5
An	36.4	34.1	26.5	29.0	33.3	33.3	33.3	28.7	44.3	38.5
Or	0.5	0.6	0.9	0.7	0.6	0.8	0.9	0.9	0.5	0.9

Sample Key	21-4 6	21-5 6	21-7 6	21-11 6	24-2 6	24-3 6	24-5 6	24-9 6	24-10 6	24-11 6
SiO <sub>2</sub>	62.06	61.10	61.21	59.55	61.62	61.41	58.48	58.51	61.54	59.39
Al <sub>2</sub> O <sub>3</sub>	24.31	24.41	24.45	24.59	23.62	23.54	25.73	25.95	23.89	25.48
Fe <sub>2</sub> O <sub>3</sub>	0.00	0.00	0.00	0.00	0.00	0.00	0.00	0.00	0.00	0.32
CaO	5.90	6.43	6.22	6.49	5.57	5.62	7.80	7.99	5.68	7.46
Na <sub>2</sub> O	8.08	7.73	7.97	7.74	8.25	7.89	6.82	6.69	7.97	7.21
K <sub>2</sub> O	0.11	0.14	0.15	0.12	0.07	0.11	0.06	0.06	0.09	0.11
Total	100.46	99.81	100.00	98.49	99.13	98.57	98.89	99.20	99.17	99.97
Cations per 24 Oxygens										
Si	8.215	8.154	8.156	8.070	8.262	8.272	7.909	7.890	8.243	7.957
Al	3.792	3.840	3.839	3.927	3.732	3.738	4.101	4.124	3.772	4.023
Fe <sup>3+</sup>	0.000	0.000	0.000	0.000	0.000	0.000	0.000	0.000	0.000	0.036
Ca	0.837	0.920	0.888	0.942	0.800	0.811	1.130	1.154	0.815	1.072
Na	2.073	2.000	2.060	2.035	2.144	2.060	1.788	1.750	2.069	1.872
K	0.019	0.024	0.026	0.021	0.012	0.019	0.010	0.010	0.016	0.019
Total	14.936	14.938	14.969	14.995	14.950	14.900	14.938	14.928	14.915	14.979
End Member Compositions										
Ab	70.8	68.0	69.3	67.9	72.5	71.3	61.1	60.0	71.4	63.2
An	28.6	31.2	29.9	31.4	27.1	28.1	38.6	39.6	28.1	36.1
Or	0.6	0.8	0.9	0.7	0.4	0.7	0.4	0.4	0.5	0.6

Sample Key	24-12 6	24-13 6	42-1 6	42-5 6	42-6 6	42-7 6	42-11 6	42-13 6	42-14 6	42-15 6
SiO <sub>2</sub>	59.76	59.42	59.63	59.27	57.91	59.75	60.32	61.13	60.27	59.09
Al <sub>2</sub> O <sub>3</sub>	25.32	25.17	25.09	25.54	25.82	25.59	25.54	23.63	25.81	25.97
CaO	7.28	7.08	7.07	7.50	8.20	7.30	7.26	5.91	7.61	7.95
Na <sub>2</sub> O	7.29	7.06	7.04	7.14	6.49	7.38	7.16	7.79	7.21	6.91
K <sub>2</sub> O	0.12	0.11	0.13	0.15	0.16	0.07	0.14	0.10	0.15	0.13
Total	99.77	98.84	98.96	99.60	98.58	100.09	100.42	98.56	101.05	100.05
Cations per 24 Oxygens										
Si	8.003	8.018	8.036	7.958	7.868	7.977	8.016	8.243	7.974	7.906
Al	3.995	4.004	3.985	4.042	4.135	4.027	4.001	3.755	4.024	4.094
Ca	1.045	1.024	1.021	1.079	1.194	1.044	1.034	0.854	1.079	1.140
Na	1.894	1.848	1.839	1.858	1.710	1.910	1.845	2.037	1.850	1.793
K	0.021	0.019	0.022	0.026	0.028	0.012	0.024	0.017	0.026	0.022
Total	14.958	14.913	14.903	14.963	14.935	14.970	14.920	14.906	14.953	14.955
End Member Compositions										
Ab	64.0	63.9	63.8	62.7	58.3	64.4	63.6	70.0	62.6	60.7
An	35.3	35.4	35.4	36.4	40.7	35.2	35.6	29.4	36.5	38.6
Or	0.7	0.7	0.8	0.9	0.9	0.4	0.8	0.6	0.9	0.8

Sample Key	42-16 6	42-18 6	44-1 6	44-5 6	44-6 6	44-11 6	58-1 6	58-6 6	58-11 6	58-12 6
SiO <sub>2</sub>	59.79	59.54	60.16	60.86	61.47	59.67	59.88	59.56	58.49	61.00
Al <sub>2</sub> O <sub>3</sub>	25.90	25.04	25.06	24.88	23.87	25.53	25.57	24.84	25.57	24.38
CaO	7.31	7.24	7.20	6.56	5.65	7.65	7.45	6.81	7.94	6.45
Na <sub>2</sub> O	7.18	7.26	6.98	7.39	8.08	6.90	7.25	7.48	6.71	7.64
K <sub>2</sub> O	0.10	0.20	0.13	0.13	0.14	0.10	0.09	0.09	0.11	0.09
Total	100.28	99.28	99.53	99.82	99.21	99.85	100.24	98.78	98.82	99.56
Cations per 24 Oxygens										
Si	7.962	8.015	8.058	8.116	8.236	7.982	7.983	8.047	7.920	8.157
Al	4.065	3.973	3.956	3.910	3.770	4.024	4.018	3.956	4.080	3.842
Ca	1.043	1.045	1.033	0.937	0.811	1.097	1.064	0.985	1.152	0.925
Na	1.855	1.895	1.813	1.912	2.099	1.789	1.875	1.960	1.761	1.982
K	0.017	0.034	0.022	0.022	0.023	0.017	0.015	0.016	0.018	0.016
Total	14.942	14.962	14.882	14.897	14.939	14.909	14.955	14.964	14.931	14.922
End Member Compositions										
Ab	63.6	63.7	63.2	66.6	71.5	61.6	63.5	66.2	60.1	67.8
An	35.8	35.1	36.0	32.7	27.6	37.8	36.0	33.3	39.3	31.6
Or	0.6	1.2	0.8	0.8	0.8	0.6	0.5	0.5	0.6	0.5

Sample Key	58-13 6	58-14 6	68-1 6	68-3 6	68-4 6	68-5 6	68-9 6	68-10 6	65-2 0	65-3 0
SiO <sub>2</sub>	60.00	57.10	59.61	62.28	60.35	60.13	60.10	58.78	62.10	67.04
Al <sub>2</sub> O <sub>3</sub>	24.88	27.38	25.39	24.09	25.26	25.01	25.24	25.79	23.97	20.70
CaO	6.84	9.72	7.12	5.30	6.71	6.69	7.24	7.71	5.46	2.00
Na <sub>2</sub> O	7.44	5.77	7.23	8.39	7.75	7.71	7.27	6.75	8.36	10.13
K <sub>2</sub> O	0.12	0.15	0.17	0.09	0.15	0.19	0.11	0.07	0.19	0.09
Total	99.28	100.12	99.52	100.15	100.22	99.73	99.96	99.10	100.08	99.96

## Cations per 24 Oxygens

Si	8.063	7.668	7.999	8.258	8.040	8.052	8.027	7.925	8.250	8.807
Al	3.940	4.334	4.016	3.764	3.966	3.947	3.973	4.098	3.753	3.205
Ca	0.984	1.398	1.023	0.752	0.958	0.959	1.036	1.114	0.777	0.282
Na	1.939	1.502	1.880	2.157	2.001	2.001	1.882	1.764	2.153	2.580
K	0.020	0.026	0.030	0.016	0.025	0.033	0.020	0.013	0.032	0.015
Total	14.946	14.928	14.948	14.947	14.990	14.992	14.938	14.914	14.965	14.889

## End Member Compositions

Ab	65.8	51.3	64.1	73.7	67.1	66.9	64.1	61.0	72.7	89.7
An	33.5	47.8	34.9	25.7	32.1	32.1	35.3	38.5	26.2	9.8
Or	0.7	0.9	1.0	0.5	0.9	1.1	0.6	0.4	1.1	0.5

Sample Key	65-6 0	65-8 0	86-1 0	86-2 0	86-3 0	86-4 0	86-7 0	86-8 0	86-9 0	86-11 0
SiO <sub>2</sub>	62.36	60.94	60.62	61.73	61.38	61.21	61.45	62.45	61.68	61.12
Al <sub>2</sub> O <sub>3</sub>	23.76	24.34	24.30	24.00	23.89	24.13	23.91	23.91	24.28	23.64
FeO	0.00	0.00	0.00	0.00	0.00	0.00	0.00	0.00	0.00	0.61
CaO	5.57	6.17	6.07	5.32	5.74	6.06	5.66	5.22	5.92	5.53
Na <sub>2</sub> O	8.11	7.75	7.73	8.25	8.09	7.86	8.16	8.61	7.95	8.31
K <sub>2</sub> O	0.12	0.14	0.13	0.12	0.08	0.00	0.10	0.14	0.11	0.35
Total	99.92	99.34	98.85	99.42	99.18	99.26	99.28	100.33	99.94	99.56

## Cations per 24 Oxygens

Si	8.286	8.165	8.161	8.246	8.228	8.198	8.230	8.271	8.205	8.206
Al	3.721	3.843	3.855	3.778	3.774	3.809	3.774	3.733	3.808	3.741
Fe	0.000	0.000	0.000	0.000	0.000	0.000	0.000	0.000	0.000	0.069
Ca	0.793	0.886	0.876	0.761	0.825	0.870	0.812	0.741	0.843	0.796
Na	2.090	2.014	2.018	2.138	2.104	2.041	2.118	2.212	2.051	2.163
K	0.020	0.025	0.023	0.021	0.014	0.000	0.017	0.023	0.019	0.059
Total	14.910	14.933	14.933	14.944	14.945	14.918	14.951	14.980	14.926	15.034

## End Member Compositions

Ab	72.0	68.9	69.2	73.2	71.5	70.1	71.9	74.3	70.4	71.7
An	27.3	30.3	30.0	26.1	28.0	29.9	27.5	24.9	29.0	26.4
Or	0.7	0.8	0.8	0.7	0.5	0.0	0.6	0.8	0.6	2.0

Sample Key	86-12 0	90-1 *	90-2 *	90-3 *	90-4 *	90-5 *	90-6 *	90-8 *
SiO <sub>2</sub>	61.86	62.84	62.16	61.81	60.73	59.06	60.77	61.41
Al <sub>2</sub> O <sub>3</sub>	23.97	23.87	23.62	23.87	24.29	25.48	23.86	24.55
CaO	5.57	5.34	5.26	5.45	6.31	7.69	5.62	5.98
Na <sub>2</sub> O	8.35	8.22	8.07	8.19	7.80	6.76	7.86	7.78
K <sub>2</sub> O	0.07	0.20	0.17	0.11	0.11	0.15	0.17	0.13
Total	99.82	100.47	99.28	99.43	99.24	99.14	98.28	99.85
Cations per 24 Oxygens								
Si	8.239	8.300	8.305	8.257	8.152	7.961	8.218	8.176
Al	3.762	3.716	3.719	3.758	3.843	4.047	3.803	3.852
Ca	0.794	0.756	0.753	0.780	0.908	1.111	0.814	0.854
Na	2.157	2.106	2.090	2.120	2.030	1.768	2.060	2.008
K	0.011	0.033	0.029	0.019	0.019	0.026	0.029	0.022
Total	14.963	14.911	14.896	14.934	14.952	14.913	14.924	14.912
End Member Compositions								
Ab	72.8	72.7	72.8	72.6	68.7	60.9	71.0	69.7
An	26.8	26.1	26.2	26.7	30.7	38.3	28.0	29.6
Or	0.4	1.2	1.0	0.6	0.6	0.9	1.0	0.8

\* Plagioclase analyses from a quartz monzonite dyke.

DESCRIPTIONS OF PLAGIOCLASES ANALYZED BY MICROPROBE

- 55-1: Phenocryst, Gabbro #1
- 55-2: Fine grained groundmass plagioclase, Gabbro #1
- 55-3: Fine grained groundmass plagioclase, Gabbro #1
- 55-4: Phenocryst, Gabbro #1
- 55-5: Medium grained groundmass plagioclase, Gabbro #1
- 55-8: Phenocryst, Gabbro #1
- 55-9A: Medium grained, zoned (?) groundmass plagioclase, Gabbro #1
- 55-9B: Same plagioclase crystal as 55-9A
- 55-10: Phenocryst, Gabbro #1
- 74-1: Medium grained plagioclase, Gabbro #2
- 74-2: Fine grained plagioclase, Gabbro #2
- 74-3: Medium grained plagioclase, Gabbro #2
- 74-4: Fine grained plagioclase, Gabbro #2
- 74-7: Very fine grained plagioclase, Gabbro #2
- 74-8: Coarse grained plagioclase, Gabbro #2
- 74-9: Medium grained plagioclase, Gabbro #2
- 18-1: Coarse grained cumulus plagioclase, Gabbro #3
- 18-2: Medium grained cumulus plagioclase, Gabbro #3
- 18-3: Very fine grained intercumulus plagioclase, Gabbro #3
- 18-4: Coarse grained cumulus plagioclase, Gabbro #3
- 18-5: Fine grained intercumulus plagioclase, Gabbro #3
- 18-12: Coarse grained cumulus plagioclase, Gabbro #3
- 73-2: Fine grained intercumulus plagioclase, Gabbro #3
- 73-5: Fine grained intercumulus plagioclase, Gabbro #3
- 73-6: Coarse grained cumulus plagioclase, Gabbro #3
- 73-7: Medium grained cumulus plagioclase, Gabbro #3
- 73-9: Medium grained cumulus plagioclase, Gabbro #3
- 85-1: Very coarse grained cumulus plagioclase, Gabbro #3
- 85-3: Coarse grained cumulus plagioclase, Gabbro #3
- 85-7: Very fine grained intercumulus plagioclase, Gabbro #3
- 85-8: Medium grained cumulus plagioclase, Gabbro #3
- 85-9: Medium grained cumulus plagioclase, gabbro #3
- 34-2: Fine grained plagioclase, Gabbro #4
- 34-4: Fine grained plagioclase, Gabbro #4
- 34-5: Coarse grained plagioclase, Gabbro #4
- 34-7: Medium grained plagioclase, Gabbro #4
- 34-9: Medium grained plagioclase, Gabbro #4
- 34-11: Coarse grained plagioclase, Gabbro #4
- 47-1: Plagioclase inclusion (?) in larger plagioclase grain, Gabbro #4
- 47-2: Very coarse grained cumulus plagioclase containing 47-1, Gabbro #4

- 47-3: Coarse grained cumulus plagioclase, Gabbro #4  
 47-4: Fine grained intercumulus plagioclase, Gabbro #4  
 47-5: Coarse grained cumulus plagioclase, Gabbro #4  
 38-1: Medium grained cumulus plagioclase, diorite  
 38-2: Medium grained cumulus plagioclase, diorite  
 38-3: Medium grained cumulus plagioclase, diorite  
 38-4: Coarse grained cumulus plagioclase, diorite  
 38-10: Coarse grained cumulus plagioclase, diorite  
 38-11: Very coarse grained cumulus plagioclase, diorite  
 39-1: Medium grained groundmass plagioclase, quartz diorite  
 39-3: Coarse grained phenocryst, quartz diorite  
 39-4: Very coarse grained phenocryst, quartz diorite.  
 39-5: Fine grained groundmass plagioclase, quartz diorite  
 39-6: Fine grained groundmass, plagioclase, quartz diorite  
 39-8: Medium grained groundmass plagioclase, quartz diorite  
 41-1: Coarse grained phenocryst, diorite  
 41-4: Medium grained groundmass plagioclase, diorite  
 41-6: Medium grained groundmass plagioclase, diorite  
 41-7: Very coarse grained phenocryst, diorite  
 41-11: Coarse grained phenocryst, diorite  
 41-12: Fine grained groundmass plagioclase, diorite  
 70-1: Coarse grained phenocryst, diorite  
 70-4: Plagioclase inclusion (?) in coarse grained alkali feldspar phenocryst, diorite  
 70-6: Medium grained groundmass plagioclase, diorite  
 70-8: Medium grained groundmass plagioclase, diorite  
 70-9: Medium grained groundmass plagioclase, diorite  
 70-11: Medium grained groundmass plagioclase, diorite  
 70-12: Medium grained groundmass plagioclase, diorite  
 21-1: Medium grained plagioclase, granodiorite  
 21-2: Medium grained plagioclase, granodiorite  
 21-4: Medium grained plagioclase, granodiorite  
 21-5: Medium grained plagioclase, granodiorite  
 21-7: Medium grained plagioclase, granodiorite  
 21-11: Medium grained plagioclase, granodiorite  
 24-2: Fine grained groundmass plagioclase, granodiorite  
 24-3: Fine grained groundmass plagioclase, granodiorite  
 24-5: Medium grained groundmass plagioclase, granodiorite  
 24-9: Medium grained groundmass plagioclase, granodiorite  
 24-10: Coarse grained phenocryst, granodiorite  
 24-11: Medium grained groundmass plagioclase, granodiorite  
 24-12: Medium grained groundmass plagioclase, granodiorite  
 24-13: Coarse grained phenocryst, granodiorite

- 42-1: Coarse grained phenocryst, granodiorite  
42-5: Fine grained groundmass plagioclase, granodiorite  
42-6: Medium grained groundmass plagioclase, granodiorite  
42-7: Fine grained resorbed (?) groundmass plagioclase, granodiorite  
42-11: Medium grained groundmass plagioclase, granodiorite  
42-13: Fine grained resorbed plagioclase enclosed (?) in perthite grain, granodiorite  
42-14: As 42-13  
42-15: Coarse grained phenocryst, granodiorite  
42-16: Coarse grained phenocryst, granodiorite  
42-18: Coarse grained phenocryst, granodiorite  
44-1: Coarse grained phenocryst, granodiorite  
44-5: Medium to coarse grained phenocryst, granodiorite  
44-6: Fine grained groundmass plagioclase, granodiorite  
44-11: Medium grained groundmass plagioclase, granodiorite  
58-1: Medium grained groundmass plagioclase, granodiorite  
58-6: Very fine grained plagioclase grain surrounded by alkali feldspar, granodiorite  
58-11: Medium grained groundmass plagioclase, granodiorite  
58-12: Fine grained groundmass plagioclase, granodiorite  
58-13: Medium grained groundmass plagioclase, granodiorite  
58-14: Coarse grained phenocryst, granodiorite  
68-1: Very coarse grained phenocryst, granodiorite  
68-3: Medium grained groundmass plagioclase, granodiorite  
68-4: Medium grained groundmass plagioclase, granodiorite  
68-5: Coarse grained phenocryst, granodiorite  
68-9: Medium grained groundmass plagioclase, granodiorite  
68-10: Medium grained groundmass plagioclase, granodiorite  
65-2: Medium grained groundmass plagioclase, quartz monzonite  
65-3: Medium grained groundmass plagioclase, quartz monzonite  
65-6: Medium grained groundmass plagioclase, quartz monzonite  
65-8: Coarse grained phenocryst, quartz monzonite  
86-1: Medium grained groundmass plagioclase, quartz monzonite  
86-2: Medium grained groundmass plagioclase, quartz monzonite  
86-3: Fine grained groundmass plagioclase, quartz monzonite  
86-4: Medium grained groundmass plagioclase, quartz monzonite  
86-7: Coarse grained phenocryst, quartz monzonite  
86-8: Fine grained groundmass plagioclase, quartz monzonite  
86-9: Fine grained groundmass plagioclase, quartz monzonite  
86-11: Medium grained groundmass plagioclase, quartz monzonite  
86-12: Medium grained groundmass plagioclase, quartz monzonite  
90-1: Fine grained groundmass plagioclase, quartz monzonite dyke  
90-2: Fine grained groundmass plagioclase, quartz monzonite dyke

- 90-3: Fine grained groundmass plagioclase, quartz monzonite dyke
- 90-4: Coarse grained plagioclase phenocryst, quartz monzonite dyke
- 90-5: As 90-4
- 90-6: As 90-4
- 90-8: Medium grained groundmass plagioclase, quartz monzonite dyke

## b) Alkali Feldspar Analyses

Sample Key	18-13 3	85-13 3	47-6 4	38-7 5	38-13 5	39-2 5	39-7 5	41-5 5	41-14 5	70-5 6
SiO <sub>2</sub>	64.41	64.17	64.00	65.36	64.46	64.09	63.24	64.97	64.50	63.95
Al <sub>2</sub> O <sub>3</sub>	18.66	17.93	18.06	18.84	18.61	18.15	18.53	18.15	17.83	18.56
CaO	0.00	0.00	0.00	0.00	0.00	0.02	0.00	0.00	0.00	0.00
Na <sub>2</sub> O	1.60	0.77	0.50	1.60	1.36	0.00	0.89	0.59	0.00	1.32
K <sub>2</sub> O	14.31	15.81	15.50	14.71	14.65	16.53	14.87	16.08	16.59	14.35
BaO	1.52	0.71	0.67	0.58	0.88	0.68	1.49	0.75	0.51	1.51
Total	100.50	99.39	98.73	101.09	99.96	99.47	99.02	100.54	99.43	99.69
Cations per 24 Oxygens										
Si	8.931	8.999	9.005	8.954	8.951	8.990	8.919	9.006	9.037	8.937
Al	3.050	2.963	2.995	3.042	3.046	3.001	3.080	2.964	2.944	3.057
Ca	0.000	0.000	0.000	0.000	0.000	0.002	0.000	0.000	0.000	0.000
Na	0.430	0.209	0.136	0.425	0.365	0.000	0.244	0.158	0.000	0.357
K	2.532	2.829	2.782	2.571	2.595	2.958	2.676	2.844	2.966	2.559
Ba	0.083	0.039	0.037	0.031	0.048	0.037	0.082	0.041	0.028	0.083
Total	15.026	15.039	14.955	15.023	15.005	14.988	15.001	15.013	14.975	14.993
End Member Compositions										
Ab	14.5	8.3	4.7	14.2	12.4	0.0	8.3	5.3	0.0	12.3
An	0.0	0.0	0.0	0.0	0.0	0.1	0.0	0.0	0.0	0.0
Or	85.5	91.7	95.3	85.5	87.6	99.9	91.7	94.7	100.0	87.7

Sample Key	70-10 6	21-8 6	42-2 6	42-8 6	42-12 6	44-4 6	44-8 6	58-4 6	58-7 6	68-2 6
SiO <sub>2</sub>	64.58	64.16	64.35	64.60	63.82	64.47	64.21	64.30	64.74	63.89
Al <sub>2</sub> O <sub>3</sub>	17.73	17.83	17.84	17.88	18.10	17.90	18.17	17.95	18.39	19.70
CaO	0.00	0.00	0.00	0.00	0.00	0.00	0.00	0.00	0.00	1.55
Na <sub>2</sub> O	0.00	0.57	0.61	0.55	0.69	0.00	0.39	0.00	0.45	3.06
K <sub>2</sub> O	16.77	16.16	16.07	16.26	15.59	16.64	16.18	16.68	16.39	11.21
BaO	0.38	0.36	0.39	0.00	1.24	0.00	0.70	0.43	0.66	0.44
Total	99.46	99.08	99.26	99.29	99.44	99.01	99.65	99.36	100.63	99.85
Cations per 24 Oxygens										
Si	9.045	9.013	9.020	9.029	8.971	9.038	8.985	9.017	8.974	8.784
Al	2.927	2.953	2.947	2.946	2.998	2.958	2.996	2.967	3.005	3.192
Ca	0.000	0.000	0.000	0.000	0.000	0.000	0.000	0.000	0.000	0.229
Na	0.000	0.155	0.164	0.150	0.189	0.000	0.107	0.000	0.121	0.815
K	2.997	2.896	2.873	2.899	2.796	2.975	2.888	2.984	2.899	1.967
Ba	0.021	0.020	0.022	0.000	0.068	0.000	0.039	0.024	0.036	0.024
Total	14.990	15.037	15.026	15.024	15.022	14.971	15.015	14.992	15.035	15.011
End Member Compositions										
Ab	0.0	5.1	5.5	4.9	6.3	0.0	3.5	0.0	4.0	27.1
An	0.0	0.0	0.0	0.0	0.0	0.0	0.0	0.0	0.0	7.6
Or	100.0	94.9	94.5	95.1	93.7	100.0	96.5	100.0	96.0	65.3

Sample Key	65-1	65-4	65-5	65-7	65-9	86-5	86-10
	0	0	0	0	0	0	0
SiO <sub>2</sub>	64.29	64.11	64.45	63.76	64.47	64.39	64.21
Al <sub>2</sub> O <sub>3</sub>	18.30	18.08	18.18	18.20	18.19	17.83	18.31
Na <sub>2</sub> O	1.55	0.00	0.55	0.00	0.00	0.00	0.00
K <sub>2</sub> O	14.75	16.63	16.05	16.50	16.61	16.72	16.61
BaO	0.31	0.72	0.48	0.70	0.58	0.45	0.65
Total	99.20	99.54	99.71	99.16	99.85	99.39	99.78
	Cations per 24 Oxygens						
Si	8.973	8.994	8.993	8.975	9.000	9.030	8.978
Al	3.010	2.990	2.990	3.020	2.993	2.947	3.018
Na	0.420	0.000	0.149	0.000	0.000	0.000	0.000
K	2.625	2.976	2.857	2.963	2.958	2.992	2.963
Ba	0.017	0.039	0.026	0.039	0.032	0.025	0.035
Total	15.045	14.999	15.015	14.997	14.983	14.994	14.994
	End Member Compositions						
Ab	13.8	0.0	5.0	0.0	0.0	0.0	0.0
An	0.0	0.0	0.0	0.0	0.0	0.0	0.0
Or	86.2	100.0	95.0	100.0	100.0	100.0	100.0

c) Oxide Minerals

Atomic proportions calculated using the computer program "FORMULA" (Ercit, 1987).

Magnetite Analyses

Sample	73-8B	73-10A	85-4A	85-6	34-3B	34-10A	38-5B	38-8A	41-13	21-10
Key	3	3	3	3	4	4	5	5	5	6
SiO <sub>2</sub>	0.34	0.37	0.00	0.00	0.26	0.00	0.00	0.00	0.00	0.00
TiO <sub>2</sub>	0.86	0.00	0.00	0.00	1.07	2.07	0.00	0.00	0.00	0.00
Al <sub>2</sub> O <sub>3</sub>	0.00	0.00	0.00	0.00	0.27	0.00	0.00	0.00	0.00	0.00
Fe <sub>2</sub> O <sub>3</sub>	64.47	66.67	66.66	67.13	63.50	62.19	67.50	67.91	67.15	67.65
FeO	32.50	31.75	32.59	32.00	33.50	34.44	32.22	32.16	31.68	32.08
MnO	0.00	0.00	0.00	0.00	0.00	0.32	0.00	0.00	0.00	0.00
Cr <sub>2</sub> O <sub>3</sub>	0.59	0.37	0.00	0.00	0.37	0.33	0.00	0.00	0.00	0.43
V <sub>2</sub> O <sub>5</sub>	0.31	0.25	0.94	0.65	0.73	1.05	0.67	0.58	0.53	0.52
Total	99.07	99.41	100.19	99.77	99.70	100.40	100.39	100.65	99.36	100.68

Based on 32 anions and 24 cations

Si	0.105	0.115	0.000	0.000	0.080	0.000	0.000	0.000	0.000	0.000
Ti	0.201	0.000	0.000	0.000	0.248	0.477	0.000	0.000	0.000	0.000
Al	0.000	0.000	0.000	0.000	0.098	0.000	0.000	0.000	0.000	0.000
Fe <sup>3+</sup>	15.052	15.527	15.427	15.602	14.711	14.330	15.592	15.648	15.674	15.581
Fe <sup>2+</sup>	8.433	8.217	8.382	8.265	8.625	8.818	8.272	8.235	8.217	8.210
Mn	0.000	0.000	0.000	0.000	0.000	0.083	0.000	0.000	0.000	0.000
Cr	0.145	0.091	0.000	0.000	0.090	0.080	0.000	0.000	0.000	0.104
V	0.064	0.051	0.191	0.133	0.148	0.212	0.136	0.117	0.109	0.105
Total	24.000	24.000	24.000	24.000	24.000	24.000	24.000	24.000	24.000	24.000

Note: Fe<sub>2</sub>O<sub>3</sub> and Fe<sup>3+</sup> determined by stoichiometry.

Sample	44-7	58-8	58-15	68-7	70-7	70-15	65-10
Key	6	6	6	6	6	6	0
SiO <sub>2</sub>	0.00	0.39	0.33	0.26	0.00	0.00	0.39
TiO <sub>2</sub>	0.00	0.00	0.00	0.00	0.00	0.00	0.00
Al <sub>2</sub> O <sub>3</sub>	0.00	0.00	0.00	0.00	0.00	0.00	0.00
Fe <sub>2</sub> O <sub>3</sub>	67.36	66.86	66.19	67.86	66.87	67.19	67.95
FeO	32.01	32.07	31.89	31.40	31.38	32.03	31.80
MnO	0.00	0.00	0.00	0.00	0.00	0.00	0.00
Cr <sub>2</sub> O <sub>3</sub>	0.27	0.00	0.00	0.53	0.00	0.31	0.63
V <sub>2</sub> O <sub>5</sub>	0.57	0.38	0.48	0.00	0.47	0.60	0.00
Total	100.21	99.70	98.89	100.05	98.72	100.13	100.77

Based on 32 anions and 24 cations

Si	0.000	0.120	0.103	0.080	0.000	0.000	0.119
Ti	0.000	0.000	0.000	0.000	0.000	0.000	0.000
Al	0.000	0.000	0.000	0.000	0.000	0.000	0.000
Fe <sup>3+</sup>	15.587	15.527	15.499	15.711	15.709	15.559	15.610
Fe <sup>2+</sup>	8.232	8.275	8.300	8.080	8.194	8.244	8.119
Mn	0.000	0.000	0.000	0.000	0.000	0.000	0.000
Cr	0.066	0.000	0.000	0.129	0.000	0.075	0.152
V	0.116	0.077	0.099	0.000	0.097	0.122	0.000
Total	24.000	24.000	24.000	24.000	24.000	24.000	24.000

Note: Fe<sub>2</sub>O<sub>3</sub> and Fe<sup>3+</sup> determined by stoichiometry

Ilmenite Analyses

Sample Key	55-11 1	55-12 1	18-9 3	73-8A 3	73-10B 3	85-4B 3	34-3A 4
TiO <sub>2</sub>	50.00	50.77	50.73	49.82	50.81	51.30	50.85
Fe <sub>2</sub> O <sub>3</sub>	4.85	3.90	3.44	4.15	2.20	2.62	2.99
FeO	42.05	42.84	42.36	42.01	42.78	43.11	44.36
MnO	2.87	2.78	3.22	2.75	2.87	2.98	1.35
Total	99.78	100.29	99.74	98.74	98.66	100.01	99.55

Based on 6 anions and 4 cations

Ti	1.907	1.926	1.934	1.920	1.958	1.950	1.943
Fe <sup>3+</sup>	0.185	0.148	0.131	0.160	0.085	0.100	0.114
Fe <sup>2+</sup>	1.784	1.807	1.796	1.801	1.833	1.823	1.885
Mn	0.123	0.119	0.138	0.119	0.125	0.128	0.058
Total	4.000	4.000	4.000	4.000	4.000	4.000	4.000

Sample Key	34-10B 4	38-5A 5	38-8B 5	41-13 5	21-10 6	42-17 6
TiO <sub>2</sub>	50.32	50.39	50.88	50.59	50.49	51.26
Fe <sub>2</sub> O <sub>3</sub>	3.98	4.46	3.97	3.34	3.62	2.41
FeO	43.76	42.26	42.31	41.20	40.34	38.77
MnO	1.47	3.01	3.40	4.24	5.00	7.23
Total	99.53	100.13	100.56	99.36	99.44	99.67

Based on 6 anions and 4 cations

Ti	1.924	1.915	1.925	1.936	1.931	1.954
Fe <sup>3+</sup>	0.152	0.170	0.150	0.128	0.138	0.092
Fe <sup>2+</sup>	1.861	1.786	1.780	1.753	1.715	1.644
Mn	0.063	0.129	0.145	0.183	0.215	0.310
Total	4.000	4.000	4.000	4.000	4.000	4.000

Note: Fe<sub>2</sub>O<sub>3</sub> and Fe<sup>3+</sup> determined by stoichiometry.

## DESCRIPTIONS OF OXIDE MINERALS ANALYZED BY MICROPROBE

Magnetite

- 73-8B: Fine grained euhedral magnetite surrounded by biotite. Contains ilmenite lamellae as well as internal and external granular exsolutions. No titanite rim.
- 73-10A: Fine grained euhedral magnetite within biotite grain in aggregate of mafic minerals. Contains ilmenite lamellae and internal sandwich exsolutions. No titanite rim.
- 85-4A: Fine grained euhedral magnetite in aggregate of mafic minerals and partially enclosed in biotite. Contains internal granular ilmenite. No titanite rim.
- 85-6: Fine grained subhedral to anhedral magnetite in aggregate of mafic minerals.
- 34-3B: Fine grained, anhedral magnetite in aggregate of mafic minerals with core of ilmenite. No titanite rim.
- 34-10A: Fine grained anhedral magnetite inclusion in amphibole grain with ilmenite exsolutions (?). No titanite rim.
- 38-5B: Medium grained anhedral opaque grain in aggregate of mafic minerals comprised of intergrown magnetite and ilmenite. No titanite rim.
- 38-8A: Fine grained euhedral opaque grain interstitial to plagioclase comprised of magnetite and ilmenite. No titanite rim.
- 41-13: Magnetite with internal granular exsolutions.
- 21-10: Fine to medium grained subhedral inclusion of magnetite in coarse grained primary biotite. Grain is bounded by several apatite inclusions in the biotite. Contains small internal granular exsolutions of ilmenite. Titanite rim.
- 44-7: Fine grained anhedral magnetite adjacent to amphibole. Thick titanite rim.
- 58-8: Fine grained subhedral magnetite as inclusion in mafic mineral grain. Titanite rim.
- 58-15: Fine grained isolated subhedral magnetite grain with partial titanite rim.
- 68-7: Fine grained subhedral magnetite partially enclosed in biotite grain. Thin titanite rim.

- 70-7: Fine grained subhedral magnetite partially surrounded by biotite. Metamict core? Thick titanite rim.
- 70-15: Fine to very fine grained magnetite in aggregate of mafic minerals. Thick titanite rim.
- 65-10: Fine grained, euhedral interstitial magnetite. No titanite rim.

#### Ilmenite

- 55-11: Fine grained euhedral ilmenite intergrown with fine grained biotite. Thick titanite rim.
- 55-12: Fine grained subhedral ilmenite surrounded by fine grained biotite. Titanite rim.
- 18-9: Fine to medium grained euhedral magnetite in aggregate of mafic minerals. Thin titanite rim.
- 73-8A: Ilmenite lamellae and internal granular exsolutions in magnetite.
- 73-10B: Ilmenite exsolutions in magnetite.
- 85-4B: Internal granular ilmenite exsolutions in magnetite.
- 34-3A: Ilmenite core in magnetite.
- 34-10B: Ilmenite exsolution (?) in magnetite.
- 38-5A: Ilmenite intergrown with magnetite.
- 38-8B: Intergranular ilmenite exsolution in magnetite.
- 41-13: Ilmenite exsolution in magnetite.
- 21-10: Ilmenite exsolution in magnetite.
- 42-17: Fine grained anhedral ilmenite within aggregate of amphibole and biotite. Thick titanite rim.

## d) Pyroxenes

Sample Key	18-10 3	73-3 3	85-5 3	39-10 5	41-2 5	41-9 5	70-2 6	24-7 6	42-3 6	42-9 6
SiO <sub>2</sub>	50.97	51.32	51.52	50.87	51.27	51.13	51.76	51.48	50.17	51.71
TiO <sub>2</sub>	0.32	0.65	0.49	0.37	0.22	0.48	0.22	0.55	0.79	0.17
Al <sub>2</sub> O <sub>3</sub>	1.16	1.86	0.75	1.95	1.12	1.87	1.30	1.13	3.38	1.36
FeO	11.08	9.67	13.50	10.26	10.63	10.62	10.98	9.24	11.86	11.11
MnO	0.31	0.38	0.49	0.23	0.39	0.35	0.51	0.51	0.36	0.28
MgO	12.63	13.16	11.36	13.44	11.77	12.83	12.34	12.38	13.59	13.30
CaO	20.68	21.30	20.39	19.83	21.88	20.96	22.51	23.62	17.33	19.53
Na <sub>2</sub> O	0.00	0.00	0.00	0.00	0.00	0.00	0.00	0.00	0.60	0.00
K <sub>2</sub> O	0.04	0.07	0.00	0.19	0.12	0.14	0.26	0.09	0.39	0.33
Cr <sub>2</sub> O <sub>3</sub>	0.00	0.00	0.00	0.00	0.00	0.00	0.00	0.00	0.21	0.00
Total	97.19	98.41	98.50	97.14	97.40	98.38	99.88	99.00	98.68	97.79
Cations per 24 Oxygens										
Si	7.892	7.806	7.947	7.830	7.931	7.810	7.841	7.832	7.639	7.926
Ti	0.037	0.074	0.057	0.043	0.026	0.055	0.026	0.063	0.090	0.020
Al	0.212	0.334	0.136	0.354	0.204	0.337	0.232	0.202	0.607	0.246
Fe	1.435	1.230	1.741	1.321	1.376	1.356	1.391	1.175	1.511	1.425
Mn	0.041	0.049	0.064	0.030	0.051	0.045	0.065	0.065	0.046	0.037
Mg	2.914	2.983	2.612	3.083	2.715	2.921	2.785	2.807	3.084	3.039
Ca	3.431	3.471	3.370	3.270	3.627	3.431	3.653	3.851	2.826	3.207
Na	0.000	0.000	0.000	0.000	0.000	0.000	0.000	0.000	0.177	0.000
K	0.008	0.013	0.000	0.037	0.025	0.026	0.050	0.018	0.076	0.065
Cr	0.000	0.000	0.000	0.000	0.000	0.000	0.000	0.000	0.026	0.000
Total	15.970	15.960	15.927	15.968	15.955	15.981	16.043	16.013	16.082	15.965
End Member Compositions										
Wo	43.1	43.7	42.8	41.1	46.0	43.0	45.5	48.1	36.1	40.7
En	37.8	39.4	33.8	41.0	35.4	38.5	35.8	36.0	44.1	40.1
Sample Key	44-2 6	44-9 6	58-9 6							
SiO <sub>2</sub>	51.67	52.39	51.35							
TiO <sub>2</sub>	0.13	0.35	0.22							
Al <sub>2</sub> O <sub>3</sub>	1.11	1.77	1.14							
FeO	11.40	11.34	11.26							
MnO	0.41	0.38	0.48							
MgO	12.49	14.40	12.10							
CaO	20.87	17.15	21.12							
Na <sub>2</sub> O	0.00	0.00	0.00							
K <sub>2</sub> O	0.10	0.16	0.11							
Total	98.18	97.94	97.78							
Cations per 24 Oxygens										
Si	7.928	7.949	7.920							
Ti	0.015	0.040	0.026							
Al	0.201	0.316	0.207							
Fe	1.463	1.439	1.453							
Mn	0.053	0.049	0.063							
Mg	2.856	3.256	2.781							
Ca	3.431	2.788	3.490							
Na	0.000	0.000	0.000							
K	0.020	0.032	0.021							
Total	15.967	15.869	15.961							
End Member Compositions										
Wo	43.2	35.7	44.1							
En	37.1	44.2	36.2							
Fo	19.7	20.1	19.7							

## e) Amphiboles

Sample Key	55-7 1	74-5 2	74-6 2	18-8 3	18-11 3	73-4 3	85-2 3	85-12 3	34-6 4	34-8 4
SiO <sub>2</sub>	48.34	53.70	52.07	44.31	46.62	52.05	54.05	54.32	54.62	40.50
TiO <sub>2</sub>	0.10	0.13	0.12	2.26	0.47	1.35	0.00	0.00	0.00	0.23
Al <sub>2</sub> O <sub>3</sub>	5.59	2.92	4.34	6.57	5.53	3.07	0.40	0.32	0.68	16.96
FeO	18.43	10.04	10.77	19.58	20.63	13.44	16.04	16.11	18.63	16.52
MnO	0.30	0.15	0.00	0.41	0.38	0.28	0.38	0.49	0.75	0.00
MgO	11.08	17.46	16.67	9.24	9.26	13.78	13.53	13.82	18.37	8.66
CaO	12.38	12.55	12.21	11.89	12.32	13.19	12.60	12.65	3.68	11.78
Na <sub>2</sub> O	0.54	0.00	0.57	0.55	0.51	0.00	0.00	0.00	0.00	2.08
K <sub>2</sub> O	0.49	0.00	0.10	0.94	0.74	0.16	0.10	0.04	0.02	0.34
Cl	0.00	0.00	0.00	0.12	0.00	0.00	0.00	0.00	0.00	0.00
Total	97.25	96.95	96.85	95.87	96.46	97.32	97.10	97.75	96.75	97.07

## Cations per 24 Oxygens

Si	7.583	8.017	7.833	7.185	7.496	7.915	8.301	8.290	8.297	6.357
Ti	0.012	0.015	0.013	0.275	0.057	0.155	0.000	0.000	0.000	0.027
Al	1.033	0.513	0.769	1.255	1.048	0.551	0.072	0.057	0.122	3.137
Fe	2.418	1.254	1.355	2.655	2.774	1.710	2.060	2.057	2.367	2.168
Mn	0.039	0.019	0.000	0.057	0.051	0.037	0.050	0.063	0.096	0.000
Mg	2.591	3.885	3.738	2.235	2.220	3.122	3.097	3.144	4.159	2.026
Ca	2.081	2.008	1.968	2.066	2.123	2.150	2.073	2.068	0.599	1.981
Na	0.166	0.000	0.166	0.173	0.159	0.000	0.000	0.000	0.000	0.634
K	0.097	0.000	0.018	0.194	0.152	0.031	0.020	0.007	0.005	0.069
Cl	0.000	0.000	0.000	0.000	0.000	0.000	0.000	0.000	0.000	0.000
Total	16.020	15.711	15.860	16.095	16.080	15.671	15.673	15.686	15.645	16.399

Sample Key	38-9 5	41-3 5	41-10 5	24-8 6	42-4 6	42-10 6	44-3 6	44-10 6	58-10 6	68-6 6
SiO <sub>2</sub>	45.39	46.74	50.94	46.73	45.17	46.31	53.61	46.69	47.04	46.10
TiO <sub>2</sub>	0.38	0.70	0.29	0.77	1.61	1.19	0.21	0.44	0.67	0.99
Al <sub>2</sub> O <sub>3</sub>	7.65	6.08	2.59	6.23	6.71	6.77	1.38	6.23	5.73	6.24
FeO	20.27	18.09	15.75	17.66	19.35	18.14	14.96	18.90	18.22	17.93
MnO	0.36	0.46	0.46	0.46	0.53	0.50	0.45	0.45	0.43	0.40
MgO	9.00	10.69	13.06	11.04	9.69	10.47	14.31	10.07	10.60	10.22
CaO	12.44	12.25	12.95	12.40	11.95	12.00	12.88	12.38	12.38	11.96
Na <sub>2</sub> O	0.51	0.00	0.00	0.55	0.94	0.85	0.00	0.00	0.00	0.69
K <sub>2</sub> O	0.75	0.80	0.21	0.71	0.92	0.87	0.21	0.75	0.60	0.79
Total	96.75	95.81	96.25	96.55	96.87	97.10	98.01	95.91	95.67	95.32

## Cations per 24 Oxygens

Si	7.270	7.460	7.943	7.402	7.227	7.321	8.137	7.471	7.513	7.412
Ti	0.045	0.084	0.034	0.092	0.194	0.142	0.024	0.053	0.080	0.120
Al	1.443	1.143	0.475	1.164	1.265	1.261	0.247	1.175	1.079	1.182
Fe	2.716	2.415	2.054	2.339	2.589	2.398	1.898	2.529	2.433	2.411
Mn	0.049	0.062	0.060	0.061	0.072	0.067	0.058	0.061	0.058	0.055
Mg	2.149	2.543	3.035	2.606	2.312	2.467	3.237	2.402	2.524	2.450
Ca	2.135	2.095	2.163	2.105	2.048	2.032	2.094	2.123	2.118	2.060
Na	0.158	0.000	0.000	0.170	0.292	0.262	0.000	0.000	0.000	0.215
K	0.154	0.163	0.043	0.143	0.189	0.175	0.041	0.153	0.123	0.163
Total	16.119	15.965	15.807	16.082	16.188	16.125	15.736	15.967	15.928	16.068

## DESCRIPTIONS OF AMPHIBOLES ANALYZED BY MICROPROBE

- 55-7: Fine grained, anhedral granulated (?) groundmass amphibole.
- 74-5, 74-6: Coarse grained subhedral amphibole, possibly after pyroxene.
- 18-8: Fine grained anhedral amphibole surrounding biotite in aggregate of mafic minerals.
- 18-11: Amphibole rim on subhedral pyroxene grain (18-10).
- 73-4: Amphibole rim on anhedral pyroxene grain (73-3) in aggregate of mafic minerals.
- 85-2: Aggregate of fine grained, possibly recrystallized amphibole interstitial to plagioclase.
- 85-12: Aggregate of fine grained amphibole within large aggregate of mafic minerals.
- 34-6: Fine grained amphibole in aggregate of mafic minerals.
- 34-8: Fine grained, anhedral granulated amphibole in aggregate of mafic minerals.
- 38-9: Fine grained, subhedral interstitial amphibole.
- 41-3: Amphibole rim on fine to medium grained subhedral pyroxene grain (41-2) within aggregate of mafic minerals.
- 41-10: As in 41-3. Pyroxene probe point is 41-9.
- 24-8: Fine grained subhedral amphibole occurring with several grains of biotite and pyroxene all interstitial to coarse grained plagioclase.
- 42-4: Amphibole rim on coarse grained subhedral pyroxene grain (42-3).
- 42-10: Amphibole rim on medium grained rounded pyroxene grain (42-9).
- 44-3: Amphibole rim on fine to medium grained, anhedral pyroxene grain (44-2).
- 44-10: Amphibole rim on coarse grained subhedral to euhedral pyroxene grain (44-9).
- 58-10: Amphibole rim on medium grained subhedral pyroxene grain (58-9).
- 68-6: Medium grained subhedral amphibole.

## f) Biotites

Sample Key	55-6 1	18-7 3	73-1 3	85-10 3	85-11 3	34-1 4	38-6 5	39-9 5	41-8 5	70-14 6
SiO <sub>2</sub>	36.30	34.89	36.11	35.84	35.83	36.13	35.42	36.57	36.41	36.65
TiO <sub>2</sub>	2.34	2.17	2.23	2.99	2.94	1.73	2.20	1.82	1.58	1.62
Al <sub>2</sub> O <sub>3</sub>	15.50	14.81	15.52	13.93	13.92	17.25	15.26	14.23	14.70	14.39
FeO	23.02	24.07	20.01	24.13	24.44	17.09	24.73	20.92	21.43	21.40
MnO	0.00	0.00	0.00	0.29	0.21	0.00	0.00	0.23	0.19	0.33
MgO	9.16	7.59	10.68	8.39	8.24	13.19	8.31	10.05	10.45	10.52
CaO	0.00	0.00	0.00	0.00	0.00	0.29	0.00	0.00	0.00	0.00
K <sub>2</sub> O	10.10	9.19	9.54	9.95	9.81	9.45	9.92	9.86	9.61	10.07
Cl	0.00	0.18	0.00	0.00	0.00	0.00	0.00	0.00	0.00	0.00
Total	96.42	92.90	94.09	95.52	95.39	95.13	95.84	93.68	94.37	94.98
Cations per 24 Oxygens										
Si	6.098	6.133	6.114	6.140	6.149	5.954	6.051	6.270	6.198	6.218
Ti	0.296	0.287	0.284	0.386	0.380	0.214	0.282	0.234	0.203	0.207
Al	3.069	3.069	3.098	2.813	2.816	3.351	3.071	2.876	2.949	2.878
Fe	3.233	3.538	2.833	3.457	3.508	2.355	3.532	3.000	3.051	3.037
Mn	0.000	0.000	0.000	0.042	0.031	0.000	0.000	0.034	0.027	0.047
Mg	2.294	1.988	2.694	2.143	2.107	3.240	2.116	2.567	2.653	2.660
Ca	0.000	0.000	0.000	0.000	0.000	0.051	0.000	0.000	0.000	0.000
K	2.164	2.061	2.060	2.174	2.147	1.985	2.161	2.157	2.088	2.180
Cl	0.000	0.000	0.000	0.000	0.000	0.000	0.000	0.000	0.000	0.000
Total	17.154	17.076	17.083	17.155	17.138	17.150	17.213	17.138	17.169	17.227

Sample Key	21-9 6	24-6 6	58-3 6	68-8 6	86-13 0	90-7 *	90-9 *
SiO <sub>2</sub>	37.22	36.49	36.78	36.26	35.41	36.38	36.73
TiO <sub>2</sub>	2.02	2.22	1.78	4.23	1.81	1.64	1.68
Al <sub>2</sub> O <sub>3</sub>	14.37	14.39	14.61	14.12	16.46	16.10	16.01
FeO	19.75	21.01	21.40	21.32	21.99	20.37	20.49
MnO	0.29	0.33	0.33	0.27	0.37	0.30	0.37
MgO	10.76	10.72	10.35	10.55	7.91	9.64	10.07
K <sub>2</sub> O	9.73	10.03	10.12	7.64	9.34	10.15	9.76
Total	94.14	95.19	95.37	94.39	93.29	94.58	95.11
Cation per 24 Oxygens							
Si	6.296	6.168	6.211	6.107	6.109	6.157	6.165
Ti	0.257	0.283	0.227	0.535	0.235	0.208	0.212
Al	2.865	2.867	2.908	2.803	3.347	3.211	3.168
Fe	2.793	2.969	3.021	3.004	3.173	2.883	2.876
Mn	0.042	0.047	0.047	0.038	0.055	0.043	0.052
Mg	2.712	2.700	2.604	2.648	2.035	2.432	2.520
K	2.100	2.163	2.180	1.643	2.056	2.191	2.090
Total	17.065	17.197	17.198	16.778	17.010	17.125	17.083

\* Biotite analyses from a quartz monzonite dyke.